Università degli Studi di Catania
Facoltà di Scienze Matematiche, Fisiche e Naturali
Dipartimento di Fisica ed Astronomia

Dottorato di Ricerca in Fisica
Ciclo XXIV
Sezione Astrofisica

Luminous – Early Interactive Type II Supernovae

Supervisori:
Chiar.mo Prof. Gaetano BELVEDERE
Dott. Massimo TURATTO

Coordinatore:
Chiar.mo Prof. Francesco RIGGI

Dottorando:
Cosimo INSERRA

December 10, 2011

"Non chi comincia
ma quel che persevera"
Leonardo da Vinci, aforisma

Contents

List of Figures

List of Tables

1

Introduction

1.1 The Supernova event

The word *Supernova* has been coined by the astronomers Baade and Zwicky in 1934, referring to what appears to be a very bright new star shining in the celestial sphere and adding the suffix "*super*" respect to the standard *Nova* (it means "new" in Latin) to distinguish the two events. The Novae are cataclysmic events, instead the Supernovae (hereafter SNe) are catastrophic events and the objects belonging to this class must have a magnitude < -14. With the impulse of Zwicky, a systematic search began and a large number of new SNe were discovered in the following years.

Now it is know that massive stars finish their life as SNe when the energy source produced by the nuclear reactions in the cores of the star is exhausted. SNe are powerful explosions that mark not only the final stage of single stars but also of compact stars in binary system. The SN explosion can completely destroy the star, like the thermonuclear SNe, or can leave a compact nucleus, like the core-collapse SNe (hereafter CC-SNe). In these explosions kinetic energies of $\sim 10^{51}$ ergs are released, although in the events produced by the gravitational collapse of the nucleus, most energy escapes as neutrinos (E_ν $\sim 10^{53}$ ergs, 99% of the total energy). Only the 1% of energy is spent to eject matter at velocity of the order of $\sim$ 10000 $\mathrm{km\,s^{-1}}$. Despite the great energy only a factor of 10^{-4} of that is emitted in visible light. In our own Galaxy a Supernova (SN) event may even be visible in daylight. The interstellar medium (ISM) is enriched by

heavy elements synthesized by the star during its evolution and explosion. After a period of the order of decades post the explosion, Supernova Remnants (SNRs) are formed and drive the chemical evolution of the whole galaxy.

The role of SNe is not only related to the explosion of the stars itself, but is extremely important in the modern astrophysics because links several fields of research. The energy inputs of SNe influence the birth of new stars, compressing the ISM through their shocks. Also in the dust production have an important role, indeed they are one of the only two mechanisms known as responsible of dust creation. Moreover, SNe can be used in theoretical fields as probes of the stellar evolution, or in the case of the Galaxy CC-SNe as "laboratory" to study the strong neutrino emission. In cosmology SNe are among the best tools as distance indicators or in the star formation history at redshift $z>1$ ($z = (\lambda_{obs} - \lambda_{emi})/\lambda_{emi}$). Recently has been discovered a link between the CC-SNe and the production of long duration γ-ray bursts (GRBs) that can lead to better understand these complex events.

In this Section has been introduced the event of Supernova, subsequently will point out the differences among the SN types, focusing on the objects described in this thesis: the type II SNe. The Chapter is organized as follows: in Sect. 1.2 we introduce the different SNe types and in Sect. 1.3 the general properties of the various types dedicating various subsections to each kind of SN. In Sect. 1.4 we describe the explosion mechanism of CC-SNe, instead in Sect. 1.5 we present some of open issues about the type II SNe. At least Sect. 1.6 describes the motivation and the outline of the thesis.

1.2 Supernovae classification

As written above, after the introduction of the SNe class, started a campaign to discover new SNe, this led in a brief period to collect a number of SNe (19 during the first systematic campaign by Baade and Zwicky) and cataloguing them trough the discovery year followed by a letter of the alphabet indicating the chronological order of the discovery. The first division, based on spectroscopic differences, had been made by Minkowski (153), who divided the SNe into two types, depending on the absence (type I) or presence (type II) of H lines in the

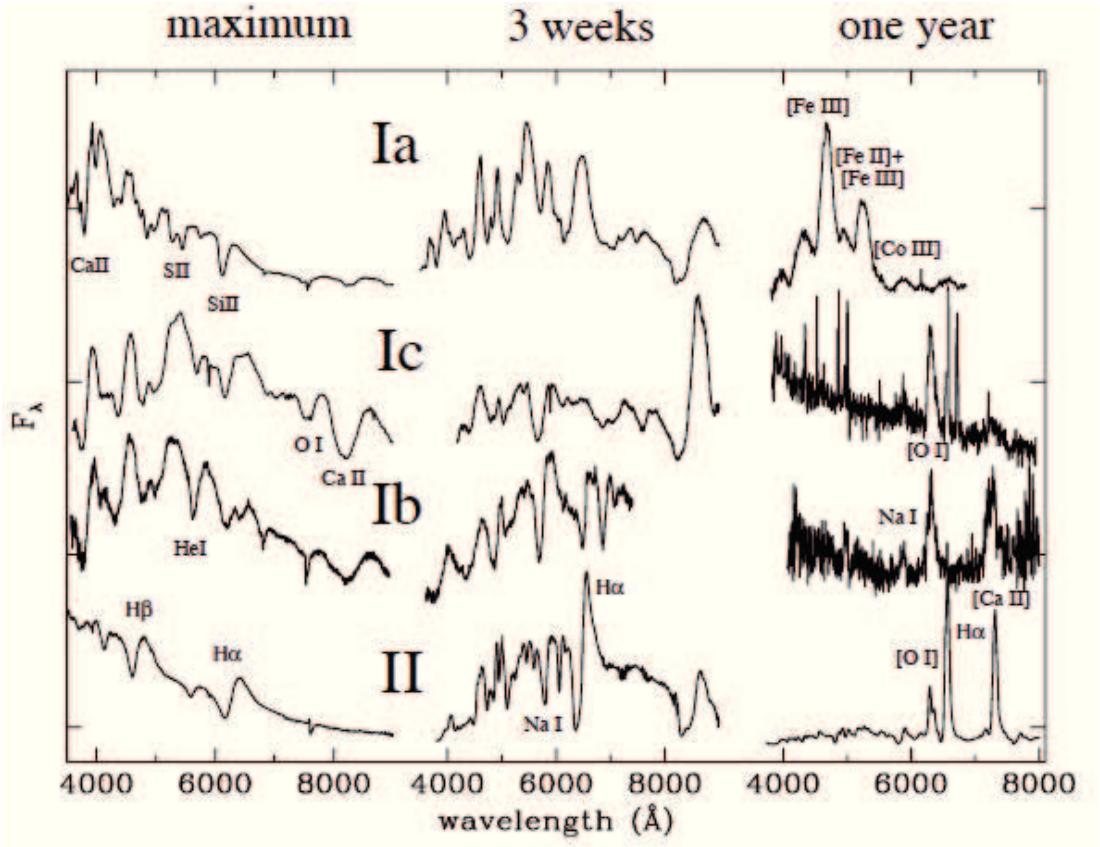

Figure 1.1: Schematic spectra of type Ia, Ib/c and II at maximum, tree weeks and a year after maximum (236).

spectra. Subsequently Zwicky added other three categories (III, IV, V) that had H in the spectra and peculiar light curves. The last types were scarcely populated and had been generally included among type II SNe.

Thanks to the new discoveries in the 80's a new classification scheme started to take shape. The classification is based on the early optical spectroscopy (cfr. Fig. 1.1,Turatto (236)) and divides the SNe into four main classes:

- **SNe Ia**: the spectra show Si II lines but not H I. This class correspond to the type SNe I by Minkovsky;
- **SNe Ib**: the spectra have not Si II or H I lines and are dominated by He I lines;

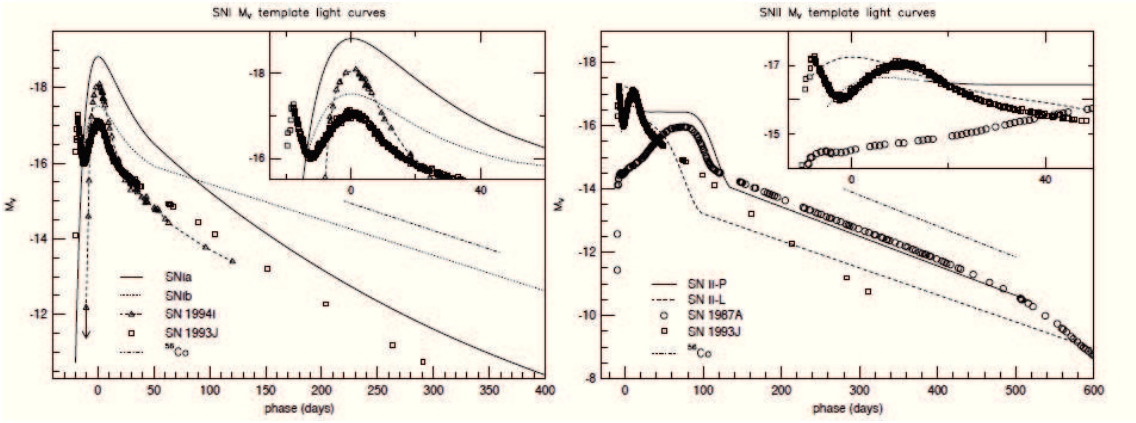

Figure 1.2: Comparison between photometric evolution (251) of SNe Ia and Ib/c (left panel) and type II (right panel).

- **SNe Ic**: the spectra have not Si II and H I lines, despite the He I lines are really weak or absent. There is a general consensus that there is a continuos transition between this class and the class before;

- **SNe II**: the spectra show H I lines, that dominate at all epochs. This class correspond to the type II by Minkovsky.

Subsequently, thanks to the informations about the light curves (cfr. Fig. 1.2, Wheeler and Benetti (251)) and the late spectra, the classification has been refined introducing a few subclasses for the SNe II:

- **SNe IIP**: have light curve that after maximum show a period of almost constant luminosity, called plateau, lasting from a few weeks to more than 100 days;

- **SNe IIL**: show a linear, uninterrupted decline of luminosity after maximum. These classes (type IIP and IIL) were earlier proposed by Barbon, Ciatti, and Rosino (15);

- **SNe IIb**: photometrically analogies with SNe Ib/c, while spectra show strong H I lines for the first few weeks after the explosion. Later on, the spectra become dominated by He I lines, resemble that of SNe Ib. They are therefore the link between these two classes, supporting the idea that

SNe II and SNe Ib/c come form the same kind of progenitors and explosion mechanism;

- **SNe IIn**: show light curves declining very slowly. The spectra show blue continua with multicomponent emission lines lacking the broad P-Cygni absorptions typical of other types. Narrow emission lines, sometimes with P-Cygni profiles, are also visible on the top of the broader components.

The large number of follow-up campaigns of SNe in the recent years and the improved observational capabilities and quality of the obtained data showed an unexpected diversity of SN properties. Individual objects can have properties intermediate between two SN types, and an exact classification is not always trivial, e.g. SNe 1990aj, 1993R (236), 2001ic (93), 2006jc (142), 2008S (30) and 2008ha (243). Other SNe have behaviours different form previous classification scheme, like the *Hypernovae*, possibly associated with GRBs, whose spectra resembling SNe Ib/c show very broad P-Cygni features and overluminous light curves (162). In Fig. 1.3 is reported the current classification scheme from Turatto, Benetti, and Pastorello (234).

1.3 General properties of Supernovae

1.3.1 Supernovae Ia (Thermonuclear SNe)

Type Ia SNe have become very popular in the last decade because of their role in determining the geometry of the Universe with their high luminosity and relatively small luminosity dispersion at maximum. SNIa are discovered in all types of galaxies, also in ellipticals (13), and are not associated with the arms of spirals as strongly as other SN types (248).

It is believed that type-Ia SNe originate from the thermonuclear disruption of CO white dwarfs (WDs) in binary systems, which accrete mass via material transfer from companion stars (thus, SNe Ia are also called thermonuclear SNe). The material reinvigorates the WDs which, after to have reached the Chandrasekhar limit (1.4 $M_\odot$), explode as SNe Ia. This occurs when the rate of accretion is sufficiently fast, i.e. 10^{-6}–10^{-9} $M_\odot$ year^{-1}. The nature of the companion is not

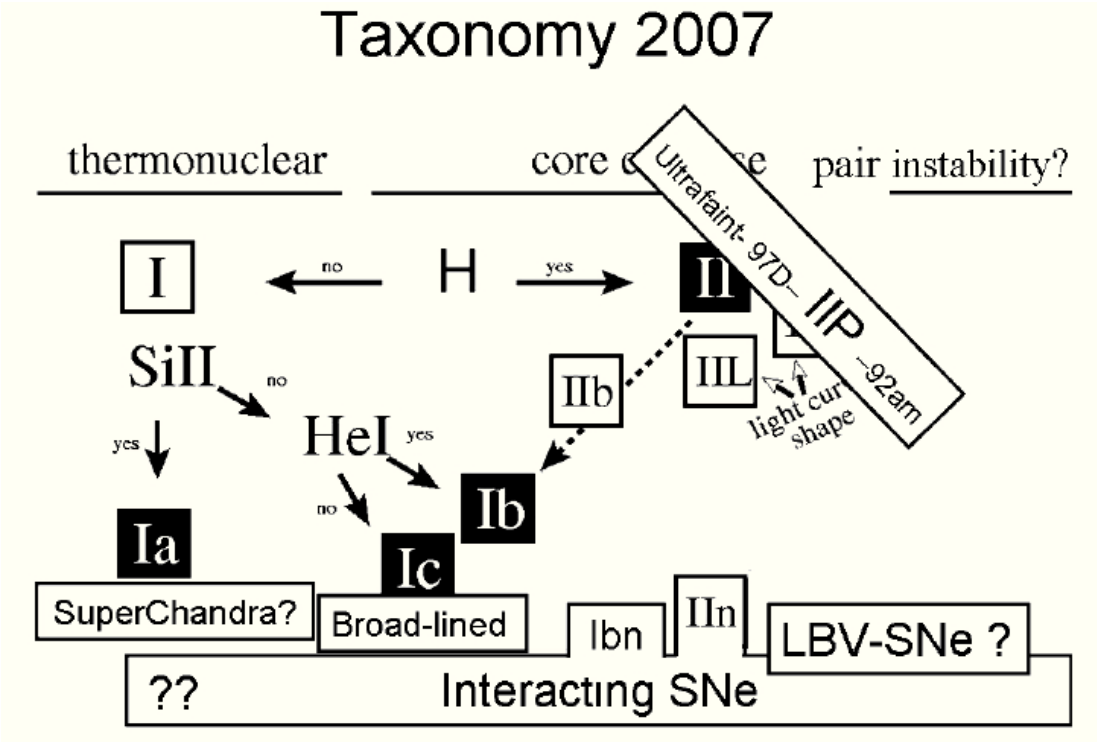

Figure 1.3: Classification scheme of SNe (234).

fully understood. Two scenarios, in which the companion is a main sequence star or a degenerate star are still debated (163); furthermore, different mechanisms of explosion, as merging of two massive degenerate stars, has been considered to explain extremely luminous SNe Ia, called "*Superchandra*", for what the progenitor was estimated to be 2.1 $M_{\odot}$ (110, 119). However also the possible interpretation with a Chandrasekhar mass model has been proposed (107).

The spectra are characterized by lines of intermediate mass elements such as Ca II, O I, Si II and S II during the peak phase and by the absence of H at any time (cfr. Fig. 1.1). With age metal lines as Fe and Co become prominents. The nebular spectra are dominated by strong [Fe II] and [Fe III] lines (cfr. Fig. 1.1). The spectra of a few SNe Ia appear to be significantly different form the average, especially in the strength of Si II lines.

The light curves of SNe Ia are relatively homogenous, even if important differences among them have to be pointed out. Thanks to the use of the Cepheids as calibrators, for the absolute magnitude of a number of type Ia the average values founded ranging from M_V=-19.34 to M_V=-19.64 with small dispersion (91, 223). It is also been observed (181) that the magnitudes at the B maximum in all bands are also correlated with the post maximum decline rate Δm_B^{15}. It is known that the peak luminosity of SNe Ia is directly linked to the amount of radioactive ^{56}Ni produced in the explosion (7, 8). Hence SNe Ia, having different magnitudes at maximum, are probably the result of the synthesis of different amounts of radioactive ^{56}Ni. Moreover, there are indications of large variances (up to a factor 2) in the total mass of the ejecta (36). Nevertheless, during the recent years, suggestion of significant differences among SNe Ia have been confirmed by new, high signal to noise data.

Based on the analysis of the photometric and spectroscopic properties of a sample of 26 objects Benetti *et al.* (22) have identified three subclasses of SNIa with distinct physical properties, the main characterizing parameter is the gradient of expansion velocity of the photosphere. Faint SNe Ia (similar to SN 1991bg) are fast decliners both in luminosity and expansion velocity, have typically low expansion velocities and occur in early-type galaxies. High– (HVG) and low–velocity (LVG) gradient SNIa include normal objects, although the LVG group also includes all the brightest, slow declining SNe (like SN 1991T). Even if the

statistical analysis suggests that LVG and HVG are two distinct groups, they may possibly represent a continuum of properties. Indeed a recent analysis by Maeda *et al.* (136) has brought new evidence on the possibility that the differences in the spectral evolution are related to an asymmetric explosion.

Other SNe Ia show anomalies as detection of an evanescent CSM around as for SN 2006X (178) and a strong circumstellar matter (CSM)–ejecta interaction with pronounced H emission lines as for SNe 2002ic and 2005gj (3, 93).

The study of the thermonuclear SNe is beyond the aims of this thesis.

1.3.2 Supernovae Ib/c

Type Ib and Ic appear only in spiral type galaxies (13) and have been associated with a parent population of massive stars, perhaps more massive than SNe II progenitors (248). It is believed that they are produced by the core-collapse of very massive stars which have been stripped, before the explosion, of their envelope of H (type Ib) or of both H and He (type Ic). Therefore, at some epoch of their evolution, they exhibit relatively strong radio emission with steep spectral indices and fast turn-on/turn-off, which is thought to arise from the SN shock interaction with the dense circumstellar medium (46, 47).

As written above, the characterizing spectral features of SNe Ib are the absence of H and Si II lines and the presence of He I. The excited levels of He producing such lines are thought to be populated by fast electrons accelerated by γ-rays from the decay of ^{56}Ni and ^{56}Co (133). It was soon recognized that some objects did not show strong He lines (253) and the class of helium poor type Ic was proposed. Prominent lines in photospheric spectra of both SN types are: Ca II, O I, Na I, Fe II, Ti II. The nebular spectra are dominated by [O I] and [Ca II], but also Na I and Ca II are visible (see Fig. 1.1).

In order to investigate the physical differences between these two subclasses, the signatures of He were searched carefully in SNe Ic. The He I 10830 line in type Ic was first found in the spectra of SN 1994I (76). The He lines have expansion velocities much lower than other lines, indicating that the ejecta interacts with a dense shell of almost pure He originating from a stellar wind or mass transfer

to a companion. Helium has been unambiguously identified also in the spectra of other SNe Ic as SN 1999cq (141).

Weak absorption features attributed to Hα were first identified in the spectra of the SNe Ib 1983N and 1984L (252). Analyses of the spectra of a few other SNe Ib have suggested that detached H is frequently present in SNe Ib (31). The optical depths of H and He are not very high, so that modest differences in the He I line optical depths might transform type Ib into type Ic objects.

The SNe Ib/c are typically fainter than SNe Ia (at maximum, $M_B \sim 18$, with a larger dispersion, 200, 251). The light curves of type Ib/c SNe have been divided in two groups depending on the luminosity decline rate (51). However, the suggestion that type Ic SNe include both fast and slow decliners while Ib seem to prefer slow decliners has been challenged by the existence of SNe Ib with fast light curves, e.g. SNe 1999I and 1991D.

Recently, SNe Ic have deserved large attention because of their relation to GRBs. Indeed, long-duration GRBs at sufficiently close distance have been related to bright, highly energetic SNe Ic. The first SN associated with a GRB has been SN 1998bw related with GRB980425 and having broad–line SN Ic features (118). Other SNe with GRBs associated were discovered as SN 2003dh/GRB030329 (219), SN 2003lw/GRB031203 (140) and SN 2010bh/GRB100316. Detailed analysis showed that these SNe require even more than 10^{52} ergs, somewhat less in case of asymmetric explosion, have exceptionally high expansion velocities (>30000 $\mathrm{km\,s^{-1}}$) and very luminous curves, justifying the introduction of the term "Hypernovae" (118). They are believed to be the outcome of very energetic black hole forming explosions of massive stars (30-50 $M_\odot$) which synthesize large amounts of ^{56}Ni (0.3-0.5 $M_\odot$). Furthermore, there are a number of broad–line SNIc for which an accompanying GRB has not been detected, e.g. SNe 1997ef (117), 2002ap (146), 2003jd (244). These SNe have a tendency to have smaller luminosity, mass of the ejecta and explosion energy than GRB–SNe but it is not clear whether the non-detection of the GRB is a geometric effect due to asymmetries or an intrinsic property of the explosion.

1.3.3 Supernovae IIb

A few objects have been found to have early time spectra similar to type II (i.e. with prominent H lines) and late time spectra similar to type Ib/c. For this reason they have been called type IIb SNe. The first discovered was SN 1987K (77), but the best studied example, and one of the best studied SNe ever, was SN 1993J in M81 (e.g. 14). In addition to SNe 1987K and 1993J, few other similar objects have been discovered (SNe 1996cb, 2001gd, 2001ig, 2008ax, 2008bo and 2011dx).

While the early spectrum of SN 1993J was almost featureless with a blue continuum and broad H and He I λ 5876 lines typical of SN II, already three weeks later it displayed progressively stronger He I $\lambda\lambda$ 5876, 6678 and 7065 lines characteristic of SN Ib.

The light curve of SN 1993J was unusual with a narrow peak followed by a secondary maximum, recalling the behavior of SN 1987A if the time axis were reduced by a factor of four. After another rapid luminosity decline around 50 days past the explosion, the light curve settled into an almost exponential tail with a decline rate faster than normal SN II and similar to that of SN Ia, indicative of a small mass for the ejecta.

The progenitor stars of SNe IIb are expected to have lost most of their mass before explosion. This scenario is supported by a few observational properties: (1) the nebular spectra of SN 1993J show, at late time, Balmer emission lines of H with boxy profiles, consistent with the interaction with circumstellar material lost by the progenitor; (2) circumstellar gas in proximity to the exploding star was also revealed through the detection of narrow coronal lines persisting for a few days after the explosion (24, 179); (3) the luminosity evolution closely resembles that of SNe Ib, with a steep post-maximum decline rate typical of explosions with low mass ejecta.

1.3.4 Supernovae II

Type II SNe are characterized by the obvious presence of H in their spectra. They avoid early type galaxies (13), are strongly associated with regions of recent star formation (248) and are commonly related with the core collapse of massive stars (259). SNe II display a wide variety of properties both in their light curves

(180) and in their spectra (75) and represent core-collapse explosions occurring in progenitor stars still retaining the H envelopes. They are principally divided into two subclasses, on the basis of the shape of their optical light curves (15). SN IIL (Linear) and SN IIP (plateau) constitute the bulk of SN II and are often referred as normal SN II. Indeed the two classes are not separated and there are a few intermediate cases with short plateaus, e.g., SN 1992H (52).

The properties and mass of the progenitor star and the environment in which the SN explosion occurs are the main factors determining the display of SNe II, thus, modeling the observations helps to identify the progenitors. Another approach to this key issue is based on the direct detection of progenitor stars on high quality archive images obtained before the SN explosion (209).

SNe IIL are characterized by light curves showing a linear, uninterrupted decline of luminosity after maximum, probably because of the relatively low mass envelope. The absolute magnitude is similar to that of SNe Ib/c, even if with a slightly smaller scatter, as reported by Richardson *et al.* (200). From ∼50 days after the explosion the light curves settle onto an exponential decline: this behaviour is consistent with constant trapping of the energy release of the radioactive decay of ^{56}Co to ^{56}Fe.

SNe IIP constitute a very heterogeneous class of CC SNe, whose light curves show different characteristics both in shape and luminosity at maximum. The average absolute magnitude at maximum of SNe IIP is fainter than that of SNe IIL, i.e. M_B ∼-17, but has a very large dispersion (σ=1.12, 200). After maximum, the luminosity declines for a few days, until it reaches the plateau, a period of constant luminosity. This period is due to the recombination of the ionized matter. Depending on the envelope mass and explosion energy, this phase may be particularly long-lasting (∼100 days) or extremely short (∼20 days). After this, the light curve shows an evolutionary path similar to that of SNe IIL.

At nebular epochs the observed decline rate can be modified by two effects. The first one is the dust formation within the ejecta. The light at optical wavelengths is absorbed by newly formed dust grains and re-emitted in the near infrared (NIR). This makes to increase the opacity, and thus the luminosity decreases faster. A second effect may be caused by the presence of high density circumstel-

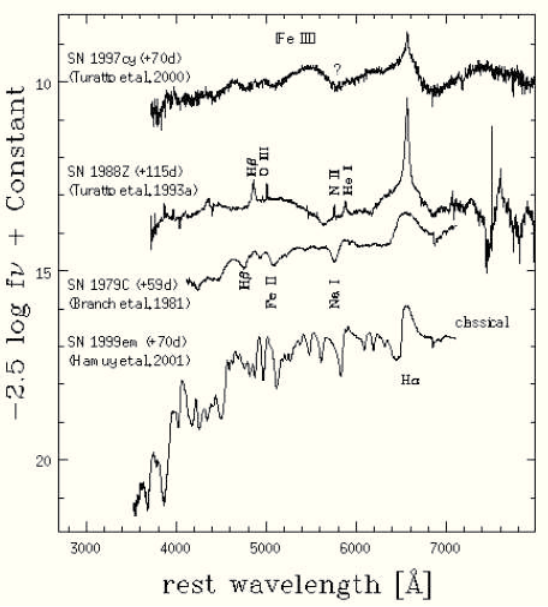

Figure 1.4: SNe II spectra at ∼3 months after explosion (95).

lar medium (CSM): if the SN environment is rich of material, this may interact with the fast ejecta, providing additional energy to the luminosity.

The spectra of both classes are dominated by the H Balmer lines (Fig. 1.4). He I lines are visible only for a few days after the explosion, then disappear and other lines (e.g. Na I, Ca II, Fe II, Sc II, Ba II) become prominent during the late photospheric phase. The nebular spectra show strong H I, [O I], Ca II, [Ca II] and [Fe II] emission lines. The absorption features in the photospheric spectra of plateau SNe are possibly stronger than those observed in the spectra of type IIL.

The spectral and photometric behaviour of type IIL is consistent with the core-collapse explosion of moderately massive stars (8-10 $M_{\odot}$), which eject low-mass envelopes (1-2 $M_{\odot}$, 33). The envelope masses are smaller than those ejected by the SNe IIP, but larger than those of SNe IIb. A general scenario has been proposed in which common envelope evolution in massive binary systems with varying mass ratios and separations of the components can lead to various degrees of stripping of the envelope (164). According to this scenario the sequence of types IIP–IIL–IIb–Ib–Ic in Fig. 1.3 is ordered according to a decreasing mass of the envelope. SNe IIP are thought to be produced by the explosion of stars

spanning a large range of masses which probably did not suffer significant mass loss phenomena before the explosion. Therefore the study of SNe IIP, not affected by phenomena of ejecta-CSM interaction, provides important information on the nature of the progenitor stars.

Sometimes type IIL show radio emission attributed to interaction with a CSM, e.g. SN 1979C (157). Other SNe IIL that have shown interaction, due to the presence of a double P-Cygni profile or a flattening light curve in late stages, were SNe 1994aj, 1996L, 1996al, 2000P (23). These SNe show also a broadening of the spectral lines, and Hα flux unusually high.

1.3.5 Supernovae IIn

A number of peculiar SN II, larger with the pass of the years, have been grouped into the class of SN IIn (n denoting narrow emission lines, 206). The spectra of these objects have a slow evolution and are dominated by strong H Balmer emission lines without the characteristic broad absorptions. The early time continua are very blue, He I emission is often present and, in some cases, narrow Balmer and Na I absorptions are visible corresponding to expansion velocities of about 1000 $\mathrm{km\,s^{-1}}$ (176). Unresolved forbidden lines of [O I], [O III] (two SNe at the top of Fig. 1.4) and of highly ionized elements such as [Fe VII] and [Fe X] are sometimes present.

What we observe in these objects are the results of the interaction between ejecta and CSM, rather than the SN itself. The interaction of the fast ejecta with the slowly expanding, dense CSM generates a forward shock in the CSM and a reverse shock in the ejecta. The shocked material emits energetic radiation whose characteristics strongly depend on the density of both the CSM and the ejecta, and on the properties of the shock (44). Sometimes the pressure and temperature behind the shock are sufficiently high that the post-shock ejecta and CSM may become powerful X-rays emitters. At the same time synchrotron radiation is generated by electrons accelerated up to relativistic energies at the shock front. Thus the great diversity of observed SN IIn can provide clues to the different history of the mass-loss in the late evolution of progenitors. This source

of energy largely dominates (sometimes for many years) over the usual sources powering the energy output of other SN types.

As written above, late time signatures of interaction with a CSM are frequent also among type II SNe. Especially for the subclass of type IIn SNe, mass loss during the progenitor pre-explosion phase is a key parameter. In fact, the CSM structure, density and kinematics strongly affect both the SN spectroscopic and photometric evolution. Typical mass loss rates are in the order of 10^{-6}–10^{-5} $M_{\odot}yr^{-1}$, but this value may change significantly, depending on several factors. The density profile and the distance of the CSM play also a major role.

Despite the apparently complicated CSM configuration, the study of Hα multi-component profile is an information source about the kinematic and structure of the gas surrounding the star both in pre- and post-explosion phase. Hα typically exhibits a narrow unresolved component (FWHM $\sim$ 200 km s^{-1}) superposed on a base of intermediate width (FWHM $\sim$ 1000–3000 km s^{-1}); sometimes a very broad component (FWHM $\sim$ 5000–10.000 km s^{-1}) is also present (75). The extremely narrow feature can give us information about the kinematics of the unperturbed CSM released by the progenitor. Generally, the velocity span from $\sim$10 to $\sim$100 order of km s^{-1} and increase with progenitor mass: 10-20 km s^{-1}for AGB, 20-40 km s^{-1} for RSG and 100-200 for LBV winds (212). Studying the intermediate component is possible retrieve informations about the kinematic of the slower, smaller radiating layer, having a velocity of a few hundreds of km s^{-1}. Instead the broadest component of a few thousand of km s^{-1} is given by SN ejecta. Broad components are seen also in emission lines of O III and Ca II, instead narrow emission lines have been seen for Fe group lines (203), maybe caused by photoionization of the CSM by the UV flash (or X-ray photons produced during the initial flash).

The best studied object of this class is SN 1988Z, detected also in radio and X-rays (238). This object is considered the prototype of this class, although a common evolutionary path for these SNe does not really exist. SNe IIn are a heterogeneous group of CC SNe whose properties are determined by the distribution of the CSM around the SN, the amount of material and its density. They are commonly brighter than SN IIP. More recently SN 1998S has been extensively studied also with the Hubble space Telescope (HST).

1.4 CC-SNe: physics of the explosion

SNe II of all subclasses, SNe Ib/c and transitional SNe IIb introduced in the previous Sect. 1.3.2; 1.3.3; 1.3.4; 1.3.5, belong to the family of SNe produced by the gravitational collapse of the core of the star (CC-SNe). At the end of their evolution, massive stars may develop iron cores surrounded by shells of lighter element until the original H atmosphere.

The mass of the Fe core will continue to grow until it approximately reaches the Chandrasekhar mass. At this mass, electron degeneracy pressure can no longer withstand the gravitational forces and, consequently, the Fe core starts to contract. Due to electron captures in the Fe core, $e^- + p \rightarrow n + \nu_e$, the number of electrons decreases and the pressure reduces accordingly. Furthermore, energetic photons in the core start to photo disintegrate Fe into α particles and baryons. The process is endothermic which remove the support of energy and pressure from the star, leading to its collapse. This process leads to the formation, generally, of a neutron star (NS) and, as consequence, a large amount of energy is released. The total energy liberated by the explosion is about 10^{53} ergs. Most of this energy is lost via neutrino escape, while about 1% is released as kinetic energy at the base of the envelope.

The passage of the shock-wave produced by the collapse through the inner layers of the star increases the temperatures, favouring the synthesis of iron peak elements. One of the most important elements in this phase is the radioactive ^{56}Ni. This elements, that decays following the sequence ^{56}Ni$\rightarrow^{56}$Co$\rightarrow^{56}$Fe, is the main fuel powering the SN light curve at late phases (for exceptions see Sec. 1.3.4). When the shock-wave reaches the surface of the star (a few hours after the collapse), the SN becomes visible producing an UV burst which generates a narrow spike in the bolometric light curve (shock breakout).

After the shock breakout, the adiabatic expansion of the envelope causes a rapid decline of the temperature and luminosity, until the diffusion of internal energy from the bulk of the envelope and/or the contribution of the radioactive decays begin to become important, increasing the SN luminosity. In this phase the light curve reaches the optical maximum.

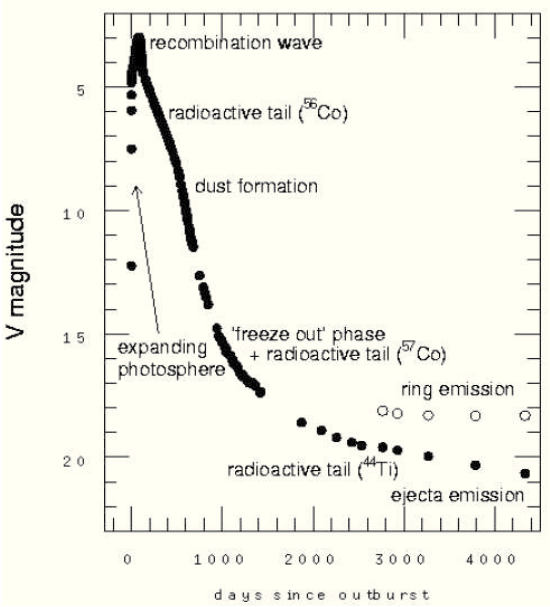

Figure 1.5: Light curve of the well studied SN 1987A in V band. The main process involved in shaping the light curve are also reported (128).

At this stage, the SN shock wave has already propagated through the envelope of the progenitor star redistributing the explosion energy through it. From this moment onward the envelope is essentially free-coasting and in homologous expansion.

As mentioned before as the SN expands and cools, the ionized matter begins to recombine. A recombination wave moves inward in mass through the ejecta, recombinating the hydrogen. The opacity goes to zero and the residual trapped internal energy can be released. This phase, whose duration depends on the envelope mass and the explosion energy, hence the expansion velocity, corresponds to the plateau in the SN IIP. During this phase the temperature remains constant.

Once the H envelope is recombined, the envelope is transparent, the SN light curve settles into the exponential tail, during which the radioactive decay of ^{56}Co represent the main energy source, and the luminosity decline is 0.098 mag/day as predicted by the decay. At this phase the luminosity depends on the amount of radioactive material ejected. Later other radioactive isotopes may also contribute to the luminosity (mainly ^{57}Co and ^{44}Ti).

The complete sequence of process typical of the SN IIP light curve is visible in Fig. 1.5 for the case of SN 1987A which, because of its proximity, has been followed for long time, allowing us to observe the complete evolution of its light curve. It is also noticeable that at late time (∼4 years after the explosion) the emission of the circumstellar ring dominates over that of the ejecta.

In summary the physics behind the SN event is the same for all the core collapse, but the shape of the spectra and light curves depend mainly on the properties of progenitor star and the environment in which the SN explosion occurs.

The range of masses for the progenitors of CC-SNe is very large, from ∼8 to tens $M_\odot$, sometimes also to hundred $M_\odot$. From a theoretical point of view, massive stars end their lives in the following manners (161):

- 8–10 $M_\odot$ stars: These stars are on the AGB phase when the O+Ne+Mg core collapses due to electron captures. The exact mass range depends on the mass loss during the AGB phase. They undergo weak explosions being induced by neutrino heating. These stars produce little α-elements and Fe-peak elements, but are important sources of Zn and light p–nuclei. These AGB supernovae may constitute a sub-class of type IIn supernovae. The explosion might produce also a SN IIL.

- 10 - 90 $M_\odot$ stars: These stars undergo Fe-core collapse to form either a neutron star (NS) or a black hole (BH), and produce large amounts of heavy elements from α-elements and Fe-peak elements. Observations have shown that the explosions of these Fe-core collapse supernovae are quite aspherical. In the extreme case, the supernova energy is higher than 10^{52} ergs s^{-1}, i.e. a Hypernova. Nucleosynthesis in these jet-induced explosions is in good agreement with the abundance patterns observed in extremely metal-poor stars. The resulting SN should appear as a type IIP ($M< 35M_\odot$), IIb, Ib, Ic in order of mass loss and explosion energy.

- 90 - 140 $M_\odot$ stars: These massive stars undergo nuclear instabilities and associated pulsations (ϵ-mechanism) at various nuclear burning stages depending on the mass loss and thus metallicity. In particular, if the mass

loss is negligible, pulsations of O-cores and/or Si-cores due to O, Si-burning could produce dynamical mass ejection. Eventually, these stars undergo Fe-core collapse.

- If the progenitor exceeds these ranges the SN mechanism is the pair instability (PISN). The star is completely disrupted without forming a BH and thus ejects a large amount of heavy elements, especially Fe.

1.5 CC-SNe: open issues

In the previous Sections we have described the general phenomenology of CC-SNe and the physical scenario which overall accounts for the observations. Anyway, a very large array of open issues still remain to be clarified. Among these we list the following:

- **Mass of progenitor**. While the theoretical progenitors scenario is that described in Sect. 1.4, the observations of the progenitors of CC-SNe are all limited to stars with M $<$ 17 $M_{\odot}$, the so called RSG problem (cfr. Sect. 1.5.1).

- **Dust Formation**. The observations of high-z objects calls for the production of large dust masses by massive stars while the observation of nearby SNe indicate much lower amounts of produced dust (cfr. Sect. 1.5.2).

- **Ejecta CSM interaction**. In addition to the above mentioned SNe IIn, there is now evidence for ejecta CSM interaction by many types of SNe (cfr. Sect. 1.5.3).

- **Use of Core Collapse SNe as distance indicators**. CC-SNe are very heterogenous but there are ways to exploit also these SNe for measuring the distances in ways completely independent from thermonuclear SNe, e.g. with the Expanding Photosphere Method (EPM) (207) or the Spectral-tting Expanding Atmosphere Method (SEAM) (18).

- **Existence of pair Production SNe**. In the last years very peculiar SNe characterized by bright and broad light curves have been discovered (e.g. 2007bi, 2006jc; 83, 178, respectively). These have been associated to Pair Production SNe but the issue is still open.

- **Very faint SNe or SNe impostor**. Recently, thanks to the"SNe search" surveys, have been identified an increasing number of SN imposters of unknown physical origin. These may be ultra-faint SNe, luminous blue variable (LBV) eruptions, or other types of proposed exotic eruptive variables (such as stellar mergers). A subset of them have absolute magnitudes between -12 and -14, narrow hydrogen emission line spectra and red colours. The debate on their nature is highlighted by the invocation of new labels, and associations with previously known transient phenomena: luminous red novae, Intermediate luminosity transients, giant eruptions of LBVs, faint core-collapse SNe. As the diversity of these labels suggest, their nature is a complete mystery.

- **Faint SNe and black hole formation**. Some theoretical models (e.g. 105) suggest that massive stars may generate very faint SNe, with much of the radioactive ^{56}Ni falling back onto a black hole. Indeed there may be no visible explosion at all.

- **Ultra bright type I SNe**. They are remarkably bright ($M_u \simeq -22$) and are all associated with very faint host galaxies (typically $M_g > -17$). The spectral evolution links this family of transients to Wolf-Rayet progenitors, and also to the broad lined type Ic SNe which are associated with gamma-ray bursts (GRBS). However a major puzzle is that the enormous luminosity at peak cannot be powered by radioactive ^{56}Ni, which is the canonical energy source for SNe Ic emission.

In this thesis we will focus mainly on type II–IIP SNe more luminous than common and that show phenomena of interaction between ejecta and CSM, even if sometimes these phenomena are hidden and do not appear clearly to a fast analysis. In the following, we shortly describe a few important topics related to this thesis.

1.5.1 Progenitor Masses

One of the key issue of CC-SNe is the mass of the exploding stars. The classical approach is to model the observations in order to obtain information about the progenitor star. In the last decade, a different approach has been also introduced based on the direct detection of the progenitor star of CC-SNe on high quality archive images obtained before the explosion (209, 210, 245). The detection of the progenitor (or measurement of upper magnitude limits) on images obtained with different filters allows to estimate the absolute luminosity and the colour of the candidate progenitor and hence, from theoretical evolutionary tracks, to infer its mass. Tab. 1.1 summarizes the status of these direct mass determinations.

With reference to the topic of this thesis, it is interesting to note that the detected progenitors of IIP have masses between 8 and 15 $M_{\odot}$ (cfr. Tab. 1.1). The issue is generally known as the "Red Supergiant problem" (209, 210). Indeed the observed distribution has been fitted with a Salpeter IMF, a minimum mass of $m_{min} = 8.5^{+1}_{-1.5}$ $M_{\odot}$, and a maximum mass of $m_{max} = 16.5 \pm 1.5$ $M_{\odot}$. Comparing this to the Local Group massive stellar populations immediately raises the question of the lack of detected RSG progenitors with initial masses between 17–30 $M_{\odot}$. Many possible explanations have been proposed (210), but given the recent works on the initial masses of the progenitors of CC-SNe as Smith *et al.* (211) seems that the problem could not exist at all.

1.5.2 Dust

Another major issue related to SNe II is whether core-collapse SNe could be major contributors to the universal dust budget.

Already 40 years ago it has been suggested that SNe could be an important source of dust in the interstellar medium (ISM) (41, 109). This has been partly due to the fact that, given the large amounts of dust produced in the winds of low-mass stars in the local Universe, the possibility that SNe might produce significant dust was not widely explored (cfr. 121). However, evidences in favor of enormous amounts of dust ($\gtrsim 10^8$ $M_{\odot}$) in galaxies at high redshifts ($z \gtrsim 6$) have been found: millimetric observations of the most distant quasars (25), obscuration by dust of quasars in damped Ly-α systems (DLAs) (183) and measurements of

Table 1.1: Results of the homogenous analysis of CC-SNe progenitors through archival images obtained before the SN explosion.

SN name	SN type	Host Galaxy	Progenitor Mass ($M_\odot$)	Reference
1980K	IIL	NGC 6946	< 18	2
1987A	II pec	LMC	20	e.g. 3
1993J	IIb	M81	13-22	4
1997bs	IIn	M66	>20-30	5
1999an	II	IC755	< 18	1
1999br	IIP	NGC 4900	< 15	1
1999em	IIP	NGC1637	< 15	1
1999ev	IIP	NGC 4274	16^{+6}_{-4}	1
1999gi	IIP	NGC 3184	< 14	1
2001du	IIP	NGC 1365	< 15	1
2002hh	IIP	NGC 6946	< 18	1
2003gd	IIP	NGC 628	7^{+6}_{-2}	1
2003ie	II?	NGC 4051	< 25	1
2004A	IIP	NGC 6207	7^{+6}_{-2}	1
2004am	IIP	NGC 3034	12^{+7}_{-3}	1
2004dg	IIP	NGC 5806	< 12	1
2004dj	IIP	NGC 2403	15 ± 3	1
20004et	IIP	NGC 6946	9^{+5}_{-1}	1
2005cs	IIP	NGC 5194(M51)	7^{+3}_{-1}	1
2006bc	IIP	NGC 2397	< 12	1
2006my	IIP	NGC 4651	< 13	1
2006ov	IIP	NGC 4303	< 10	1
2007aa	IIP	NGC 4030	< 12	1
2008bk	IIP	NGC 7793	9^{+4}_{-1}	1
2008cn	II	NGC 4603	15 ± 2, $\lesssim 14$	6
2009kr	IIL	NGC 1832	18-24	7
2009hd	IIL	NGC 3627(M66)	< 20	8
2011dh	IIP	NGC 5194(M51)	13 ± 3	9

1 - Smartt *et al.* (210), 2 - Thompson (228), 3 - Woosley *et al.* (258), 4 - Van Dyk *et al.* (246), 5 - Van Dyk *et al.* (247), 6 - Elias-Rosa *et al.* (65), 7 - Elias-Rosa *et al.* (64), 8 - Elias-Rosa *et al.* (63), 9 -Maund *et al.* (144).

metal abundances in DLAs (185). The existence of large amounts of dust when the Universe was relatively young poses problems for the low-mass star origin of dust, since the main-sequence evolution timescales of these stars (up to 1Gyr) begin to become comparable to the age of the Universe. SNe arising from short-lived population III stars could be a viable alternative.

Recently studies on the origin of dust (60, 166, 229) have supported this view, calling for core-collapse SNe as a major source of dust in the Universe. In fact a number of nearby objects have shown clear evidence of dust formation, e.g. the type IIn SNe 1998S (90, 193), 1995N (89), and 2005ip (79), the type IIP SNe 1999em (68), 2004et (121, 139) and 2004dj (226), the type IIb SN 1993J (89), and the peculiar SN 1987A (5, 134), SN 2006jc (142) and SN 2008S (30).

However, the amount of dust produced by these SNe is highly variable and uncertain. Pozzo *et al.* (193) evaluated a dust mass of $\sim 10^{-3} M_{\odot}$ in the type IIn SN 1998S. For the type IIP supernova SN 1999em, Elmhamdi *et al.* (68) obtained a lower limit to the dust mass of just $10^{-4} M_{\odot}$. In the case of the type II SN 2003gd the MIR flux at about 16 months was consistent with emission from just $4 \times 10^{-5} M_{\odot}$ of newly condensed dust in the ejecta (150).

Another channel to obtain informations about dust formation in SNe environment is via the study of supernova remnants (SNRs). Studies based on three young SNRs reveal dust masses that vary by roughly two orders of magnitude: no more than $8 \times 10^{-4} M_{\odot}$ of dust at $\sim$120 K associated with one of the remnant have been found by Stanimirović *et al.* (220), for the other two remnants Sandstrom *et al.* (204) and Rho *et al.* (199) derive dust masses of $3 \times 10^{-3} M_{\odot}$ at about 70 K and $10 \times 10^{-2} M_{\odot}$ of dust at $\sim$60 K. Estimates for the Crab and Keplers SNRs based on Spitzer MIR data are similar, with 10^{-3}–$10^{-4} M_{\odot}$ of dust (227) and $3 \times 10^{-3} M_{\odot}$ at $\sim$85 K (27), respectively. Thus, the bulk of MIR/FIR studies of SNRs yield dust masses which are at least a factor of 10 less than the minimum required to account for the high-redshift dust. It is possible that most of the SNR dust is very cold ($\lesssim$30 K) and hence has escaped detection in these studies. Attempts have been made to detect very cold dust using sub-mm measurements of the Cas A and Kepler SNRs. Observations using SCUBA led (62) to claim that at least 2 $M_{\odot}$ of dust formed in the supernova, with their model including a dust component at 18 K. However, Krause *et al.* (124) used the same data together with

observations from Spitzer to show that most of the emission originates from a line-of-sight molecular cloud, and not from dust formed in Cas A. In particular, they point out that iron or graphite needles could reduce the dust mass required to explain the sub-mm observations (61). Instead the same analysis applied to the Kepler remnant, considering also a model fit component at 17 K, gives a dust mass of $\sim$1 $M_\odot$ (155). We conclude that, so far, the direct sub-mm evidence in favor of large masses of ejecta dust is relatively weak. On the other hand, several studies have highlighted the destruction of dust grains by the reverse shock as the supernova ejecta crashes into the ambient medium and makes the transition into the remnant phase (e.g. 165). This implies that the dust masses that condense in SN ejecta at early epochs (few years) should be several times higher than during the remnant phase.

Though these data support the scenario of CC-SNe as important dust producers, the amounts of dust (0.1–1.0 $M_\odot$, 60, 150) required to explain the dust at high redshift ($z \gtrsim 6$) is a orders of magnitude larger (2 - 3) than those measured in individual local core-collapse SNe. It is also unknown if there is a link between the metallicity at the site of SN (and then of the progenitor itself) and the amount of new produced dust during the SN event.

1.5.3 Role of the interaction ejecta-CSM

In the last years a few SNe, in addition to the above mentioned, have shown clear evidence of ejecta-CSM interaction, e.g. type Ia SNe 2002ic (93), 2003du (88), 2002bo (145) and type IIP SNe 1999em and 2004dj (49), reviving the interest for the studies of the interacting SNe. Upper limits for the mass loss rates of the progenitors (standard, excluding peculiar stars) have been estimate to be the order of $\dot{M} \approx 10^{-4}$ $M_\odot$ year^{-1}, value consistent for the case of SN 1999em ($\dot{M} \approx 10^{-6}$ $M_\odot$ year^{-1} 190) , while the observed data of SN 2001ic are consistent with an extremely high mass loss rate ($\dot{M} \approx 10^{-2.4}$ $M_\odot$ year^{-1}) of the progenitor. Other parameters that can lead to different observables are the density profile, the distance of the CSM (depending by the structure of the progenitor star), the shock acceleration of the gas during the explosion and the kind of progenitor.

The impact between the fast ejecta and the low CSM causes the conversion of the ejecta kinetic energy to radiation and the creation of a forward (moving into the CSM) and a reverse (moving into the ejecta) shock spatially generated in the contact discontinuity between the two different medium. Sometimes the pressure and the temperatures behind the shock are high enough to produce X-ray emission and synchrotron radiation generated by electrons accelerate at relativistic energies by the shock front. The X-ray emission is generally produced behind the reverse shock, where a cool dense shell ($\sim 10^7$ K) formed, otherwise behind the forward shock a hotter shell ($\sim 10^9$ K) has been generated (44).

As suggested by Chevalier and Fransson (44), the interaction produced also ionizing photons that ionize the cool SN gas. The dimension of the ionized region is due to the production rate of ionizing photons, which can be related to Hα luminosity. Most of these photons are produced at the reverse shock front in the SN ejecta environment. If the SN density profile is flat, the reverse shock wave has a high velocity and the emission is at X-ray wavelength. Instead if the profile is steep, as for RSG model, the velocity of the reverse shock is low and the shock emission is at far-UV wavelengths. Similar structure has been found in quasar ionization structure.

Moreover, the shocked SN gas (ejecta) is expected to undergo an early radiative phase, the time of this phase increases if the SN density profile is steeper. The dense shell of gas, created by the cooling, is important for absorbing X-rays produced by the cooling at the reverse shock.

In addition, the CSM interaction models suggest that the line widths are expected to decrease with time.

CC-SNe show spectra with features deriving from ejecta-CSM interaction. Most of them probably have lost considerable amount of material via strong stellar winds or through the tidal interaction with companion stars in binary systems. Recent studies (49) have been shown as also the type IIP can display such evidence.

Generally, the SNe showing narrow lines produced by the interaction with a CSM are the Hypernovae as SNe 1997cy and 1999E (237), the long duration SNe IIn (e.g. 1988Z, 1995G and 1995N) and SNe IIn with short duration interaction, having either linear (e.g. SN 1998S) or plateau (e.g. SN 1979C) light curves.

If the ejecta mass is comparable with that of CSM, the CSM can produce a significant deceleration of the ejecta (maybe visible also in the absorption profile) and a conversion of the kinetic energy into radiative energy. Obviously, more luminous SNe requires progenitors with higher mass loss rates or slower wind speeds.

How an early interaction can change the observables (and some physical parameters) of a type II SN is still unclear and this issue needs more dedicated studies.

1.6 Motivation of the thesis and outline

The study of CC-SNe has a fundamental interest in astrophysics to understanding the physical mechanism controlling the final evolutionary stages of massive stars, the nucleosynthesis processes, the nature of the remnants, etc. The discovery of peculiar objects, inside the same category (e.g. type II), points out the necessity to better understand how the environment of the explosion can change or not the observables. Moreover, there are some kinds of objects among the classes that have a low rate of detection and consequently there is a lack of informations about them.

The studies of Hamuy (94) and Pastorello (175) suggest a continuum in the properties of CC-SNe revealing several relations between physical parameters, as most sit in the region of $M_{ej} \approx 12 - 17$ $M_{\odot}$, regardless of the mass of radioactive ^{56}Ni, and only for relatively large ^{56}Ni masses ($\geq 10^{-2}$ $M_{\odot}$) M_{ej} increases with M_{Ni}. This suggests a possible bi-modal distribution of M_{ej} versus other observables. However, the sample of bright type II was poor (SNe 1992H, 1992am, 1995ad and 1996W).

In this thesis, first of all, we increase the data set of bright type II SNe available in literature, mainly focusing on plateau events. Even if in our sample there is also a SN initially labelled as type IIn and revealed as a normal type II during the photospheric period. The other goal of the thesis is verify if more of these bright objects have clues of CSM close to the SN, leading to imagine a scenario with interaction, weaker than that shown by type IIn, occurs at early phase. The possibility that the mass loss during the final stage of evolution could be

more common than expected, can give us new informations about the evolution of these objects and their counterparts as Supernovae. At the same time a better knowledge of this events can lead to propose a new scheme (taxonomy) about SNe, based more on the physical condition than the observable data.

The thesis focuses on the study of the properties of a selected sample of bright CC-SNe, reporting both spectroscopic and photometric observations. New data, together with other material from the Padova-Supernova Archive are presented and discussed. The new observations have been obtained using many telescopes in different sites (Italy, Chile, Spain, Russia, Finland); some of these has been taken by the author of the thesis that has learned how to manage observations of transient objects at the Copernico Telescope (1.82m at Asiago) and increased his experience acquiring data as visitor astronomer at the NOT telescope (2.5m at La Palma, Canary island) and (twice) at the NTT (3.6m at La Silla, Chile). An extensive work of data reduction has been carried out; the knowledge about the not trivial data reduction of transient objects has been obtained thanks to the teaching received by astronomers and astrophysicists of european institutes as the INAF-OACt (optical photometry and spectroscopy), the INAF-OAPd (near infrared photometry and spectroscopy, ultraviolet photometry) and the Queen's University of Belfast (optical photometry and spectroscopy, near infrared photometry) were the author has been hosted as guest researcher/astronomer. An important work of data analysis has been performed on the reduced data thanks to the education received at the INAF-OACt (experimental/observational learning) and at the University of Oklahoma (theoretical learning). Thanks to these knowledge the author has contributed as co-author on three different paper about the SNe 2009jf (Ib), 2009dc (Ia) and 1999dn (Ib) and reduced data for the SNe 2010al (IIn pec) and 2010jp (IIn) (Pastorello et al. in preparation).

Although SNe IIP appear to be an heterogenous class of SNe in the individual properties, a number of common peculiarities have been found in our database of 8 bright type II SNe.

The plan of the thesis is the following:

Chapter 1 introduces the event of SN and its role in the modern astrophysics, showing also the diversities among the SNe type and subtype, the

physics of the explosion and illustrating some key problematics relate to the study of the H-rich CC events.

Chapter 2 describes all the instruments used to obtain the (new) data presented in the thesis. A discussion about data reduction techniques is also reported.

Chapter 3 presents the data, the analysis and the results of a new group of bright type II-IIP SNe. These SNe show peculiar properties: luminous light curves at photospheric period for all the objects, some of them have short plateau (∼30-50d), other luminous plateau coupled with low/normal luminosity tail, HV features of Balmer series during the photospheric period, Hα flat top profile in the early spectra, presence of CNO elements in photospheric spectra and dust formation in a cool dense shell (CDS) in the nebular phase. To two SNe of the sample have been applied parametrized codes for synthetic spectra; the LTE code `SYNOW` has been applied to identify many ions in the case of SN 2009bw, while a more extensive analysis through the use of the NLTE code `PHOENIX` is presented for the photospheric spectra of SN 2007od. An entire Section is devoted to the late interaction with a CSM observed in the case of SN 2007od and the consequentially dust formation in the CDS formed after the interaction. Discussions on all the SNe are reported, with great interest on the two well followed objects of the sample (SN 2007od Inserra *et al.* (116) and SN 2009bw Inserra *et al.* (114)) for which are also presented the parameters about the explosions and the possible progenitors. The work relate to the use of the parameterized codes has been performed in collaboration with the group of E. Baron and D. Branch at the University of Oklahoma. Instead the work relate to the determination of the physical parameters of the SNe has been performed in collaboration with M.L. Pumo and L. Zampieri at INAF-OAPd.

Chapter 4 shows the photometry and the spectra of three objects founded in the Padova SNe archive and chosen thanks to the luminous peak/plateau and the similarities in the spectra with those presented in Chapter 3. Two of these object are already shown in Pastorello (175), here we present only

the data and the new interpretation of some evidences, useful to pursuit the final goals of this elaborate.

Chapter 5 is devoted to the geometrical and physical understanding of the early interaction between CSM and ejecta of the SNe presented in the previous chapters. The analysis performed shows as the CSM ejected by the progenitor could be aspherical and the spectral and photometric evidences depend by the mass/density (or mass loss rate) of CSM and by the observer angle.

Chapter 6 presents a short summary of the main results of the thesis, the final comments on the status of the research about these kind of SNe and possibles future studies to improve our knowledge.

Appendix A reports the magnitudes of the local sequences of stars used to calibrate the SNe.

Appendix B reports the spectroscopic journal of all SNe presented in the thesis.

2

Observations and data processing

Along with material from literature, in this thesis new data for five SNe II are presented for the first time. The new material has been collected during a large number of observing nights at several telescopes around the globe performed by the members of the Asiago-Padova SNe Group (among which the thesis author), in the framework of a larger collaboration with other SN groups from Belfast (Queen's University, UK), Garching (ESO and Max-Planck-Institut fuï Astrophysik, Germany), Stockholm (Stockholm University, Sweden), Turku (University of Turku, Finland), Bellaterra (IEEC-CSIC, Spain) and Lisbon (CENTRA, Portugal) between years 2007 and 2011, and using many different telescopes and instrumental configurations. Particular attention and an enormous amount of time have been devoted during the preparation of this thesis to reduce the huge amount of data. The set here analyzed includes 98 spectra, of which 30 already present in archive, and 237 photometric epochs (with an average of 4 filters for epoch), of which 41 in archive, of SNe never published before (except the data presented in Inserra *et al.* (116) and Inserra *et al.* (114)). Being targets of the Padova-Asiago Supernova Follow-up, their finding charts, coordinates and updated observational status (related to an observational log visible only to registered people) are reported at the webpage `http://graspa.oapd.inaf.it/` that the author has designed and managed together of the entire website with E. Cappellaro (OAPd) and A. Harutyunyan (TNG).

In this chapter we introduce the instrumental configurations used to observe the SNe discussed in this thesis (Sect. 2.1), and describe the adopted techniques

of photometric (Sect. 2.2.1) and spectroscopic (Sect. 2.2.2) data reduction.

2.1 Instrumental configuration

In the following we will shortly describe the most important technical characteristics of the different instrumental configurations used for the observations of the SNe presented in this thesis:

Asiago-Ekar 1.82m Copernico Telescope + AFOSC - Copernico Telescope is located on the top of Mount Ekar, near Asiago (Italy). The instrument AFOSC (Asiago Faint Object Spectrograph and Camera) was equipped with a Tektronix TK1024 Thinned Back Illuminated CCD, 1024 x 1024, with pixel size 24 μm, pixel scale 0.473 arc-sec/pixel, and the field of view is 8'.14 x 8'.14. The estimated Conversion Factor (CF) and the Read Out Noise (RON) of the detector are 1.86 e^-/ADU and 9.6 e^-. For photometry the Johnson U, B, V, R and Gunn i filter were adopted. For spectroscopy, we used the grism #2 (wavelength region 5000-11000 Å) and the grism #4 (wavelength region 3360-7440 Å).

Asiago-Pennar 1.22m Galilei Telescope + B&C - Galileo Telescope is located on the top of Mount Pennar, near Asiago (Italy). The Boller and Chivens (B&C) spectrograph has been equipped with the Dioptric Blue Galileo Camera. There are five gratings available for the B&C spectrograph. The 300 r grooves mm^{-1} grating was usually used to get spectra with a dispersion of 4.06 Å/pixel. The scale of the CCD along the slit is 1.11 arc-sec/pixel.

TNG +DOLORES - The Device Optimized for the LOw RESolution (DOLORES) is installed at the Nasmyth B focus of the 3.5m TNG (Telescopio Nazionale Galileo) in La Palma (Spain). The detector is a Loral thinned and back illuminated 2048x2048 CCD. The scale is 0.275 arc-sec/pixel (μm 15), which yields a field of view of about 9'.4 x 9'.4. The CF is 0.97 e^-/ADU and the RON 2 e^-. We used the Johnson filters U, B, V, and Cousins R, I; for the spectroscopy we used LR-B (wavelength range 3000-8800 Å) and LR-R (wavelength range 4470-10070 Å).

TNG + NICS - The Near Infrared Camera Spectrometer (NICS) is the TNG infrared (0.9-2.5 μm) multimode instrument which is based on a HgCdTe Hawaii 1024 x 1024 pixel CCD. The latter has a pixel scale of 0.25 arc-sec/pixel. The field of view is 4'.2 x 4'.2. The filters used for the observations are the J, H and K'. Instead for the spectroscopy we used the IJ grism (range 9000–14500 Å) and the HK grims (range 14000–25000 Å).

Calar Alto 2.2m + CAFOS - The 2.2m Calar Alto telescope, located in Sierra de Los Filabres, Andalucia (Spain) is equipped with CAFOS (Calar Alto Faint Object Spectrograph), a 2048x2048 SITe #1d CCD (pixel size 24 μm, image scale 0.53 arc-sec/pixel, total field 18' x 18', CF = 2.3 e^-/ADU and RON = 5.060 e^-). For photometry the Johnson U, B, V, R, I filters were used; for spectroscopy the grism B-200 (range 3200-7000 Å), the grism R-200 (range 6300-11000 Å) and the grism G-200 (range 4000 - 8500 Å) were adopted.

Liverpool Telescope + RATCAM - The 2m robotic Liverpool Telescope (LT) at La Palma (Spain) with the optical RATCAM CCD Camera. The CCD is a 2048x2048 pixel EEV CCD42-40, with pixel size 13.5 μm, pixel scale 0.135 arc-sec/pixel and field of view 4'.6 x 4'.6. The CF is 2.72 e^-/ADU and the RON is 5 e^-. The photometry was obtained using the Sloan u, r, i and Bessell B, V filters.

NOT + ALFOSC -The detector that was used for the ALFOSC (Andalucia Faint Object Spectrograph and Camera) instrument mounted at the 2.5m Nordic Optical Telescope (NOT) in La Palma (Spain) is a EEV42-40 2Kx2K Manufacturer (CCD42–40) back illuminated, a 2048x2048 chip of pixel size 13.5 μm and 0.19 arc-sec/pixel. The CF has been estimated to be 0.726 e^-/ADU and the RON = 5.3 e^-. For the photometry we used Bessel U, B, V, R filters and i interference filter and for the spectroscopy the grism #4 (low resolution visual grism, range 3200-9100 Å) and the grism #5 (low resolution red grism, range 5000-10250 Å).

REM + ROSS - The Rapid Eye Movement (REM) 0.6m Telescope is an automatic telescope located at La SIlla (Chile). The REM Optical Slitless

SPectrograph (ROSS) camera mounts an Apogee Alta CCD with pixel scale 0.575 arc-sec/pixel and a field of view 10' x 10'. We used the Johnson V filter and the Cousins R, I filters.

REM + REMIR - REMIR camera mounts a Rockwell HAWAII HgCdTe with pixel scale 1.2 arc-sec/pixel and a field of view 10' x 10'. We used the J, H, K filters.

Swift + UVOT - The 0.3m UV/Optical Telescope is mounted on the NASA Space Telescope Swift. It has an intensified CCD with an array of 2048x2048 pixels, a virtual pixel scale of 0.506 arc-sec/pixel and a filed of view of 17' x 17'. The CF is 1.0 count/ADU. We used the UVOT filters uvw2, uvm2, uvw1, u, b, v.

ESO NTT + EFOSC2 - EFOSC2, or the ESO Faint Object Spectrograph and Camera, is the new ESO instrument mounted on the 3.6m New Generation Telescope (NTT) at La Silla (Chile). Thanks its multi mode capabilities EFOSC2 is especially suitable for low resolution photometry and spectroscopy. The CCD #40, which is particularly sensitive to UV photons, is a Loral/Lesser, thinned, AR coated, UV flooded, MPP chip controlled by ESO-FIERA. It is composed by 2048 x 2048 pixel; the pixel size and pixel scale are 15μm and 0".157 arc-sec/pixel, respectively. The field of view is 5'.2 x 5'.2. The CF and RON in slow mode are 1.3 e^-/ADU and 10.2 e^-. For the photometry we used Bessel U, B, V, R filters and i Gunn filter. Instead for the spectroscopy we used the grism #11 (range 3380–7520 Å), the grism #13 (range 3685–9315 Å) and the grism #16 (range 6015–10320 Å).

ESO NTT + SOFI - Son OF Isaac (SOFI) provides both infrared spectroscopy and imaging. The CCD is an Hawaii HgCdTe 1024x1024, with pixel size 18.5 μm and 0.288 arc-sec/pixel. The CF and RON are 5.4e^-/ADU and 2.1 ADU respectively. We used the filters J, H, Ks for the imaging and the Grism Blue (range 9500–16400 Å) and Grism Red (range 15300–25200 Å) for spectroscopy.

ESO NTT + EMMI - EMMI (ESO Multi-Mode Instrument) splits the light into two "arms" with high efficiency in the wavelength ranges 3000–5000 Å (blue arm) and 4000-10000 Å (red arm), and with two separate detectors. Each arm was available both for spectroscopy and imaging. The blue arm mounted the ESO CCD 31, a Tektronix TK1034 chip, 1024x1024 pixels, with pixel size of 24 μm, pixel scale of 0.37 arc-sec/pixel, field size of 6'.2 x 6'.2, CF 2.88 e^-/ADU, RON 6.5 e^-. The red arm mounted the ZEUS and MICHELE chips, both are FIERA MIT/LL CCD chips, 2048x4096 pixels, with pixel size 15μm, pixel scale of 0.166 arc-sec/pixel, field size of 9'.9 x 9'.1. We used only the grism 2 (range 3800–9200 Å) for spectroscopy.

Hale Telescope - Hale telescope is the 5.1m telescope located at Palomar Observatory (San Diego, CA, USA). We used the Double Spectrograph mounting as red detector the CCD 21, with a pixel size of 24μm, a CF of 2.0 e^-/ADU and RON of 7.5 e^-. We used the red grism (range 4700–10000 Å).

SAO RAS BTA + SCORPIO - The Big Telescope Alt-azimuth (BTA) 6m Telescope of the Special Astrophysics Observatory is located at Mt. Pastukhov, Russia. The Spectral Camera with Optical Reducer for Photometrical and Interferometrical Observations (SCORPIO) has CCD EEV 42-40 with size 2048x2048 pixels and pixel scale 0.18 arc-sec/pixel. The field of view is 6'.1 x 6'.1 and the RON is 3e^-. We used the grism VPHG400 (range 3500–9500 Å).

SAO-RAS Zeiss - The Zeiss 1m telescope has a CCD photometer with a pixel scale 0.48 arc-sec/pixel and a field of view of 2'.38 x 3'.53. For this instrument we used the Johnson U, B, V filters and the Cousins R, I filters.

Taurus Hill Observatory - The Taurus Hill Observatory is owned by an amateur astronomical association and it is located on the top of Hill Härkämäki, near Kangaslampi, Finland. The telescope is the Meade 12" LX200 OTA Schmidt-Cassegrain telescope (focal length 3048 mm), which has as detector a CCD KAF-1603ME mounted on the camera SBIG ST-8XME with

567 x 532 pixels. The pixel-scale is 0.9 arc-sec/pix. Images were acquired without filters and with Bessel B, V and R filters.

WHT + ISIS - WHT is the William Herschel 4.2m Telescope (WHT) at La Palma (Spain) equipped with ISIS (Intermediate dispersion Spectrograph and Imaging System), on which the CCD EEV12 (2148x4200 pixels, pixel size 13.5 μm, scale 0.19 arc-sec/pixel) is mounted. The blue arm uses the R158B grating (with dispersion 1.62 Å/pixel) and R300B grating (with dispersion 0.86 A/pixel). At the red arm the grating R158R (with dispersion 1.81Å/pixel) is adopted. ISIS has a CF of 2.3 e^-/ADU and RON 6 e^-.

S50 and M70 - During the follow up of SN 2009bw a few imaging points have been obtained by D. Tzvetkov. The S50 is a 0.6m Newton Telescope located at Tatranska Lomnica, Slovakia; while the M70 is a 0.7m Cassegrain Telescope located at Moscow, Russia. These telescopes used the Johnson U, B, V filters and Cousins R, I filters.

2.2 Data reduction

The data obtained with the instruments described in Sect. 2.1 have been processed using IRAF programs. The NIR imaging and spectroscopic data have been reduced with IRAF tasks, while for the optical photometry a number of tasks developed by the Padova-Asiago SNe Group have been used. Furthermore the optical data (imaging+spectroscopy) acquired since January 2009 have been reduced a second time with a python pipeline created by S. Valenti to test and refine it. Only the Swift data have been reduced using the HEASARC (NASA's High Energy Astrophysics Science Archive Research Center) software.

Before the measurement, it is important to remove any peculiar instrumental signature due to the detector and the instrument. This step is called pre-reduction and is developed, through the IRAF tasks (*ccdred* package) as follows.
Bias subtraction. The bias level is an electronic offset added to the signal from the CCD to make sure that the Analogue-to-Digital Converter (ADC) always receives a positive value. It is common practice to create a master bias image from the median of several (>10) bias images in order to reduce the RON and to

get rid of cosmic rays.
Overscan correction. In principle the bias level is constant, but it can slightly change during the night because of external factors (like temperature variations). To monitor this effect, the bias level of each image is measured in the "overscan" region (a stripe of a few columns/rows at the edge of the CCDs, which is not exposed to the light) and removed from the whole frame, before the bias images combination.
Trimming. After use, the overscan region can be cut off trimming the images.
Flat fielding. Due to construction faults, to variation of transmissivity of the CCD coating, and to dust contamination, the CCD response to the incident light is not uniform and can show variation on different scales from that of the whole frame to pixel-to-pixel. So, it is necessary to divide the data by a sensitivity map (flat-field) created from calibration exposures. Usually, a flat-field is obtained by imaging a uniformly illuminated screen inside the telescope dome (dome-flats) or, better, the sky at twilight/dawn (sky-flat). In order to have a better statistic, to reduce the poisson statistics and to get rid of cosmic rays, a number of flats are averaged to obtain a master-flat. For the spectroscopic master-flats another process has to be added, i.e. their normalization along the dispersion axis.
For the IR magnitudes, additional reduction steps are required. These include the subtraction of sky images obtained by combining several dithered exposures. Then NIR images of the SN field for each band were obtained by combining several, sky-subtracted, dithered exposures. Particular care has to be devoted to the sky subtraction from all science frames due to the rapid variation in the IR and to image co-addition due to very short integration time of each exposure. In the case of the UVOT filter the pre-reduction is provided by the HEASARC tool *imsum* that aligns and sums the images for each filter.

2.2.1 Photometry

Detailed information on the photometry of each SN will be reported in the relative Sections. Usually U, B, V R, I photometry was obtained, even if for the recents SNe also NIR observations (J, H, K filters) have been provided. Since 2005 also

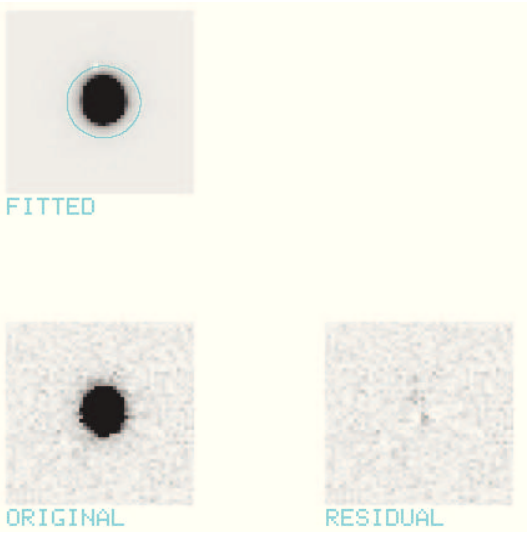

Figure 2.1: PSF-fitting technique applied to SN 2007od: the original image of the SN is shown (bottom-left panel); the SN contribution (fitted star), obtained after that the background at the SN position has been estimated fitting the region with a bidimensional polynomial of fixed degree (upper-left panel); and residual background (bottom-right).

ultraviolet photometry has been provided, thanks to the Swift satellite in the filters uvw2, uvm2, uvw1 mounted on UVOT.

The observations consist of short exposures at early times and dithered multiple exposures at late epochs. In the latter case, the images in each filter were first geometrically aligned (registered) and then combined to produce a single deep image. After the pre-reduction described in Sect. 2.2 the magnitude measurements have been performed. To this aim, two different techniques have been used according to the background conditions:

1. **PSF-Fitting Technique.** If the SN exploded onto a relatively flat background, or when its luminosity largely dominates that of the surrounding background, the PSF-fitting technique can be used with excellent results. This method consists in performing the fit of stellar profile on a number of preselected, isolated field stars and subtracting the background galaxy contamination at the SN position, reconstructed with a polynomial surface, using as input the background just outside the SN PSF area. For this

purpose the Padova team developed SNOoPY (SuperNOvaPhotometrY), a package originally designed by F. Patat and later implemented in IRAF by E. Cappellaro. It is based on IRAF *daophot* package which allows to fit the SN profile with a PSF obtained from a set of local, unsaturated stars. An example of the application of this method is shown in Fig. 2.1 in the case of SN 2007od. The extraction of SN appears to be satisfactory, even if, in general, in such critical cases the errors on the magnitude estimated with the PSF-fitting technique may be significantly large. Uncertainties in the instrumental photometry are estimated by placing artificial stars with the same magnitude and profile as the SN, at positions close (within a few arcsec) to that of the SN, and then computing the deviations of the artificial star magnitudes. The final errors are computed as the square root of the quadratic sum of instrumental and calibration errors. This technique has been applied to the entire data set of SN 2007od and the photospheric data (until $\sim$ 80-90d) of SN 2009bw, SN 2009dd, SN 2007pk and SN 2010aj.

2. **Template Subtraction Technique.** This procedure is adopted when high quality images of the host galaxy, obtained before or long time after the SN explosion, when the SN luminosity fades from detection, are available. This technique has been proved useful when the SN explodes in a complex background area e.g. close to the galactic nucleus, H II region, spiral arms, and in general when the SN is faint. The procedure used is based on the ISIS template subtraction program (2) and runs in IRAF environment. The initial step is the geometrical and photometrical registration of both images in order to correct for different instrumental pixel scales (image stretching), spatial orientation and position (frame rotation and shifting). Subsequently, degradation of the better-seeing image to the poorer one and scaling of the two frames to the same intensity. In the end, the reference template image is subtracted from the scientific frame of the SN image. In the ideal case, the resulting image is flat, except for variable objects or accidental bodies in the field. In the real case number of blemishes show up (saturated stars, cosmic rays, hot pixels and bad columns). After that, the instrumental magnitude of the SN can be measured using the aperture photometry (e.g.

IRAF task *imexamine*) or the PSF-fitting technique through the SNOoPY package. This technique has been applied to the last photospheric and nebular points of SN 2009bw, SN 2009dd, SN 2007pk and SN 2010aj.

Since SNe are variable objects each observation is unique and non re-producible. For this reason an effort is done to use all available data, even those obtained under non ideal conditions. In order to calibrate the photometry obtained in non-photometric nights we make use of a set of local standards in each SN field. These stars are chosen among the isolated stars in the field in order to avoid the contamination by nearby objects. Also, they should be non-variable star or galaxies. Stars too bright or too faint could be useful in the photospheric and nebular periods respectively. In turn, the local stars are a posteriori calibrated by mean of observations of standard stars during a subset of photometric nights. Photometric zero-points and colour terms are computed through observations of Landolt standard (127) on the photometric nights. Finally a check of the photometric quality of each of the observing nights has been performed on the local sequence. If the mean difference between the magnitudes of the sequence stars in a non-photometric night and those of the photometric ones is higher than 0.1–0.2 mag (the difference depends of the luminosity of the sequence stars), a correction is applied to the zero points used for that nights. The new values of the constant terms allow to estimate the final calibrated magnitudes of the object.

In the case of the IR magnitudes particular attention has been devoted to the sky subtraction and to the image coaddition. This because of in the IR the varying sky contribution must be removed from all science frame, and it is necessary to combine a number of dithered images in order to improve the signal to noise ratio. IR magnitudes have been obtained with the PSF-fitting technique as for the optical photometry. Also for the calibration we have made use of the same local sequence stars used in optical and calibrated by the 2MASS survey. However, because of the number of IR standard fields observed each night was small, we adopted average color terms provided by the telescope teams. For the K band the different filters had different transmission curve from that of the standard K filter. In the case of the NICS K' filter we do not apply any kind of transformation because the filter resembles the standard K filter and that used

also by REM. Instead for Ks band filter used in SofI, the transmission curve is slightly different from that of a standard K filter. Following Lidman *et al.* (132) we have transformed the Ks magnitudes to K by mean of the relation K - Ks = -0.005 x (J - K).

For the UVOT magnitudes the pre-coadded images have been reduced following the guidelines in Poole *et al.* (189) through the HEASARC task *uvotsource* setting the SWIT calibration data (to use zero point and colour term), a curve of growth applied to aperture correction, a sigma equals to 3 for the rejection, a circle centered to SN coordinates with an aperture greater than 2.3 times the sigma and an annulus ad hoc chosen to have the better background. Then aperture magnitudes so measured, have been transformed from the Swift system to Johnson magnitudes through the colour transformations of Li *et al.* (130). However, by comparing the space and the ground-based SN magnitudes at corresponding significant epochs we found differences of an average ΔU $\sim$0.2, ΔB $\sim$0.05 and ΔV $\sim$0.09 for the various SNe treated in this thesis. These corrections have been applied to all UVOT magnitudes and the resulting magnitude values are reported in the Tabs. relative to the photometry of the SNe. We noted also that the largest differences are for the U band in which the specific detector responses and the variable transmission at atmospheric cutoff can generate quite different passbands.

When the SN luminosity fades, deep imaging even at large telescopes may not be sufficient to detect the SN. In the cases when the SN is invisible in the image, it is worthy to establish at least the maximum threshold of the SN luminosity, i.e. un upper limit on the magnitude. The limits calculation was accomplished with the creation of artificial stars using the PSF of the sequence stars present in the field and manually added in the image near the SN position. This has been done for all the SNe and in all the bands available, when needed.

2.2.2 Spectroscopy

In addition to the photometry we present also the spectral evolution of the SNe studied in this thesis. The optical spectra, as the IR, have been reduced using standard IRAF tasks from the *ctioslit* and *ccdred* packages. After the pre-

reduction steps described in Sect. 2.2, the reduction includes the following steps. The one-dimensional spectrum of the SN is extracted across the dispersion axis and the adjacent galaxy contribution is subtracted via a polynomial fit (task *apall*).

Then, the observation of lamp spectra (usually He-Ne, He-Ar, Hg-Cd lamps), obtained with the same instrumental configuration, allow the wavelength calibration of the SN spectrum with errors in the wavelength < 2Å, verified thanks to the position of the background sky lines in the spectra.

The subsequent step is the flux calibration. The response curve of the instrumental configuration is obtained observing spectroscopic standard stars from the lists of Oke (168) and Hamuy *et al.* (98, 99). This response curve is obtained by comparing the observed standard star spectrum to the tabulated flux for the star. The flux calibration is typically accurate within 20% due to poor photometric conditions or object non centered in the slit A check with the photometry allows to verify the correct flux calibration of the spectra.

Sometimes broad telluric absorptions contaminate the SN spectra, this can be removed if a spectrum of a standard star obtained with the same resolution and at the same zenith distance is available. The observed standard star spectrum is divided by the same spectrum from which the telluric absorptions have been identified and removed. The resulting spectrum (equal to 1 everywhere, except in coincidence with the telluric bands) is multiplied by the object spectrum. For the atmospheric extinction correction, we used the average extinction curves available for each site.

To perform the analysis, the SN spectra were corrected for the redshift of the host galaxy to identify the spectral lines and to estimate the expansion velocities. Furthermore, the correction for interstellar extinction is necessary to compute the continuum temperature. In order to have a full wavelength coverage in the optical region, we combined the spectra obtained using different grating/grisms. These operation have been performed with standard IRAF tasks.

In the case of IR spectra the procedure is slightly different because the source spectra are usually obtained at two position along the slit. After the pre-reduction steps we need to create difference images of the SN spectra and combined them before the wavelength calibration. The telluric absorption correction is obtained

removing the H lines in the standard (normally a solar analogue taken close before or after the SN observation) and subsequently dividing the SN spectrum by the standard spectrum without the telluric absorption. The last step is the flux calibration, obtained multiply the SN spectrum for a vega spectrum (without H lines) and for a factor related to the exposure time of the objects (SN and standard star) and the apparent magnitude of the standard star. As for the optical spectra, to have full wavelength coverage, we combined the spectra obtained using different grisms.

3

SNe IIP early interacting: The main set

3.1 Introduction

Integral part of the work of this thesis has been the organization of the observational campaign for each object. It includes:

1. early classification with any of the available telescopes in Time of Opportunity (ToO) mode. This allowed the selection of the targets and the activation of the observational campaign.

2. Set up of the campaign through the selection of the more suitable telescopes and the decision of the observing strategy.

3. Daily surveillance of the monitoring carried out in Service Mode and through direct observation at several sites in visitor mode (cfr. Tab. 3.1).

4. Management of the target webpages on the collaboration website.

5. Data reduction.

6. Data analysis.

Our sample of bright SNe, with possible early interaction, includes both objects followed during this thesis (SN 2007od, SN2009bw, SN 2009dd, SN 2007pk

Table 3.1: Direct observations operated by the author during the observational campaign of the SNe of the thesis.

Telescope	Site	Obs run	SN	filter	grism
Copernico	Asiago	09/05/25	SN 2009bw	UBVRI	-
NOT	La Palma	09/08/12-13	SN 2009dd	BVRi	gm4
NOT	La Palma	09/08/13	SN 2009bw	UBVRi	gm4
NTT	La SIlla	11/01/25	SN 2010aj	BVRI	-

Table 3.2: Quantitative information about reduced data by the author.

Object	Photometric points	Bands number*	Spectra	Instruments configuration
SN 2007od	204	11	19	9
SN 2009bw	227	12	20	14
SN 2009dd	113	11	8	6
SN 2007pk	110	8	13	7
SN 2010aj	80	8	8	5
Total	**734**	-	**68**	-

* Optical, NIR, UV and X bands.

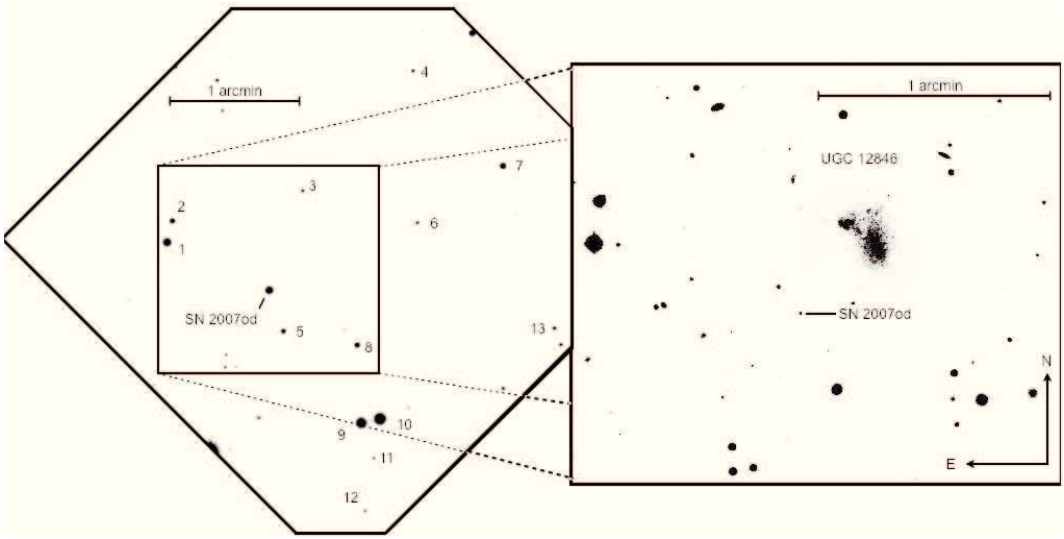

Figure 3.1: (Left) R band image of SN 2007od in UGC 12846 obtained on November, 2007 with the 1.82-m Copernico telescope + AFOSC at Mt. Ekar (Asiago, Italy). The exposure is so short that the low surface brightness parent galaxy is barely visible. The sequence of stars in the field used to calibrate the optical and NIR magnitude of SN 2007od is also labelled. (Right) Blow-up of the region of the parent galaxy in an R-band frame obtained on July 16, 2008 with the 2.2-m telescope of Calar Alto equipped with CAFOS

and SN 2010aj, cfr. Tab. 3.2), which are the subject of this chapter, and objects with observations already available in the Padova-Asiago SN archive (presented in the next Chapter).

3.2 Individual SNe

3.2.1 SN 2007od

SN 2007od was discovered on 2007 November 2.85 UT in the nearby galaxy UGC 12846 (152). Blondin and Calkins (28) classified it as a normal SN IIP about two weeks after explosion, and reported some similarity with the spectrum of type II SN 1999em 10 days after explosion. On November 6, the SN was detected by Swift with UVOT, although not with XRT (3σ upper limit $< 1.4{\times}10^{-13}$ ergs/cm^2/s^{-1}, 113). The main data of SN 2007od are reported in Tab. 3.3.

Table 3.3: Main data of SN 2007od

position (2000.0)		$23^h55^m48^s.68$	$+18^o24^m54^s.8$
parent galaxy		UGC 12846, Sm:	
offset wrt nucleus		38" E	31" S
adopted distance modulus	$\mu = 32.05 \pm 0.15$		
SN heliocentric velocity	1734 ± 3 km s^{-1}		
adopted reddening	E_g(B-V)= 0.038	E_{tot}(B-V)= 0.038	
	peak time (JD 2454000+)	peak observed magnitude	peak absolute magnitude
U	409 ± 2	13.49 ± 0.04	-18.7 ± 0.18
B	409 ± 2	14.46 ± 0.03	-17.8 ± 0.18
V	411 ± 2	14.14 ± 0.02	-18.0 ± 0.23
R	411 ± 2	13.95 ± 0.02	-18.1 ± 0.21
I	411 ± 2	13.82 ± 0.02	-18.2 ± 0.23
uvoir	410 ± 2	$L_{bol} = 6.0 \times 10^{42}$ erg s^{-1}	
rise to R max	~ 5 days		
explosion day	$\sim 404 \pm 5$	$\sim$ 30 Oct. 2007	
		late time decline mag(100d)$^{-1}$	interval days
V		0.94	208–434
R		1.00	208–434
I		1.08	208–434
uvoir		1.053	208–434
UBVRI		1.065	208-434
M(Ni)			0.02 $M_\odot$
M(ejecta)			5-7.5 $M_\odot$
explosion energy			0.5×10^{51} ergs

The coordinates of SN 2007od have been measured on our astrometrically calibrated images at two different epochs: $\alpha = 23^h55^m48^s.68 \pm 0.1^s$ and $\delta = +18^o24'54".8 \pm 0.1"$ (J2000). The SN is located in a peripheral region of UGC 12846, 38" East and 31" South of the core of the galaxy (Fig. 3.1). This position, slightly revised with respect to previous determinations (152), corresponds to a linear distance of $\sim$6 kpc from the nucleus (assuming a distance to UGC 12846 of $\sim$26 Mpc).

The Galactic reddening to UGC 12846 was estimated as E_g(B-V)=0.038 ($A_g(B)$ = 0.155, Schlegel, Finkbeiner, and Davis (205)). In our best resolution optical spectra (cfr. Sect. 3.4.1), the absorption features due to interstellar NaID ($\lambda\lambda$5890,5896) lines of the Galaxy are present with average EW$_g$(NaID)$\sim$ 0.42

Å. According to Turatto, Benetti, and Cappellaro (235), this corresponds to a galactic reddening E_g(B-V)$\sim$0.07 mag (which can be transformed through the standard reddening law of Cardelli, Clayton, and Mathis (38) to A_g(B)$\sim$0.28). Interstellar NaID lines at the redshift of UGC 12846 are not detected even in our best signal-to-noise NTT spectrum of November 27 (EW$_i$(NaID)$<$ 0.10 Å) suggesting that the extinction in the host galaxy is negligible. This is not surprising, considering the position of the SN well outside the main body of the galaxy, and the absence of foreground/background structure at its location even in our late, deep images. Throughout this thesis, therefore, for SN 2007od we will assume a total reddening of E_g(B-V)=0.038 mag.

NED provides a heliocentric radial velocity of v_{hel}(UGC12846)= 1734± 3 km s^{-1}. Correcting for the Virgo infall (V_{Virgo}=1873 ± 17km s^{-1}, 157) and adopting H_0=73 km s^{-1}Mpc^{-1}, we obtain a distance modulus μ=32.05±0.15 which will be used throughout this thesis. This is in agreement with the distance modulus μ=31.91 (H_0=75 km s^{-1}Mpc^{-1}) provided by Tully (233). NED provides also the recession velocities corrected for the Virgo Cluster, the Great Attractor, and the Shapley Supercluster velocity fields (Virgo+GA and Virgo+GA+Shapley). Both are marginally lower and their use would produce distance moduli smaller (and absolute magnitudes fainter) by about 0.1 mag.

Assuming the above distance and extinction values, we find $M_U^{max} = -18.7 \pm 0.18$, $M_B^{max} = -17.8 \pm 0.18$, $M_V^{max} = -18.0 \pm 0.23$, $M_R^{max} = -18.1 \pm 0.21$ and $M_I^{max} = -18.2 \pm 0.23$, where the reported errors include the uncertainties of our photometry, the adopted distance modulus, and the interstellar reddening.

In Fig. 3.1 the sequence stars used for the calibration of the photometry are shown, while the magnitudes are listed in Tab. A.1 in Appendix A. Our SNe measurements are reported in Tab. 3.4 along with early magnitudes from (152). The treatment of the Swift magnitudes has been not simple. Aperture magnitudes were transformed from the Swift system to Johnson magnitudes through the colour transformations of Li *et al.* (130). By comparing the space and the ground-based SN magnitudes at corresponding epochs we found an average difference (ground–space) $\Delta U \sim 0.19 \pm 0.03$, $\Delta B \sim 0.04 \pm 0.03$, $\Delta V \sim 0.09 \pm 0.03$. These corrections have been applied to all UVOT magnitudes and the resulting magnitude values are reported in Tab. 3.5.

Table 3.4: Ground-based UBVRI magnitudes of SN 2007od and assigned errors (in brackets).

Date	JD	U	B	V	R	I	Inst.
dd/mm/yy	(+2400000)						
02/11/07	54407.35				14.4 (-)		7
03/11/07	54408.30		14.5 (-)		13.9 (-)		7
06/11/07	54411.57			14.14 (.03)	13.95 (.02)	13.82 (.02)	2
08/11/07	54413.21		14.46 (.03)	14.26 (.03)	13.99 (.02)	13.87 (.03)	1
09/11/07	54413.62			14.35 (.03)	14.10 (.03)	13.89 (.03)	2
12/11/07	54416.64			14.39 (.03)	14.15 (.03)	13.85 (.03)	2
12/11/07	54417.42		14.66 (.04)	14.33 (.03)	14.08 (.03)	14.01 (.02)	1
16/11/07	54421.43	14.35 (.03)	14.90 (.03)	14.49 (.03)	14.07 (.03)	13.91 (.03)	3
16/11/07	54421.54			14.42 (.03)	14.11 (.03)	13.61 (.02)	2
21/11/07	54425.53			14.47 (.05)	14.13 (.04)	13.89 (.03)	2
24/11/07	54428.58			14.54 (.05)	14.14 (.05)	13.93 (.06)	2
27/11/07	54432.54			14.56 (.03)	14.19 (.03)	13.97 (.02)	2
01/12/07	54435.56			14.53 (.03)	14.19 (.03)	13.96 (.02)	2
05/12/07	54439.34		15.50 (.03)	14.71 (.03)	14.20 (.03)	13.98 (.02)	1
06/12/07	54441.35	15.87 (.04)	15.57 (.03)	14.78 (.03)			4
07/12/07	54441.55			14.71 (.03)	14.25 (.03)	13.97 (.03)	2
11/12/07	54445.55			14.76 (.03)	14.29 (.03)	14.11 (.03)	2
15/12/07	54450.34	16.31 (.04)	15.78 (.03)	14.80 (.03)			4
15/12/07	54450.45	16.20 (.04)	15.81 (.03)	14.76 (.03)	14.37 (.02)	14.23 (.02)	3
21/12/07	54455.55			14.87 (.09)	14.45 (.02)	14.44 (.03)	2
25/12/07	54459.53			14.98 (.13)	14.52 (.03)	14.22 (.03)	2
25/12/07	54460.33	16.83 (.04)	16.02 (.03)	15.01 (.03)			4
28/12/07	54462.20		16.23 (.03)	15.10 (.03)	14.57 (.02)	14.37 (.02)	1
29/12/07	54463.53			15.02 (.06)	14.45 (.02)	14.23 (.02)	2
13/01/08	54479.36	17.51 (.04)	16.62 (.03)	15.35 (.03)	14.69 (.02)	14.59 (.02)	6
28/01/08	54494.26		17.18 (.03)	15.72 (.03)	14.87 (.02)	15.01 (.02)	1
17/02/08	54514.25			16.93 (.03)	16.20 (.03)	15.98 (.03)	1
05/07/08	54653.62		22.39 (.20)	21.71 (.16)	20.75 (.06)	20.88 (.26)	5
16/07/08	54664.62			21.99 (.10)	21.06 (.06)		5
04/09/08	54714.59			22.33 (.06)	21.56 (.03)	21.31 (.03)	3
17/09/08	54727.42			> 22.0	> 21.2	> 21.2	5

1 = Copernico, 2 = REM, 3 = TNG, 4 = LT, 5 = CAHA, 6 = NOT, 7 = CBET 1116. Unfiltered photometry from CBET 1116 is considered most similar to the R-band Johnson-Bessell system.

Table 3.5: Swift magnitudes of SN 2007od and assigned errors (in brackets). The UBV magnitudes have been corrected for the small systematic differences mentioned in the text.

Date dd/mm/yy	JD (+2400000)	uvw2	uvm2	uvw1	U	B	V
04/11/07	54409.50	14.68 (.05)	14.52 (.06)	14.15 (.06)	13.49 (.04)	14.34 (.06)	14.19 (.04)
07/11/07	54411.52	14.90 (.05)	14.74 (.06)	14.36 (.05)	13.66 (.05)	14.41 (.05)	14.22 (.04)
09/11/07	54413.78	15.32 (.06)	15.20 (.06)				
11/11/07	54415.79	15.70 (.05)	15.54 (.06)	15.03 (.06)	14.11 (.05)	14.60 (.05)	14.35 (.04)
13/11/07	54417.80	16.13 (.06)	16.00 (.06)	15.37 (.06)	14.30 (.05)	14.68 (.05)	14.36 (.04)
17/11/07	54421.88	15.97 (.03)	16.74 (.07)	15.97 (.07)	14.90 (05)	14.90 (.05)	14.41 (.04)
23/11/07	54427.83	17.63 (.07)	17.63 (.08)	16.69 (.07)	15.40 (.05)	15.24 (.05)	14.59 (.04)
04/12/07	54438.55	18.31 (.08)	18.25 (.11)	17.28 (.08)	15.78 (.05)	15.56 (.05)	14.71 (.04)
14/12/07	54448.52	18.76 (.11)	18.92 (.13)	17.69 (.08)	16.20 (.06)	15.74 (.05)	14.84 (04)
07/01/08	54473.16	19.58 (.13)	19.69 (.22)	18.33 (.10)	17.33 (.07)	16.38 (.05)	15.25 (.04)
04/08/08	54683.02	> 20.9			> 20.9	> 21.2	> 20.2
23/08/08	54701.96	> 20.4	>19.6	> 21.3	> 21.0	> 21.0	> 20.2

To check for possible biases due to the peculiar pass bands of UVOT (and other instruments), in Fig. 3.2 we show the residuals with respect to a low order polynomial fit of all the available values. The agreement of the ground-based data is overall good with few measurements deviating by more than 0.05 mag. SWIFT data deviate more. The largest differences are for the U band in which the specific detector responses and the variable transmission at atmospheric cut-off can generate quite different effective wavelengths. This analysis have been done for all the SNe with optical measurement by Swift. The average difference (ground–space) founded for the other SNe of this sample are comparable with that shown here.

uvw2, uvm2, uvw1, U, B, V, R, I, J, H, and K light curves of SN 2007od are plotted in Fig. 3.3. This figure includes also photometric data from Andrews *et al.* (4). As stressed by these authors, the F606W and the Gemini r filters (transformed respectively to the V and R) include the Hα line, and care should be used when comparing these data with standard photometry of other SNe. Both in the photospheric and in the nebular phases the data of Andrews *et al.* (4) are in good agreement with our data.

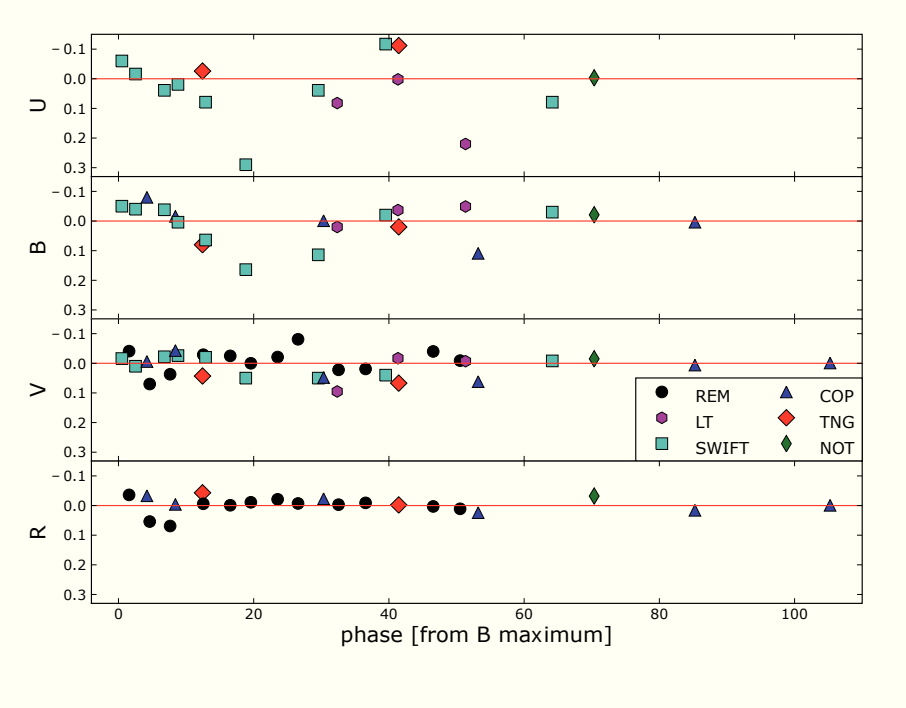

Figure 3.2: U, B, V and R band residuals in the first 106 days with respect to low order polynomial fits of all available data. Different instruments are marked with different symbols.

Table 3.6: JHK magnitudes of SN 2007od and assigned errors (in brackets). We accounted for both measurement errors and uncertainties in the photometric calibration.

Date dd/mm/yy	JD (+2400000)	J	H	K	Inst.
06/11/07	54410.57	13.71 (.05)	13.60 (.07)		2
09/11/07	54413.62		13.63 (.04)	13.80 (.09)	2
12/11/07	54416.64	13.75 (.04)	13.63 (.05)		2
16/11/07	54421.54	13.73 (.05)	13.65 (.04)	13.59 (.12)	2
21/11/07	54425.53	13.82 (.02)	13.64 (.02)	13.70 (.08)	2
24/11/07	54428.58		13.64 (.04)	13.61 (.06)	2
27/11/07	54432.54	13.79 (.02)	13.64 (.03)	13.65 (.05)	2
01/12/07	54435.56	13.84 (.02)	13.57 (.05)	13.56 (.05)	2
07/12/07	54441.55	13.80 (.04)			2
11/12/07	54445.55	13.85 (.03)	13.63 (.02)	13.60 (.07)	2
21/12/07	54455.55	13.84 (.04)	13.61 (.03)	13.58 (.06)	2
25/12/07	54459.53	13.79 (.05)	13.69 (.04)	13.94 (.13)	2
29/12/07	54463.53	13.94 (.02)	13.77 (.04)	13.77 (.07)	2
12/01/08	54478.31	14.33 (.04)	14.23 (.04)	13.90 (.03)	3
11/06/08	54629.73	19.61 (.03)	19.30 (.05)		3

2 = REM, 3 = TNG (K' filter).

The R-band light curve shows a fast rise to the peak, estimated to occur around JD 2454409.0±2.0. In fact, early unfiltered observations from Mikuz and Maticic (152) showed that the SN was still rising to the R-band maximum at discovery (Nov 2.85 UT). This is also consistent with the phases derived for the first spectra of SN 2007od through a cross-correlation with a library of supernova spectra performed with the "GELATO" code (100). Therefore, hereafter we will adopt JD 2454404±5 (October 30.5 UT) as an estimate for the epoch of shock breakout.

In Fig. 3.3 an early (short) post-peak decline is visible mainly in the BVR bands, while the U band shows a monotonic decline.

A short, flat plateau is visible at longer wavelengths with $m_R \sim 14.3$ ($M_R \sim -17.8$) between about day 15 and day 45. The plateau of SN 2007od is, therefore, relatively luminous when compared with that of more typical SNe IIP (180, 200) and similar to those of SNe 1992H (52) and 2004et (121, 139).

The SN was recovered about 240 days after maximum light. Unfortunately,

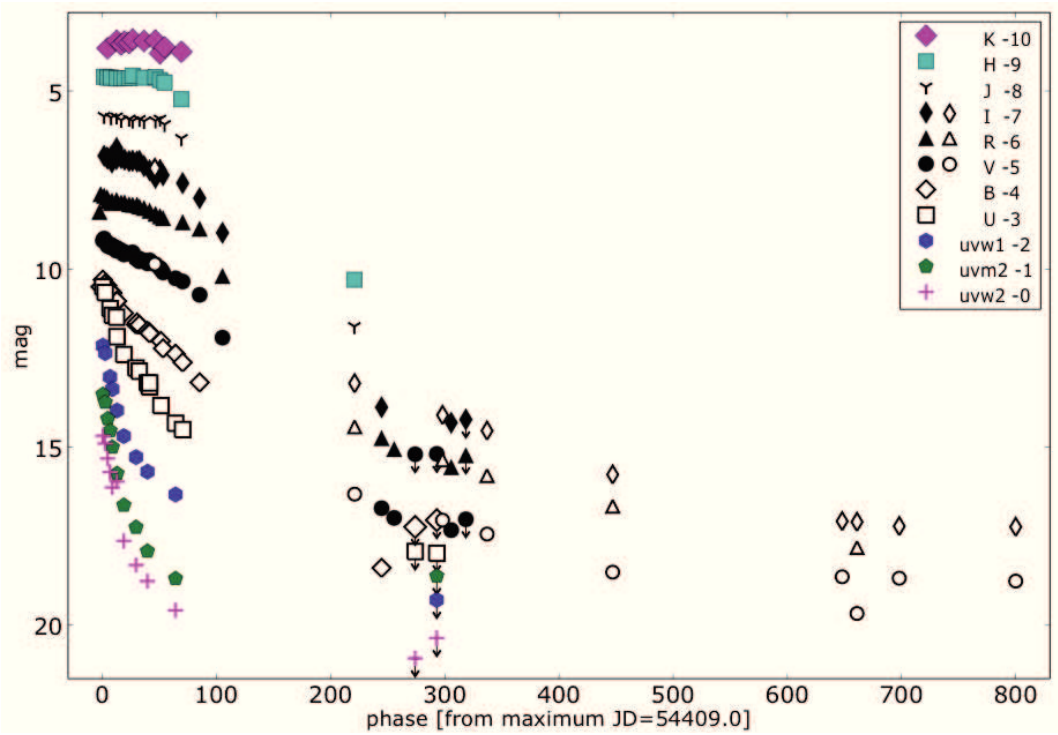

Figure 3.3: Synoptic view of the light curves of SN 2007od in all available bands. The U, B, V light curves include data both from ground-based telescopes and SWIFT, RIJHK light curves from ground-based telescope images, and uvw2, uvm2 and uvw1 light curves only from SWIFT. The magnitude shifts from the original value reported on Tab. 3.4 are in the legend. Open VRI symbols are magnitude values reported in Andrews *et al.* (4).

our observations do not cover the plateau-tail transition which would allow interesting diagnostics for the explosion parameters (67). It is remarkable that from the plateau to the first point of the radioactive tail there is a drop of ∼6 mag in about 200 days, which is much larger than that seen in normal SNe IIP. Afterwards, the late time decline rates in the different bands (cfr. Tab. 3.3), computed including also data from Andrews *et al.* (4), are rather similar to those of most normal SNe IIP (180, 239). The V band decline rate is 0.94 mag $(100\mathrm{d})^{-1}$, close to the 0.98 mag $(100\mathrm{d})^{-1}$ (e-folding time 111.26 days) expected if the luminosity is powered by the decay of ^{56}Co to ^{56}Fe.

3.2.2 SN 2009bw

SN 2009bw was discovered in UGC 2890 on 2009 March 27.87 UT Nissinen, Heikkinen & Hentunen (167). Stanishev, Adamo, and Micheva (221) classified it as a normal type II SN soon after explosion, showing spectrum with narrow Hα emission superimposed on a broader base.

The coordinates of SN 2009bw have been measured on our astrometrically calibrated images: $\alpha = 03^h56^m06^s.92 \pm 0^s.05$ $\delta = +72^o55'40".90 \pm 0."05$ (J2000). The object is located in the inner region of the highly (i=90, LEDA) inclined UGC 2890, 11" East and 22" North of the center of the galaxy (Fig. 3.4). This corresponds to a projected distance of ∼2.4 Kpc from the nucleus assuming a distance to UGC 2890 of ∼20 Mpc (z=0.003853).

The Galactic reddening to UGC 2890 is E_g(B-V) = 0.231 mag ($A_g(B) = 0.996$ mag) according to Schlegel, Finkbeiner, and Davis (205), a relative large value consistent with the low Galactic latitude of UGC 2890 (b_2=$14^o.7$, LEDA). In the optical spectra of SN 2009bw (cfr. Sect. 3.4.2) the absorption features due to interstellar NaID ($\lambda\lambda$5890,5896) of the Galaxy are present, with an average EW_g(NaID)∼1.37 Å, as determined by our best resolution spectra. According to Turatto, Benetti, and Cappellaro (235) this corresponds to a Galactic reddening E_g(B-V)∼0.22 mag (A_g(B)∼0.92 mag). This is in good agreement with Schlegel, Finkbeiner, and Davis (205). With the same method we can estimate the reddening inside the parent galaxy. Interstellar NaID components within the host galaxy have been measured with an average EW_i(NaID)∼ 0.52 Å that corresponds to a

Table 3.7: Main data of SN 2009bw.

position (2000.0)		$03^h56^m02^s.92$	$+72^o55^m40^s.9$
parent galaxy		UGC 2890, Sdm pec:	
offset wrt nucleus		11" E	22" N
adopted distance modulus	$\mu = 31.53 \pm 0.15$		
SN heliocentric velocity	1155 ± 6 km s^{-1}		
adopted reddening		E_g(B-V)= 0.23	E_{tot}(B-V)= 0.31
	peak time (JD 2454000+)	peak observed magnitude	peak absolute magnitude
B	923 ± 1	15.18 ± 0.01	-17.72 ± 0.15
V	925 ± 1	14.88 ± 0.06	-17.67 ± 0.16
R	925 ± 1	14.55 ± 0.02	-17.82 ± 0.15
I	929 ± 1	14.33 ± 0.01	-17.83 ± 0.15
UBVRI	925 ± 2	$L_{bol} = 2.6 \times 10^{42}$ erg s^{-1}	
rise to R max	~ 8 days		
explosion day	$\sim 916.5 \pm 2$	$\sim$ 25 Mar. 2009	
		late time decline mag(100d)$^{-1}$	interval days
V		1.00	139–239
R		1.09	139–239
I		1.13	139–239
UBVRI(tot)		1.06	139–239
UBVRI(1seg)		0.70	139–156
UBVRI(2seg)		1.16	161–239
M(^{56}Ni)			0.022 $M_\odot$
M(ejecta)			8.3 – 12 $M_\odot$
explosion energy			0.3 $\times 10^{51}$ ergs

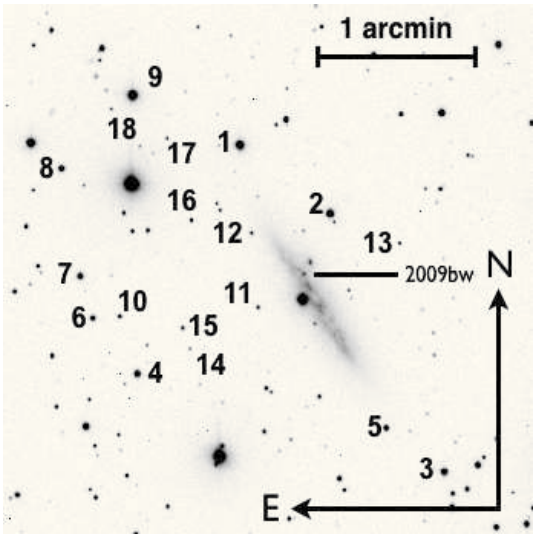

Figure 3.4: R band image of SN 2009bw in UGC 2890 obtained with CAHA+CAFOS on August 30th, 2009. The sequence of stars in the field used to calibrate the optical and NIR magnitude of the 2009bw is indicated.

low internal reddening E_i(B-V)$\sim$0.08 mag or A_i(B)$\sim$0.35 mag. We should warn the reader that recently Poznanski *et al.* (191) have shown that NaID lines in SNIa spectra are poor tracers of dust extinction. However, having no alternative throughout this paper we have adopted a total reddening E_{tot}(B-V) = 0.31$\pm$0.03 mag.

NED provides a heliocentric radial velocity of $v_{hel}(UGC2890) = 1155 \pm 6$ km s^{-1}. Adopting $H_0 = 73$ km s^{-1} Mpc^{-1} and a velocity corrected for the Virgo infall of $v_{Virgo} = 1473 \pm 16$ km s^{-1} (157) we obtain a distance modulus $\mu = 31.53 \pm 0.15$ mag which will be used throughout this thesis.

Assuming the above distance and extinction values, we find $M_B^{max} = -17.72 \pm 0.15$, $M_V^{max} = -17.67 \pm 0.16$, $M_R^{max} = -17.82 \pm 0.15$ and $M_I^{max} = -17.83 \pm 0.15$, where the reported errors include the uncertainties on the adopted distance modulus, reddening and magnitude measurements.

Principal data of SN 2009bw are shown in Tab. 3.7. In Fig. 3.5 the uvw2,uvm2, uvw1,U,B,V,R,I,J,H,K′ light curves of SN 2009bw are plotted. The relative magnitudes are reported in Tab. 3.8, 3.9 & 3.10, while the magnitudes of the sequence stars shown in Fig. 3.4 are listed in Tab. A.2. The B-, V-, I- and more clearly

Table 3.8: UBVRI magnitudes of SN 2009bw and assigned errors in brackets.

Date yy/mm/dd	JD (+2400000)	U	B	V	R	I	Inst.
09/03/27	54918.42				15.88 (.02)		7
09/03/30	54921.40		15.49 (.02)	15.22 (.01)	15.09 (.01)		6
09/03/31	54922.24		15.38 (.02)	15.01 (.01)	14.90 (.01)		6
09/04/01	54923.32		15.18 (.01)	14.96 (.01)	14.72 (.01)		7
09/04/03	54925.31				14.55 (.02)		7
09/04/03	54925.50		15.32 (.10)	14.88 (.06)	14.68 (.01)	14.44 (.02)	6
09/04/04	54926.24	14.51 (.05)	15.30 (.05)	14.95 (.02)	14.65 (.01)	14.37 (.03)	9
09/04/07	54929.33			14.99 (.02)	14.64 (.02)	14.33 (.01)	8
09/04/08	54930.46				14.65 (.07)		7
09/04/09	54931.30	14.79 (.07)	15.36 (.03)	15.03 (.02)	14.67 (.02)	14.34 (.03)	9
09/04/12	54934.25	14.95 (.15)	15.57 (.05)	15.08 (.05)	14.72 (.03)	14.40 (.03)	9
09/04/12	54934.31	15.11 (.03)	15.55 (.02)	15.18 (.02)	14.74 (.02)	14.49 (.02)	1
09/04/14	54936.40	15.49 (.02)	15.73 (.02)	15.20 (.02)	14.77 (.02)	14.50 (.02)	2
09/04/14	54936.45				14.77 (.18)		7
09/04/15	54937.39	15.52 (.02)	15.82 (.02)	15.17 (.01)	14.78 (.02)	14.50 (.02)	4
09/04/19	54941.26	15.85 (.11)	15.96 (.03)	15.25 (.02)	14.81 (.02)	14.45 (.03)	9
09/04/19	54941.39	16.05 (.02)	15.98 (.02)	15.28 (.02)	14.80 (.02)	14.48 (.02)	4
09/04/22	54944.28	16.29 (.13)	16.16 (.05)	15.30 (.03)	14.88 (.02)	14.49 (.03)	9
09/04/22	54944.34				14.81 (.01)		7
09/04/23	54945.28	16.49 (.03)	16.34 (.05)	15.29 (.02)	14.86 (.02)	14.51 (.02)	6
09/04/26	54948.28		16.36 (.04)	15.40 (.03)	14.94 (.02)	14.53 (.03)	9
09/04/28	54950.34	16.54 (.19)	16.26 (.10)	15.40 (.20)	14.93 (.12)	14.61 (.12)	1
09/04/29	54951.29		16.44 (.04)	15.47 (.03)	15.02 (.02)	14.58 (.02)	9
09/04/30	54952.38				14.97 (.25)		7
09/05/03	54955.33	17.27 (.03)	16.70 (.02)	15.57 (.02)	15.03 (.02)	14.65 (.02)	1
09/05/03	54955.38	17.26 (.04)	16.75 (.02)	15.60 (.02)	15.10 (.04)	14.69 (.02)	3
09/05/04	54956.28		16.81 (.06)	15.61 (.04)	15.03 (.03)	14.57 (.03)	9
09/05/08	54960.44				15.01 (.13)		7
09/05/14	54966.45				15.11 (.05)		7
09/05/18	54970.34		17.08 (.07)	15.79 (.03)	15.16 (.03)	14.65 (.03)	9
09/05/18	54970.44				15.20 (.15)		7
09/05/21	54973.42	18.19 (.15)	17.01 (.05)	15.76 (.02)	15.19 (.02)	14.70 (.03)	5
09/05/25	54977.39	18.26 (.19)	17.27 (.04)	15.83 (.02)	15.17 (.02)	14.74 (.02)	5
09/05/25	54977.42				15.17 (.30)		7
09/05/26	54978.33			15.78 (.15)	15.17 (.10)	14.66 (.15)	9
09/05/30	54982.63	18.28 (.09)	17.29 (.02)	15.75 (.02)	15.17 (.02)	14.73 (.02)	1
09/05/31	54983.32				15.22 (.15)	14.70 (.16)	9
09/06/26	55009.58		17.63 (.02)	15.94 (.02)	15.31 (.02)	14.82 (.02)	1
09/07/04	55017.46			16.04 (.15)	15.31 (.12)		10
09/07/19	55032.68		18.15 (.04)	16.29 (.02)	15.60 (.02)	15.12 (.02)	3
09/07/23	55036.58		18.26 (.08)	16.38 (.02)	15.62 (.02)	15.13 (.02)	5
09/07/26	55039.43				15.71 (.05)		7
09/07/30	55043.42		18.32 (.17)	16.57 (.10)	15.76 (.10)	15.30 (.10)	9
09/07/30	55043.65		18.43 (.03)	16.52 (.03)	15.74 (.03)	15.23 (.03)	1
09/08/05	55049.35		18.62 (.30)	16.93 (.10)	16.11 (.10)	15.61 (.10)	9
09/08/10	55054.40			18.52 (.30)	17.54 (.16)	17.00 (.15)	9
09/08/12	55056.43			18.78 (.20)	17.90 (.18)	17.35 (.30)	9
09/08/12	55056.54	20.04 (.40)	20.79 (.09)	18.90 (.10)	17.93 (.06)	17.36 (.08)	1
09/08/13	55057.59	21.18 (.38)	20.74 (.09)	18.96 (.12)	18.01 (.04)	17.41 (.07)	2
09/08/20	55063.61		20.80 (.21)	19.23 (.11)	18.12 (.17)	17.47 (.13)	5
09/08/23	55067.29				18.03 (.15)	17.59 (.30)	9
09/08/29	55073.55			19.06 (.15)	18.05 (.10)		11
09/08/30	55074.52				18.05 (.15)		11
09/08/30	55074.57		20.81 (.04)	19.14 (.13)	18.19 (.08)	17.57 (.08)	1
09/09/04	55079.44		21.02 (.05)	19.19 (.04)	18.14 (.04)	17.55 (.07)	1
09/09/04	55079.53			19.15 (.16)	18.14 (.12)	17.51 (.27)	11
09/09/05	55080.47				18.12 (.12)		11
09/09/06	55081.43				18.15 (.12)		11
09/10/12	55116.74		21.03 (.11)	19.48 (.29)	18.51 (.57)	18.10 (.15)	3
09/10/18	55123.62			19.62 (.13)	18.70 (.11)	18.20 (.12)	5
09/11/07	55143.50			20.09 (.27)	19.01 (.15)		11
09/11/09	55145.47			20.13 (.21)	19.05 (.18)		11
09/11/10	55146.46		21.41 (.12)	20.11 (.19)	19.05 (.56)	18.68 (.22)	3
09/11/17	55153.42			20.36 (.21)	19.22 (.12)		11
09/11/22	55157.85			20.40 (.21)	19.36 (.24)	18.78 (.25)	1
10/08/24	55433.69			> 21.9	> 20.3	> 19.5	3

1 = CAHA, 2 = NOT, 3 = TNG, 4 = LT, 5 = Copernico, 6 = SAO-RAS, 7 = THO, 8 = S50, 9 = M70, 10 = C50, 11 = C60.

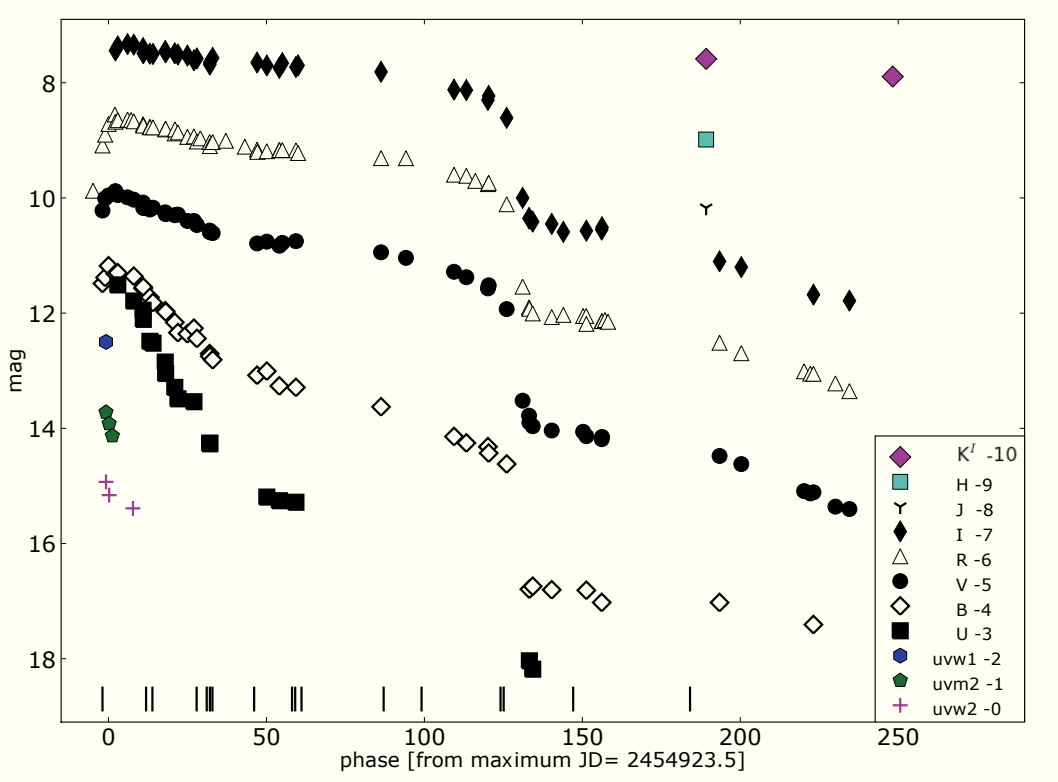

Figure 3.5: Synoptic view of the light curves of SN 2009bw in all available bands. The shifts from the original values reported on Tab. 3.8 are in the legend. Vertical marks at the bottom indicate the epochs of available spectra.

Table 3.9: JHK' magnitudes of SN 2009bw and assigned errors, we take into account both measurement errors and uncertainties in the photometric calibration. The measures have been taken at TNG.

Date	JD	J	H	K'
yy/mm/dd	(+2400000)			
09/10/07	55112.49	18.17 (.18)	17.99 (.15)	17.59 (.13)
09/12/05	55171.50			17.89 (.08)

Table 3.10: Swift magnitudes of SN 2009bw and assigned errors.

Date	JD	uvw2	uvm2	uvw1
yy/mm/dd	(+2400000)			
09/04/01	54922.51	14.93 (.06)	14.72 (.07)	14.50 (.10)
09/04/02	54923.51	15.16 (.06)	14.92 (.08)	
09/04/03	54924.52		15.13 (.09)	
09/04/09	54931.05	15.39 (.06)		

R-band light curves show a rise to the peak, estimated to be occurred around the JD 2454923.5±1.0 in the B band. Thus the discovery of the SN happened close to the shock breakout. The maximum epoch is also consistent with the phases derived for the first spectra of SN 2009bw as deduced from the comparison of the early spectra with a library of supernova spectra performed with the "GELATO" code (100). Therefore, hereafter we will adopt JD 2454916.5±3 (March 25.0 UT) as an estimate for the epoch of shock breakout.

An initial slow decline of ∼30 days, during which the SN decreases by about 0.5 mag in the V and R bands, is followed by a plateau lasting for 50 to 100 days. The plateau is flat from V to I ($m_R \sim 15.0$, i.e. $M_R \sim -17.4$), whilst it is less pronounced in blue bands, even though possibly shorter and slanted. It turns out that the plateau luminosity of SN 2009bw is more luminous than that of common SNe IIP (more than 1 mag, see 180, 200) and similar to those of SNe 1992H (52), 2004et (139) and 2007od (116, and this thesis).

As shown in Fig. 3.5 , after ∼110d BVRI light curves show a decline from the plateau. Though very fast (∼2.2 mag in only 13 days) the jump is less pronounced

than in other SNe IIP e.g. 6 mag in SN 2007od (116), >3.5 mag in SN 1994W (216), 3.6 mag in the low luminosity SN 2005cs (171).

After the drop, the light curve settles onto the radioactive tail. The late time decline rates in various bands are reported in Tab. 3.7. Although with same variations, these share overall similarity with those of most SNe IIP (e.g. 180, 239) and are close to 0.98 mag $(100d)^{-1}$, which is the decay rate of ^{56}Co to ^{56}Fe (corresponding to a lifetime of 111.26 days).

3.2.3 SN 2009dd

SN 2009dd was discovered in NGC 4088 by Cortini and Dimai (53) on 2009 April 13.97. Elias-Rosa *et al.* (66) classified it as a young type II with a strong absorption due to Na ID, which indicates a somewhat high interstellar absorption suffered by the supernova inside the parent galaxy. In the first month various X-ray observations have been carried out through Swift+XRT, detecting an X-ray source at the optical SN position with a 4.5σ significance (111). Over the course of the Swift XRT observations, the X-ray source continuously brightened from 8 x 10^{38} erg/s to 1.7 x 10^{39} erg/s (0.2-10 keV) (111). Instead, in the same period, no radio emission was detected at SN position with 3σ upper limits of 0.35 mJy at a resolution of 0.38" at 1.3 cm, and of 0.15 mJy at a resolution of 1.1" at 3.5 cm (222).

The coordinates of SN 2009dd have been measured on our astrometrically images at two different epochs: $\alpha = 12^h05^m34^s.10 \pm 0.05^s$ $\delta = +50^o32'19".40$ ± 0.05" (J2000). The object is located in an inner region 1".5 West and 4" South from the nucleus of SABbc NGC 4088. This position slightly revised with respect to previous determination (53), corresponds to a linear distance of $\sim$0.3 Kpc from the nucleus (assuming a distance to NGC of $\sim$14 Mpc derived by Virgo Infall only).

The Galactic reddening toward NGC 4088 was estimated as E_g(B-V)=0.02 (A_g(B)=0.085 205). In our best resolution optical spectra (cfr. Sect. 3.4.3), the absorption features due to interstellar Na ID ($\lambda\lambda$5890,5896) lines of the Galaxy are present with average EW_g(NaID)$\sim$ 0.13 Å. According to Turatto, Benetti, and Cappellaro (235) this corresponds to a galactic reddening E_g(B-V)$\sim$0.02 mag

Table 3.11: Main data of SN 2009dd

position (2000.0)		$12^h05^m34^s.10$	$+50^o32'19".40$
parent galaxy		NGC 4088, SAB(rs)bc	
offset wrt nucleus		1.5" W	4" S
adopted distance modulus		$\mu = 30.74 \pm 0.15$	
SN heliocentric velocity		1025 ± 15 km s^{-1}	
adopted reddening		E_g(B-V)= 0.02	E_{tot}(B-V)= 0.45
	peak time (JD 2454000+)	peak observed magnitude	peak absolute magnitude
U	937 ± 4	$> 14.74 \pm 0.01$	$> -17.82 \pm 0.11$
B	937 ± 4	$> 15.07 \pm 0.06$	$> -17.49 \pm 0.13$
V	937 ± 4	$> 14.87 \pm 0.06$	$> -17.80 \pm 0.12$
R	937 ± 4	$> 14.60 \pm 0.06$	$> -17.96 \pm 0.16$
I	937 ± 4	$> 14.62 \pm 0.04$	$> -17.99 \pm 0.17$
UBVRI	937 ± 4	$L_{bol} = 2.16 \times 10^{42}$ erg s^{-1}	
explosion day	$\sim 925.5 \pm 5$	$\sim$ 04 Apr. 2009	
		late time decline mag(100d)$^{-1}$	interval days
B		1.20	117–219
V		1.15	117–277
R		1.18	117–277
I		0.80	117–219
UBVRI		1.07	117-277
M(Ni)			0.034 $M_\odot$

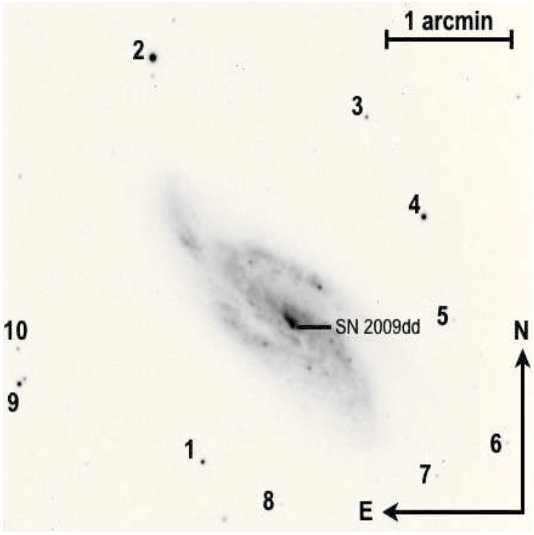

Figure 3.6: R band image of SN 2009dd in NGC 4088 obtained with CAHA+CAFOS on November 19th, 2009. The local sequence of stars used to calibrate the optical and NIR magnitudes of the SN 2009dd is indicated.

(A_g(B)$\sim$0.087), that considering the large uncertainties in the measurements and in the empirical method and the blend of these lines with those of the parent galaxy, is in surprise agreement with the previous estimate.

With the same method we can estimate the reddening inside the parent galaxy. Interstellar Na ID components within the host galaxy have been measured with an average EW$_i$(NaID)$\sim$2.7 Å that correspond to an internal reddening E$_i$(B-V)$\sim$0.43 mag or A$_i$(B)$\sim$1.81. Missing other more precise methods of determination of reddening we have adopted a total reddening to SN 2009dd E$_{tot}$(B-V)=0.45. This is consistent with the position of the SN inside the parent galaxy and what reported in Elias-Rosa *et al.* (66).

NED provides an heliocentric radial velocity of V_{hel}(NGC4088)= 757$\pm$ 1 km s^{-1}. Adopting H$_0$=73 km s^{-1}Mpc^{-1} and a velocity corrected for the Virgo infall of V_{Virgo} = 1025$\pm$15km s^{-1} (157) we obtain a distance modulus μ=30.74$\pm$0.15 which will be used throughout this thesis.

Assuming the above distance and extinction values, we find $M_U^{max} = -17.82 \pm 0.11$, $M_B^{max} = -17.49 \pm 0.13$, $M_V^{max} = -17.80 \pm 0.12$, $M_R^{max} = -17.96 \pm 0.16$ and

Table 3.12: UBVRI magnitudes of SN 2009dd and assigned errors.

Date	JD	U	B	V	R	I	Inst.
yy/mm/dd	(+2400000)						
09/04/14	54936.67	14.74 (.02)	15.07 (.06)	14.87 (.05)	14.60 (.06)	14.62 (.04)	1
09/05/19	54971.58	17.99 (.10)	16.87 (.02)	15.48 (.01)	14.67 (.04)	14.57 (.05)	2
09/07/20	55033.41	20.01 (.13)	18.21 (.09)	16.28 (.06)	15.45 (.05)	15.17 (.04)	2
09/07/21	55034.31		18.20 (.06)	16.35 (.01)	15.47 (.02)	15.14 (.02)	3
09/07/23	55036.39		18.36 (.02)	16.38 (.01)	15.53 (.05)	15.19 (.10)	3
09/08/12	55056.50		19.63 (.04)	17.79 (.09)	16.74 (.02)	16.66 (.05)	1
09/08/20	55064.36		19.73 (.20)	17.92 (.03)	16.84 (.08)	16.72 (.02)	3
09/09/04	55079.31			18.20 (.04)	17.04 (.19)	16.99 (.20)	4
09/11/19	55155.65		20.82 (.03)	18.92 (.10)	17.76 (.09)	17.36 (.06)	4
09/11/21	55157.70		20.93 (.04)	18.98 (.12)	17.83 (.10)	17.44 (.04)	4
10/01/19	55216.20			19.73 (.20)	18.83 (.20)		3
10/05/17	55334.43		> 20.7	> 20.1	> 19.8	> 19.3	2
10/10/25	55495.67		> 20.7	> 20.6	> 19.9	> 20.0	4

1 = NOT, 2 = TNG, 3 = Ekar, 4 = CAHA.

$M_I^{max} = -17.99 \pm 0.17$ (maximum of our data set), where the errors reported include the uncertainties on the distance modulus adopted and observations.

In Fig. 3.6 the sequence stars used for the calibration of the photometry are shown, while the magnitudes are listed in Tab. A.3 in Appendix A. Our SNe measurements are reported in Tab. 3.12. The Swift data have been treated as in previous Sec. 3.2.1. By comparing the space and the ground-based SN magnitudes, evaluated interpolating the light curves using low-order polynomials, at corresponding epochs we found an average difference (ground–space) $\Delta U \sim 0.20 \pm 0.03$, $\Delta B \sim 0.06 \pm 0.03$, $\Delta V \sim 0.10 \pm 0.03$. These corrections have been applied to all UVOT magnitudes and the resulting magnitude values are reported in Tab. 3.13.

Main data of SN 2009dd are shown in Tab. 3.11. In Fig. 3.7 the uvw2,uvm2, uvw1,U,B,V,R,I,J,H,K' light curves of SN 2009dd are plotted. The relative magnitudes are reported in Tab. 3.12. No band shows a rise to the the peak, thus we take as reference the magnitude maxima the values on the first epoch. Lacking any other constrain we have adopted as epoch of explosion JD 2454925.5±5 (April 04 UT) consistent with the epoch of the first spectra derived with the cross correlation with a library of supernova spectra performed with the "GELATO" code (100).

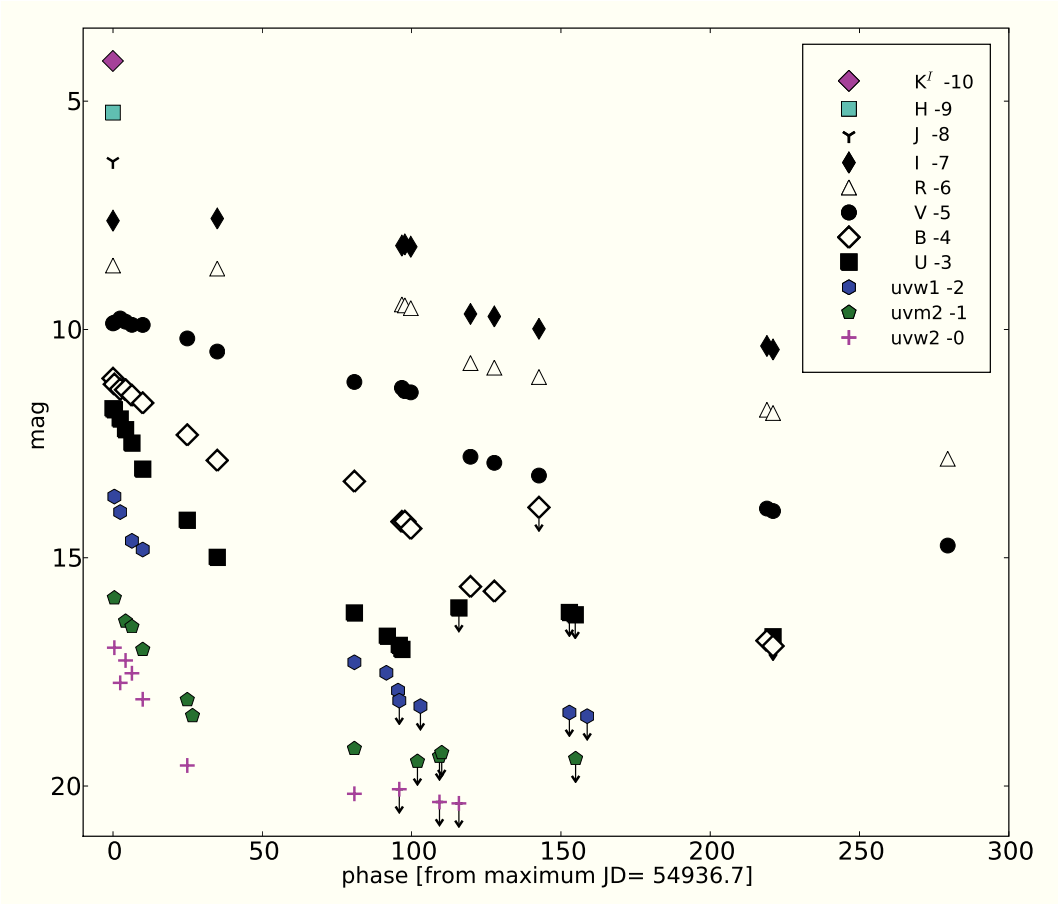

Figure 3.7: Synoptic view of the light curves of SN 2009dd in all available bands. The U, B, V light curves include data both from ground-based telescopes and SWIFT, RIJHK light curves from ground-based telescopes, and uvw2, uvm2 and uvw1 light curves from SWIFT only. The magnitude shifts from the original values reported on Tab. 3.12 are in the legend.

Table 3.13: Swift magnitudes of SN 2009dd and assigned errors (in brackets). The UBV magnitudes have been corrected for the small systematic differences mentioned in the text.

Date	JD	uvw2	uvm2	uvw1	U	B	V
yy/mm/dd	(+2400000)						
09/04/15	54937.12	16.97 (.07)	16.88 (.05)	15.66 (.05)	14.76 (.09)	15.20 (.08)	14.85 (.08)
09/04/17	54939.08	17.44 (.13)		16.00 (.04)	14.96 (.06)	15.31 (.06)	14.76 (.06)
09/04/19	54940.87	17.25 (.08)	17.39 (.09)		15.19 (.05)	15.32 (.06)	14.83 (.04)
09/04/21	54943.00	17.53 (.07)	17.51 (.09)	16.63 (.08)	15.49 (.06)	15.44 (.08)	14.90 (.04)
09/04/25	54946.62	18.10 (.11)	18.01 (.10)	16.82 (.09)	16.06 (.06)	15.61 (.05)	14.90 (.04)
09/05/10	54961.54	19.55 (.08)	19.11 (.08)		17.18 (.06)	16.31 (.05)	15.20 (.04)
09/05/11	54963.29		19.46 (.09)				
09/07/05	55017.50	20.17 (.15)	20.18 (.12)	19.29 (.10)	19.21 (.06)	17.33 (.05)	16.15 (.04)
09/07/15	55028.21			19.52 (.11)			
09/07/16	55028.54				19.72 (.06)		
09/07/19	55032.12			19.91 (.13)			
09/07/20	55032.54	> 20.1		> 20.1	19.92 (.13)		
09/07/26	55038.62		> 20.4				
09/07/27	55039.62			> 20.2			
09/08/02	55046.00	> 20.3	> 20.3				
09/08/03	55046.75		> 20.2				
09/08/09	55052.50	> 20.4			> 19.2		
09/09/13	55088.50			> 20.3			
09/09/14	55089.50				> 19.2		
09/09/16	55091.58		> 20.4				
09/09/21	55095.46			> 20.5	> 19.3		

Table 3.14: JHK' magnitudes of SN 2009dd and assigned errors, we take into account both measurement errors and uncertainties in the photometric calibration. The measures have been taken at TNG.

Date	JD	J	H	K'
dd/mm/yy	(+2400000)			
09/04/15	54936.63	14.32 (.04)	14.25 (.05)	14.12 (.05)

An initial decline of ∼0.7 mag in ∼30 days is visible from U to V. It is followed by a plateau of 50–70 days, roughly visible from B to I bands, with magnitude m_V∼16.1 (M_V∼ −16.4). The plateau luminosity of SN 2009dd is therefore more luminous than common SNe, but slightly lesser than the luminous IIP 1992H (52), 2004et (139), 2007od (116, and this thesis) and 2009bw (114, and this thesis). The post plateau decline visible in the BVRI light curves guides them to the nebular phase. The drop in magnitude between the photospheric and the nebular phase is ∼1.4 mag in ∼20d that is somewhat common in type II. The late decline rates in various bands are reported in Tab. 3.11. The V band decline rate is 1.15 mag mag $(100d)^{-1}$, close to 0.98 mag $(100d)^{-1}$that is the decay rate of ^{56}Co to ^{56}Fe.

3.2.4 SN 2007pk

SN 2007pk discovered in NGC 579 by Parisky and Li (170) on 2007 November 10.31 UT has been classified by Filippenko, Silverman, and Foley (74) as a young-"peculiar" type IIn SNe, with early time spectra resembling those of SN 1998S. Immler *et al.* (112) reported that a bright X-ray source was detected within 23".5 the position of the SN. Inspection of the XRT raw image indicated that some of the X-ray flux might be due to the SN, although the results were not conclusive due to the large point-spread-function of the XRT instrument (18" half-power diameter at 1.5 keV). An X-ray flux of $(2.9\pm0.5)\times10^{-13}$ erg cm^{-2} s^{-1} and a luminosity of $(1.7\pm0.3)\times10^{40}$ erg s^{-1} have been calculated. Instead no radio emission has been detected at VLA in 8.46 GHz band as reported by (42).

The coordinates of SN 2007pk have been measured on our astrometrically calibrated images at three different epochs: $\alpha = 01^h31^m47^s.07 \pm0.04^s$ $\delta = +33^o36'54".70$ ±0.04" (J2000) and are really close ($\Delta \sim 0".5$ in δ) with that provided by Parisky and Li (170). The object is located in an inner region of the Spiral parent galaxy, 7".4 East and 1".6 South (slightly revised with respect to the Parisky and Li (170) determination) from the nucleus of NGC 579. The position of SN corresponds to a projected distance of ∼2.5 Kpc from the center.

The galactic reddening toward NGC 579 was estimated as E_g(B-V)=0.054 (A_g(B)=0.225, 205). We have evaluated the Na ID lines of the Galaxy in our

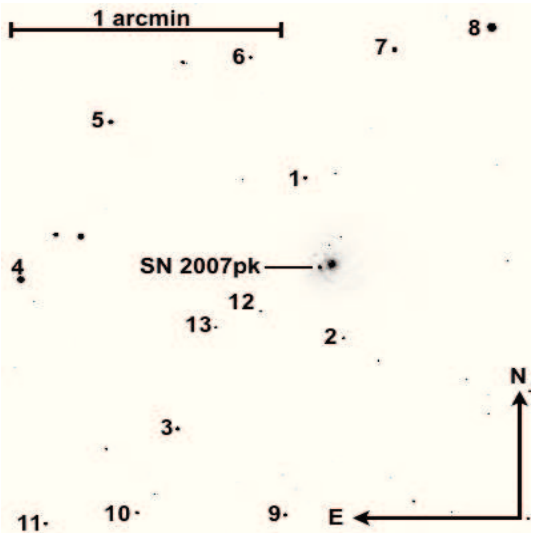

Figure 3.8: R band image of SN 2007pk in NGC 579 obtained with NOT+ALFOSC on January 11th, 2008. The sequence of stars in the field used to calibrate the optical magnitude of the 2007pk is indicated.

Table 3.15: Main data of SN 2007pk

position (2000.0)		$01^h31^m47^s.07$	$+33^o36'54".70$
parent galaxy		NGC 579, Scd:	
offset wrt nucleus		7".4 E	1".6 S
adopted distance modulus		$\mu = 34.23 \pm 0.15$	
SN heliocentric velocity		5116 ± 16 km s^{-1}	
adopted reddening		E_g(B-V)= 0.054	E_{tot}(B-V)= 0.106
	peak time (JD 2454000+)	peak observed magnitude	peak absolute magnitude
B	417 ± 1	16.00 ± 0.14	-18.64 ± 0.15
V	420 ± 1	16.09 ± 0.06	-18.55 ± 0.11
R	421 ± 1	15.88 ± 0.04	-18.76 ± 0.16
I	417 ± 4	15.89 ± 0.54	-18.75 ± 0.40
UBVRI	420 ± 2	$L_{bol} = 6.26 \times 10^{42}$ erg s^{-1}	
explosion day	$\sim 412 \pm 5$	$\sim$ 07.5 Nov. 2007	

Table 3.16: UBVRI magnitudes of SN 2007pk and assigned errors.

Date	JD	U	B	V	R	I	Inst.
yy/mm/dd	(+2400000)						
07/11/10	54415.30				17.00 (-)		99
07/11/11	54416.40		16.25 (.02)	16.37 (.02)	16.37 (.03)	16.45 (.03)	1
07/11/12	54417.50		16.00 (.15)	16.17 (.25)	16.20 (.34)	15.89 (.55)	1
07/11/16	54421.50	15.20 (.04)	16.14 (.04)	16.20 (.03)	15.88 (.04)	15.99 (.03)	2
07/12/04	54439.39		16.62 (.24)	16.31 (.24)	16.14 (.27)	16.01 (.29)	1
07/12/08	54443.50	16.65 (.03)	16.86 (.02)	16.43 (.02)	16.23 (.02)	16.00 (.02)	3
07/12/13	54448.40			16.51 (.02)	16.38 (.09)	16.00 (.04)	1
07/12/14	54449.50	17.29 (.03)	17.21 (.03)	16.62 (.03)	16.36 (.03)	16.01 (.03)	3
07/12/24	54459.50	18.02 (.10)	17.65 (.04)	16.82 (.03)	16.41 (.03)	16.19 (.02)	3
07/12/28	54463.29		17.92 (.12)	16.96 (.10)	16.53 (.05)	16.26 (.04)	1
08/01/09	54475.39		18.14 (.23)	17.13 (.22)	16.63 (.18)		1
08/01/11	54477.40	18.73 (.05)	18.34 (.03)	17.19 (.02)	16.69 (.03)	16.40 (.03)	4
08/01/28	54494.36		18.49 (.93)	17.46 (.16)	17.04 (.16)	16.69 (.13)	1
08/09/04	54714.64			> 19.8	>19.6	> 19.4	2
08/09/14	54723.69		>19.8	> 20.1	>19.6		5

1 = Ekar, 2 = TNG, 3 = LT, 4 = NOT, 5 = CAHA, 99 = CBET

best resolution spectra, finding an average of EW_g(NaID)$\sim$0.57 Å that corresponds to a galactic reddening of E_g(B-V)$\sim$0.09 mag (A_g(B)$\sim$0.380), that is 1.5 times larger than previous estimate. With the same method (cfr. Sec. 3.2.1 & 3.2.2) we estimated the reddening inside the parent galaxy. The interstellar Na ID components within the host galaxy have been measured with an average EW_i(NaID)$\sim$0.33 that corresponds to a reddening E_i(B-V)$\sim$0.052 mag or A_i(B)$\sim$0.221. Missing other methods of reddening determination, throughout this work, therefore, we have adopted a total reddening to SN 2007pk E_{tot}(B-V)=0.106.

NED provides an heliocentric radial velocity of V_{hel}(NGC579)= 4993± 4 km s^{-1}. Adopting H_0=73 km s^{-1}Mpc^{-1} and a velocity corrected for the Virgo infall of V_{Virgo} = 5116±16km s^{-1} (157) we obtain a distance modulus μ=34.23±0.15 which will be used throughout this thesis.

Assuming the above distance and extinction values, we find $M_B^{max} = -18.64 \pm 0.15$, $M_V^{max} = -18.55 \pm 0.11$, $M_R^{max} = -18.76 \pm 0.12$ and $M_I^{max} = -18.75 \pm 0.40$, where the errors reported include the uncertainty on the distance modulus adopted and observations.

Table 3.17: Swift magnitudes of SN 2007pk and assigned errors (in brackets). The UBV magnitudes have been corrected for the small systematic differences mentioned in the text.

Date	JD	uvw2	uvm2	uvw1	U	B	V
yy/mm/dd	(+2400000)						
07/11/13	54417.66			14.50 (.04)			
07/11/14	54418.65	14.54 (.06)		14.64 (.05)	15.13 (.05)	16.05 (.06)	16.15 (.04)
07/11/15	54420.24	14.92 (.05)		14.78 (.04)	15.17 (.05)	16.07 (.06)	16.09 (.04)
07/11/16	54420.66	15.14 (.06)		14.87 (.05)	15.19 (.05)	16.08 (.06)	16.09 (.04)
07/11/17	54421.68	15.45 (.06)		15.08 (.05)	15.22 (.06)	16.14 (.06)	16.23 (.05)
07/11/20	54425.08	16.03 (.06)		15.48 (.05)			
07/11/25	54429.65	16.91 (.07)		16.32 (.08)	15.69 (.06)	16.28 (.06)	16.23 (.04)
07/11/29	54433.91	17.85 (.09)		17.02 (.08)	16.13 (.06)	16.42 (.07)	16.27 (.05)
07/12/02	54436.96	18.44 (.10)		17.64 (.09)	16.45 (.06)	16.57 (.06)	16.27 (.05)
07/12/06	54440.81	19.01 (.10)		18.07 (.10)	16.61 (.06)	16.69 (.07)	16.32 (.05)
07/12/17	54451.65				17.39 (.06)	17.27 (.07)	16.68 (.05)
07/12/27	54462.01				18.20 (.08)	17.78 (.08)	16.95 (.05)
08/01/08	54474.09				18.52 (.08)	18.11 (.10)	17.09 (.06)

The Swift data have been treated as in previous Sec. 3.2.1. By comparing the space and the ground-based SN magnitudes, evaluated interpolating the light curves using low-order polynomials, at corresponding epochs we found an average difference (ground–space) $\Delta U \sim 0.20 \pm 0.05$, $\Delta B \sim 0.06 \pm 0.02$, $\Delta V \sim 0.07 \pm 0.03$. These corrections have been applied to all UVOT magnitudes and the resulting magnitude values are reported in Tab. 3.17.

Main data of SN 2007pk are shown in Tab. 3.15. In Fig. 3.5 the uvw2, uvw1,U,B,V,R,I light curves of SN 2007pk are plotted. The relative magnitudes are reported in Tab. 3.16, while the magnitudes of the sequence stars shown in Fig. 3.8 are listed in Tab. A.4. The slight, slow rise to the peak shown by R band supports the classification of this object as type IIn, even if after a period of 10 days post maximum in B band, estimated around JD 2454417.5±1.0, the light curves resemble those of a normal type II. The day of the maximum is also consistent with the phases derived for the first spectra of SN 2007pk through the cross-correlation with "GELATO" (used also for the other SNe of the sample and explained in detail in 100). Therefore, hereafter we will adopt JD 2454412±5 (November 07.5 UT) as an estimate for the epoch of shock breakout.

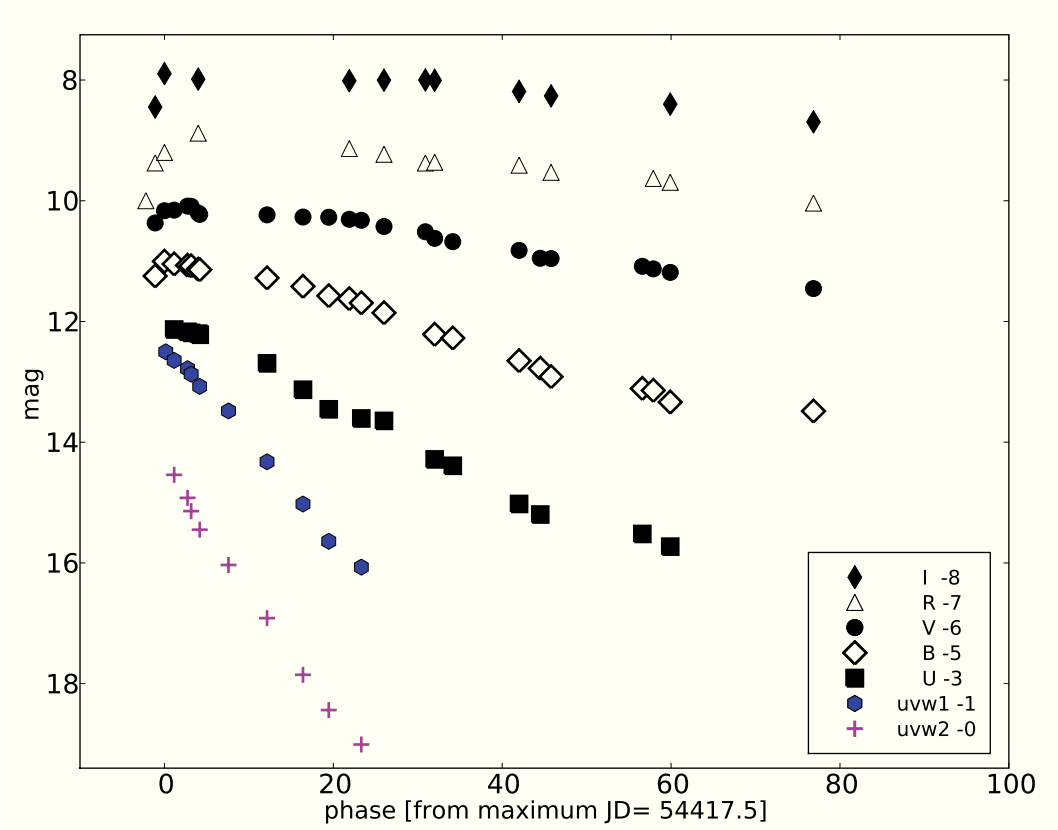

Figure 3.9: Synoptic view of the light curves of SN 2007pk in all available bands. The U, B, V light curves include data both from ground-based telescopes and SWIFT, RI light curves from ground-based telescope images, and uvw2 and uvw1 light curves only from SWIFT. The magnitude shifts from the original value reported on Tab. 3.16 are in the legend.

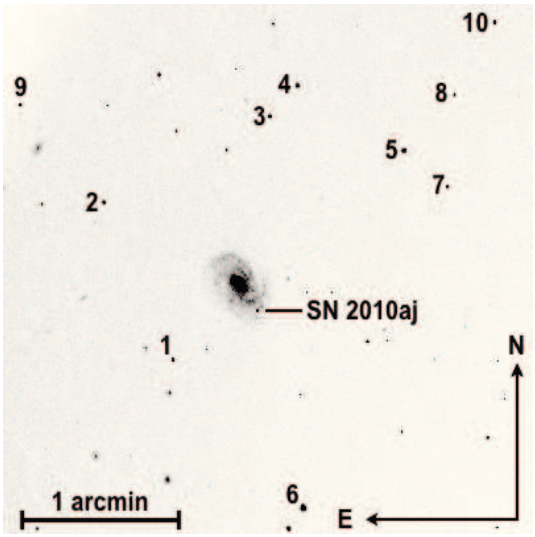

Figure 3.10: R band image of SN 2010aj in MGC -01-32-035 obtained with TNG+DOLORES on May 22th, 2010. The sequence of stars in the field used to calibrate the optical and NIR magnitude of the 2010aj is indicated.

After the peak, the decline of the light curves seems similar to type IIL, with no sign of plateau in all bands. The behavior of the light curves is certainly more similar to that of type IIL SNe as SN 1979C respect to the plateau SNe proposed for comparison in Fig. 3.17. In fact the average decline rate by Patat *et al.* (180) is β^B_{100}(07pk)$\sim$3.7 mag $(100\mathrm{d})^{-1}$, typical of type IIL. Unfortunately we have not nights during the nebular phase, but only a couple of points after 300d that give us weak constraints on the nebular magnitudes.

3.2.5 SN 2010aj

SN 2010aj was discovered in MGC -01-32-035 by Newton, Puckett, and Orff (160) on 2010 March 12.39 UT and confirmed the next day (March 13.29 UT). Cenko *et al.* (40) classified it as a young type II SNe that resembles type IIP SN 2006bp near maximum brightness.

The coordinates of SN 2010aj have been measured on our astrometrically calibrated images at $\alpha = 12^h40^m15^s.16 \pm 0.05^s$ δ = -09^{o}18'14".30 $\pm$0.05" (J2000). The object is located in an arm of the SABbc: parent galaxy, 12".4 West and

Table 3.18: Main data of SN 2010aj

position (2000.0)	$12^h40^m15^s.16$	-09°18'14".30 ±0.05" (J2000)	
parent galaxy	MGC -01-32-035, SAB(rs)bc		
offset wrt nucleus	12".4 W	11".7 S	
adopted distance modulus	$\mu = 34.71 \pm 0.15$		
SN heliocentric velocity	6386 ± 20 km s^{-1}		
adopted reddening	E_g(B-V)= 0.036	E_{tot}(B-V)= 0.036	
	peak time (JD 2455000+)	peak observed magnitude	peak absolute magnitude
R	269 ± 4	17.00	-17.86 ± 0.15
UBVRI	269 ± 4	$L_{bol} = 2.68 \times 10^{42}$ erg s^{-1}	
explosion day	$\sim 265.5 \pm 8$	$\sim$ 10 Mar. 2010	
		late time decline mag(100d)$^{-1}$	interval days
UBVRI		4.06	87–103
M(Ni)			<0.004 $M_\odot$

11".7 South of the center of galaxy (Fig. 3.10). This offset corresponds to a linear distance of ∼7.3 Kpc form the nucleus, assuming the distance to MGC of ∼ 87.5 Mpc (z=0.021185). As shown by the spectra in Fig. 3.27 a strong H II region is present on the same position and becomes the main light source after 350d (Fig. 3.27).

The Galactic reddening in the direction to MGC -01-32-035 was estimated as E_g(B-V)=0.036 ($A_g(B)$=0.148, 205). Unfortunately, the available spectra do not show both the Na ID lines of the parent galaxy and our Galaxy. Maybe due to a combination of resolution and presence of metal lines. Indeed, throughout this thesis, for SN 2010aj we will assume a total reddening of E_{tot}(B-V)=E_g(B-V)=0.036 mag, due only to the Galaxy absorption.

NED provides a heliocentric radial velocity of v_{hel}(MGC)= 6351± 4 km s^{-1}. Correcting for the Virgo infall (V_{Virgo} = 6386 ± 20km s^{-1}, 157) and adopting H_0=73 km s^{-1}Mpc^{-1}, we obtain a distance modulus μ=34.71±0.15 which will be used throughout this thesis.

U, B, V, R, I, J, H, K light curves of SN 2010aj are plotted on Fig. 3.11. As said before, the R band is the only one to show the rise to the peak, estimated to occur around JD 2455269.5±4.0 (March 13 UT) and in agreement with the spectra classification reported by Cenko *et al.* (40). This is also consistent with the

Table 3.19: UBVRI magnitudes of SN 2010aj and assigned errors.

Date	JD	U	B	V	R	I	Inst.
yy/mm/dd	(+2400000)						
12/03/10	55268.50				17.1 (-)		99
13/03/10	55269.50				17.0 (-)		99
24/03/10	55280.50		17.92 (.05)	17.75 (.03)	17.55 (.03)	17.34 (.05)	1
27/03/10	55282.95		18.30 (.04)	17.78 (.03)	17.57 (.02)	17.33 (.04)	1
16/04/10	55303.50		18.72 (.13)	18.16 (.03)	17.82 (.03)	17.45 (.06)	2
24/04/10	55311.52		19.30 (.11)	18.29 (.04)	17.83 (.03)	17.54 (.03)	3
05/05/10	55321.90	20.21 (.17)	19.55 (.09)	18.48 (.06)	17.99 (.03)	17.85 (.03)	1
07/05/10	55324.00	20.27 (.21)	19.65 (.12)	18.62 (.07)	18.11 (.04)	17.81 (.06)	1
18/05/10	55334.95	20.36 (.25)	19.90 (.12)	18.83 (.07)	18.24 (.05)	18.13 (.08)	1
22/05/10	55339.38	20.44 (.23)	19.97 (.10)	18.93 (.07)	18.32 (.05)	18.23 (.06)	3
26/05/10	55342.92	20.51 (.23)	20.30 (.15)	19.17 (.07)	18.53 (.06)	18.43 (.06)	1
09/06/10	55356.93		22.82 (.24)		21.01 (.19)	20.74 (.30)	1
12/06/10	55359.89		>20.7	21.91 (.30)	21.16 (.28)	21.03 (.20)	1
16/06/10	55363.94		>20.7	22.28 (.21)	21.18 (.11)	21.11 (.11)	1
17/06/10	55365.14			>20.6	> 20.2	>20.0	2
21/06/10	55368.91		>20.5	>20.5	21.25 (.14)	21.17 (.12)	1
24/06/10	55371.91		>20.7	>20.7	21.58 (.04)	21.31 (.14)	1
08/07/10	55386.46		>20.9	>20.6	>20.1	>20.4	3
01/01/11	55563.31		>20.5	>20.6	>20.2	>20.0	2
25/01/11	55587.30		>20.6	>20.6	>20.3	>20.5	2

1 = LT, 2 = NTT, 3 = TNG, 99 = CBET

Table 3.20: JHK magnitudes of SN 2010aj and assigned errors, we take into account both measurement errors and uncertainties in the photometric calibration. The measures have been taken at NTT.

Date	JD	J	H	K
dd/mm/yy	(+2400000)			
10/04/18	55305.50	19.42 (.04)	20.19 (.08)	20.21 (.05)

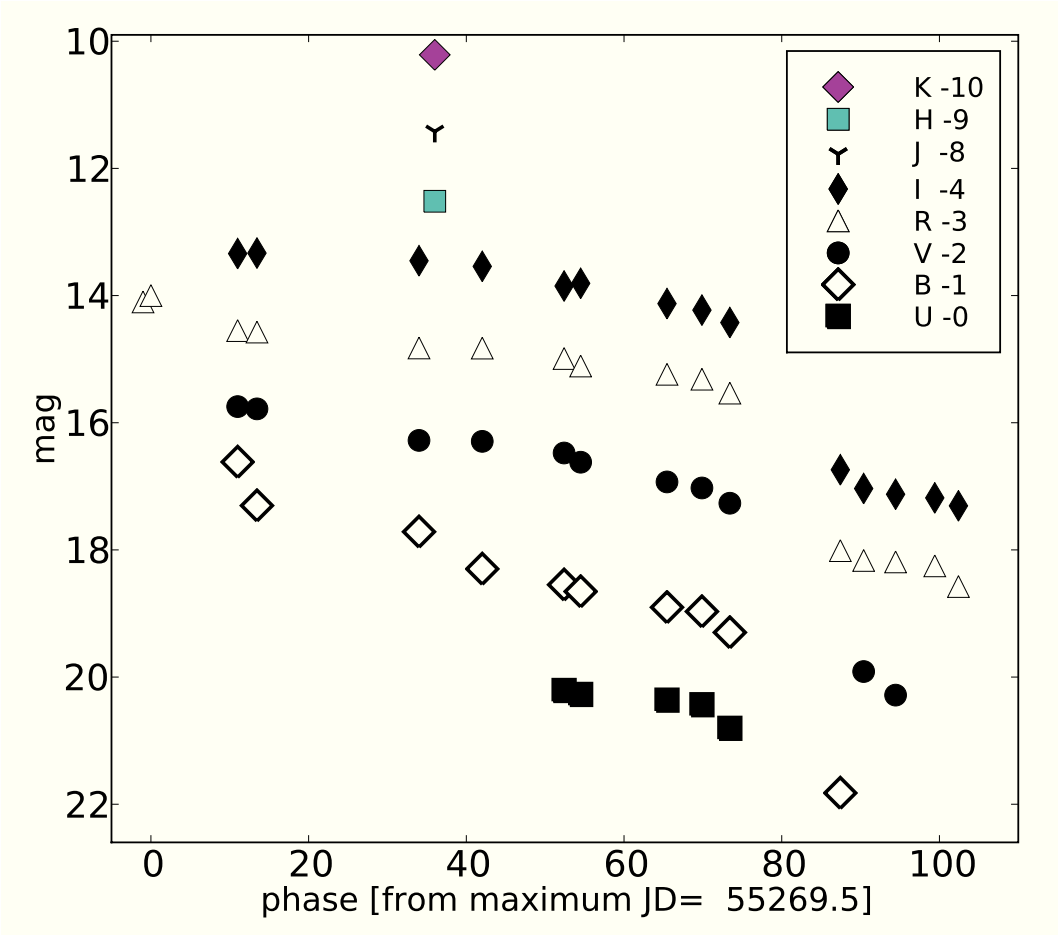

Figure 3.11: Synoptic view of the light curves of SN 2010aj in all available bands. The magnitude shifts from the original value reported on Tab. 3.19 are in the legend.

phase derived for the first spectra through GELATO (100). Therefore, hereafter we will adopt JD 2455265.5±8 (March 10 UT) as an estimate for the epoch of shock breakout.

A decline after maximum is visible only in R band (∼0.6 mag in 13d), missing data in all other bands. From about 15d onward we observe a long slanted plateau during which magnitudes decline faster at shorter wavelengths. The plateau is visible in V and R bands with m_R ∼17.82 and m_V ∼18.28 (M_R ∼-17.04, M_V ∼-16.58), while the B band shows a monotonic decline. The tail has been observed from V to I band, while in B band there is a single point. The drop in magnitude between the photospheric and the nebular phase is ∼2.5 mag in ∼16d (R band taken as reference), similar to SN 2009bw (∼2.2 mag in ∼13d). We could not compute the decline rate on the radioactive tail because of the lack of late time data (last observation is at 103d).

Assuming the above distance and extinction values, we find $M_B^{max} = -17.20 \pm 0.12$, $M_V^{max} = -17.11 \pm 0.11$, $M_R^{max} = -17.86 \pm 0.11$ and $M_I^{max} = -17.52 \pm 0.11$, where the reported errors include the uncertainties of our photometry, the adopted distance modulus, and the interstellar reddening. As shown in Fig. 3.11 only the R band has a real peak, the other values refer to the maximum values of our data set.

3.3 Colour curves and bolometric light curves

In order to estimate the intrinsic luminosity of the objects of our sample, it is essential to establish their distances, the phases and the extinctions to which they are subject. All this informations have been presented in the previous Section. Only for the SN 2010aj are missing informations about a possible extinction related to the SN position in the parent galaxy. Differently, the peripheral position of SN 2007od respect to the nucleus of its host galaxy is in agreement with the absence of extinction due to the position in UGC12846.

As we will show in Sec. 3.4, the SNe, presented as new set of luminous objects in this section, show early spectra with blue continua (except the SN 2010aj for which the first spectrum is at ∼22d post explosion) and broad P-Cygni of H (Balmer series) and He I λ5876 lines, typical of young type II. As reported in

Table 3.21: Main parameters of type II SNe used in the comparisons with our SNe sample.

SN	μ^*	E(B–V)	Parent Galaxy	References
1979C	31.16	0.009	NGC4321	1
1987A	18.49	0.195	LMC	2
1992H	32.38	0.027	NGC 5377	3
1998S	31.08	0.232	NGC 3877	4
1999em	29.47	0.1	NGC 1637	5,6
2004et	28.85	0.41	NGC 6946	7
2005cs	29.62	0.05	M 51	8
2006bp	31.44	0.031	NGC 3953	9

* Reported to a $H_0 = 73\ km\,s^{-1}\ Mpc^{-1}$ distance scale
REFERENCES: 1 - Balinskaia, Bychkov, and Neizvestnyi (12), 2 - Arnett *et al.* (6), 3 - Clocchiatti *et al.* (52), 4 - Fassia *et al.* (71), 5 - Elmhamdi *et al.* (68), 6 - Baron *et al.* (17), 7 - Maguire *et al.* (139), 8 - Pastorello *et al.* (171), 9 - Quimby et al. (197).

the previous Sec. 3.2 both spectroscopic and photometric evidences lead us to conclude that these SNe have been discovered close to explosion. More uncertain is the explosion epoch of SN 2010aj, for which we have assumed that it exploded 3 days before discovery (cfr. Sect. 3.2.5).

Considering the distance moduli and the absorption corrections already determined for these objects we can draw the colour curves of this sample. These curves are compared with those of SN 1987A, the faint SN 2005cs, the normal SN 1999em and the luminous SN 1992H and SN 2004et. All distances have been reported to an H_0=73 $km\,s^{-1}Mpc^{-1}$ distance scale. In Fig. 3.12 we show the time evolution of B–V, V–I and J–H color curves of our sample, together with those of the other SNe, dereddened according to the values of Tab. 3.21. All these SNe IIP show quite similar colour evolutions with a rapid increase of the B–V colour as the supernova envelope expands and cools down. After about 40 days the colour varies more slowly as the rate of cooling decreases, reaching a value of $\sim$1.5 at $\sim$100d. SN 2007od, SN 2009bw, SN 2009dd and SN 2007pk follow this behavior, also the SN 2010aj seems to follow the trend despite the scattering of some points due to the errors. The only exception to this smooth trend is SN 2005cs which shows a red spike at about 120d (when data of SN 2007od are missing). Such a red spike seems to mark low-luminosity SNe IIP in correspondence to the steep

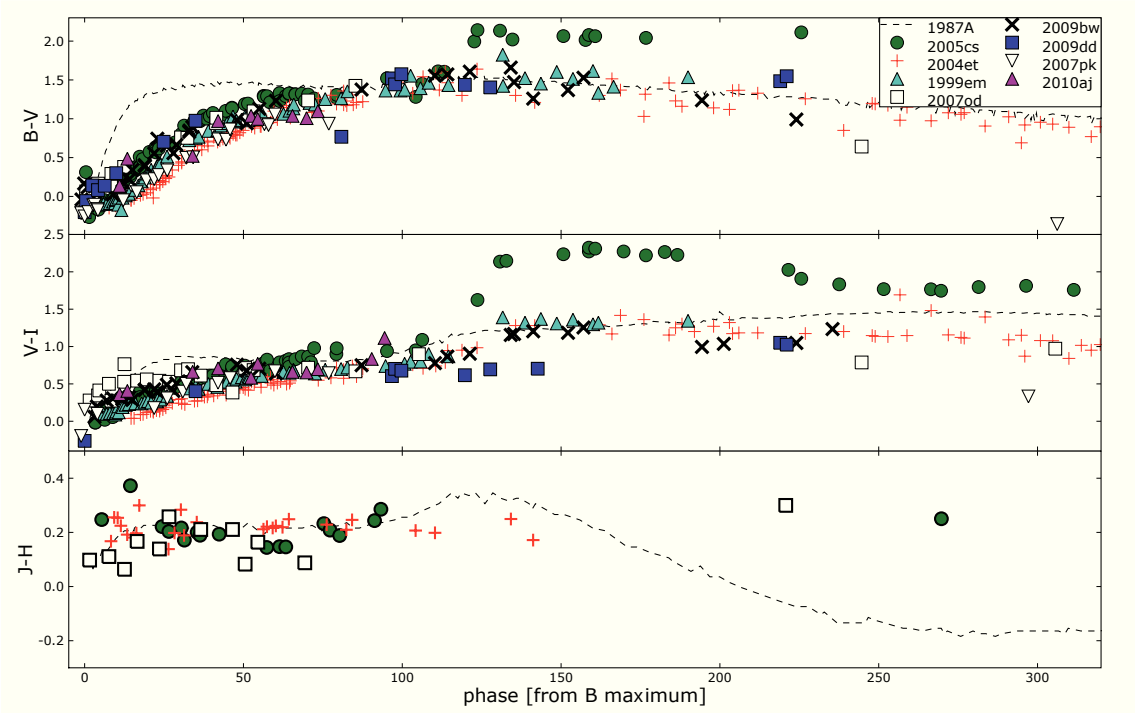

Figure 3.12: Comparison of the dereddened colours of SN 2007od, SN 2009bw, SN 2009dd, SN 2007pk, SN 2010aj, SN 1987A, SN 2005cs, SN 1999em and SN 2004et. The phase of SN 1987A is respect to the explosion date

post-plateau decline (174). The B–V trend of the SN 2009bw and SN 2009dd in the first day seems redder than normal type II as SN 1999em and more similar to that of SNe 2005cs and 2007od (cfr. Fig. 3.13). The last two points of SN 2009bw suggest a decrease to the blue faster than normal SN II and similar to SN 2007od, but the errors of these points are large.

The V–I colour of our sample increases in a linear fashion for all SNe IIP during the plateau phase, and remains roughly constant (∼0.5) during the nebular phase (Fig. 3.12). The colour evolution of SN 2007od is similar to that of other type IIP SNe, although it is redder at early phases, as for the SN 2010aj, and in a similar way also the SN 2009bw seems redder than the others. SN 2009dd shows a constant behaviour longer than the other SNe. The fast decline of the SN 2010aj light curves during the nebular phase can suggest an early dust formation, making the object a clone of SN 2007od. In the nebular phase, the colour curve of

SN 2007od seems to become bluer, especially the B–V curve, similarly to SN 2004et. Note, however, that such claim is based on a single point affected by large uncertainty. The other two SNe with nebular points in V–I (SN 2009bw and SN 2009dd) have the same behaviour of SN 2004et and SN 1999em. The last two points of SN 2009bw suggest a decrease to the blue faster than normal SN II and similar to SN 2007od, but the errors of these points are large. The similarity of SN 2007od with SN 2004et in the nebular phase is supported by the V–I colour evolution.

Only sparse data are available for type IIP SNe in the NIR, especially during the nebular phase, and also our sample show this lack, except the SN 2007od. For this reason in this domain we compared only a few well-studied, recent events such as SNe 2005cs and 2004et, plus the reference type II SN 1987A. Their J–H colour curves (Fig. 3.12) remain constant at J–H $\approx$ 0.2 mag until the phase of $\sim$ 120 days. For the later nebular phase, the single epoch J–H measurement of SN 2007od was found consistent with a similar measurement for SN 2005cs and very different from SN 1987A.

The (uvoir) bolometric light curves of our SNe sample (Fig. 3.14, 3.15 & 3.17) were obtained by converting the observed broad band magnitudes (in the available bands) into fluxes at the effective wavelengths, then correcting for the adopted extinctions (cfr. Sect. 3.2.1; 3.2.2; 3.2.3; 3.2.4; 3.2.5), and finally integrating the resulting Spectral Energy Distribution (SED) over wavelength, assuming zero flux at the integration limits. Fluxes were then converted to luminosity by using the distances adopted in Sect. 3.2.1; 3.2.2; 3.2.3; 3.2.4; 3.2.5. The emitted fluxes were computed at the phases in which R or V observations were available. When observations in a bandpass were unavailable in a given night, the magnitudes were obtained by interpolating the light curves using low-order polynomials, or were extrapolated using constant colours. In the SN 2007od, SN 2007pk and SN 2010aj cases, the pre-maximum bolometric is based mainly on R band observations and should be regarded as uncertain, especially for the SN 2010aj because of the reasons explained in Sec. 3.2.5.

SN 2007od is our best studied object. The peak of the uvoir bolometric light curve is reached very close in time to the R maximum, on JD^{bol}_{max} = 2454410.0 $\pm$ 2.0, and at a luminosity L_{bol} = 6.0 x 10^{42} erg s^{-1}. In Fig. 3.14, together

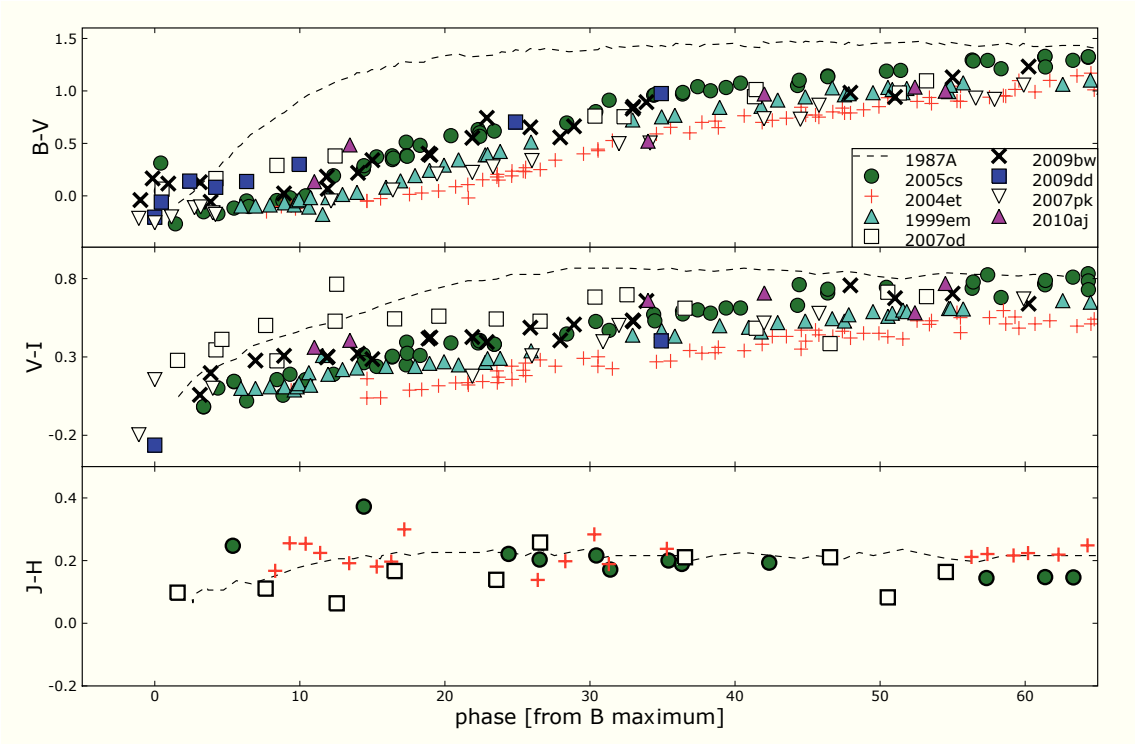

Figure 3.13: Zoom of Fig. 3.12 in the first 65d.

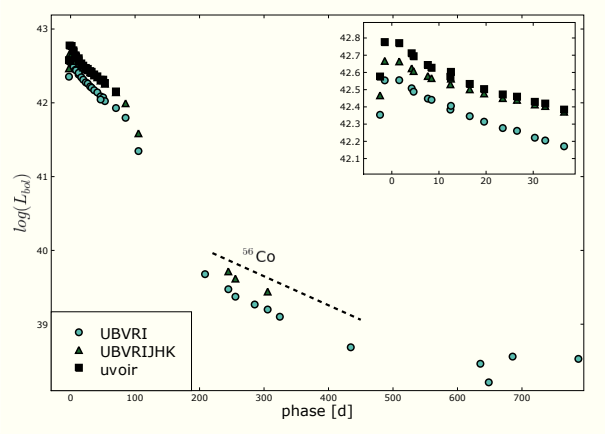

Figure 3.14: *uvoir* (black squares), UBVRIJHK (green triangles) and UBVRI (cyan circles) light curves of SN 2007od. Also reported is the extension of the UBVRI light curve to late phases obtained with data of Andrews *et al.* (4). The slope of ^{56}Co to ^{56}Fe decay is also displayed for comparison. A blow-up until 40d post maximum is shown in the upper–right corner. Distance modulus and reddening are those reported in Tab. 3.3.

with the uvoir light curve, we also plot the light curves obtained by integrating UBVRI and UBVRIJHK contributions only. The light curve (from U to K) of SN 2007od shows a significant NIR (JHK) contribution, as displayed in Fig. 3.16. The progressive rise of the NIR flux in the photospheric phase is similar to that of other SNe IIP while the contribution in the nebular phase is constant at least until ∼220d (Fig. 3.16). This result is similar to that found by Maguire *et al.* (139) for SN 2004et. As for individual bands, the nebular tail of the bolometric light curve closely matches the slope expected from the decay of ^{56}Co to ^{56}Fe, suggesting complete γ-ray trapping. The measured slope is $\gamma \sim 1.053$ mag $100d^{-1}$, close to the canonical value of $\gamma \sim 0.98$ mag $100d^{-1}$ of ^{56}Co decay. After day 500, the curve, based only on data by Andrews *et al.* (4), flattens.

The early luminosity of SN 2007od is comparable to those of the luminous SN 1992H and SN 2004et. The behavior of the light curve is certainly more similar to that of Type IIP SNe with respect to the Linear SN II 1979C proposed for comparison (the average decline rate by Patat *et al.* (180) is $\beta^B_{100}(07od) \sim 3.2$ mag $(100\mathrm{d})^{-1}$, typical of SN IIP). The similarity to SN 1992H is noticeable in

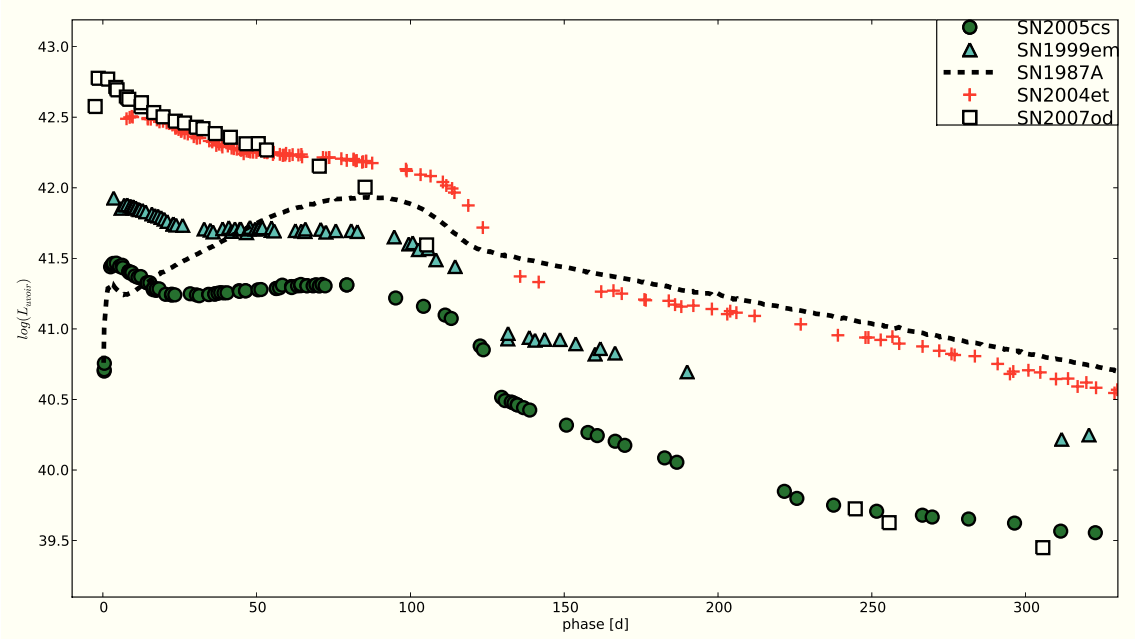

Figure 3.15: Comparison on the whole optical-to-NIR (UBVRIJHK) domain of SN 2007od with those of other type II SNe.

the photospheric phase where both SNe present the same early decline and short plateau, a possible evidence of a low-mass H envelope. On the other hand, the radioactive tail of SN 2007od is more than 1 dex fainter than that of SN 1992H.

The comparison among the bolometric light curves of our sample is reported in Fig. 3.15 & 3.17. The peak of the SN 2009bw bolometric (UBVRI) light curve is reached about the R maximum on JD^{bol}_{max} = 2454925.3± 2.0 at a luminosity L_{bol} = 2.6 x 10^{42} erg s^{-1}. Unfortunately, because of the lack of simultaneous optical–NIR observations it is impossible to obtain a true bolometric light curve for SN 2009bw. In fact extended coverage from B to K′ is available only in the late radioactive tail. The nebular tail of the bolometric light curve declines at a rate $\gamma \sim 1.06$ mag $(100d)^{-1}$, measured from 138d–239d since explosion, suggesting complete γ-ray trapping. However, we noticed that the tail can be divided into two different segments: a flatter one from 138d to 156d with $\gamma \sim 0.70$ mag $(100d)^{-1}$ resembling that of the early tail of SN 1999em and present in many SNe, and a second one (161d–239d) with $\gamma \sim 1.16$ mag $(100d)^{-1}$. The last two points at ∼234-240d seem to suggest a further increase of the decline rate, maybe

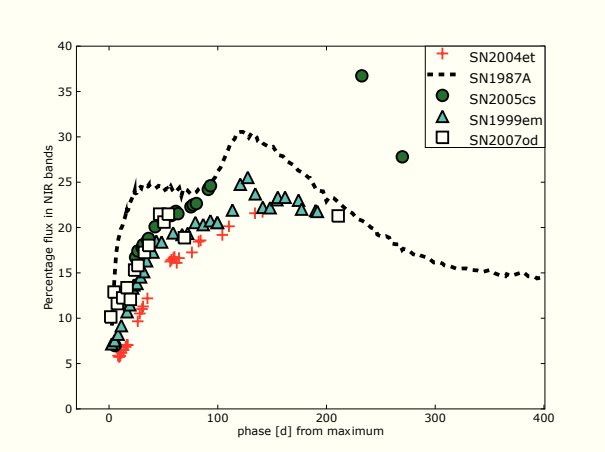

Figure 3.16: Flux contribution of NIR bands to the U-to-K bolometric light curve for a sample of SNe IIP.

due to dust formation. However, due to the relatively large errors this is not significant and we will not elaborate it any further.

The peaks of the SN 2009dd, SN 2007pk, SN 2010aj bolometric (UBVRI) light curve are reached around the R maximum (only for SN 2009dd is around the V maximum) on $JD^{bol}_{max} = 2454925 \pm 2.0$ at a luminosity $L_{bol} = 2.16$ x 10^{42} erg s^{-1}, on $JD^{bol}_{max} = 2454412.0 \pm 5.0$ at a luminosity $L_{bol} = 6.26$ x 10^{42} erg s^{-1} and on $JD^{bol}_{max} = 2455265.5 \pm 8.0$ at a luminosity $L_{bol} = 2.68$ x 10^{42} erg s^{-1}, respectively. The tail of the SN 2009dd bolometric light curve has slopes of $\gamma \sim 1.07$ mag $(100\mathrm{d})^{-1}$, close to that of the decay of ^{56}Co. Instead, the observations of SN 2010aj stop before the radioactive tail, in the last segment available $\gamma \sim 4.06$ mag $(100\mathrm{d})^{-1}$.

The comparison points out the large drop in magnitude ($\sim$ 6 mag) from the plateau to the radioactive tail of SN 2007od and its small amount of ^{56}Ni. Also evident is the fast drop of SN 2009bw and the early but slow transition to the nebular phase shown by SN 2010aj. The SNe chosen for the comparison are those reported in Tab. 3.21. Unfortunately, not many of them have spectral coverage from the optical to the NIR, and therefore the comparison was done either for UBVRIJHK (cfr. 3.15) or UBVRI (cfr. 3.17) bolometric curves.

The early luminosity of SN 2009bw, as those of SN 2009dd and SN 2010aj, are slightly lesser than the luminous SNe 2007od, 2004et, 1992H. The duration

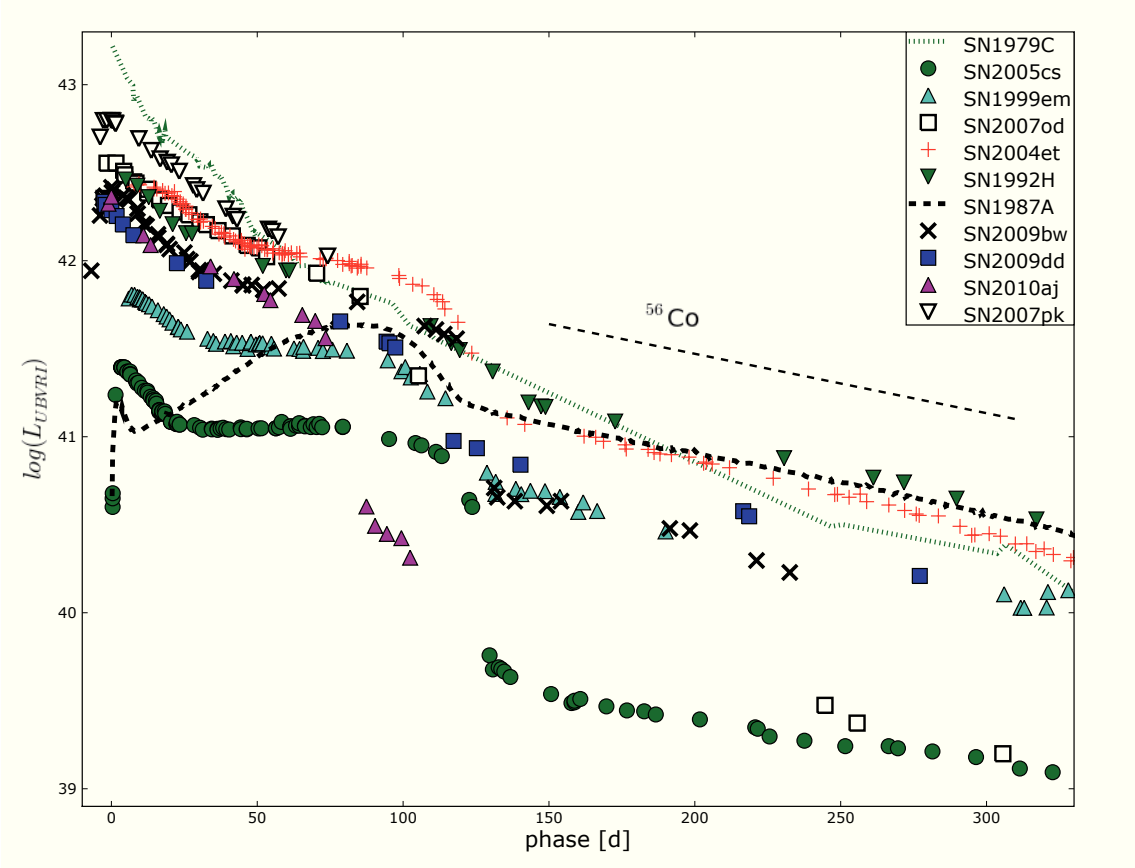

Figure 3.17: Comparison of quasi-bolometric light curves of our sample with those of other type II SNe. For SN 1992H the data are limited to BVR, while for SN 1979C are UBVR. Hence the reported values are lower limits The distances and reddenings adopted for the comparison with our SN sample are reported in Tab. 3.21. Minor misalignments in the epoch of maxima are due to the different epochs adopted for the maxima of the reference band light curve and the quasi-bolometric curve.

of the SN 2009bw plateau resembles that of SN 1999em, then longer than the peculiar SN 2007od. However, the luminosity drop from the plateau to the tail of the SN 2007od is much larger from that of SN 2009bw.

The SN 2009dd plateau luminosity is similar to that of SN 2009bw and SN 2010aj, but the drop in magnitude that leads the bolometric curve to the nebular phase occurs slightly before the other SNe of the comparison (except SN 2010aj) and it is similar in phase to that of SN 2007od.

In our sample only SN 2007pk shows a linear decline during the photospheric phase with a peak luminosity higher than all the other IIP and a behaviour resembling that of the type IIL SN 1979C. The average decline rate computed according Patat *et al.* (180) is $\beta^B_{100}(07pk) \sim 3.7$ mag $(100\mathrm{d})^{-1}$, typical of SN IIL. As written before, the peak luminosity of SN 2010aj is similar to that of SN 2009dd and SN 2009bw. It shows a dramatic drop from plateau similar to that of SN 2007od. This can suggest a progenitor with a small H layers and/or early dust formation as for SN 2007od.

The ^{56}Ni mass ejected in the nebular phase by our SNe can be derived by comparing the bolometric light curve (Fig. 3.17 or Fig. 3.15) to that of SN 1987A assuming a similar γ-ray deposition fraction

$$M(^{56}Ni)_{SN} = M(^{56}Ni)_{87A} \times \frac{L_{SN}}{L_{87A}} M_{\odot} \tag{3.1}$$

where $\mathrm{M}(^{56}\mathrm{Ni})_{87A} = 0.075 \pm 0.005$ $\mathrm{M}_{\odot}$ is the mass of ^{56}Ni ejected by SN 1987A (5), and L_{87A} is the bolometric luminosity at comparable epoch. The comparison gives $\mathrm{M}(^{56}\mathrm{Ni})_{07od} \sim 0.003$ $\mathrm{M}_{\odot}$, $\mathrm{M}(^{56}\mathrm{Ni})_{09bw} \sim 0.022$ $\mathrm{M}_{\odot}$, $\mathrm{M}(^{56}\mathrm{Ni})_{09dd} \sim 0.034$ $\mathrm{M}_{\odot}$. We can not evaluate with this method the $\mathrm{M}(^{56}\mathrm{Ni})_{10aj}$ because at the phase available neither SN 1987A nor SN 2010aj are on the nebular tail, instead we can not evaluate the $\mathrm{M}(^{56}\mathrm{Ni})_{07pk}$ because of the lack of nebular data. Making the reasonable assumption that γ-rays from ^{56}Co decay are fully thermalized at this epoch, we crosschecked these results with the formula

$$M(^{56}Ni)_{SN} = (7.866 \times 10^{-44})\, L_t exp\left[\frac{(t-t_0)/(1+z)-6.1}{111.26}\right] M_{\odot} \tag{3.2}$$

from Hamuy (94), where t_0 is the explosion epoch, 6.1d is the half-life of ^{56}Ni and 111.26d is the e-folding time of the ^{56}Co decay, which releases 1.71 MeV and

3.57 MeV respectively as γ-rays (36, 257). This method provides $M(^{56}Ni)_{07od} \sim$ 0.003 $M_\odot$, fully consistent with the previous estimate, $M(^{56}Ni)_{09bw} \sim$ 0.021 $M_\odot$, $M(^{56}Ni)_{09dd} \sim$ 0.027 $M_\odot$ and $M(^{56}Ni)_{10aj} \sim$ 0.004 $M_\odot$ as upper limit (taken on the last available epoch). Despite the lack of NIR data, the reliability of Eq. 3.2 is supported by the little contribution of the NIR bands at the nebular phase ($\sim$20%–15% of total flux, cfr 3.16). These results find graphic confirmation from the inspection of Fig. 3.17.

The luminous plateau of SN 2007od, comparable with that of the brightest SNe IIP, coupled to an under-luminous tail is very unusual (175). In Sect. 3.4 we will show that on day 310 (but also in the spectra on day 226 by Andrews *et al.* (4)) there is evidence of dust formation. Thus the low luminosity in the nebular phase may be due not only to a low ^{56}Ni production. The value determined above should be considered as a lower limit. Indeed, the late-time MIR (mid infrared) data published from Andrews *et al.* (4) allows us to study the SED up to the M band. The IR bands show clear evidence of strong blackbody emission due to the re-emission of radiation absorbed at shorter wavelengths. Adding this contribution to the bolometric flux, Eq. 3.2 provides $M(^{56}Ni)_{07od} \sim 0.02$ $M_\odot$ at the first two epochs of MIR observations. The estimate on a third epoch is less reliable because based only on 3.6 and 4.5 μ observations. We address the issue of dust formation in Sec. 3.6.

Good sampling of the end of the plateau phase and the beginning of the radioactive tail allows us to estimate the steepness function S (maximum value at the transition phase of the first derivative of the plateau absolute visual magnitude) and in turn the ^{56}Ni mass using the method devised by Elmhamdi, Chugai, and Danziger (67). We evaluated $S = 0.57$ corresponding to 0.002 $M_\odot$ of ^{56}Ni, typical of faint CC-SNe and very different from the previous estimates. The S value is larger than in all SNe of the sample of Elmhamdi, Chugai, and Danziger (67) and extremely different from the values of SN 1992H ($S = 0.048$) and SN 1999em ($S = 0.118$). This result suggests that in this case the anti-correlation between steepness function and ^{56}Ni mass does not work, implying something uncommon in the hight photospheric luminosity or a transition masked by some effect. We will address this issue on Sect. 3.7.2.2.

To summarize, the unusual behavior of the SN 2009bw bolometric light curve lies in: the luminous plateau coupled with a luminosity tail typical of normal type IIP (e.g. SN 1999em) and the very rapid drop (2.2 mag in 13d) from the plateau to the tail giving $S = 0.57$.

The behaviour of SN 2009dd is quite common, the only peculiarity is the short plateau similar to that of SN 1992H, instead the begin of the nebular phase of SN 2010aj after ∼80d is anomalous and maybe due to an early dust formation.

3.4 Spectroscopy

In this Section we present the spectroscopic evolution of the five luminous SNe introduced in the Sect. 3.2. The journals of spectroscopic observation are reported in Tab. B.1; B.2; B.3; B.4; B.5. All reductions and part of the observation have been obtained during this thesis.

SN 2007od and SN 2009bw have been well monitored at all phases, the SN 2007pk has a good coverage during the early three months plus a number of nebular spectra, instead for the SN 2009dd and SN 2010aj only 6 and 5 spectra, respectively, are available. The spectra of SN 2007pk, SN 2009dd and SN 2010aj are shown here for the first time, while those of SN 2007od and SN 2009bw are published during the preparation of this thesis (114, 116).

The temporal coverage is different for various objects because of the imperceptibility of explosion, weather conditions and availability of telescopes. Nevertheless, also for those not well sampled we can provide the photospheric velocities and the continuum temperatures. Thanks to a semi-analitical code (described in detail in 261) and a radiation-hydrodynamics code (described in detail in Pumo, Zampieri, and Turatto (195) and Pumo & Zampieri, submitted), we can estimate the physical parameters of the explosions with these data (cfr. Sect. 3.7).

3.4.1 SN 2007od

Fig. 3.18 shows the entire evolution of SN 2007od from the first spectrum (near the R-band maximum) to about 1 year later. The evolution is very well sampled

in the photospheric phase. As for the photometry, the transition from photospheric to nebular stages was not observed because the SN was behind the Sun. Line identification at two epochs is shown in Fig. 3.19. It relies on qualitative arguments based on the presence of lines of the same ions at consistent velocity and by comparison with template spectra of other SNe IIP, e.g., 2005cs (173), 2004et (139) and 1999em (17, 68, 175). For most of them detailed line identification was carried out also with spectral modeling (we have to remember that also for SN 2007od we will show a spectral modeling).

The first spectra (5-13 days) are characterized by a blue continuum, yet cooler than those of SNe 1999em and 2005cs. The most prominent features (Fig. 3.19, top) are the H Balmer lines and He I λ5876, all with a normal P-Cygni profile except Hα which shows a weak absorption component and a boxy emission. This profile, which resembles a detached atmosphere profile (120), might be the signature of a weak interaction with a low density CSM (e.g. SN 1999em 190). Two absorption features are worth mentioning: one is prominent on the blue side of Hβ at about 4440Å (marked as high velocity, HV Hβ in Fig. 3.19 Top), the other, much fainter, on the blue side of Hα, at about 6250Å in the first spectrum (marked as Si II in Fig. 3.19 top). These lines were noted before in the spectra of SNe IIP. In the case of SN 2005cs (173) the feature near 4440Å was identified as N II λ4623, supported by the presence of another N II line at about 5580Å. The latter line is not seen in the spectra of SN 2007od at the expected position. Baron *et al.* (17) discussed such lines in an early spectrum of SN 1999em. While the parametrized `SYNOW` code suggested that the 4400Å feature was consistent with N II, the non-LTE code `PHOENIX` rejected this identification because of the absence of the feature around 5580Å. Instead, the positions of both features were consistent with being Balmer lines produced in a high–velocity (HV) layer. Such combined identification does not seem plausible in the case of SN 2007od because the expansion velocity of the HV Hβ line is much faster than that of the putative HV Hα (25000 vs. 15000 $\mathrm{km\,s^{-1}}$).

In our first set of spectra (5d - 13d), another absorption line is visible around 3980Å, between Hγ and the H&K doublet of Ca II. This feature (marked as HV Hγ in Fig. 3.19 top) has the same velocity of the mentioned HV Hβ ($\sim$ 25000 $\mathrm{km\,s^{-1}}$) and might therefore be produced in the same layer. Up to phase $\sim$ 13d

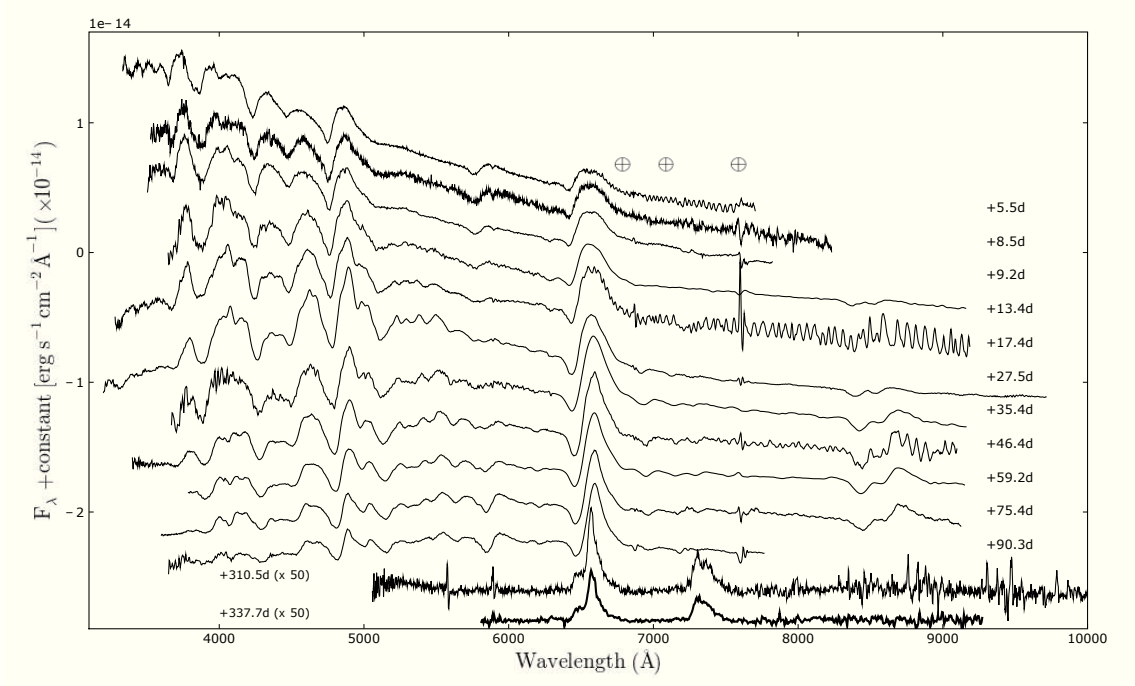

Figure 3.18: The overall spectral evolution of SN 2007od. Wavelengths are in the observer's rest frame. The phase reported for each spectrum is relative to the explosion date (JD 2454404). The $\oplus$ symbols mark the positions of the strongest telluric absorptions. The ordinate refers to the top spectrum; the other spectra are shifted downwards with respect to the previous one by 2×10^{-15} (second spectrum), 4.3×10^{-15} (third) and 2.2×10^{-15} erg s^{-1} cm^{-2} Å^{-1}(others).

the trend of these lines is the same. From day 17 the HV Hγ disappears, likely hidden by the increasing strength of metal lines such as Fe II and Ti II. We suggest that these are indeed HV Balmer lines and that the HV Hα component is missing because Hα level is mostly populated collisionally, similarly to what is seen in SN IIL (34). This difference among the Balmer lines can be noted also in the early spectra of SN 1993J, which showed a more pronounced P-Cygni absorption for Hβ and Hγ than for Hα.

In the early spectra of SN 2007od, H&K of Ca II and a combination of Fe I, Ti II and Sc I around 4000Å are also identified. The line at about 6250Å is probably Si II λ6355 as suggested by the expansion velocity, consistent with that of the other metal ions. The presence of Si II is fully blown at early times in type Ia, but also proposed in several type II SNe such as 2005cs (173), 1992H (52), 1999em (58) and 1990E (208). In the spectrum of November 12 (phase = 13.4 days) a faint feature appears at about 6200Å and is probably due to Sc II (λ6300) or Fe II (λ6305). In this spectrum there is also evidence of a feature at about 6375 Å, close to the blue edge of the Hα absorption, possibly due to Fe II λ6456. The 13.4d spectrum, the first extending to 1 micron, shows the presence of the Ca II IR triplet ($\lambda\lambda$ 8498, 8542, 8662).

In the subsequent set of spectra (phase 17-90 days) a number of well developed features with P-Cygni profiles appear, in addition to the persistent Balmer lines of H (Fig. 3.19, bottom). In the region between Hβ and Hγ, a group of lines identified as Sc II, Ti II and Fe II around 4420Å, Ba II at λ4450 and Sc II λ4670 (on the blue side of Hβ) become more prominent than in earlier spectra. At this phase several other metal lines appear. The Fe II multiplet 42 lines ($\lambda\lambda$ 4924, 5018, 5169) are visible to the red side of Hβ along with Fe I and Sc II in the region between 5200Å and 5500 Å and, starting from day 17, Sc II λ5658. Other features are identified as a blend of Ba II λ4997 and Sc II λ5031 on the red side of Hβ and Sc II λ6245. On day 27 the He I λ5876 line is weak and blended with Na ID which becomes progressively stronger and replaces He I in subsequent spectra.

The presence of C I lines in spectra of type IIP SNe was claimed in some objects, e.g., in SNe 1995V (72) and 1999em (175). In spectra of SN 2007od at $\sim$ 75 days a faint absorption on the red wing of Ca II IR triplet could be attributed to C I λ9061 but no other C I lines are visible to support this finding.

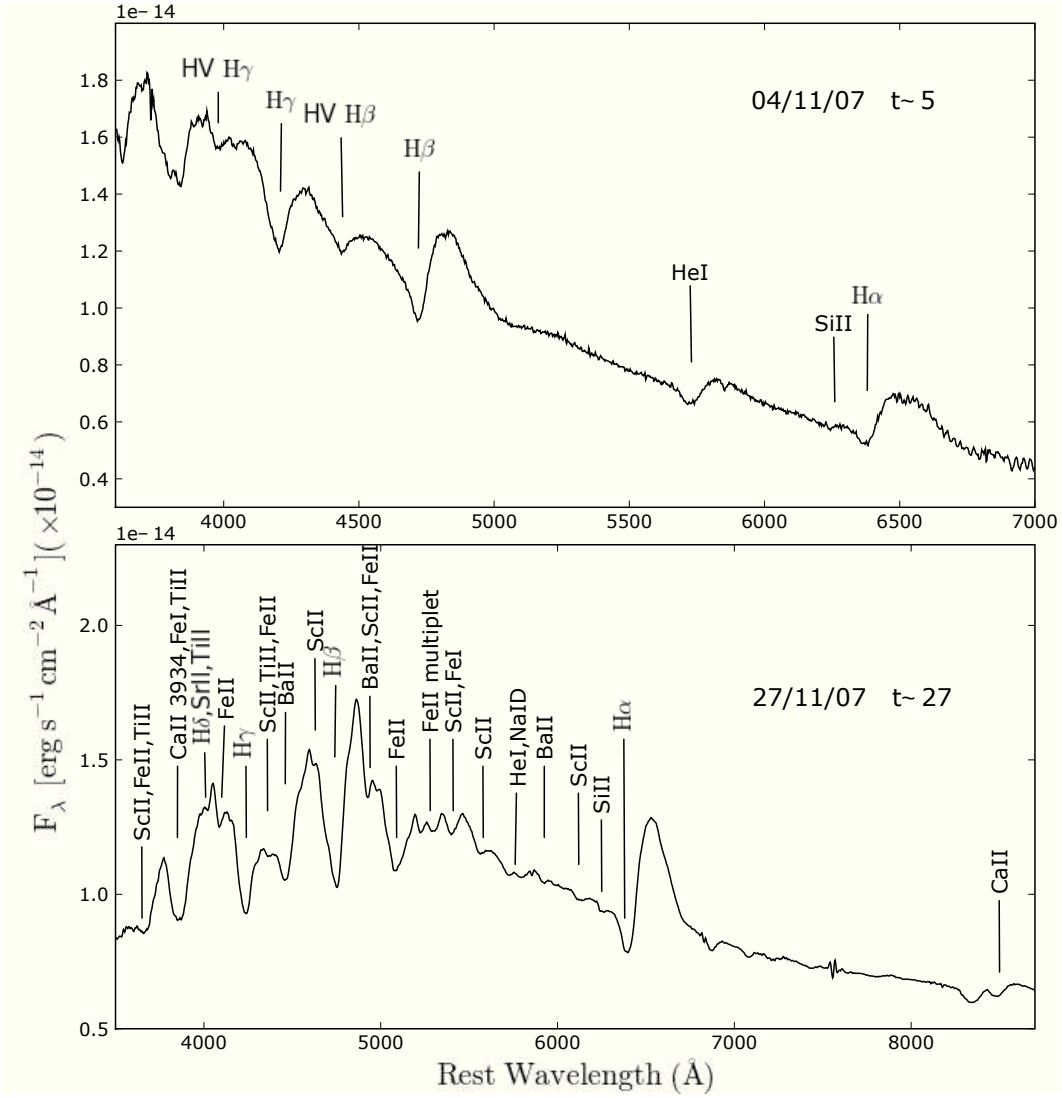

Figure 3.19: Top: optical spectrum of SN 2007od, obtained 5 days past explosion (JD 2454404). Bottom: optical spectrum of SN 2007od, 27 days past explosion. Both spectra have been corrected for absorption in our galaxy and corrected by redshift. The most prominent absorptions are labelled.

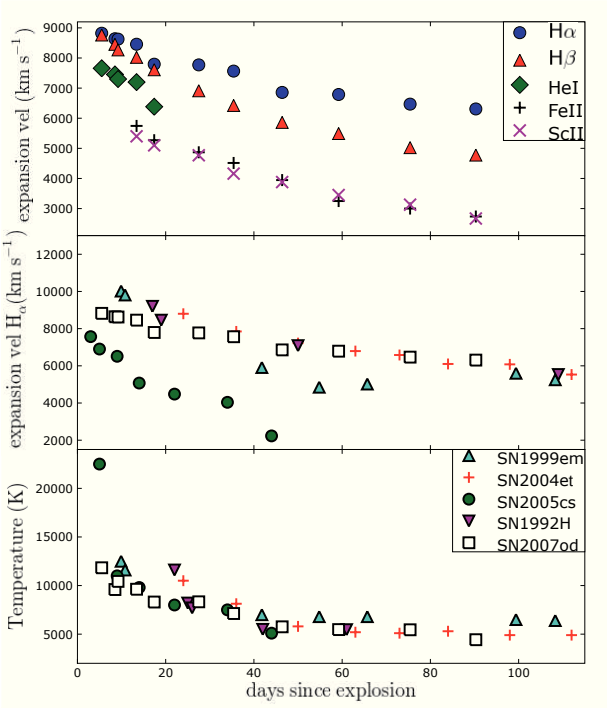

Figure 3.20: Top: expansion velocity of Hα, Hβ, He I λ5876, Fe II λ5169 and Sc II λ6246 as measured from the minima of the P-Cygni profiles. Middle: comparison of the Hα velocity of SN 2007od with those of other SNe II. Bottom: Evolution of the continuum temperatures T_{bb} for the same SN sample.

Two spectra are available in the nebular phase (310-338 days). In both spectra the peaks of the Hα emission are blue-shifted by the same amount ($\sim$1500 km s^{-1}). The line shows a multi–component structure that will be discussed in Sec. 3.6. These spectra show also forbidden emission lines of [Ca II] $\lambda\lambda$7291, 7324, and weak evidence of [O I] $\lambda\lambda$6300, 6364 and [Fe II] λ7155, which are common features in SNe IIP.

The expansion velocities of Hα, Hβ, He I 5876Å, Fe II 5169Å and Sc II 6246Å, derived from fits to the absorption minima, are reported in Tab. 3.22 and plotted in Fig. 3.20 (Top panel). Error estimates are derived from the scatter of several independent measurements. The velocities of Hα are comparable with those of Hβ during the first 20 days, and progressively higher afterwards. During the 20 days in which the He I line remains visible the velocity is about 1000 km s^{-1} smaller

Table 3.22: Observed black-body temperatures and expansion velocities of SN 2007od.

JD +2400000	Phase* (days)	T (K)	v($H\alpha$) ($\mathrm{km\,s^{-1}}$)	v($H\beta$) ($\mathrm{km\,s^{-1}}$)	v(He I) ($\mathrm{km\,s^{-1}}$)	v(Fe II) ($\mathrm{km\,s^{-1}}$)	v(Sc II) ($\mathrm{km\,s^{-1}}$)
54409.5	5.5	11830 ± 350	8822 ± 104	8764 ± 164	7658 ± 122		
54412.5	8.5	9591 ± 350	8639 ± 62	8455 ± 140	7454 ± 150		
54413.2	9.2	10429 ± 350	8626 ± 60	8270 ± 140	7301± 100		
54417.4	13.4	9620 ± 350	8457 ± 82	8023 ± 150	7199 ± 105	5745 ± 132	5400± 200
54421.4	17.4	8305 ± 350	7794 ± 66	7610 ± 114	6382 ± 137	5270 ± 280	5100 ± 200
54431.5	27.5	8328 ± 350	7771 ± 75	6912 ± 130		4869 ± 200	4770 ± 110
54439.4	35.4	7123 ± 350	7565 ± 75	6425 ± 400		4515 ± 110	4161± 250
54450.4	46.4	5755 ± 350	6857 ± 75	5863 ± 133		3946 ± 120	3880 ± 200
54463.2	59.2	5470 ± 350	6788 ± 75	5493 ± 128		3250 ± 116	3450 ± 300
54479.4	75.4	5450 ± 350	6468 ± 95	5024 ± 100		3001± 120	3130 ± 200
54494.3	90.3	4429 ± 350	6308 ± 101	4777 ± 102		2736 ± 110	2670 ± 100

* with respect to the explosion epoch (JD 2454404)

than that of Hα. Fe II velocity, which is a good indicator for the photospheric velocity because of the small optical depth, is lower than that of H and He I, and decreases below 3000 $\mathrm{km\,s^{-1}}$ at about three months. Sc II is also a good indicator of the photospheric velocity and its velocity is very close to that of Fe II, supporting the identifications of both ions.

In Fig. 3.20 (middle) we compare the Hα velocity evolution of SN 2007od with those of our comparison sample of type IIP. In the first months, the Hα velocity of SN 2007od is comparable to those of SN 1999em, SN 2004et, SN 1992H, and higher than that of SN 2005cs, which is known to have slow photospheric expansion. As a major difference from other objects the velocity decrement is always rather constant, even in early phases. The early velocity of SN 2007od, lower than those of the other SNe of our sample, might be attributed to early-phase interaction with a low density, thin CSM.

The early spectra of SN 2007od are fairly blue, suggesting moderately hot black-body temperatures ($T_{bb} = 1.1\times10^4$ K). temperature evolution of SN 2007od is rather normal, although its temperature during the very first days past explosion never reached 12000 K. About 40 days after explosion the temperature becomes constant, in analogy to what observed in SNe 2004et, 1999em and 1992H.

This phase corresponds to the beginning of the H envelope recombination.

3.4.2 SN 2009bw

Fig. 3.21 shows that the entire evolution of SN 2009bw from ∼2 days before maximum to over six months past peak, well sampled both in the photospheric and nebular stages. The evolution is well sampled in photospheric and in the transition from the photospheric to nebular stages. Line identification was made by mean of the parametrized LTE code SYNOW (17, 78) and will be presented in Sec. 3.5.2.

The first spectrum, used for classification by Stanishev, Adamo, and Micheva (221), shows a blue continuum typical of SNe II at the same age. An unusual, prominent feature at 4600Å appears near maximum. The feature is not present in the subsequent spectrum (18d), and is most likely related to the SN since it is relatively broad (FWHM∼140Å) and has a short life. No significant emission of the underlying HII region, well seen at other wavelengths, is present in this range even in the deepest nebular spectra (N II, N III, O II and forbidden Fe III lines are present in the spectra of typical HII regions at about 4600Å, cfr. 231). The FWHM of the 4600Å feature corresponds to a velocity v∼9100 $\mathrm{km\,s^{-1}}$, larger than the velocity of Hα∼7000 $\mathrm{km\,s^{-1}}$, leading us to explore the possibility of a very special line formation mechanism or to a very peculiar line blending. Concerning the opacity, its component related to the bound free process has a saw-tooth behaviour and in this wavelength region, in a window of the order of 10^2 Å, it is in a minimum (202). Assuming the decrease of the opacity, the emission from lines due to highly ionized elements like N III, N IV and C V is allowed. On the other hand, we can not exclude the possibility of an extreme toplighting effect (concerning a flip of the P-Cygni profile, see 32) relative to Hβ and not observed in the Hα due to a difference in the optical depth (maybe due to the interaction). However to observe this effect the interaction should be really strong and anything in the light curve suggests such strong interaction. Actually, the comparison with SN 2006bp and SN 1998S shown in panel a) of Fig. 3.33 (top panel) suggests the identification of this feature as a blend of highly ionized N and C. Indeed, the feature is closer to that observed in SN 1998S, identified by

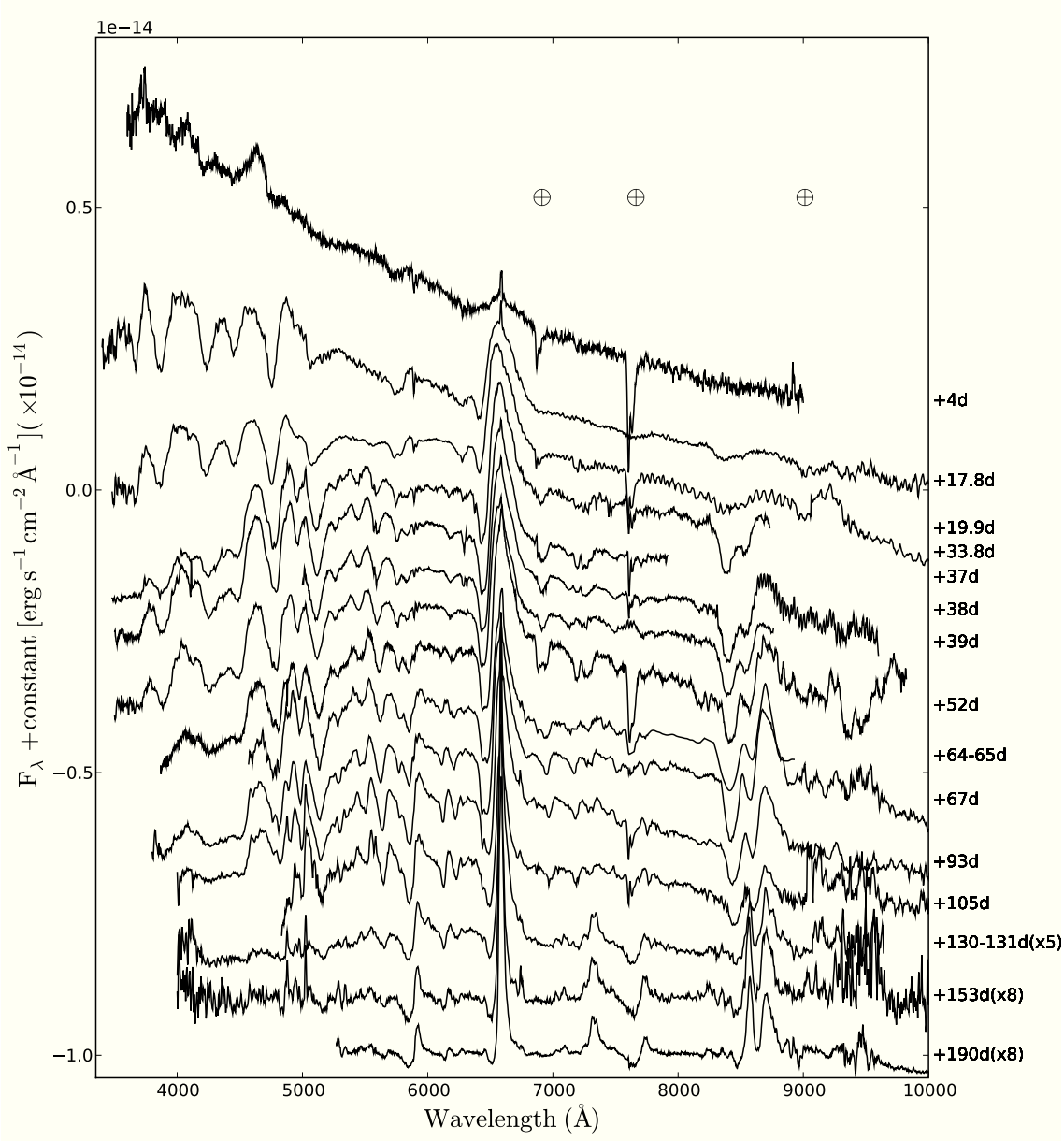

Figure 3.21: The overall spectral evolution of SN 2009bw. Wavelengths are in the observer rest frame. The phase reported for each spectrum is relative to the explosion date (JD 2454916.5). The $\oplus$ symbols mark the positions of the most important telluric absorptions. The ordinate refers to the first spectrum. The second spectrum is shifted downwards by 2×10^{-15} units, the third by 3.3×10^{-15} units with respects to the second, others by 1.5×10^{-15} erg s^{-1} cm^{-2} Å^{-1} with respect to the previous.

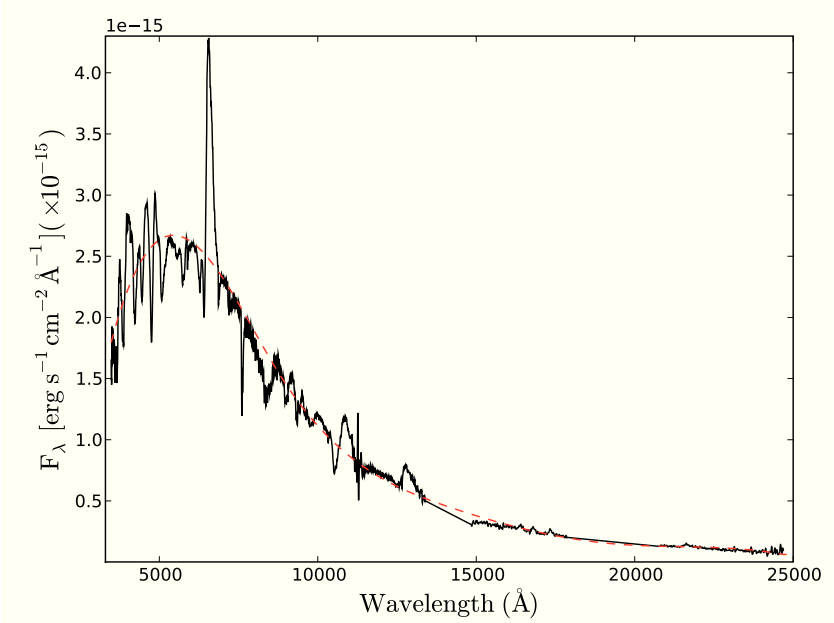

Figure 3.22: Composed spectrum of SN 2009bw, from optical to NIR, at $\sim$ 20d past explosion date (JD 2454916.5). A black body fit at $\sim$7900 K is over-plotted.

Fassia *et al.* (71) as CIII/NIII emission, rather than that in SN 2006bp attributed to He II λ4686 by Quimby et al. (197).

The spectra at 18 and 20 days are characterized by a blue continuum, comparable to that of SN 1992H and slightly bluer than that of SN 1999em at a similar age. For the visible spectral features we identified H Balmer lines, He I 5876Å and some Fe II multiplet lines. The line at about 6250Å has been identified as Si II λ6355 with expansion velocity comparable to those the other metal ions. As written above the presence of Si II is full blown in CC-SNe. In this set of spectra a narrow Hα emission due to an underline H II region is visible.

In the NIR spectrum (20d), combined with the optical spectrum of 19.8d (Fig. 3.22), are visible the P-Cygni profile of Paschen series. Especially of Paschen β, γ, δ. The Paschen γ is blended with He I λ10830, that has a velocity greater (Δv$\sim$2200 km s^{-1}) than the He I 5876Å.

The subsequent set of spectra (33-39 days) shows well developed P-Cyg profiles of Balmer and metal lines. Sc II λ5031 on the red side and Sc II λ4670 on

the blue side of Hβ are visible, as well as the Fe II multiplet 42 lines ($\lambda\lambda$ 4924, 5018, 5169), Fe II at about 4500Å, Fe I, and Sc II in the region between 5200Å and 5500 Å. Starting from day ∼34, the He I λ5876 forms a blend with the Na ID. The Ca II IR triplet ($\lambda\lambda$ 8498, 8542, 8662) is well developed, while the H&K Ca II feature blends with Ti II. O I at about 7700Å starts to be visible. Si II λ6355 has now disappeared, and the bottom of the Hα absorption shows a flat profile. We address this issue up ahead.

In late plateau phase the spectra continue to show the elements identified at earlier phases, complemented by Ba II and Ti II, whose presence indicate a temperature of ∼5000 K. Both ions are required for explaining several features between 4000 and 5000 Å. In particular, Ba II λ6142 is also clearly visible. Probably in this phase there is also the presence of Ba I that contributes to the blending of the metal lines in the range 5000–6000Å and of Mg II around 9140Å as visible in Fig. 3.47. Interesting line identifications are in the red side (>7000Å) of these spectra, where absorption lines due to the elements of CNO cycle appear. We will address this issue in Sec. 3.5.2.

Three nebular spectra of SN 2009bw have been collected between 130 and 190 days. A narrow component appears at the host galaxy rest position, confirming that it is due to an underlying H II region. The broad Hα emission, attributed to the SN ejecta, is also centered at the rest wavelength and shows a residual absorption. Na ID and Ca II IR triplet absorptions are clearly visible. The spectra show also evidence of the forbidden emission of the [Ca II] $\lambda\lambda$7291, 7324 doublet. Compared to other SNe IIP (cfr. Fig. 3.35) the absence of [O I] $\lambda\lambda$6300,6363 even in the latest available SN 2009bw spectrum, and the relatively narrow lines (FWHM(Hα) ∼1900 $\mathrm{km\,s^{-1}}$) are a peculiarity.

The photospheric expansion velocities of Hα, Hβ, He I λ5876, Fe II λ5169 and Sc II λ6246 are reported in Tab. 3.23 and plotted in Fig. 3.23 (top panel). They have been derived through the minima of P-Cygni profiles. Error estimates have been derived from the scatter of several independent measurements. Hα is always the strongest line, and the derived velocities are systematically the largest. During the first 20 days when He I λ5876 dominates over Na ID, the He I velocity is comparable with that of Hβ. The Fe II velocity, which is considered to be a good indicator for the photospheric velocity because of the small optical depth,

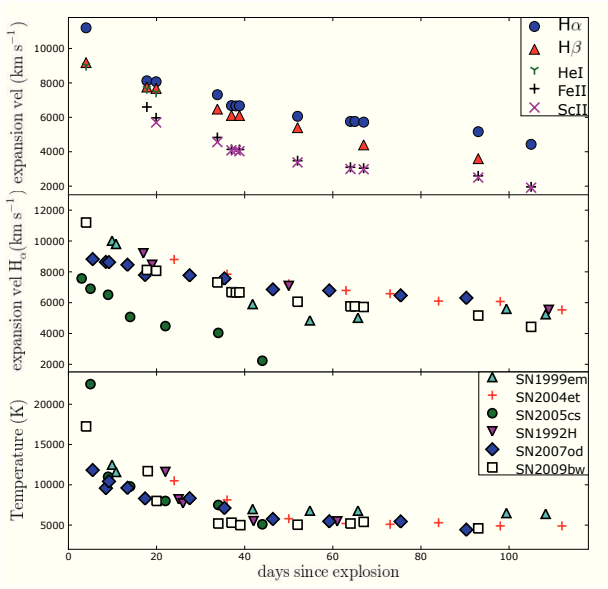

Figure 3.23: Top: expansion velocity of Hα, Hβ, HeI λ5876, FeII λ5169 and Sc II λ6246 measured from the minima of P-Cygni profiles. Middle: comparison of the Hα velocity of SN 2009bw with those of other SN II. Bottom: Evolution of the continuum temperature of SNe 2009bw, 2007od, 1999em, 2004et, 2005cs, 1992H.

Table 3.23: Observed blackbody temperature and photospheric velocities of SN 2009bw.parameters for SN 2009bw. For the Balmer lines the velocities were measured on the red wing component.

JD +2400000	Phase* (days)	T (K)	v(H_α) (km s^{-1})	v(H_β) (km s^{-1})	v(He I) (km s^{-1})	v(Fe II) (km s^{-1})	v(Sc II) (km s^{-1})
54920.5	4.0	17250 ± 1000	11200 ± 2000	9180 ± 1200	9000 ± 500		
54934.3	17.8	11700 ± 700	8122 ± 200	7760 ± 120	7658 ± 122	6600 ± 400	
54936.3	19.8	8000 ± 500	8067 ± 80	7682 ± 150	7454 ± 100	5970 ± 400	5700 ± 600
54950.3	33.8	5200 ± 400	7313 ± 300	6480 ± 300		4828 ± 300	4560 ± 200
54953.5	37	5300 ± 500	6680 ± 200	6110 ± 200		4138 ± 100	4080 ± 140
54954.5	38		6660 ± 300				4080 ± 140
54955.3	38.8	5000 ± 500	6670 ± 200	6109 ± 130		4130 ± 100	4030 ± 200
54968.5	52	5050 ± 250	6060 ± 60	5400 ± 400		3480 ± 100	3380 ± 120
54980.5	64	5200 ± 300	5760 ± 300			3097 ± 80	3000 ± 200
54981.5	65		5759 ± 180			3000 ± 200	
54983.5	67	5400 ± 300	5720 ± 300	4400 ± 230		3045 ± 150	2980 ± 200
54509.5	93	4600 ± 200	5165 ± 150	3600 ± 180		2600 ± 300	2500 ± 150
55021.5	105		4430 ± 100			1960 ± 300	1910 ± 110

* with respect to the explosion epoch (JD 2454916.5)

is lower than those of H and He, reaching 3000 km s^{-1} at about two months. Sc II is also a good indicator of the photospheric velocity and indeed its velocity is very close to that of Fe II, supporting the identification of the lines of both ions.

In Fig. 3.23(middle) we compare the Hα velocity evolution of SN 2009bw with those of the type IIP SNe. The velocity of SN 2009bw in the two months is comparable to those of type IIP as SNe 1999em, 2004et, 1992H and 2007od but higher than that SN 2005cs known to have an exceptionally slow photospheric expansion. Afterwards, the photospheric velocity of SN 2009bw slowly decreases, showing a trend that is slightly different from that of other type II SNe. This may be attributed to the presence of a moderate/low-density CSM that changes the shape of the absorption profile of Hα (see Sec. 3.7.2.2).

In Fig. 3.23 (bottom) the evolution of the photospheric temperature, derived from a blackbody fit to the spectral continuum, is shown and is compared to those of the reference sample. We already mentioned that the first spectrum of SN 2009bw is quite blue, indicating high black-body temperatures (1.7±0.1 x 10^4 K). The temperature remains high also at the second epoch (∼18d). Nevertheless,

the temperature evolution of SN 2009bw is normal and not so different from those of the other SNe in the sample: its ejecta is probably hotter in the first month (similar to SN 1992H) and marginally cooler than average from the plateau onward.

3.4.3 SN 2009dd

Fig. 3.24 shows the entire evolution of SN 2009dd from ∼10d post explosion to about fourteen months. In the last spectrum however it is difficult to recognize the SN spectrum from the galaxy background.

The first spectrum shows a blue continuum comparable to other SNe at this stage. It is characterized by line absorptions of Balmer series, He I λ5876 and Fe II multiplet lines ($\lambda\lambda$ 4924, 5018, 5169) are also visible as the H&K of Ca II. The interesting features of this spectrum are in the region of 6200Å where three absorption components lie on the blue side of Hα. The blue one, at ∼6174Å is related to Si II, with expansion velocity comparable to those of the other metal ions and it is confirmed in type II SNe (e.g. SN 1992H, SN 2007od, SN 2009bw). The other one seems to be related with possible metal ions at these wavelengths as Fe II λ6456, because of its velocity, even if the strength of the line suggest an optical depth uncommon for metal lines at this stage. As a matter of fact also the Fe II multiplet has a strength uncommon for this phase. The possibility of an HV Hα is intriguing, but no other HV lines related to Balmer series are clearly visible, as for the Hβ where a rough absorption profile is visible at ∼4620Å, but the velocity of this line should be higher than the putative HV Hα (HV Hα 13800 $\mathrm{km\,s^{-1}}$, HV Hβ 14800 $\mathrm{km\,s^{-1}}$). The presence of HV features could be related to an early interaction with a CSM, supported also by the X-ray observations, but we do not have other spectra at this phase to stress this issue.

The second spectrum is in the plateau phase and shows well developed P-Cygni profiles for Balmer lines and many metal elements as Fe II at ∼4500 and Sc II λ5031 on the red side of Hβ. Fe I and Sc II are visible at about 5500Å, while Na ID has replaced the He I. Other metal lines clearly visible between Na ID and Hα are Ba II λ6142 and Sc II λ6245. In the red side (>7000 Å) is visible the Ca II IR triplet ($\lambda\lambda$ 8498, 8542, 8662) and maybe the N II at ∼8100Å, even if

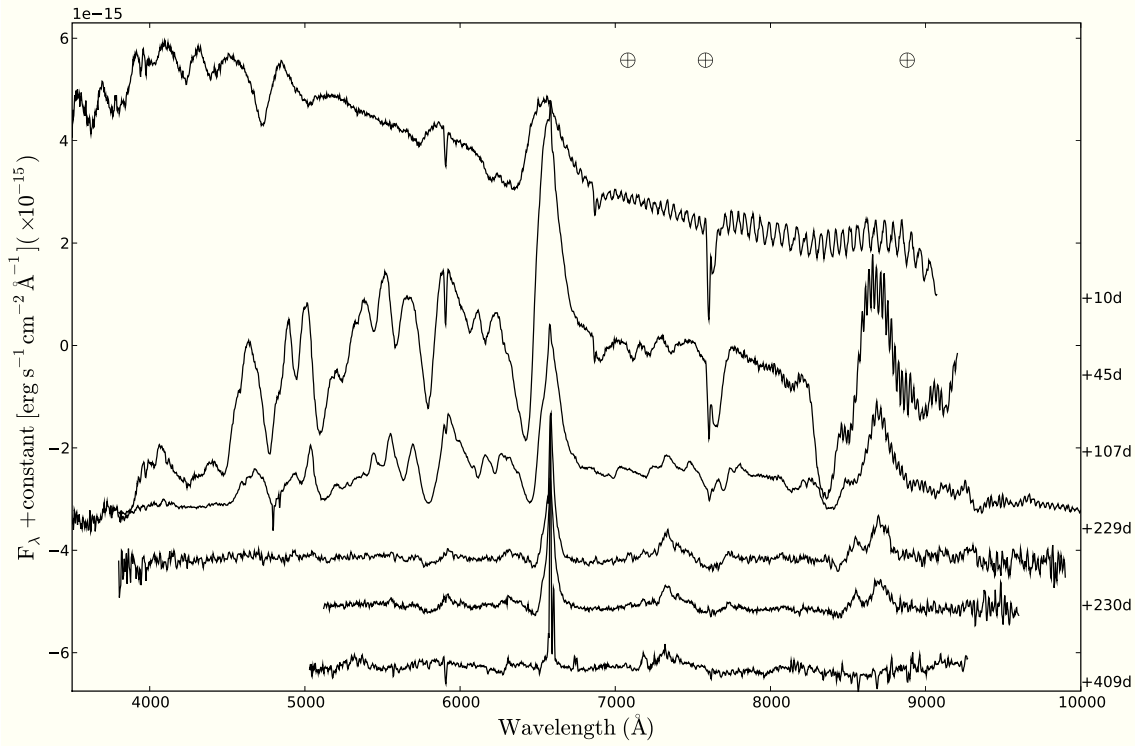

Figure 3.24: The overall spectral evolution of SN 2009dd. Wavelengths are in the observer's rest frame. The phase reported for each spectrum is relative to the explosion date (JD 2454925.5). The $\oplus$ symbols mark the positions of the strongest telluric absorptions. The ordinate refers to the top spectrum; the other spectra are shifted downwards with respect to the previous one by 4×10^{-15} (second and third) and 1.2×10^{-15} (others).

Table 3.24: Observed black-body temperatures and expansion velocities of SN 2009dd.

JD +2400000	Phase* (days)	T (K)	v($H\alpha$) (km s^{-1})	v($H\beta$) (km s^{-1})	v(He I) (km s^{-1})	v(Fe II) (km s^{-1})	v(Sc II) (km s^{-1})
54936.7	11.7	14700 ± 2000	10970 ± 150	9500 ± 370	8500 ± 700	9000 ± 500	
54971.6	46.6	5500 ± 200	7680 ± 250	6600 ± 100		5500 ± 500	5040 ± 100
55033.4	108.4	5300 ± 700	6500 ± 300	5120 ± 230		3400 ± 1000	2200 ± 200

* with respect to the explosion epoch (JD 2454925)

the telluric absorption could have changed the spectra profile at that wavelength. The lines are the same in the third spectrum (+107d).

The last set of spectra (229-409) shows the Na ID in emission, the Hα, the [Fe II] λ7155 and also [Ca II] $\lambda\lambda$7291, 7324 doublet and the Ca IR triplet. Also the [O I] $\lambda\lambda$6300, 6363 doublet is barely visible. When the SN has been recovered at 409d post maximum the principal source of Hα seems tied to the H II region, as the emission lines on its red side that is [S II] $\lambda\lambda$6717,6731 doublet typical of H II region. In this spectrum are barely visible [O I], [Fe II] and [Ca II].

The expansion velocities of Hα, Hβ, He I 5876Å, Fe II 5169Å and Sc II 6246Å are reported in Tab. 3.24 and plotted in Fig. 3.28 (Left panel). Error estimates are derived from the scatter of several independent measurements. The velocities of Hα are higher than those of Hβ. In the only epoch in which the He I line remains visible the velocity is about 2500 km s^{-1} smaller than that of Hα. Fe II velocity, decreases below 4000 km s^{-1} at about three months, when the Sc II, that is a good indicator of the photospheric velocity, decreases below 3000Å.

In Fig. 3.29 (Top panel) is compared the Hα evolution of SN 2009dd with those of the type II SNe, included our sample. The first velocity of SN 2009dd is comparable to those of SNe 2009bw, 1992H and 2004et. After that, the velocity follows the behaviour of the other SNe, even if the values are greater than the other SNe, especially the value at ∼108d. In the same figure, bottom panel, are compared the evolution of temperature with those of the sample. The trend is similar to that of SN 2009bw in the early phase and similar to those of all the type II SNe during the plateau phase.

3.4.4 SN 2007pk

Fig. 3.25 shows the entire evolution of SN 2007pk from few days post explosion (∼4d) to about three months, plus two spectra at about ten and eleven months after the explosion when the SN was barely seen and only underlying H II region is seen.

The first set of spectra (4d-8d) show a blue continuum and no prominent absorption features. Hα and Hβ have only emission components as the prominent feature on Hβ blue side related to He II λ4686 maybe contaminated by CIII/NIII as in the case of SN 1998S (71). From the third spectrum (8d) the absorption components of the Balmer series are roughly visible but the emission components are still predominant. As reported in Filippenko, Silverman, and Foley (74), there are some peculiarities similar to type IIn.

The spectrum of ∼27d shows well developed P-Cygni profiles for metal elements as Fe II at ∼4500Å and Sc II λ5031. Also the Fe II multiplet $\lambda\lambda$4924, 5018, 5169 and Sc II λ6245 are visible. The Na ID is blended with He I. The Hα and Hβ still show a prominent emission component plus an absorption component comparable with those of other SN II at the same phase. The profile of the Balmer lines shows also a blue flat shoulder that could be tied to the interaction ejecta-CSM.

Differently from the early ones, the last set of photospheric spectra (50d-81d) shows spectra of a typical type II. At this phase are visible other metal lines as the Fe I and Sc II at ∼5500Å or the Ba II λ6142, while Na ID have permanently replaced the He I. In this set is also visible the Ca IR triplet ($\lambda\lambda$8498, 8542, 8662).

In the NIR spectrum (20d) are visible the P-Cygni prole of Paschen series. Especially of Paschen β, γ and δ. The Paschen γ is partially blended with He I λ10830.

The two spectra collected during the late phase do not show sign of SNe emission. The only emissions are related to the H II region in which the SNe exploded, these are the Hα (Δv∼600 km s^{-1}, too narrow to be a SN feature) and the [S II] $\lambda\lambda$6717, 6731 doublet.

The expansion velocity of Hα, Hβ, He I, Fe II 5169Å and Sc II 6246Å are plotted in Fig. 3.28 (Middle panel) and reported in Tab. 3.25. The velocities of

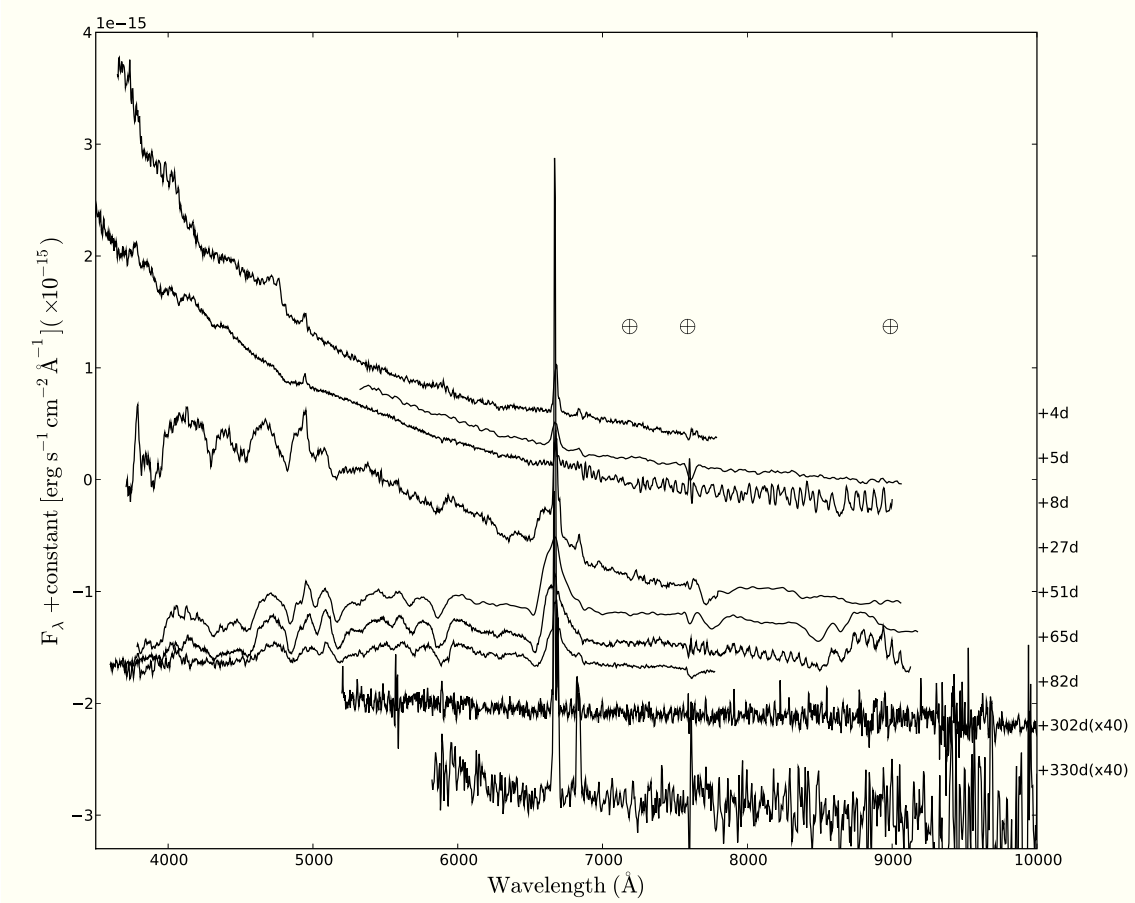

Figure 3.25: The overall spectral evolution of SN 2007pk. Wavelengths are in the observer's rest frame. The phase reported for each spectrum is relative to the explosion date (JD 2454412). The ⊕ symbols mark the positions of the strongest telluric absorptions. The ordinate refers to the top spectrum; the other spectra are shifted downwards with respect to the previous one by 7×10^{-16}, except the third shifted by 1×10^{-15}.

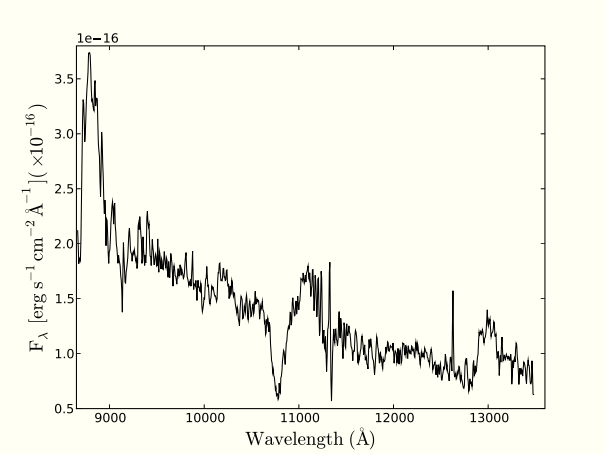

Figure 3.26: NIR spectrum of SN 2007pk at $\sim$ 66d past explosion date (JD 2454412). Wavelengths are in the observer rest frame.

Table 3.25: Observed black-body temperatures and expansion velocities of SN 2007pk.

JD +2400000	Phase* (days)	T (K)	v($H\alpha$) (km s^{-1})	v($H\beta$) (km s^{-1})	v(He I) (km s^{-1})	v(Fe II) (km s^{-1})	v(Sc II) (km s^{-1})
54416.3	4.3	14500 ± 2000	2700 ± 1200	2500 ± 1200	10900 ± 600		
54417.5	5.5	13500 ± 1000	6080 ± 1800	7454 ± 350			
54421.4	8.4	12000 ± 1000	8640 ± 280	7780 ± 1400			
54439.5	27.5	8500 ± 300	8100 ± 800	7400 ± 100		5860 ± 250	
54463.3	51.3	5500 ± 500	7060 ± 100	6040 ± 200		4875 ± 400	4040 ± 100
54477.4	65.4	5500 ± 300	6515 ± 180	5700 ± 300		4540 ± 100	3900 ± 180
54494.3	82.3	5600 ± 600	6100 ± 100	4940 ± 500		4000 ± 500	3400 ± 400

* with respect to the explosion epoch (JD 2454412)

Hα are higher than those of Hβ except for the second spectrum. The velocities evolution of Blamer series shows clearly the evolution type IIn spectra (strong interaction ejecta-CSM and lack of absorption profile) to typical type II spectra (presence of absorption component). We warn about the values of the first set of spectra, where the absorption component are barely visible and the errors are large. Fe II velocity reaches $\sim$4000 km s^{-1}at the last photospheric epoch, when the Sc II is $\sim$90% of Fe II value. For the metal lines, rose after the early stage, the behaviour is the same of the other type II SNe.

In Fig. 3.29 (Top panel) the Hα evolution is compared with those of other SNe as done for the previous SNe. The differences in the first 8 days from the type II are remarkable. After that, from 20d to the entire photospheric phase, the evolution resembles that of the other SNe chosen for comparison. In the bottom panel of Fig. 3.29 the temperature evolution has been compared. The behaviour shown by SN 2007pk is similar to those of other SNe, only the first points are too low, but we have to remember the big uncertainties related to that measures and the fact that an absorption component might be not visible because of the interaction.

3.4.5 SN 2010aj

The evolution of the collected spectra of SN 2010aj is shown in Fig. 3.27. It covers $\sim$2 months of the photospheric evolution and an epoch after a year from the estimated explosion epoch.

The first spectrum shows absorption profile of Balmer lines, as the He I λ5876, the Ca II H&K, the Fe II multiplet lines ($\lambda\lambda$ 4924, 5018, 5169) and possibly also the Si II λ6355, even if the low signal to noise of the spectrum does not help in the identification. Also the Ca II IR triplet is already visible.

In the other three spectra (38d - 73d) other metal lines are visible as those of Ti II around 4100Å and a contribution of Fe II and Ba II at $\sim$4930. The Fe I and Sc II lines at about 5500Å are also clearly visible, as the Sc II λ 6245. In these spectra the Na ID replaces the He I. In all the spectra are clearly visible the strong narrow components of the Balmer series due to the H II region superimposed to SN 2010aj.

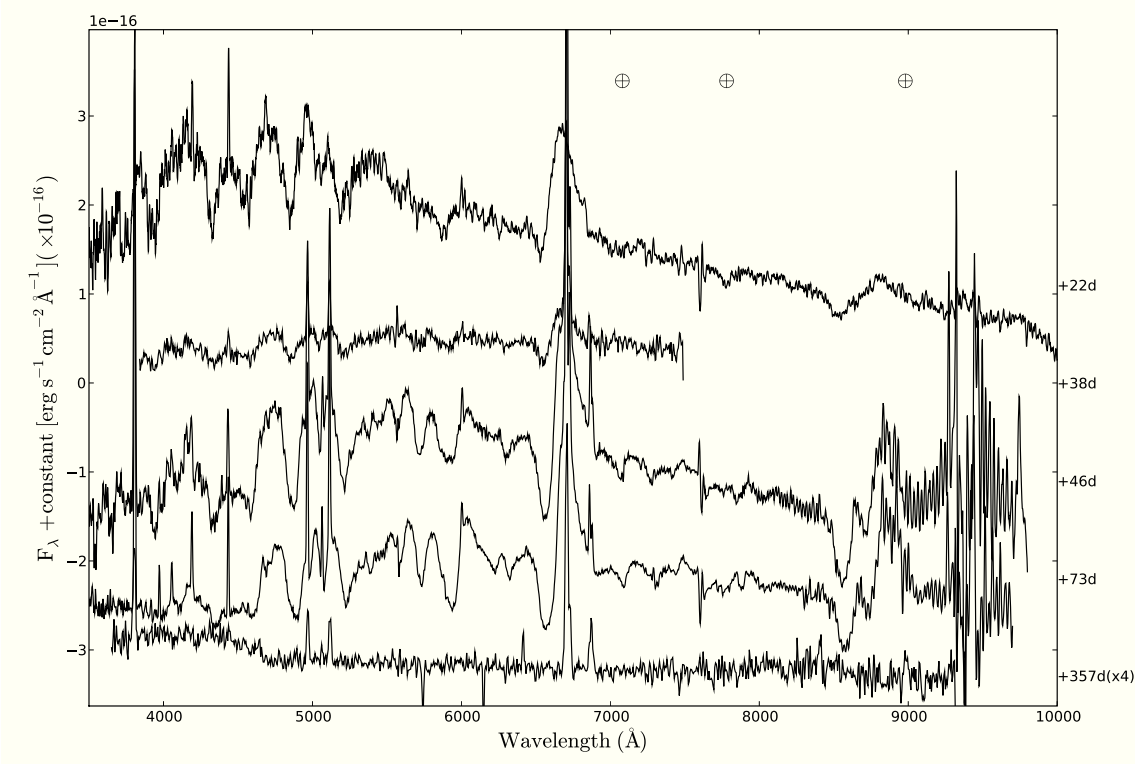

Figure 3.27: The overall spectral evolution of SN 2010aj. Wavelengths are in the observer's rest frame. The phase reported for each spectrum is relative to the explosion date (JD 2455265.5). The $\oplus$ symbols mark the positions of the strongest telluric absorptions. The ordinate refers to the top spectrum; the other spectra are shifted downwards with respect to the previous one by 2×10^{-16} and 6×10^{-16} (only the third).

Table 3.26: Observed black-body temperatures and expansion velocities of SN 2010aj.

JD +2400000	Phase* (days)	T (K)	v($H\alpha$) (km s^{-1})	v($H\beta$) (km s^{-1})	v(He I) (km s^{-1})	v(Fe II) (km s^{-1})	v(Sc II) (km s^{-1})
55287.6	22.1	8000 ± 500	8370 ± 200	7600 ± 300	6930± 1000	5900 ± 700	
55303.3	37.8	5600 ± 500	7780 ± 700	7300 ± 350		4700 ± 200	4240 ± 500
55311.5	46	5800 ± 500	7090 ± 300	6700 ± 300		4400 ± 200	4050 ± 200
55338.5	73	5200 ± 400	6080 ± 300	4750 ± 380		2890 ± 250	2500 ± 200

* with respect to the explosion epoch (JD 2455265.5)

The lonely nebular spectrum does not show any sign of lines due to the SN nebular phase. There are no signs of [O I] $\lambda\lambda$ 6300, 6364 doublet or [Ca II] $\lambda\lambda$ 7291, 7324. The Hα is extremely narrow (FWHM 23Å equal to $\sim$1000 km s^{-1}, cfr. with a spectra resolution of $\Delta\lambda$=17Å) indicating that it is due to the H II and the major contribution to its emission should be by the H II region, as suggested by the other narrow emission of the Blamer series.

The expansion velocities of Hα, Hβ, He I 5826Å, Fe II λ5169 and Sc II λ6246 are plotted in the Fig. 3.28(right panel) as derived through a gaussian fit of the absorption minima. Error estimates are derived from the scatter of several independent measurements. As usual the velocities of Hα are slightly larger than Hβ. In the only epoch in which the line remains visible, the He I velocity is lesser than the Hβ. The Fe II velocity is smaller than that of H and He and reaches 2900 km s^{-1} at about two month. Sc II velocity is very close to that of Fe II, supporting the identification of both ions.

In Fig. 3.29 (Top panel) we compare the Hα velocity evolution of SN 2010aj with those of type IIP SNe, among which those of our sample. The velocity is comparable to most of the SNe sample, especially with those of SNe 2004et, 1992H and 2007od.

In Fig. 3.29 (Bottom panel) the evolution of temperature is shown and compared to the same SNe chosen for the velocity comparison. The evolution is similar to the other type II, with the classical T$\sim$5500 K reached during the plateau phase.

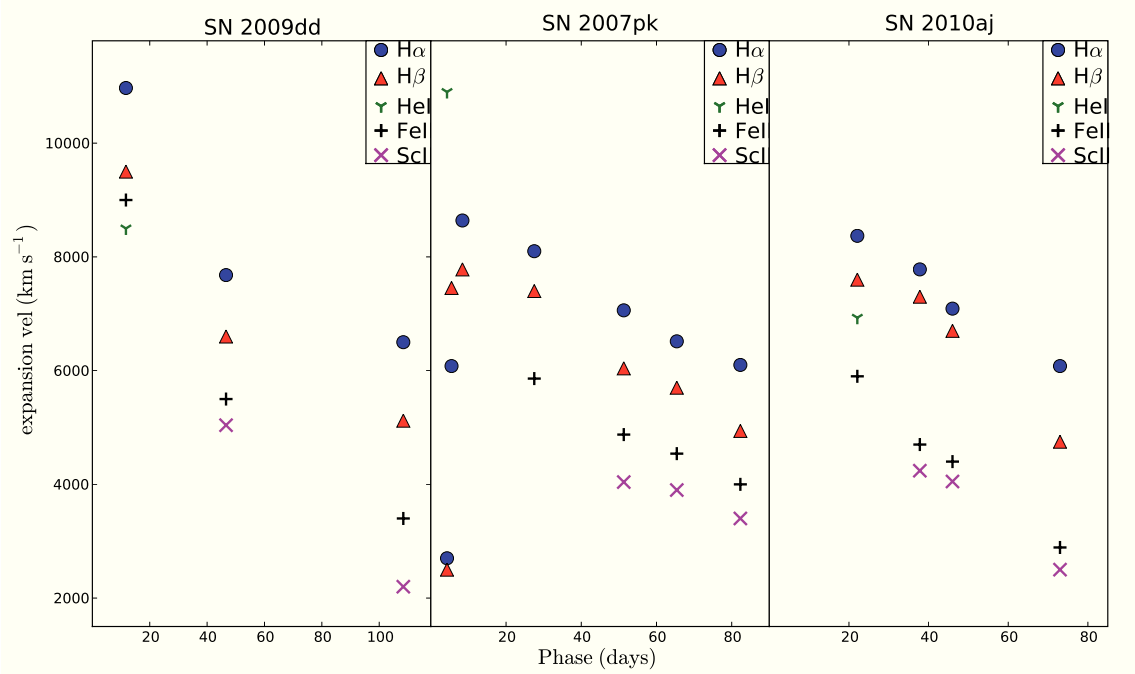

Figure 3.28: Expansion velocity of Hα, Hβ, HeI λ5876, FeII λ5169 and Sc II λ6246 measured from the minima of P-Cygni profiles for SN 2009dd,SN 2007pk and SN 2010aj.

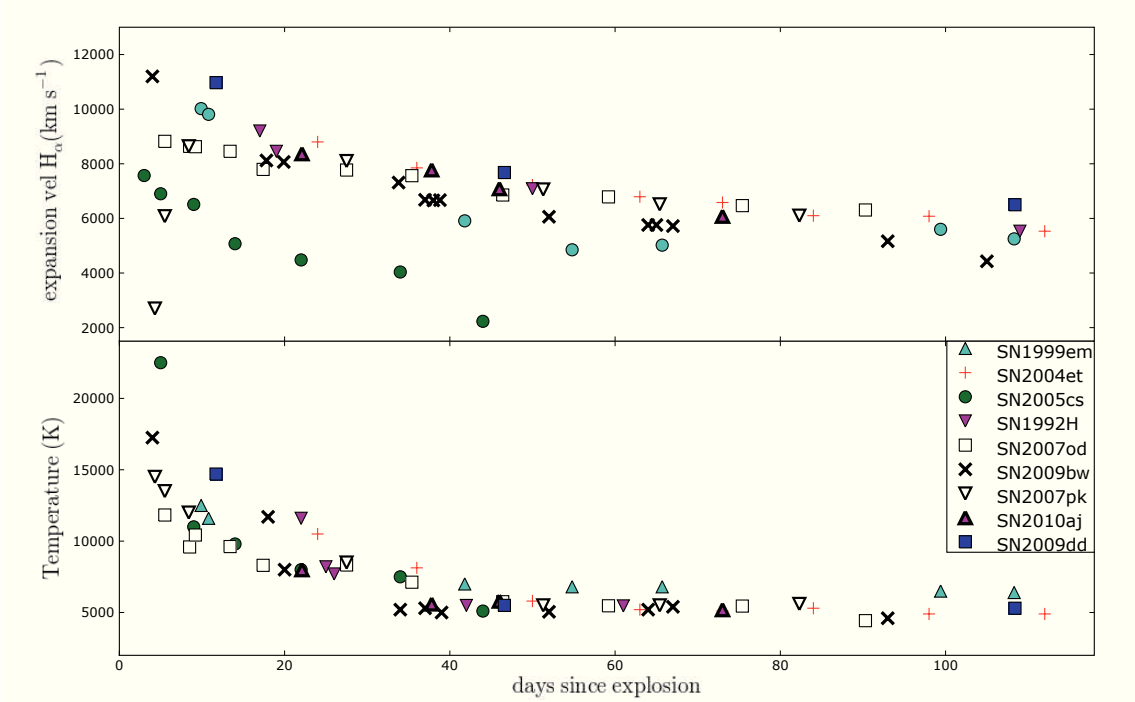

Figure 3.29: Top: comparison of the Hα velocity of our SNe sample with those of other SN II. Bottom: Evolution of the continuum temperature of SNe of our sample plus SNe 1999em, 2004et, 2005cs, 1992H.

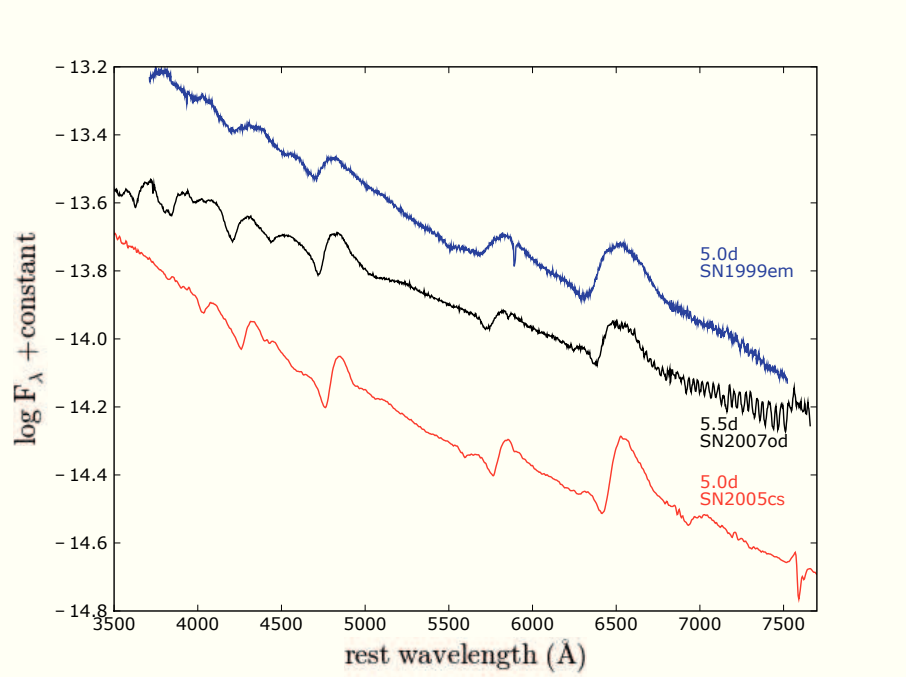

Figure 3.30: Comparison among spectra of SN 1999em, SN 2007od and SN 2005cs around 5 days after explosion. For references see Tab. 3.21.

3.4.6 Comparison among spectra of type II SNe

The material described in the previous Sections 2.2.2 & 3.4, can be compared with those of other SNe at similar phases. This helps the analysis of particular features and shows as our objects evolve compared to common or well studied SNe. SN 2007od and SN 2009bw are the best studied objects of our sample, for this reason the most of the comparisons are with them.

In Fig. 3.30 we compare the spectrum of SN 2007od at $\sim$ 5 days with two other young SNe IIP: SN 1999em (68) and SN 2005cs (173). The similarity with SN 1999em was prompted by the GELATO spectral comparison tool (100), while the comparison with the faint SN 2005cs is made because of the characteristic features on the blue side of Hβ and Si II lines. All spectra show relatively blue continua and display H Balmer lines and He I 5786Å. The spectrum of SN 2007od shows a boxy profile of Hα which suggests an ejecta-CSM interaction, but no radio or X-ray observations at early phases are available to confirm such a hypothesis.

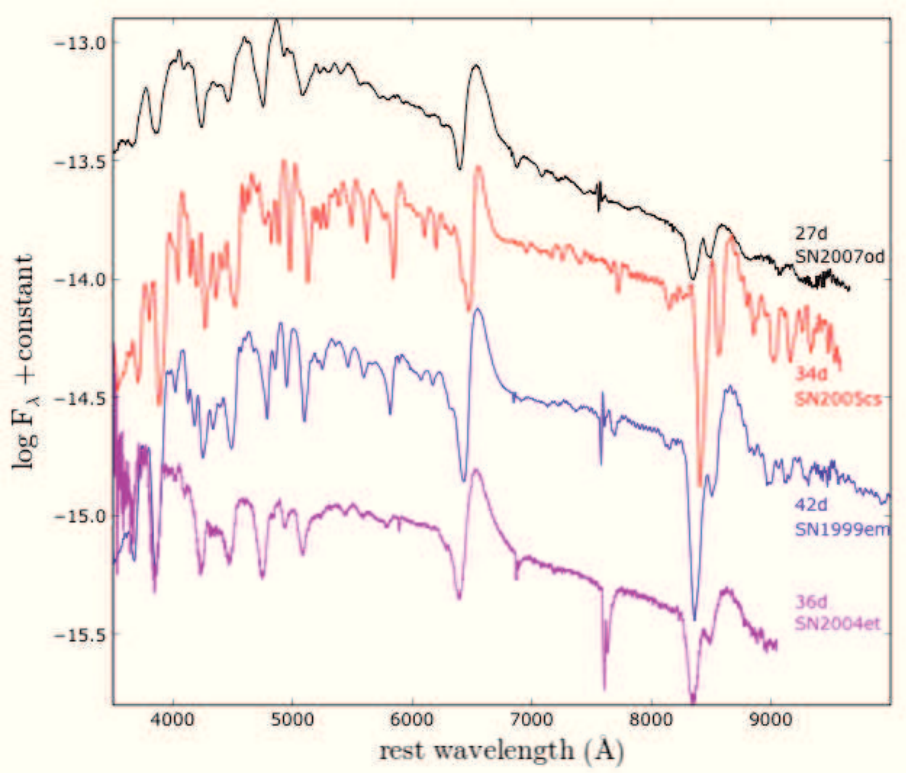

Figure 3.31: Comparison among spectra of SN 2004et, SN 2007od, SN 2005cs and SN 1999em during the plateau phase. For references see Tab. 3.21.

The feature at about 4440Å, discussed in Sec. 3.5.1, is possibly detected in SN 2005cs, but not in SN 1999em. A weak line around 5600Å, observed only in SN 2005cs (cfr. 173) and (possibly) in SN 1999em, and tentatively identified as N II, is not visible in SN 2007od.

In Fig. 3.31 a few spectra of type IIP SNe during the plateau phase are compared. The spectrum of SN 2007od seems to have shallower absorption components than other SNe at the same phase, probably because of temperature difference. Alternatively this effect may be due to circumstellar interaction through SN 1999em toplighting effect (32). In such scenario the fast ejecta catches and sweeps up the much slower circumstellar matter from the wind of the SN progenitor (or its binary companion) and produces a continuum emission above the photosphere. The global effect is to increase the total luminosity decreasing the

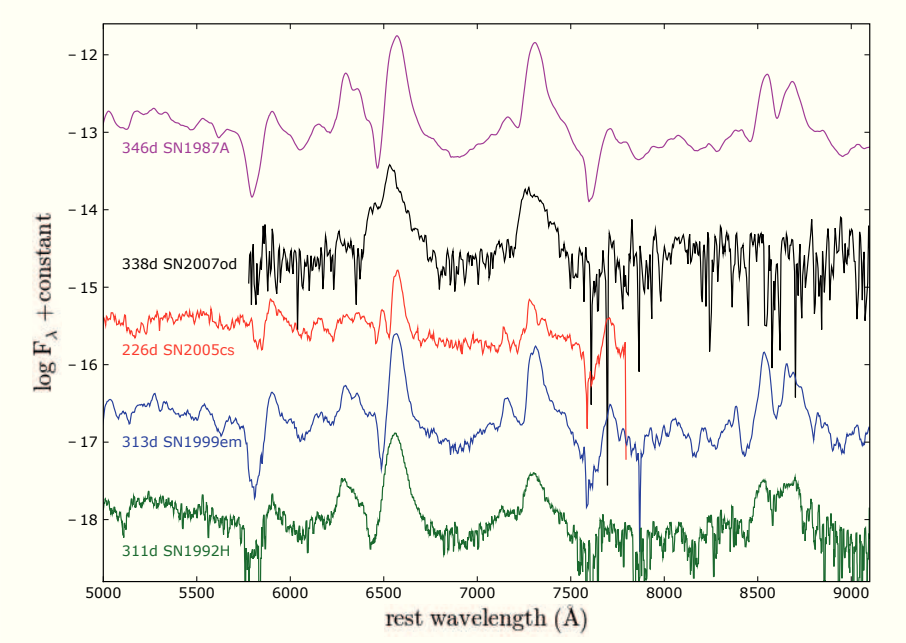

Figure 3.32: Comparison among spectra of SN 1987A, SN 2007od, SN 2005cs, SN 1999em and SN 1992H during the nebular phase. For references see Sect. 3.4.6 and Tab. 3.21.

contrast of spectral lines. It is also possible that the reverse shock decelerate the gas and produces low photospheric velocities. The lines close to the blue edge of Hα at about 6300Å are visible also in the spectrum of SN 2005cs and in SN 1999em but not in SN 2004et (139).

The third comparison about SN 2007od (Fig. 3.32) is made for the nebular phase with SN 1987A (225), SN 2005cs (171), SN 1999em (68) and the luminous SN 1992H (52). The Hα profile of SN 2007od differs from those of the other SNe. The central peak is blue-shifted and there is a boxy shoulder on the blue side (see Sec. 3.6). Also [CaII] is blue-shifted and shows an asymmetric profile. Instead, [OI] $\lambda\lambda$ 6300, 6363 doublet, [FeII] at 7000Å and NaID are barely detectable preventing a detailed analysis of the line profiles.

In Fig. 3.33(bottom) we compare the spectrum of SN 2009bw at $\sim$ 18 days with those of other young SNe IIP: SN 1999em (68) and SN 1992H (52). The similarity with SN 1992H is due to the presence of Si II and the luminosity

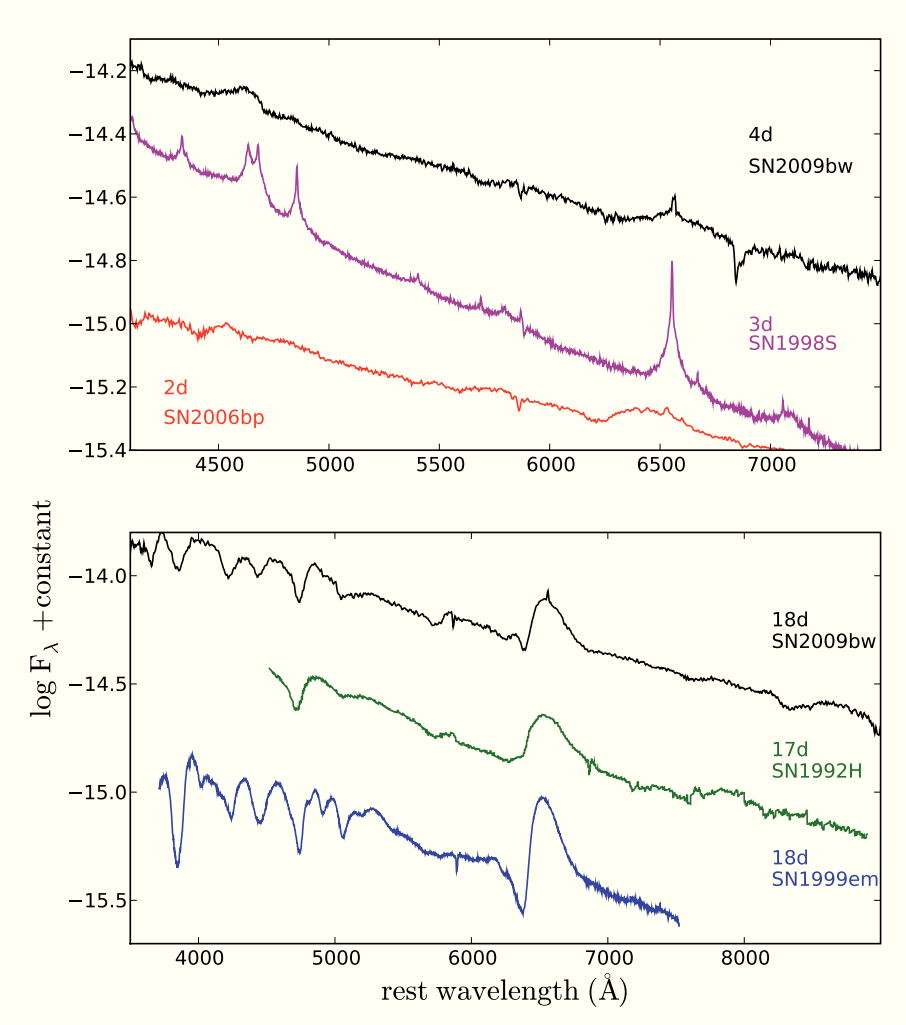

Figure 3.33: Top panel: comparison among spectra of SN 2009bw, SN 1998S and SN2006bp about ∼4d past explosion. Bottom panel: comparison among spectra of SN 2009bw, SN 1999em and SN 1992H about ∼18d past explosion. For references, see the text and Tab. 3.21.

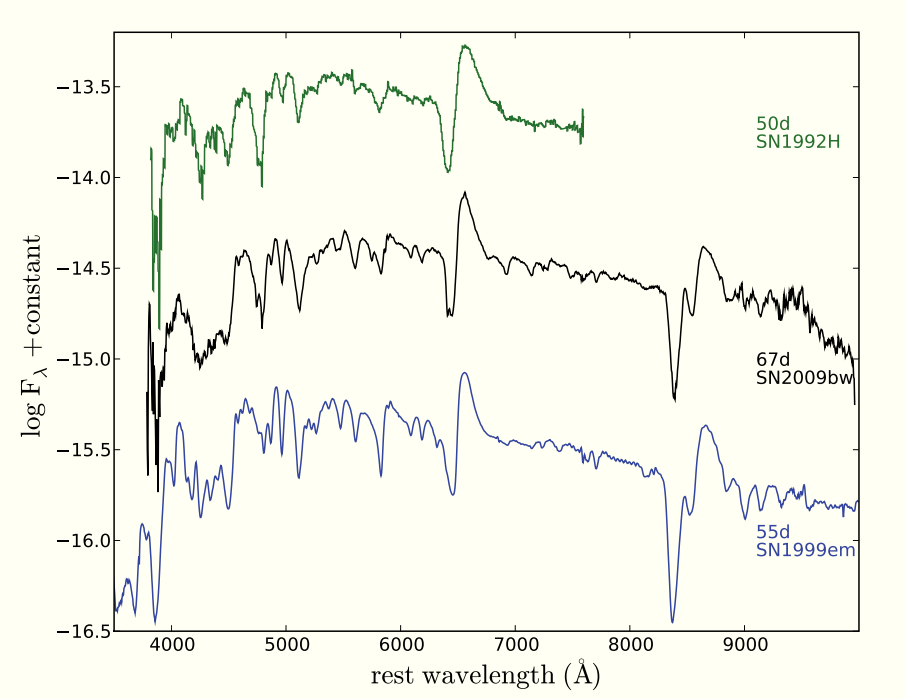

Figure 3.34: Comparison among spectra of SN 2009bw, SN 1999em and SN 1992H in the photospheric phase. For references, see the text and Tab. 3.21.

shown, while for SN 1999em is made thanks to some characteristic line elements shown during the plateau and nebular phases. All spectra show relatively blue continua and display H Balmer lines, He I 5786Å and some Fe II lines. The spectrum of SN 2009bw seems bluer than SN 1999em that at the same age shows a temperature lower than our object as confirmed by the well developed P-Cygni profile of the metal line. The spectrum of SN 1992H seems comparable both for temperature and optical depth of the lines (except the Hα).

Fig. 3.34 compares the spectra in the plateau phase. The spectrum of SN 2009bw seems much similar to the spectra of SN 1992H with all the common features shown by the SNe IIP in the plateau phase. A good evidence is the comparison with SN 1999em in the range of 9000Å that shows the presence of the line identified as C I. Unfortunately the other spectra do not cover this range. The absorption profile of Hα resembles that of SN 1999em and strengthens the idea of interaction with a CSM during the plateau phase as reported by Chugai, Cheva-

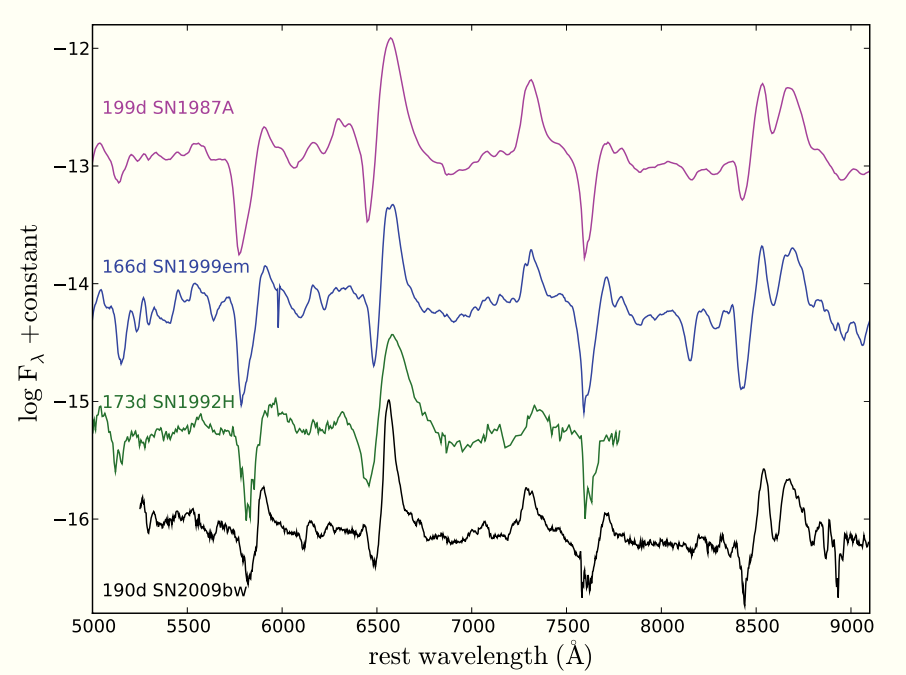

Figure 3.35: Comparison among spectra of SN 2009bw, SN 1987A, SN 1999em and SN 1992H during the nebular phase. For references, see the text and Tab. 3.21.

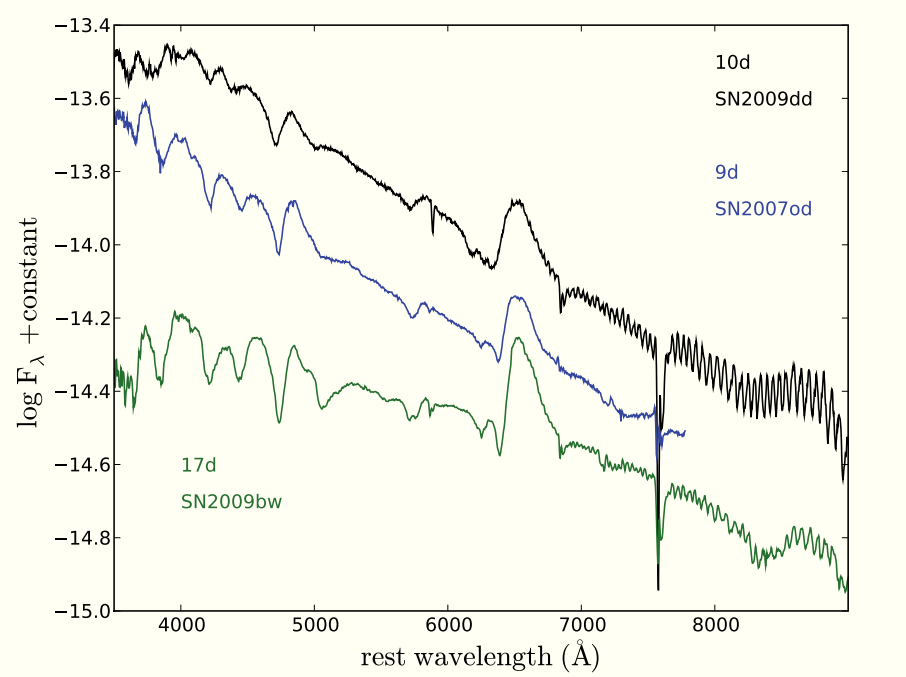

Figure 3.36: Comparison among spectra of SN 2009dd, SN 2007od and SN 2009bw during the plateau phase.

lier, and Utrobin (49).

The last comparison for SN 2009bw (Fig. 3.35) has been made for the nebular phase with SN 1987A (225) in addition to the precedent comparison. In this phase all the SNe show residual of P-Cygni profile as Ca II NIR triplet or Na ID. The [Ca II] $\lambda\lambda$7291, 7324 doublet seems similar to that of SN 1999em, while the [O I] $\lambda\lambda$6300, 6364 is not clearly visible. At this age also the 1999em does not show a clearly [O I] doublet, preventing a detailed analysis of the line profile. The entire profile of Hα is not shifted, but seems lesser (FWHM$\sim$1900 km s^{-1}) than the others SNe.

We have compared also the first spectrum of SN 2009dd with those of our sample at similar phase. All the SNe show metal lines, even if are more marked in SN 2009bw as we expected from more advanced phase (cfr. Fig. 3.36). The line of Si II λ6355, well identified in SN 2007od (cfr. 3.5.1) and SN 2009bw (cfr. 3.5.2), is clearly visible also in SN 2009dd. There are no spectra of type II

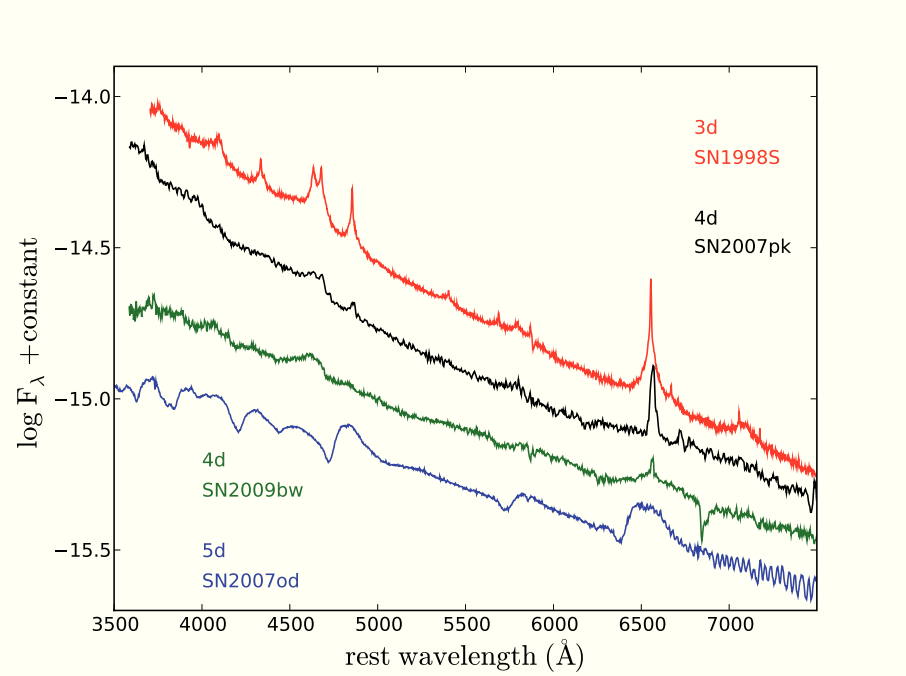

Figure 3.37: Comparison among spectra of SN 2007pk, SN 1998S, SN 2006bp and SN 2009bw about ∼4 days after explosion. For references, see the text and Tab. 3.21.

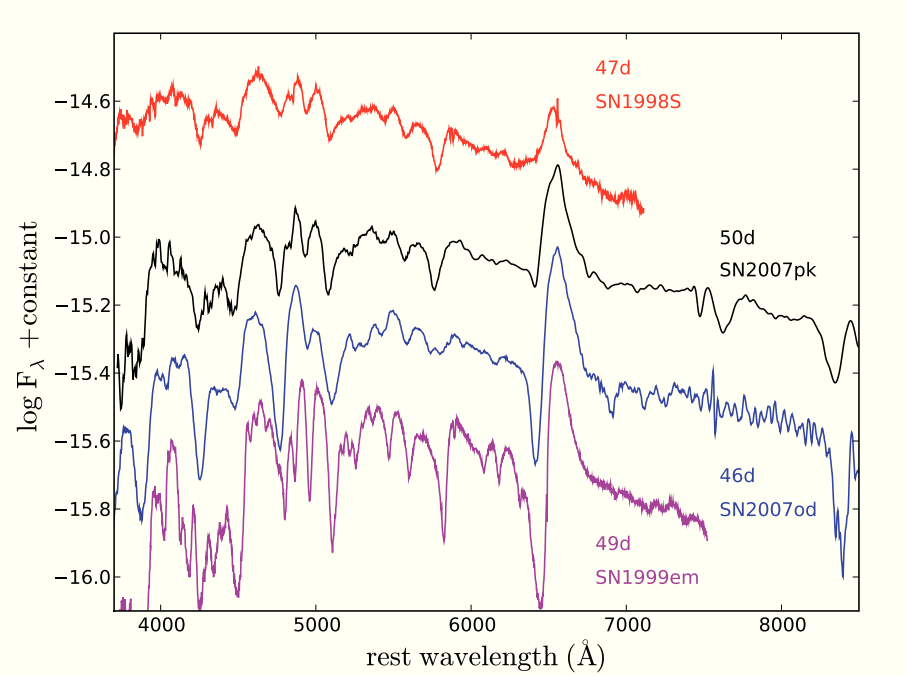

Figure 3.38: Comparison among spectra of SN 2007pk, SN 2007od, SN 1998S and SN 1999em during the plateau phase. For references, see the text and Tab. 3.21.

that show a triple absorption at about 6250Å that can be due to the interaction ejecta-CSM. One of this absorption is maybe an HV Hα, but the absence of other spectra at this epoch forbid further investigation. However, the presence of this multiple component absorption in the Hα profile and the X observation at early time point to an interaction between ejecta and CSM. The strength of the SN 2009dd iron lines resembles that of SN 2007od where the third absorption is not visible. Despite that, there are not other spectral evidences of interaction as a clear presence of HV Hβ or a flat top profile (we will address this issue in Sec. 5). In this context, thanks also the information reported by Immler, Russell, and Brown (111), that line could be identified as HV Hα due to a possible interaction ejecta-CSM.

In the first comparison of SN 2007pk (Fig. 3.37) we show the first spectrum of this SNe with those of other type IIP-IIn SNe. The similarity with the spectrum of SN 1998S is clearly visible, more than the other IIPs, even if are both peculiars

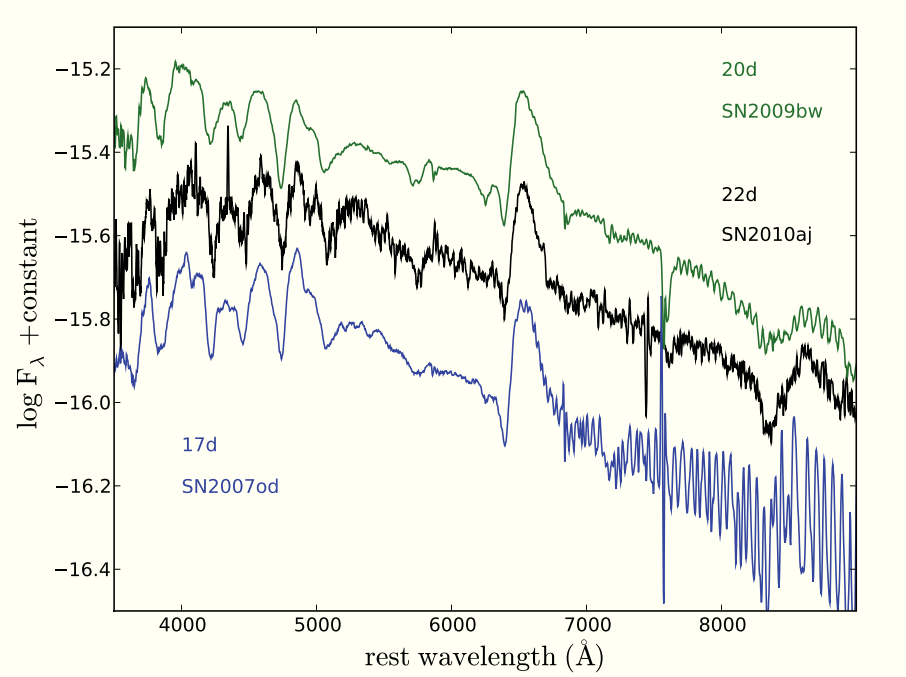

Figure 3.39: Comparison among spectra of SN 2010aj, SN 2007od and SN 2009bw at ∼22 days post explosion.

because of the early interaction. The line at ∼4600Å seems relate to highly ionization elements as CIII/NIII or maybe CIV as supported by the similarity in lambda with comparable features in SN 1998S and SN 2009bw. Maybe there is also a contribution by He II but it is not noteworthy.

Fig. 3.38 compares the spectra in the plateau phase. The spectrum of SN 2007pk seems more similar to those of type IIP SNe 1999em and 2007od respect to the type IIn SN 1998S. The spectral changing from a type IIn to a type II has been completed, at this phase SN 2007pk shows a P-Cygni also for Hα with a weak, clearly visible absorption component, not shown by type IIn at similar phase.

The last comparison of our sample shows the first spectrum of SN 2010aj with those of SN 2007od and SN 2009bw. Despite the low S/N the Si II seems to be visible also in SN 2010aj, that maybe shows presence of Sc II lines as in the red side of Hβ or the Sc II λ6246, visible thank to the comparison.

3.5 Spectral Analysis with NLTE and LTE codes

The next two subsections 3.5.1 & 3.5.2 are devoted to a detailed line analysis through two powerful tools as the LTE code SYNOW and the non-LTE code PHOENIX. Both are reported in Inserra *et al.* (114) and Inserra *et al.* (115).

3.5.1 SN 2007od with PHOENIX and SYNOW

Despite the possible presence of circumstellar interaction during the photospheric phase that could affect the spectra, due to the good temporal coverage, the position respect to the host galaxy, and low observed reddening that this supernova is a good candidate for analysis by the generalized stellar atmosphere code PHOENIX. We utilize PHOENIX in order to learn more about the physical structure of this object.

As a starting point, for the preliminary line identification in the spectra of SN 2007od we have confirmed the line ids obtained by Inserra *et al.* (116), and this work using the fast, parameterized supernova synthetic spectra code SYNOW. The code is discussed in detail by Fisher (78) and recent applications include Moskvitin *et al.* (158), Roy *et al.* (201), and Branch *et al.* (31). SYNOW assumes the Schuster-Schwarzschild approximation and the source function is assumed to be given by resonant scattering, treated in the Sobolev approximation. It correctly accounts for the effects of multiple scattering. For a subsequent more detailed analysis, in order to improve the line identification and to show possible differences between the highly parameterized SYNOW and NLTE results, we used the generalized NLTE stellar atmospheres code PHOENIX (101, 102). PHOENIX treats the fully relativistic NLTE radiative transfer problem, solving the full scattering problem, the rate equations for ions treated in NLTE, and generalized radiative equilibrium assuming the total bolometric luminosity in the observer's frame as a model parameter. The code includes a large number of NLTE and LTE background spectral lines and solves the radiative transfer equation with a full characteristics piecewise parabolic method (103) and without simple approximations such as the Sobolev approximation (151). The process that solves the radiative transfer and the rate equations, with the condition of radiative equilibrium, is repeated until the radiation field and the matter have converged to radiative equilibrium in the

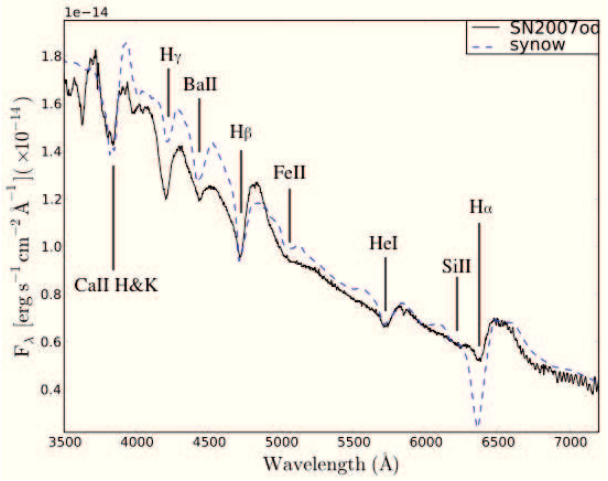

Figure 3.40: Comparison between the normalized optical spectrum of SN 2007od at 5 days post explosion (JD 2454404) and the SYNOW synthetic spectrum (for composition of synthetic spectra see text).

Lagrangian frame. These calculations assumed a compositionally homogeneous atmosphere whose density is given by a power-law in radius and steady state conditions in the atmosphere.

We have reproduced the synthetic spectra of the first six observed photospheric spectra, covering a period from 5d to 27d since the adopted explosion date JD= 2454404±5 (∼ 30 Oct. 2007, 116). The most interesting spectra are the first of the series (5d, we measure times from the assumed date of explosion), that shows an Hα flat top profile and two uncommon features at about 4400Å and 6250Å, and the last of our series (27d) which has the best signal to noise ratio during the plateau. The study of both of these epochs provides important information about the presence of certain ions and possible CSM interaction at early times.

Figure 3.40 shows the line identifications determined by the SYNOW analysis for the first spectrum, obtained using a T_{bb} ∼12000 K, a v_{phot} ∼7800 km s^{-1}, an optical depth $\tau(v)$ parameterized as a power law of index $n = 9$ and a T_{exc}=10000 K assumed to be the same for all the ions. The features visible in Fig. 3.40 are produced by only 6 chemical species. The P-Cygni profile of the Balmer lines are clearly visible, as well as He I λ5876, but there are also contributions due to Ca II,

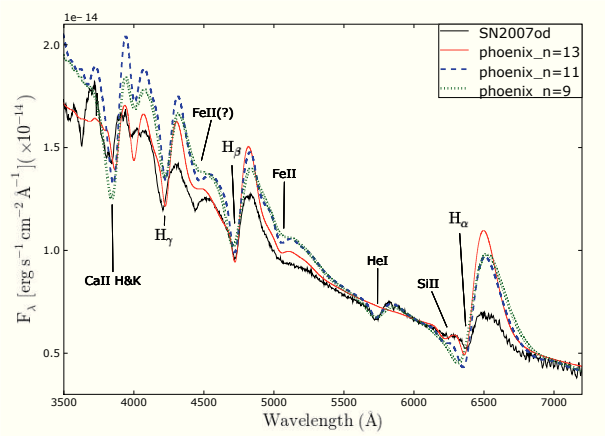

Figure 3.41: Comparison between the optical spectrum of SN 2007od at 5 days post explosion (JD 2454404) and `PHOENIX` full NLTE spectrum (for model parameters see Tab. 3.27).

Fe II, Ba II, and Si II. The Balmer lines have been detached from the photosphere to better match the observed velocity. The uncommon lines mentioned above are identified as Ba II (λ4524) and Si II (λ6355). In our attempts we have considered also the presence on N II λ4623, but the lack of the other lines of N II λ5029 and N II λ5679 (stronger than the first one), and the poor fit of the N II lead us to the conclusion that there is no evidence for enhanced nitrogen in the spectra of SN 2007od.

With the adopted reddening (E(B-V)=0.038) and the `SYNOW` ions suggested by the analysis we computed a grid of detailed fully line-blanketed `PHOENIX` models. We explored variations in multiple parameters for each epoch adjusting the total bolometric luminosity in the observer's frame (parameterized by a model temperature, T_{model}), the photospheric velocity (v_0), the metallicity (the solar abundances were those of Grevesse and Sauval (92)), the density profile (described by a power law $\rho \propto r^{-n}$) and gamma-ray deposition. Gamma-ray deposition was assumed to follow the density profile. We noticed an increase of the emission profile, especially those of Balmer series, tied to a decrease of gamma ray deposition. However, for our final models at last the gamma-ray deposition was not included. We estimated the best set of model parameters by performing a simultaneous χ^2

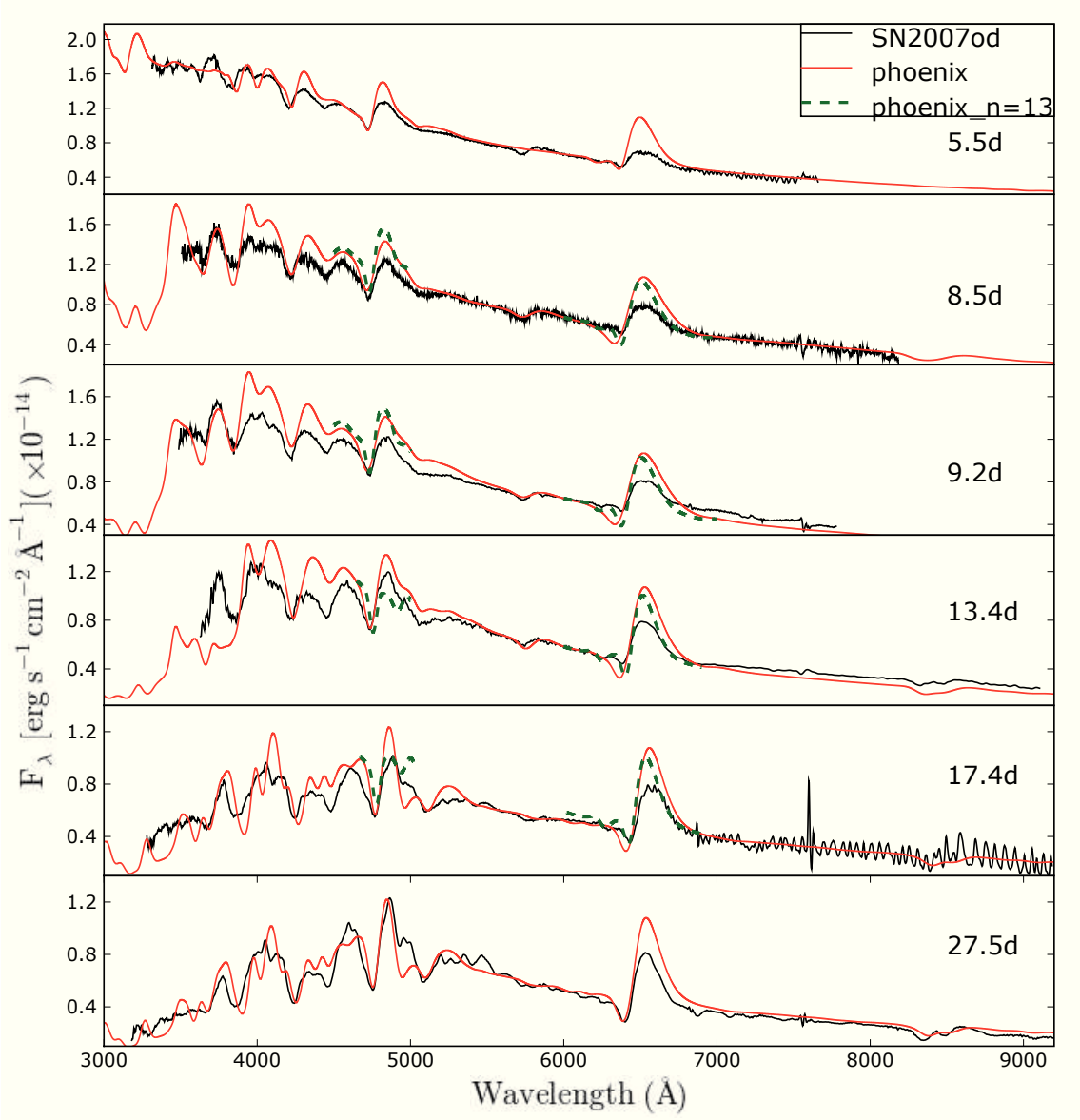

Figure 3.42: PHOENIX evolution compared to observed spectra.

Table 3.27: Parameters of PHOENIX models of SN 2007od.

JD +2400000	Phase* (days)	$T^{\diamond}_{model}$ (K)	v_0 ($km\,s^{-1}$)	n†	r (10^{14} cm)	L (10^{41} erg s^{-1})
54409.5	5.5	8000	7600	13	3.6	3.8
54412.5	8.5	7400	7200	9	5.3	6.0
54413.2	9.2	7300	7050	9	5.6	6.3
54417.4	13.4	6800	6000	9	6.9	7.2
54421.4	17.4	6200	5400	9	8.1	6.9
54431.5	27.5	6000	5000	9	11.9	13.1

* with respect to the explosion epoch (JD 2454404) from (116)

◇ with a total E(B-V)=0.038 (116)

† index of power law density function

fit of the main observables. The relevant parameters for SN 2007od for the entire early evolution are reported in Tab. 3.27. While the fits are shown in Fig. 3.42.

In the first PHOENIX spectra we treated the following ions in NLTE: H I, He I-II, Si I-II, Ca II, Fe I-II, Ba I-II. He I, Si I, Fe I and Ba I have been considered to reproduce the ionization levels of the corresponding enhanced atoms. The opacity for all other ions is treated in LTE with a constant thermalization parameter $\epsilon = 0.05$. As shown in Fig. 3.41 there is no line that corresponds to Ba II, even though such identification for the absorption at 4400Å seemed plausible in the SYNOW analysis. The temperature is too high to produce a Ba II line, all the more so with the observed strength. The presence of Ba II was checked by calculating a set of single ion spectra, that is calculating the spectrum with all continuum opacities, and only lines from Ba II as well as via the inverse procedure of turning off the line opacity from Ba II. The same procedure was performed for He I ion, that could arise in this region at λ4471; none contribution has been observed in the synthetic spectra. The closest line to 4440Å feature is due to Fe II, though it is not as strong as in the observed spectrum. The evolution of the 4440Å region (Fig. 3.43) displays the inconsistency. The Fe II line explains the feature starting from day 9, though the velocity does not match the observed position of the line.

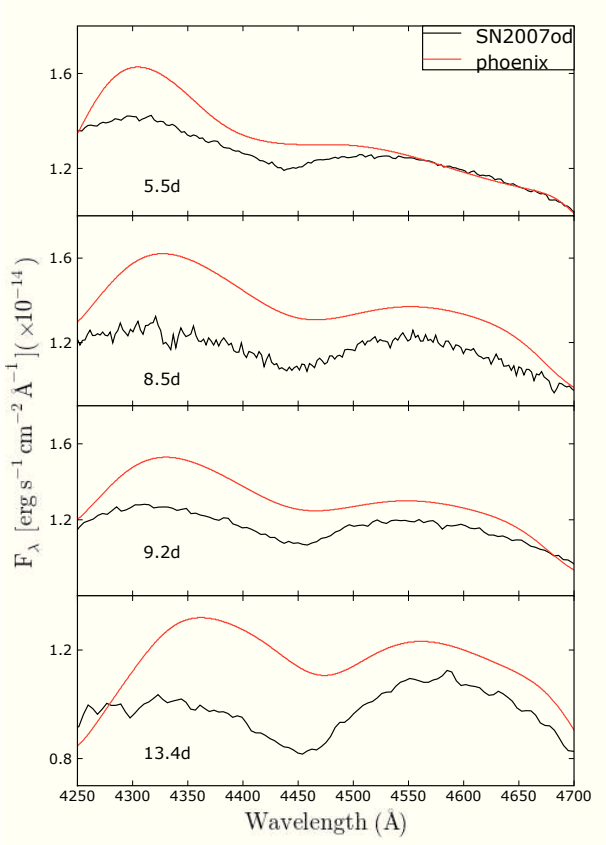

Figure 3.43: Zoom of the `PHOENIX` evolution at the 4440Å region compared to observed spectra.

It is likely that the observed profile of the 4440Å feature is due to the combination of this line with an high velocity feature (HV) of Hβ, formed by an increased line opacity that our simplified model ($\rho = \rho^n$) is not able to reproduce. While Ba II is not completely ruled out by our analysis, we consider it unlikely.

The presence of Si II at 6530Å is confirmed by `PHOENIX` despite the weakness of the synthetic feature. In Fig. 3.41 it is barely visible, but the same analysis as was performed for Ba II confirms its origin. As written before, presence of Si II in SNe IIP is not uncommon. The other absorption features are successfully reproduced, except for the Hα and the absorption lines in the region of 3600Å that are possibly related to Ti II that was not included in the first NLTE spectra in order to minimize CPU time. As shown in Fig. 3.41 we tried different density

indices to better represent the entire profile. The best match for the overall spectrum is given by the model with n=13 (note that the best `PHOENIX` model is always plotted in red), even if the strengths, with respect to the normalized continuum, of H_γ and He I are better reproduced by the model with a density exponent lower than the $n = 13$. The steeper density profile leads to emission components greater than models with flatter density profiles.

The second (8d) and third (9d) spectrum have been constructed using the same setup that was used to calculate the first spectrum, except the density index is decreased from 13 to 9. A steeper profile than that given by a density index of 9, better reproduces the absorption profile of Balmer lines, as is also the case for first epoch, but all the models show flux slightly higher blueward of 5500Å and especially at about 4000Å. Also the strength of Hγ is greater than observed in the model with $n > 9$. The flux on the blue side of Ca II H&K is lower than observed. We found that an a steeper density profile enhances the discrepancy between the observed and synthetic H&K line profile.

The behaviour of the line profiles suggests a density distribution more complex that a single power law. Our calculations suggest that perhaps a broken power law would better reproduce the observed specta, with a shallower density profile at lower velocities and a steeper density profile at higher velocities. We notice that ions as Ca II or He I are clearly better reproduced by a density index close to 9, while the metal elements which form close to the photosphere (and are relatively weak) such as Fe and Si are less sensitive to the assumed density profile. In fact, we note that Fe I-II and Si II are well reproduced with all density profiles, even if the steeper profile does a somewhat better job at reproducing the Si II profile than the flatter profile as seen in Fig. 3.41. While the more complex density profile could be inherent in the initial structure it is also possible that early interaction with a close in circumstellar region can affet the line profiles. Indeed the flat topped nature of the Balmer lines may indicate circumstellar interaction. A broken power law density distribution of the ejecta has been claimed also by Utrobin and Chugai (240) in the case of SN 2000cb. To illustrate this issue we have over-plotted in Fig. 3.45 the Hβ and Hα regions obtained by n=13 models (green dashed line) on the spectra from 8.5d to 17.4.

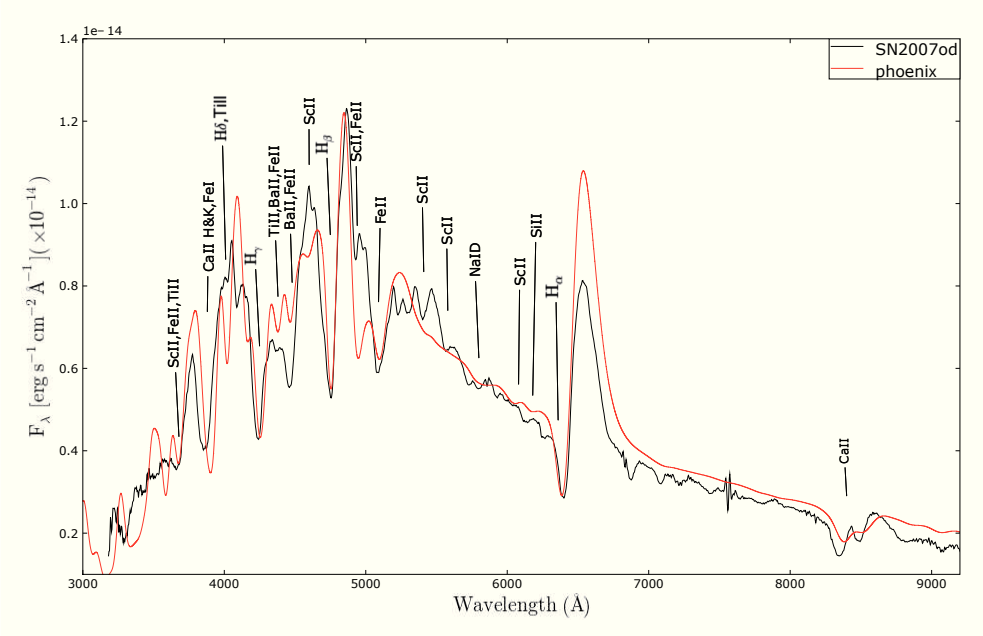

Figure 3.44: Comparison between optical spectrum of SN 2007od at 27 days post explosion (JD 2454404) and `PHOENIX` full NLTE spectrum (for model parameters see Tab. 3.27).

The spectra at 13 and 17 days show the increasing effects of a few metal lines such as Fe II λ5169 and Sc II λ6300 that indicate the lower temperature and the beginning of the plateau phase. Moreover, the presence of metal ions changes the flux at ∼3800Å in the spectra at 13d. From this epoch the 4440Å feature seems more clearly related to Fe II, strengthening our non-identification of Ba II.

The final spectrum we analyze was obtained on November 27, 2007 with the NTT (27d) when the supernova is solidly on the plateau. At this epoch the metal lines are fully developed as is the feature due to Na ID that has replaced the He I λ5876 line. Thanks to the broad wavelength coverage, the good resolution (11Å), and the high signal to noise (S/N=60) it is the best spectrum.

Fig. 3.44 displays our best NLTE model. The species treated in NLTE are H I, Na I, Si I-II, Ca II, Sc I-II, Ti I-II, Fe I-II and Ba I-II. Here, more than in the case of the earlier epochs, the presence of the neutral species change the strength of some lines, especially in the blue (< 4000Å) and around 5000Å. The H lines,

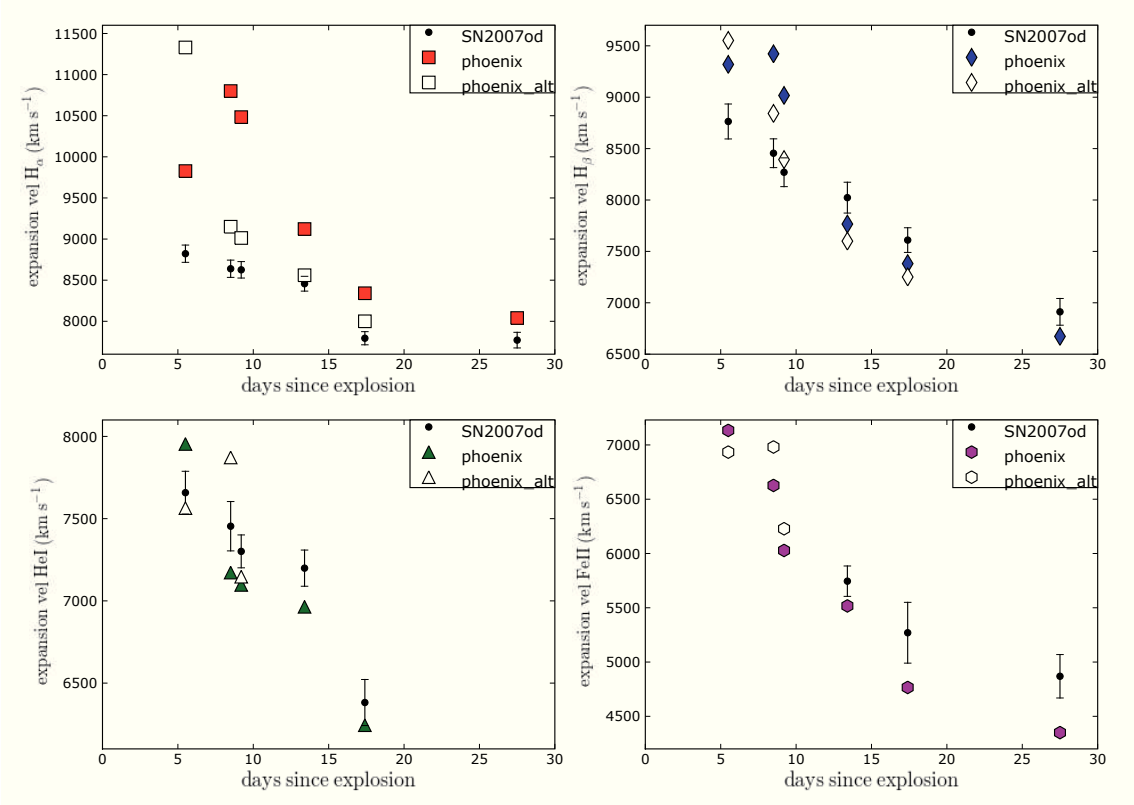

Figure 3.45: Expansion velocities measure of Hα, Hβ, He I, Fe II through `PHOENIX` NLTE spectra compared with those measured in observed spectra.

Na ID, Fe II λ5169, Sc II λ5658, and λ6245 are fit well. The Ca II lines also are well fit. Other lines fit fairly well in terms of velocity width, but not necessarily in total flux. This is due to the fact that many lines are blended with others.

All the models have solar abundances and metallicity. We studied the effects of reducing the model metallicity to that which matches metallicity deduced for the the SN 2007od environment Z<0.004 (for a detailed analysis see 116), but the changes in the spectra were negligible at the 3σ level.

The expansion velocities of Hα, Hβ, He I λ5876 and Fe II λ5169 as derived from fit to the absorption minima of the `PHOENIX` spectra, are shown in Fig. 3.45. The filled symbols indicate the spectra shown in Fig. 3.45 (reported in Tab 3.27), while the open symbols refer to spectra calculated with different density index ($n = 9$ for the first epoch, $n = 13$ for the following epochs).

As is clearly visible in Fig. 3.45 (top left panel) and Fig. 3.42 the velocities of the absorption minima in the NLTE spectra (n=9) for Hα are too blue when compared with the observed spectra, particularly for the first three epochs. Instead the n=13 models well reproduce the velocity of the same epochs. This could be due to several effects. The first could be that the simple uniform power-law density profile assumed here is not accurate enough to describe the outer layers of the ejecta. It could also be that some ionization effect perhaps due to circumstellar interaction reduces the Balmer occupations over those that are predicted in the n=9 models. Combined with the evidence of the flat-top emission, it is somewhat possible that circumstellar interaction effects are responsible for the observed shape of the Balmer lines and the different density profile with respect to the other elements present in the spectra. It is important to remember that the blue wing of Hα includes a blend of Fe II lines and indeed the effect is much smaller for Hβ. The effect disappears with time and also for Hβ the `PHOENIX` and the observed velocity from 13.4d are comparable within the errors for both the models. We noted that from the epoch above the $n = 9$ models better reproduce the Hβ profile in velocity and strength. Neither He I nor Fe II shows this behavior in the early epochs, indicating that the effect is most likely confined to the outermost layers of the ejecta. Except for the epochs reported above, all the line velocities are slightly smaller than observed. While we have not included time-dependent rates in this calculation, this effect seems not so likely to explain the discrepancy between the velocity of the synthetic and observed Hα (54, 55, 57, 241).

In general the result indicates the goodness of the fit obtained by `PHOENIX` with relatively simple assumptions except the issues of the HV Hβ and the emission profile of Hα in the first spectrum related to the possible interaction. They also highlight the importance of the distribution of the elements inside the ejecta for all epochs to obtain the correct physical structure of the ejecta, especially when the event is more peculiar than it appears at first glance.

The sample of photospheric NLTE spectra collected for the SN 2007od is also a good test for the sophisticated modeling of the Spectral-fitting Expanding Atmosphere Method (SEAM) (18, 19, 20, 21). The models predict the emitted flux as well as the shape of the spectrum. Nevertheless, the absolute flux is a

direct result of our models, and the predicted distances serve as useful check on the accuracy of synthetic spectra. We have derived the distances by subtracting our calculated absolute magnitudes from the published photometry (116) and assuming a reddening of E(B-V)$_{tot}$=0.038. Considering all the epochs we obtain the distance modulus to the supernova, μ=32.5±0.3 where the errors include the standard deviation of our fits and the error due to the uncertainty in the interstellar reddening. Since SEAM is strongly dependent on the uncertainties of the explosion date, it seems reasonable to give lower weight to early spectra, since a longer time baseline minimizes the error due to the uncertainties in the explosion day. In fact, if we consider only the later observed spectra, from 13.4d to 27.5d, we find μ=32.2±0.2, in good agreement with the value reported in Inserra *et al.* (116). Furthermore, these spectra better fit the entire spectral range than the other three and the uncertainties are comparable with the Mould *et al.* (157) measurement. It seems not unreasonable to restrict to our best fit. Indeed, a good agreement with the Inserra *et al.* (116) distance (μ=32.2±0.3) is obtained by using all spectra and by taking the explosion date to be JD 2454403 (29 October, 2007). Hence we conclude that the explosion date is October 29 ±1.5 days. In fact, the explosion date should always be determined by a χ^2 minimization in a SEAM analysis.

3.5.2 SN 2009bw with SYNOW

For the second spectrum of SN 2009bw (see Fig. 3.46) we have built the synthetic photospheric spectrum with SYNOW using a T$_{bb}$ ∼12000 K, a v$_{phot}$ ∼7000 km s^{-1}, an optical depth $\tau(v)$ parameterized as a power law of index $n = 9$ and a T$_{exc}$=10000 K assumed constant for all the ions. The main features visible in Fig. 3.46 may be reproduced with only 6 chemical species. The P-Cygni profile of Balmer lines are clearly visible, as well as He I λ5876, but there are also contribution by Ca II, Fe II, Fe I and Si II. Detached H lines better match the line troughs.

SYNOW reproduces well the best spectrum of the SN 2009bw set (∼67d) with the following parameters: T$_{bb}$ ∼5500 K, v$_{phot}$ ∼3050 km s^{-1}, optical depth $\tau(v)$ parameterized as a power law of index $n = 7$ and T$_{exc}$=5000–8000 K assumed

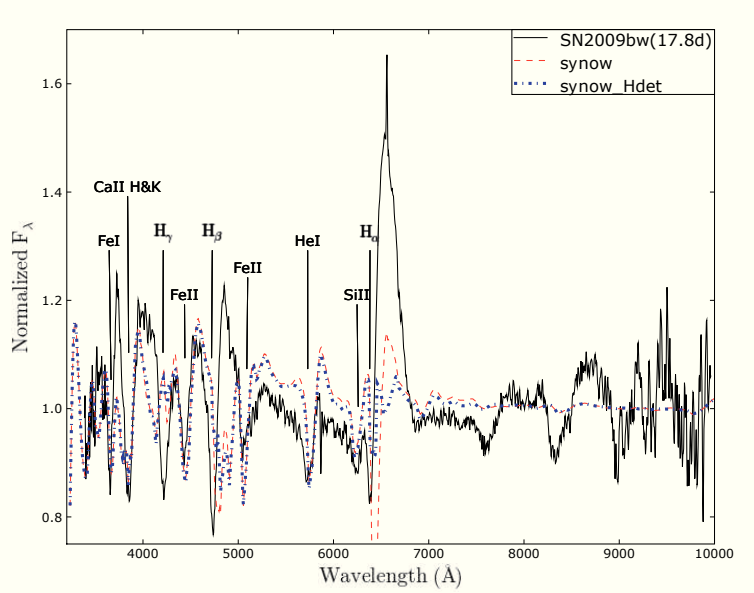

Figure 3.46: Comparison between optical spectrum of SN 2009bw at ∼18 days post explosion (JD 2454916.5) and SYNOW analytical spectra (for composition of synthetic spectra see text). Two SYNOW models are plotted having H detached (blue) or undetached (red). The spectrum has been corrected for absorption in the Galaxy and reported to the galaxy restframe. The most prominent absorptions are labelled.

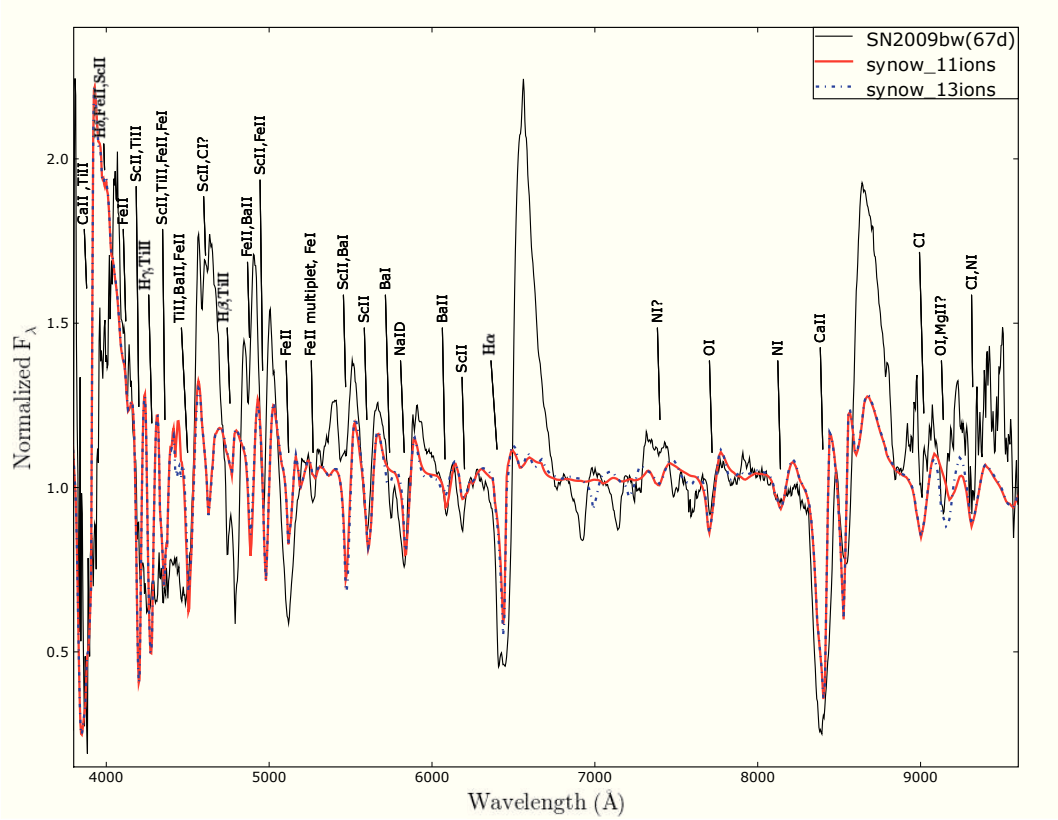

Figure 3.47: Comparison between the optical spectrum of SN 2009bw at ∼67 days post explosion (JD 2454916.5) and two SYNOW analytical spectra. The difference between the SYNOW spectra is due to the presence of Ba I and Mg II ions (red). The spectrum has been corrected for absorption in the Galaxy and reported to the galaxy restframe. The most prominent absorptions are labelled.

for the neutral atoms and T_{exc}=10000 K for the ionized species. The SYNOW spectrum (see Fig. 3.47) has been obtained considering 11 different contributing ions (red dashed line): H I, C I, N I, O I, Na I, Ca II, Sc II, Ti II, Fe I, Fe II, Ba II. WIth the inclusion of two additional ions, Ba I and Mg II, the synthetic spectrum (blue dash-dotted line) better explain the absorption on the blue side Na ID at 5745Å and the shape of the absorption at 9145Å due to a blending of O I and Mg II. The absorption features shown by the blue dash-dotted spectrum around 7100Å are to attributed to Ba I, but because of the noise and the telluric absorption in this range it is difficult to recognize. The other discrepancies between observed and synthetic spectra are explainable by NLTE effects excluded in our computation. The H I and Ca II have been detached to improve the line fit but this causes some problem to the behaviour of the absorption profile closest to the red side of these lines as clearly show the Ca II H&K, the Hγ and Hβ. Interesting line identifications are in the red side (>7000Å) of the spectrum, where absorption lines due to the elements of CNO cycle appear. O I λ7774 has been identified and is probable that there is another absorption correlated to a blending of Mg II and O I λ9260. N I has been identified around 7400Å and 8130Å. C I appears around 9010Å and 9310Å and possibly there is another C I contribution around 4615Å, close line but in this region the fit is affected by the shape of H detached that modifies the shape of the absorption close to the red side of Balmer lines. The presence of O I and N I has been identified in this phase in other SNe as 1999em (175), but the presence of C I lines in spectra of type IIP SNe has been claimed only in few objects, e.g. in SNe 1995V (72) and 1999em (175).

3.6 Dust formation and CSM late interaction in SN 2007od

There are manifold observational signatures of the formation of dust in SN ejecta. Examples are the dimming of the red wings of line profiles due to the attenuation of the emission originating in the receding layers, and the steepening of the optical light curves. These effects were observed in SN 1987A (5, 134) , SN 1998S

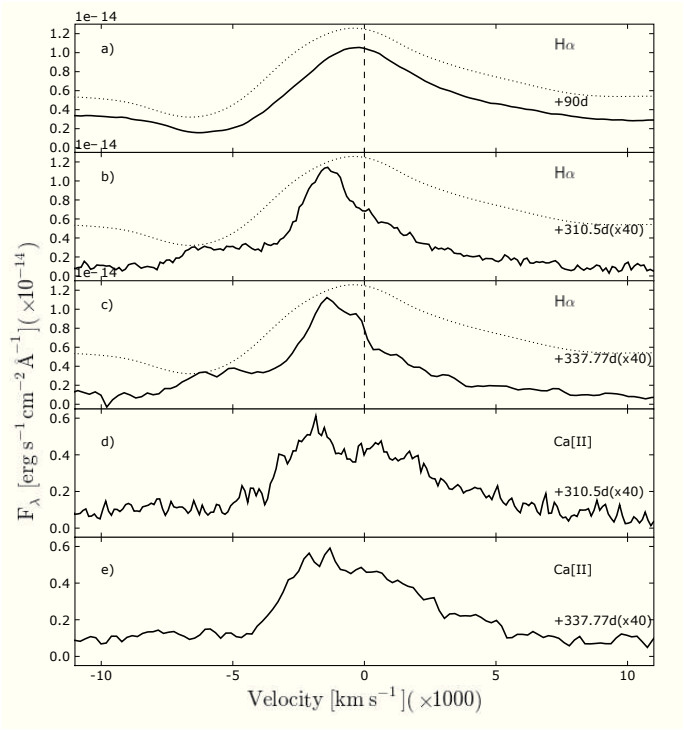

Figure 3.48: Zoom in the Hα region of the SN 2007od spectra at 90d (panel a), 310d b) and 337d c). The dotted line is the photospheric spectrum on day 60 used as a comparison. Panels d) and e) show the [CaII] profiles at late epochs. The abscissa is in expansion velocity coordinates with respect to the rest frame positions of Hα and to the average position of the [CaII] doublet. Phases relative to the explosion (JD 2454404) are indicated on the right.

Table 3.28: Evolution of the Hα line profile.

Phase* (days)	Velocity$^{\diamond}$ (km s^{-1})					Flux†
	Blue edge	Central Peak position	Central Peak FWHM	Central Peak HWHM‡	Red Edge	
60		-301				
75		-319				
90		-240				
226**	-8270	-1325	4110	2100	7770	51.20
303**	-8000	-1500	2790	2010	7860	22.50
310	-8100	-1508	2815	2230	7700	22.21
337	-8090	-1568	2623	2280	7680	12.43
342**	-8180	-1508	2615	2200	7900	14.30
452**	-8100	-1100	2970	2600	7850	5.28
666/692**	-7400					

* with respect to the explosion epoch (JD 2454404).

$^{\diamond}$ with respect to the Hα rest frame wavelength.

† 10^{-16} erg s^{-1} cm^{-2}

‡ HWHM of the blue, unabsorbed wing computed with respect to the rest frame wavelength.

** spectra from Andrews *et al.* (4), flux calibrated with broad band photometry.

(193), SN 1999em (68) and SN 2004et (139). Additional evidence is a strong IR excess observed in a few objects at late times, e.g. SNe 1998S and 2004et, but also, though very rarely, at early times, as in SN 2006jc. We stress that for the comprehension of the physical processes occurring in the aftermath of the explosions it is important to distinguish between IR thermal emission from newly formed dust within the SN ejecta and IR echoes of the maximum-light emission by pre-existing, circumstellar material (CSM).

A distinguishing precursor of dust formation is the detection of rotation-vibration molecular lines of CO, which are powerful coolants. Indeed CO was observed in several SNe, e.g., SNe 1995ad (218), 1998dl and 1999em (217), 2002hh (192), 2004dj (122) and 2004et (121, 139), in which also dust formation in the ejecta was detected. The presence of CO molecular lines seems, therefore, a necessary condition for dust condensation in the ejecta, as reported by Pozzo *et al.* (193).

Another important issue is the site of dust formation in SNe. Indeed dust in core-collapse SNe has been detected: a) deep within the ejecta, e.g., in SNe

1999em and 1987A, or b) in a cool dense shell (CDS) created by the SN ejecta/CSM interaction, e.g. in SNe 1998S, 2004dj and 2004et. The scenarios are not exclusive and evidence of both phenomena was found, as shown in Kotak *et al.* (121). Unfortunately, the paucity of MIR late time observations makes the determination of the site of dust formation very difficult.

The signature of dust formation in SN 2007od is provided by the blue-shift ($\sim$ 1500 km s^{-1}) of the peak of Hα and by the corresponding attenuation of the red wing, which is seen in late time spectra (see the panels of Fig. 3.48). On the other hand, the decay rates of the optical light curve between 208d and 434d (including also data by Andrews *et al.* (4), cfr. Tab. 3.3) are in close agreement with the decay of ^{56}Co, suggesting that the dust formed during the period of un-observability (February to May 2008), i.e. before the late-time SN recovery. Indeed Andrews *et al.* (4) show that the optical and IR SED of SN 2007od at about 300d can be fitted by the sum of a black-body originating in the SN ejecta plus a cooler black-body emission at 580 K due to dust.

In addition to the Hα skewed central peak, the line profile (Fig. 3.48) shows also the presence of structures. A boxy blue shoulder extends to about –8000 km s^{-1}(cfr. Tab 3.28), then drops rapidly to zero. This is reminiscent of the boxy profiles of late-time interacting SNe II SNe 1979C, 1980K (73, and references therein), 1986E (37) which have been interpreted as evidence of interaction of the SN ejecta with a spherical shell of CSM (44, 48). We note that, unlike other SNe, in SN 2007od a red, flat shoulder is not visible, possibly because it is attenuated by dust intervening along the line of sight.

A hint of a narrow, unresolved emission at the Hα rest wavelength, more evident in the Gemini spectra by Andrews *et al.* (4), is visible also in our latest spectrum. The peak of the [Ca II] $\lambda\lambda$ 7292, 7324 emission is also blue-skewed with attenuation of the red wing in analogy to Hα (panels d and e of Fig. 3.48). Instead, [Ca II] does not show the blue shoulder indicating that the interaction does not affect the metal-enriched ejecta, as noted in Andrews *et al.* (4).

Andrews *et al.* (4) noticed analogies between the Hα profiles of SN 2007od and SN 1998S, and tried to explain the Hα profile between 8 and 20 months as the combination of different phenomena: the interaction of the ejecta with a CSM torus and a blob of CSM out of the plane of the torus, plus the possible

presence of a light echo. Each process corresponds to specific components of the line profile (cfr. their Fig. 4): two components at about ± 1500 km s^{-1}, that arise in the radiative forward shock of the ejecta interacting with the torus which should be highly inclined to produce the low observed projected velocities; a slightly broader component at about -5000 km s^{-1} due to the ejecta–blob interaction with a larger velocity component along the line of sight; a residual ejecta component similar to that observed on day 50, required to explain the broad red wing of the line; and a light echo that became dominant about 2 yr after explosion. The blue-shifted component at -1500 km s^{-1} appears stronger than that at $+1500$ km s^{-1}. This asymmetry was attributed to strong extinction suffered by the receding component due to dust formed in the CDS. The weakness of this scenario is in the geometry of the torus. As mentioned above, the torus is required to have an inclination of the order of 80° (for H expansion velocity of the order of 10000 km s^{-1}) to explain the small projected velocities. Even for a thick torus, it is difficult to reconcile the required high inclination with the strong extinction suffered by the red component. For the same ejecta velocity the inclination of the blob along the line of sight is about 60°, i.e. it is not orthogonal to the torus.

Useful information on the phenomena taking place in SN 2007od at late times come from the comparison of the late Hα profile with those of other SNe IIP. In Fig. 3.49 all spectra were corrected for absorption and rescaled to the distance of SN 2007od. The line flux of SN 2007od is significantly smaller than those of other SNe. The blue, (likely) unabsorbed wing of the central/core Hα emission of SN 2007od roughly coincides in wavelength with the corresponding blue wings of other non-interacting SNe II at similar phases (we stress that SN 1999em at this epoch does not show sign of interaction). In particular, the HWHM(Hα)$\sim$ 2000 km s^{-1} (Tab. 3.28) of the blue side is compatible with the FWHM(Hα)$\sim$4000 km s^{-1} of the emission of SN 1992H at 311 days after explosion, a SN that has a similar kinematics to SN 2007od. Also the terminal velocities of Hα seem very similar, since the edge of the blue shoulder of SN 2007od extends out to 8000 km s^{-1}, a velocity comparable to the bluest wing of the residual P-Cyg absorption of SN 1992H. The flux of the blue wing of the central emission (at about 6500Å), likely less absorbed, coincides with those of other SNe II, e.g. SN 1999em. On the

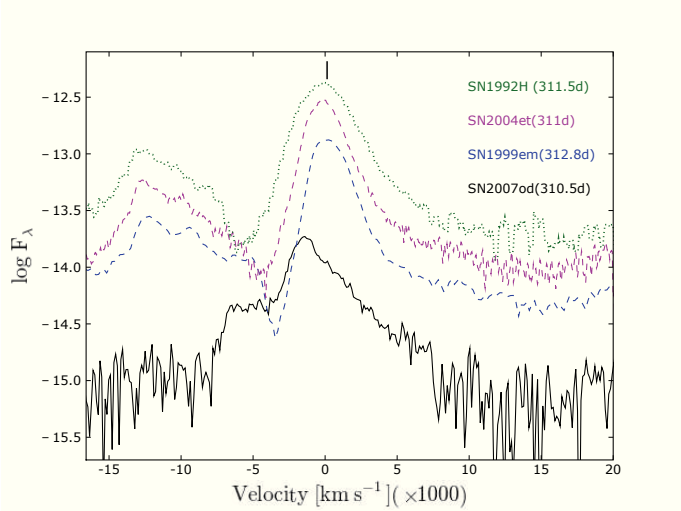

Figure 3.49: Comparison of the Hα profile of SN 2007od during the nebular phase with those of SNe 1992H, 1999em and 2004et. The spectra of all SNe were reported to the same distance of SN 2007od. The position of the Hα rest wavelength is marked with a vertical dash.

contrary, the flux at the rest wavelength is significantly depressed, and even more is the red wing, indicating the presence of dust within the ejecta. The resulting profile is skewed. The comparison, therefore, seems to point towards a common origin of the line cores extending between 6450 and 6650Å as arising from the spherical expanding ejecta.

Evidence of dust in the ejecta was also seen in SN 1987A and SN 1999em. In the case of SN 1987A the dust formed in an inner core at v$\sim$1800 km s^{-1} with optical depth $\tau \leq 1$ at a much later epoch t$\sim$526d (135) than in SN 2007od. Also in SN 1999em the dust formed late (t$\sim$500d) when no sign of interaction was present. Here the dust location, within an inner region at v$\sim$800 km s^{-1} with $\tau \geq 10$, was derived from a careful analysis of the profile of the [O I] $\lambda\lambda$6300-6363 doublet (68). As already mentioned, the [O I] doublet is barely visible in the late spectra of SN 2007od and the analysis relies on the line profile of Hα which arises mainly from the outer ejecta.

As for the CSM/ejecta geometry proposed by Andrews *et al.* (4) to explain the Hα profile, the formation of dust deep within the ejecta of SN 2007od is also

not devoid of problems. In fact, at the early epoch of occurrence (t$\leq$ 226d) the SN ejecta are expected to be too warm for dust condensation (123), while the presence of interaction at this phase justifies the dust formation in an outer CDS. It is possible that SN 2007od was intrinsically less energetic than average CC-SNe, similar to low–luminosity SNe like 1997D and 2005cs and that the temperature at about 200 days was already low enough to allow dust condensation in some regions of the SN ejecta.

Observations show first evidence of interaction already on day 226. At this epoch the ejecta reached the material expelled by the progenitor in mass loss episodes at short times before explosion. The interaction produces forward and reverse shocks (48). In general, between the two shocks the gas undergoes thermal instability and cooling, thus creating a cool dense shell (CDS) in which subsequently dust can form. The formation of a CDS can take place behind the forward shock primarily in the CSM, as invoked in the case of SN 2006jc by Mattila *et al.* (142), or behind the reverse shock as in SN 1998S (193). With a standard mass loss rate, the CDS forms behind the reverse shock, i.e. in the ejecta that are denser and chemically richer, hence more prone to dust formation (193). The presence of dense clumps in the CSM, which eventually are overcome by the fast SN ejecta, may allow the formation of a CDS (and dust) also in regions that eventually are deeply embedded in the ejecta.

We believe that the observed late-time line profiles at about 300 days can be explained schematically with: 1) a relatively broad skewed emission from SN ejecta (FWHM$\sim$2800 km s^{-1}) typical of SNe II at corresponding epochs, significantly absorbed by dust formed *within the ejecta, possibly in clumps*; 2) a distorted boxy profile with high velocity (up to 8000 km s^{-1}), evidence of the interaction of the H-rich ejecta with a *spherical* outer CSM, with the red shoulder depressed due to dust absorption. The presence of late time interaction is supported by the re-brightening of optical light curves by day $\sim$653, as shown by Andrews *et al.* (4); 3) an unresolved emission which forms in the un-shocked CSM (cfr. 4).

A plausible scenario to explain the observed structure of Hα could be similar to that proposed for SN 1988Z (50). The ejecta collides with a two-component wind: a spherically symmetric substrate composed of a relatively rarefied gas,

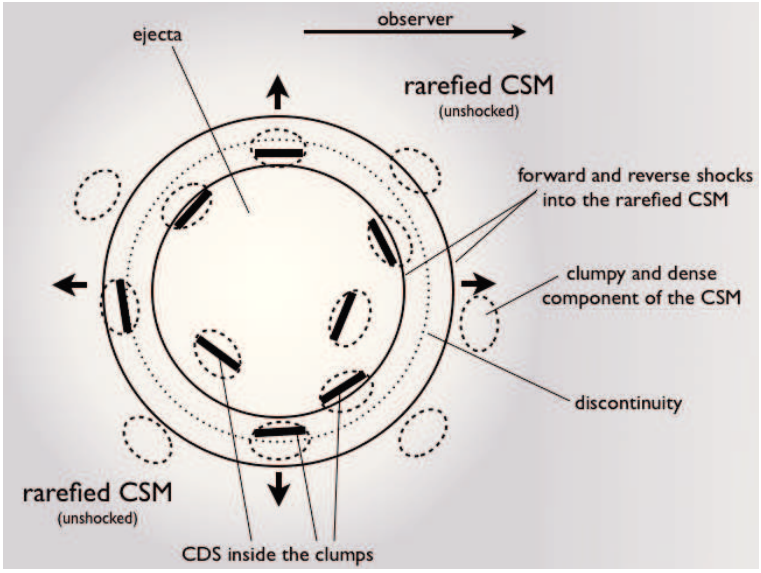

Figure 3.50: Schematic illustration of the geometry of the newly formed dust in SN 2007od. The CDS arise both inside the dense clumps and between the reverse shock and the discontinuity of the rarefied component of the CSM.

and very dense clumps (cfr. Fig. 3.50). Such structure allows the formation of the boxy profile due to the interaction between the fast expanding ejecta and the CSM and, at the same time, the early formation of dust deep in the ejecta in the CDS of the inner clumps. The dust inside the ejecta progressively screens the radiation arising from the receding layers and skews both the central profile from the unperturbed ejecta and the boxy profile from the interaction. Indeed the profile of Hα suggests the presence of dust also in the inner ejecta since dust formation in the outer CDS dims both the blue and red wings in the same way, and the red shoulder would appear boxy and not tilted (Fig. 3.48).

The analysis of the IR SED performed by Andrews *et al.* (4) shows a strong IR excess attributable to warm dust, consistent with an amorphous-carbon dominated model with 75% amorphous-carbon and 25% silicate. The radiative transfer models used by Andrews *et al.* (4) suggest up to 4.2 x 10^{-4} $M_{\odot}$ dust, mainly composed of amorphous-carbon grains formed in a CDS.

The flat blue shoulder of Hα is barely visible in the spectrum taken on day 226 but is very well formed on day ∼337 when the emission extends out to ∼8200

km s^{-1}, and remains well defined until day 680. Assuming that the CSM is due to the mass loss of material traveling at 10 km s^{-1}, this indicates the presence of CSM in a range of distances of about 1300–1950 AU and that the progenitor experienced enhanced mass loss 500–1000 yr before the explosion.

3.7 Discussion

In the following subsections we develop a discussion about SN 2007od and SN 2009bw to which we have devoted a detailed analysis in three different papers written during this PhD, Inserra *et al.* (116) and Inserra *et al.* (115) on the SN 2007od and Inserra *et al.* (114) on the SN 2009bw. For the other three objects of our sample, we have analyzed light curves and spectra in the previous Sec. 3.2 & 3.5 and founded a some cues that lead to ejecta-CSM interaction in the early phases. The brief discussion about these objects is reported in Sect. 3.7.3. The main observational data derived in this thesis for these five objects are summarized in Tab. 3.29.

3.7.1 SN 2007od

In the previous sections we presented new data of the type II SN 2007od in UGC 12846, including for the first time photometric and spectroscopic observations of the early epochs after the explosion.

Analysis of the multicolor and bolometric light curves indicates that at early times SN 2007od was a luminous SN IIP like SNe 1992H and 1992am. The absolute magnitude at maximum, $M_V = -18.0$, the bolometric luminosity $L_{bol} = 6.0 \times 10^{42}$ erg s^{-1} (see Tab. 3.3), and the relatively short plateaus in V and R suggest an envelope mass smaller than that of standard plateau events.

SN 2007od shows several interesting properties. At early epochs (t< 15d), T_{bb} and v_{exp} are lower than in other bright SNe II, e.g. SN 1992H and SN 2004et. In the same period the Hα emission component is squared, and there is evidence for HV features in Hβ and Hγ. These properties, together with bright luminosity and shallow absorption features, point towards early interaction of the ejecta with a low density CSM (cfr. 156).

Table 3.29: Main data of the SNe sample.

SNe data	2007od	2009bw	2009dd
adopted distance modulus	$\mu = 32.05 \pm 0.15$	$\mu = 31.53 \pm 0.15$	$\mu = 30.74 \pm 0.15$
SN heliocentric velocity	1734 ± 3 km s^{-1}	1155 ± 6 km s^{-1}	1025 ± 15 km s^{-1}
adopted reddening	E_{tot}(B-V)= 0.04	E_{tot}(B-V)= 0.31	E_{tot}(B-V)= 0.45
explosion day (JD)	$\sim 2454404.5 \pm 5$	$\sim 2454916.5 \pm 2$	$\sim 2454925.5 \pm 5$
L_{bol} peak	6.0×10^{42} erg s^{-1}	2.6×10^{42} erg s^{-1}	2.16×10^{42} erg s^{-1}
(JD)	(2454410 ± 2)	(2454925 ± 2)	(2454937 ± 4)
late time decline mag(100d)$^{-1}$	1.06	1.06	1.07
interval days	208–434	139–239	117–277
M(Ni)	0.02 $M_\odot$	0.022 $M_\odot$	0.034 $M_\odot$
M(ejecta)	5–7.5 $M_\odot$	8.3–12 $M_\odot$	–
explosion energy	0.5×10^{51} ergs	0.3×10^{51} ergs	–
interaction evidences	flat Hα, HVHβ	HVHα, HVHβ	X, possible HVHα

SNe data	2007pk	2010aj
adopted distance modulus	$\mu = 34.23 \pm 0.15$	$\mu = 34.71 \pm 0.15$
SN heliocentric velocity	5116 ± 16 km s^{-1}	6386 ± 20 km s^{-1}
adopted reddening	E_{tot}(B-V)= 0.11	E_{tot}(B-V)= 0.04
explosion day (JD)	$\sim 2454412 \pm 5$	$\sim 2454265.5 \pm 8$
L_{bol} peak	6.26×10^{42} erg s^{-1}	2.68×10^{42} erg s^{-1}
(JD)	(2454420 ± 2)	(2454269 ± 4)
late time decline mag(100d)$^{-1}$	–	4.06
interval days	–	87–103
M(Ni)	–	$<$0.004 $M_\odot$
M(ejecta)	–	–
explosion energy	–	–
interaction evidences	X, spectra	none

The absence of X-ray or radio detection is not against this scenario, because the distance to SN 2007od is 26 Mpc, much larger than that of SN 1999em (7.5-7.8 Mpc). If for SN 2007od we assume the same radio and X-ray luminosity of SN 1999em, the observed flux should be below the treshold of the observation. Indeed the X-ray flux of SN 1999em was close to the limit (about 10^{-14} ergs cm^{-2} s^{-1}) as well as the radio flux reported in Pooley *et al.* (190). If SN 2007d had the same emission of SN 1999em, the expected X-ray flux would be about 10^{-15} ergs cm^{-2} s^{-1}, much lower than the 3σ upper limit by Immler and Brown (113). Moreover, HV features in optical spectra were proposed by Chugai, Chevalier, and Utrobin (49), as clues of interaction and detected in SN 1999em and SN 2004dj. We claim that this is the case also for SN 2007od. A rough estimate of the CSM mass in close proximity to the progenitor can be derived starting by SYNOW parametrization of the early spectra. Through the optical depth of high-velocity lines (τ=0.8) we can gain the H density in the transition. Thanks to the Saha equation in LTE approximation it is possible to obtain the ratio between HI (n_{HI}=1.7×10^{-30} – 1.4×10^{-31} based on different assumptions) and the total H density. This ratio is roughly related to the mass of the CSM. In our case we estimated a CSM mass of the order of $\sim 10^{-3}$ – 10^{-4} $M_\odot$. This value is in agreement with the velocities of the HV lines reported in Sec. 3.4.1, in fact a greater amount of CSM would not allow reaching such velocities.

The light curves show a drop of ∼6 mag from the plateau to the tail. The tail is therefore relatively faint, corresponding to a ^{56}Ni mass M(^{56}Ni)$\sim$ 3x10^{-3} $M_\odot$, unusually small for SNe IIP that are luminous at maximum and are comparable to those estimated in faint SNe IIP such as SN 2005cs. In Sect. 3.6 we show spectroscopic evidence of dust formation at late times and therefore that the derived amount of ^{56}Ni should be considered as a lower limit. A more solid estimate, based on the bolometric flux including the MIR late time emission by Andrews *et al.* (4), is M(^{56}Ni)$\sim$ 2x10^{-2} $M_\odot$, thus indicating that about 90% of the optical+NIR emission is reprocessed by dust.

Dust formation occurs within day 226 after the explosion, quite early in comparison to other core-collapse SNe, e.g. SN 1987A, SN 1999em and SN 2004et. To our knowledge, SN 2007od is the type IIP SN showing the earliest dust formation.

Late-time optical spectroscopy shows also clear signs of strong ejecta–CSM interaction. Indeed, the complex Hα profile can be interpreted as the combination of a typical ejecta emission, ejecta–CSM interaction, and the presence of dust in clumps. However, the combined effect of interaction and dust does not affect the decline rate that is similar to that of ^{56}Co decay from 208 to ∼434 days past explosion (Fig. 3.14). CSM-ejecta interaction makes a minor contribution to the bolometric luminosity and only affects line profiles. A flattening of the light curve might be present after day 600 as shown in Andrews *et al.* (4), either because of increased interaction or a light echo, but the data are too inhomogeneous for a strong statement in this sense.

Because of the location in the outskirts of the parent galaxy, the metallicity at the position of SN 2007od could not be determined from our spectra nor were we able to find spectra of the host galaxy in the main public archives. UGC 12846 is classified as Magellanic Spiral (Sm:) of low surface brightness (LSB), as confirmed by our Fig. 3.1 (left) in which the host galaxy is barely visible. LSB galaxies are objects with peak surface brightness $\mu^B_{peak} \geq$ 22.5-23 mag arcsec^{-2} having generally low metallicity (Z$<\frac{1}{3}$Z$_\odot$ McGaugh (148); 0.1<Z(LSB)/Z$_\odot$<0.5, with no radial dependence de Blok and van der Hulst (56)). Smoker, Axon, and Davies (215) and Smoker *et al.* (214) for UGC 12846 report a central surface brightness μ^B_{peak} ∼22.65 decreasing to $\mu > 26$ mag arcsec^{-2} at position of the SN. Using $M_B = -16.79$ (215) and the diagram shown in McGaugh (148) we can consider UGC 12846 as a LSB with average oxygen abundance. Therefore, the environment of SN 2007od is likely metal poor with log(O/H) ∼ −4. In general, we expect that low metallicity stars suffer little mass loss and have big He cores and massive H envelopes when they die (105). The significant presence of CSM both at early and late times, a clear evidence of mass loss, seems in disagreement with this scenario, although recently Chevalier (43) suggested that there are mass loss mechanisms that do not decline at lower metallicities. Alternatively, the presence of companions can explain strong mass loss by metal poor stars.

In nebular spectra of core-collapse SNe the flux ratio $R = \frac{[CaII]\lambda\lambda7291,7324}{[OI]\lambda\lambda6300,6364}$ is almost constant with time (80, 81). This ratio, only marginally affected by differential reddening, is a useful diagnostic for the mass of the core and consequently for estimating the progenitor mass, with small ratios corresponding to higher

main sequence masses. In SN 1987A it was $R \sim 3$ (67), for the faint SN 2005cs it was $R \sim 4.2 \pm 0.6$ (171), while for SNe 1992H and 1999em we computed the values $R \sim 1.61$ and $R \sim 4.7$, respectively. In comparison, the measured ratio $R \sim 32 \pm 5$ of SN 2007od is very high, suggesting that the progenitor mass is quite small.

A super-asymptotic giant branch (hereafter SAGB) progenitor with a strongly degenerate Ne-O core might explain these observables. As shown by Pumo *et al.* (196), the most massive SAGB stars ($M \lesssim M_{mas} \sim 10$ – $11\ M_{\odot}$) can indeed suffer strong episodes of mass loss while still preserving significant H envelopes ($\gtrsim$ 5-9 $M_{\odot}$) at the end of their evolution. In fact, the outcome of SNe from a super-AGB progenitor can differ according to the configuration of the super-AGB star at the moment of the explosion, and may range from a type II SN (either IIP or IIL depending on the mass of the envelope) with relatively low degree of CSM interaction, to a type IIb SN having stronger interaction with the CSM, up to a stripped-envelope SN. The high value of R could be explained also with Fe core collapse SN II in the low limit of the mass range ($M_{\odot} \sim$11-12); these stars might produce oxygen-poor SN II. But these stars hardly explain the episodes of mass loss at metallicities lower than solar (254). Binary companions could easily explain the episodes of mass loss, regardless of the progenitor star. We cannot exclude *a priori* the binary system solution.

The formation of dust plays a key role in shaping the display of SNe II. In SN 1998S, Pozzo *et al.* (193) calculated a value of $\sim 10^{-3}\ M_{\odot}$ of dust in a CDS. Elmhamdi *et al.* (68) obtained a lower limit of $\sim 10^{-4} M_{\odot}$ in the ejecta of SN 1999em from the analysis of the [O I] 6300 Å evolution. For SN 1987A Ercolano, Barlow, and Sugerman (69) reported a dust mass of $7.5 \times 10^{-4}\ M_{\odot}$. For SN 2004et Kotak *et al.* (121) estimated a dust mass of $M = (2-5) \times 10^{-4}\ M_{\odot}$ in the CDS, and through hydrodynamical considerations suggested that the mass of new dust produced either in the ejecta or in a CDS never exceeded $10^{-3}\ M_{\odot}$. The formation of 1.7 to $4.2 \times 10^{-4} M_{\odot}$ of dust (4), contributes to the unusual drop of ~ 6 mag (from plateau to tail) in SN 2007od.

The dust mass estimate can change by an order of magnitude if we consider silicates or carbon grains and if we take into account the possibility of very opaque clouds (68, 193). Indeed, when forming in clumps most of the dust could be undetectable due to the clump opacities, and be in much higher amounts than

necessary to produce the observed blackbody emission. We note that the environment of this SN is different from other dust forming SNe that normally explode in spiral galaxies or in regions with solar metallicity. Indeed, the environment metallicity of SN 2007od is between solar and that of galaxies at $z \gtrsim 6$. Thus, one may speculate that larger amounts of dust are formed at high redshift because of low metallicities.

3.7.1.1 Explosion and progenitor parameters

We estimated the physical properties of the SN progenitor (namely the ejected mass, the progenitor radius, the explosion energy) by performing a simultaneous χ^2 fit of the main observables (i.e., bolometric light curve, evolution of line velocities, and continuum temperature at the photosphere) against model calculations, in analogy to the procedure adopted for other SNe (e.g., SNe 1997D, 1999br, 2005cs, 260, 261).

Two codes were used to produce models: a semi-analytic code (described in detail in 261) which solves the energy balance equation for a spherically symmetric, homologously expanding envelope of constant density, and a new, relativistic, radiation-hydrodynamics code (described in detail in Pumo, Zampieri, and Turatto 195 and Pumo & Zampieri, submitted). The latter is able to compute the parameters of the ejecta and the emitted luminosity up to the nebular stage by solving the equations of relativistic radiation hydrodynamics in spherically symmetry for a self-gravitating fluid which interacts with radiation, taking into account the heating due to decays of radioactive isotopes synthesized in the SN explosion.

The semi-analytic code was used to perform a preparatory study in order to constrain the parameter space and, consequently, to guide the more realistic but time-consuming simulations performed with the relativistic radiation-hydrodynamics code. We note that modelling with these two codes is appropriate if the emission from the supernova is dominated by the expanding ejecta. For SN 2007od the contamination from interaction and the formation of dust may in part affect the observed properties of the supernova during the first $\sim$ 20 days and

from the end of the plateau afterwards. However, there is no evidence that either interaction or dust formation are important during most of the photospheric phase ($\sim 20 - 90$ days) and hence our hydrodynamic modeling can be safely applied to SN 2007od during this time frame. This is more than sufficient for providing a reliable estimate of the main physical parameters of the ejecta, with the exception of the Ni mass that, as already mentioned, is inferred from late time optical and NIR observations.

The shock breakout epoch (JD = 2454404 ± 5) and distance modulus ($\mu = 32.05 \pm 0.15$) adopted in this thesis are used to fix the explosion epoch and to compute the bolometric luminosity of SN 2007od for comparison with model calculations. Assuming a ^{56}Ni mass of 0.02 $M_\odot$, the best fits of the semi-analytic and numerical models are in fair agreement and return values of total (kinetic plus thermal) energy of ~ 0.5 foe, initial radius of $4 - 7 \times 10^{13}$ cm, and envelope mass of $5 - 7.5$ $M_\odot$ (Fig. 3.52).

The best-fit models show some difficulty in reproducing the early part of the light curve ($\lesssim 25$ days) and the very end of the apparent plateau (at ~ 106 day). The excess at early epochs may be caused in part by the ejecta-CSM interaction (see discussion in Sect. 3.7). As for the point at $\sim$106 days, the excess may be related to the final interaction stage with the H-rich CSM that occurs at the end of the recombination phase.

In Fig. 3.52 we show also the evolution of the photospheric velocity and temperature. The agreement between our modeling and the observational data is good apart from, once again, the early phase. The reason for this difference may be due to both interaction and the approximate initial density profile used in our simulations, which may not reproduce correctly the radial profile in the outermost high-velocity shells of the ejecta formed after shock breakout (e.g., 242, Pumo & Zampieri, in prep.). For this reason, we did not include the first 3 measurements of the line velocity in the fit.

The values of the modeling reported above are consistent with the explosion and mass loss of a SAGB star with an initial (ZAMS) mass $\lesssim M_{mas}$ ($M_{mas} \sim 9.7$ to 11.0 $M_\odot$ for the environment metallicity limits of 196). The moderate ejecta mass and amount of ^{56}Ni, the relatively low explosion energy, the very large Ca/O ratio, and the presence of C rich dust fit reasonably well within this framework.

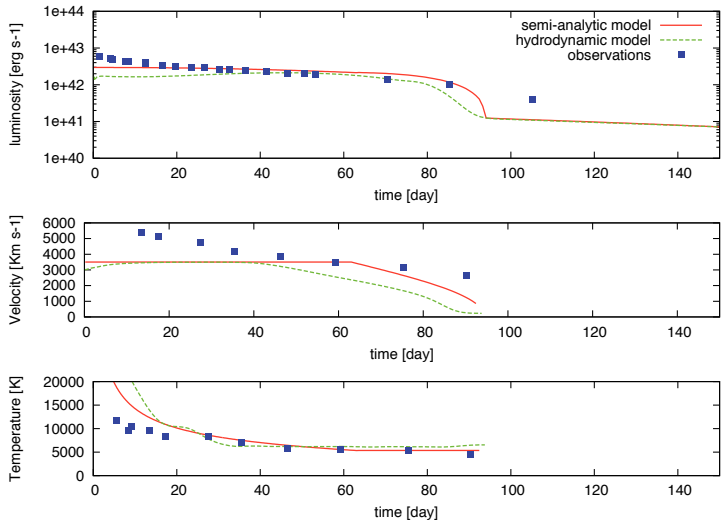

Figure 3.51: Comparison of the evolution of the main observables of SN 2007od with the best-fit models computed with the semi-analytic code (total energy ~ 0.5 foe, initial radius 4×10^{13} cm, envelope mass 5 $M_{\odot}$) and with the relativistic, radiation-hydrodynamics code (total energy ~ 0.5 foe, initial radius 7×10^{13} cm, envelope mass 7.6 $M_{\odot}$). Top, middle, and bottom panels show the bolometric light curve, the photospheric velocity, and the photospheric temperature as a function of time respectively. To estimate the photosphere velocity from observations, we used the value inferred from the Sc II lines (often considered in type II SNe good tracer of the photosphere velocity).

Some of these constraints may appear consistent with a fallback supernova from a massive star. In this scenario the mass-cut is located sufficiently far out to trap part of the ^{56}Ni and intermediate mass elements (e.g. O) that fall back onto the compact object. Also the relatively low explosion energy may be related to this mechanism (82, 262). However, significant mass loss prior to explosion is not easy to reconcile with a high mass progenitor in a low metallicity environment. Problematic are also the moderate amount of ^{56}Ni estimated including MIR data, the relatively high expansion velocity and low ejecta mass, and the C-rich dust (4), since usually these stars produce silicate-rich dust (121, and reference therein).

3.7.2 SN 2009bw

3.7.2.1 Explosion and progenitor parameters

We have estimated the physical properties of the SN progenitor (namely, the ejected mass, the progenitor radius, the explosion energy) by performing a model/data comparison based on a simultaneous χ^2 fit of the main observables (i.e. bolometric light curve, the evolution of line velocities and the continuum temperature at the photosphere), using the same procedure adopted for SN 2007od in Inserra *et al.* (116).

According to this procedure, we employ two codes, the semi-analytic code by Zampieri *et al.* (261), to perform a preparatory study in order to constrain the parameter space, and that including an accurate treatment of radiative transfer and radiation hydrodynamics (195, ; Pumo & Zampieri, 2011), for tighter grid of accurate models needed for the final comparison.

Modeling with these two codes is appropriate if the emission from the supernova is dominated by the expanding ejecta. For SN 2009bw the contamination from interaction may in part affect the observed properties. However, since there is no evidence that this effect dominates during most of the post-explosive evolution, we assume in the following that our modeling can be applied to SN 2009bw, returning a reliable estimate of the main physical parameters of this event.

The shock breakout epoch (JD = 2454916.5 $\pm$ 3) and distance modulus (μ = 31.53) adopted in this thesis are used to fix the explosion epoch and to compute the quasi bolometric (UBVRI) luminosity of SN 2009bw. In order to evaluate the

bolometric luminosity, we further assume that the supernova has the same color evolution as SN 1999em and hence

$$L_{09bw} = (L_{99em}/L_{UBVRI-99em}) * L_{UBVRI-09bw},$$

where L_{09bw}/L_{99em} and $L_{UBVRI-09bw}/L_{UBVRI-99em}$ are the bolometric and quasi bolometric luminosity of SN 2009bw and SN 1999em, respectively (data concerning SN 1999em are taken from 68).

Assuming a ^{56}Ni mass of 0.022 $M_\odot$ (see Sect. 3.3), the best fits of the semi-analytic and numerical model are in fair agreement and return values of total (kinetic plus thermal) energy of ~ 0.3 foe, initial radius of $3.6 - 7 \times 10^{13}$ cm, and envelope mass of $8.3 - 12$ $M_\odot$.

The agreement between our modeling and the observed luminosity and temperature evolution is reasonably good, except at early epochs ($\lesssim 33$ days). These discrepancies may be in part caused by the ejecta-CSM interaction (see discussion in Sect. 3.7.2.2) leading to an excess of the observed luminosity, and to the approximate initial density profile used in our simulations, that does not reproduce correctly the radial profile of the outermost high-velocity shell of the ejecta formed after shock breakout (cfr. 194)

The values of the modeling parameters reported above are consistent with a scenario leading a RSG as SN progenitor.

Unsatisfactory is the best fit of the velocity during the entire photospheric phase. This is unusual for the Pumo and Zampieri code that has proved to work well for normal SN II, indicating that for SN 2009bw other processes might be at work. This discrepancy could be related to the interaction that causes a creation of a pseudo-photosphere at a radius bigger than expected by the model. This possibility has occurred in luminous-interacting SNe as shown by Agnoletto *et al.* (1).

3.7.2.2 Conclusions about SN 2009bw

In the previous Sections we have presented and discussed the photometric and spectroscopic data of SN 2009bw in UGC 2890 from the photospheric to the nebular stages.

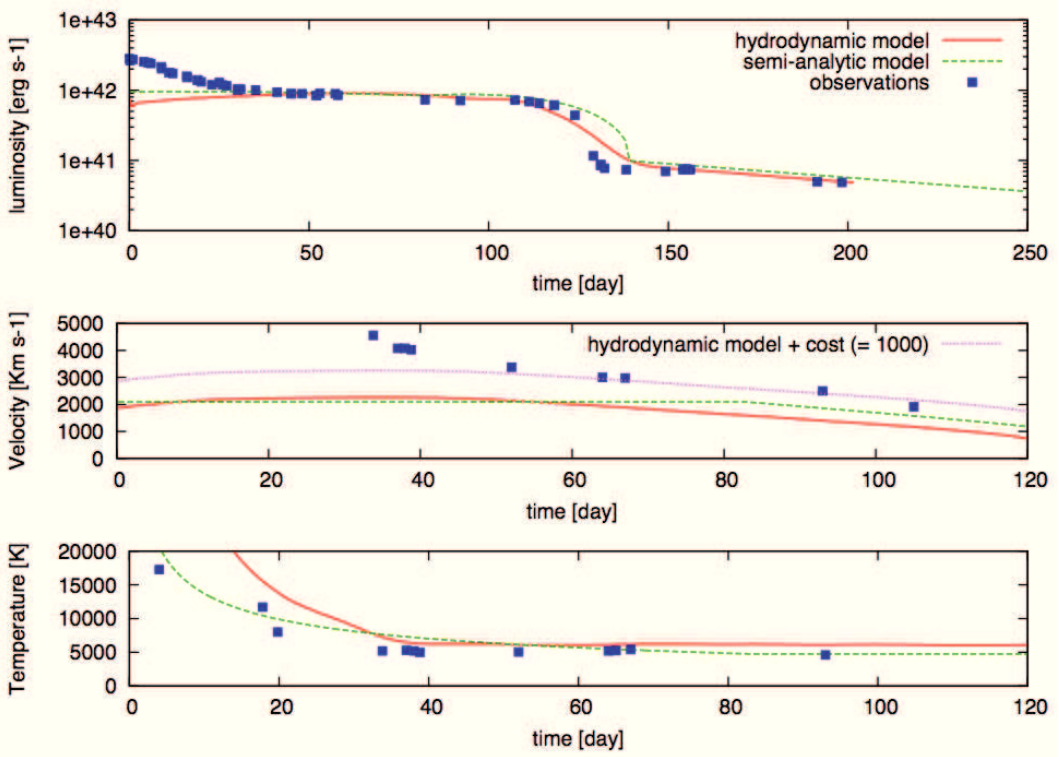

Figure 3.52: Comparison of the evolution of the main observables of SN 2009bw with the best-fit models computed with the semi-analytic code (total energy ~ 0.3 foe, initial radius 3.6×10^{13} cm, envelope mass 8.3 $M_\odot$) and with the relativistic, radiation-hydrodynamics code (total energy ~ 0.3 foe, initial radius 7×10^{13} cm, envelope mass 12 $M_\odot$). Top, middle, and bottom panels show the bolometric light curve, the photospheric velocity, and the photospheric temperature as a function of time, respectively. To estimate the photospheric velocity from the observations, we used the value inferred from the Sc II lines (often considered to be a good tracer of the photosphere velocity in type II SNe). The dotted-purple line is the radiation-hydrodynamics model shifted by 1000 $\mathrm{km\,s^{-1}}$ to reproduce the data.

The analysis of Sect. 3.3 indicates that SN 2009bw was a relatively luminous IIP with a peak luminosity similar to SN 1992H (M_V=-17.66) and a well defined plateau in V, R and I. The duration of the plateau suggests an envelope mass not dissimilar from the standard SNIIP as SN 1999em that in the nebular phase shows strong similarities with SN 2009bw both in photometry and spectroscopy. The rise to maximum seems relatively slow for a SNIIP ($\sim$ 5d) and the peak somehow roundish. The light curves show a steep but shallow drop of $\sim$2.2 mag in $\sim$13 days from the end of the plateau to the tail. The tail is flat for the first couple of months after the drop from plateau then declining at the canonical ^{56}Ni decline rate (cfr. Tab. 3.7) corresponding to a mass M(^{56}Ni)$\sim$ 2.2x10^{-2} $M_\odot$, comparable to that of SN 1999em. A broad unidentified feature is present (only) in the first photospheric spectrum at about 4600 Å. A plausible interpretation is that the feature is due to lines emerging in a region of low opacity.

The host galaxy has been classified as an highly inclined peculiar Magellanic Spiral (Sdm pec:). In the spectra is visible an unresolved component due to an underlying H II region. A reasonable assumption is to consider the SN having the same metallicity of the H II region. On the spectra obtained at Calar Alto on Apr. 9 and at TNG on Oct. 11, 2009, we have measured the N2 and (only for the CAHA spectrum) the O3N2 indexes (184) of the HII region extracted close to the SN along the slit of the spectrograph. The average relations of Pettini and Pagel (184) thus provide the O abundances which turn out to be very similar 12+log(O/H) = 8.66$\pm$0.06$\pm$0.41 (where the first error is statistical and the second one is the 95% spread of the N2 index calibrating relation). While the projected distance from the galaxy nucleus is relatively small (2.4 Kpc) we were unable to determine the deprojected one because of the very high inclination (i= 90^o) of the parent galaxy (Sect. 3.2.2). Pilyugin, Vílchez, and Contini (186) have shown that the central oxigen abundances of spiral galaxies is typically 8.3 $<$ [12+logO/H] $<$ 9.1, similar to solar abundance (8.69, 9). Therefore, with the assumption above the progenitor metallicity is close to solar and in line with the expected metallicity at the position inside the parent galaxy.

No information is available in literature on the X-ray and radio emission of the SN. An observation (8 ksec) with Swift-XRT has been obtained generating a single combined and astrometrically-corrected event file. In an aperture of 9 XRT

pixels (∼21") centered on the position of SN 2009bw we obtained a corresponding limits on total source counts of n < 5. Considering a column density of N_H= 1.9 × 10^{21} (59) we have measured an upper limit to the X-ray flux (over the energy range 0.3–10 keV) 7.9×10^{-14} ergs cm^{-2} s^{-1} corresponding to upper limits of the X-ray luminosity of $L_X < 3.77 \times 10^{39}$ erg s^{-1} (thermal bremsstrahlung model with KT = 10 Kev) and 1.5×10^{-13} ergs cm^{-2} s^{-1} corresponding to $L_X < 7.65 \times 10^{39}$ erg s^{-1} (power law model with photon index Γ=1.7). This X-ray luminosity upper limit does not preclude the possibility of a weak interaction as the SNIIP 1999em. Indeed, SN 1999em was detected at similar phase at fainter flux (∼ 10^{-14} ergs cm^{-2} s^{-1} in both the 2-8 keV and 0.4–2 keV) thanks to the superior performances of Chandra. The corresponding X-ray luminosity was one order of magnitude smaller of our upper limit (L_X(99em) ∼ 2 × 10^{38} erg s^{-1}, 0.4-8 keV, 190) because of the much shorter distance.

However, some observational evidences point in favour of weak CSM interaction in SN 2009bw. The spectral line contrast in the early photospheric period seems smaller than in other SNIIP (cfr. Fig. 3.33), as expected in the case of resonance scattering due to external illumination of the line forming region by circumstellar interaction (the so called toplighting, 32). In addition, the spectra show the presence of secondary absorptions in the H Balmer lines that we interprete as HV features. The right panel of Fig. 3.53 shows the presence of a blue Hα component at about 7300 km s^{-1} that does not evolve with time, and a redder component at decreasing progressively in velocity as other photospheric lines measured in Fig. 3.23. Careful analysis of Hβ (left panel of Fig. 3.53) shows the same bluer non-evolving component as well as the photospheric one, despite the optical depth of the line is smaller than that of Hα. Blue secondary features, constant with time, were also identified in SNe 1999em and 2004dj (49). Following Chugai, Chevalier, and Utrobin (49) such lines are HV features of Balmer lines. Their analysis shows that the CS interaction of the ejecta of a normal SN IIP with a typical red supergiant wind can be detected during the photospheric stage through the emergence of absorptions (shoulders) on the blue wing of the undisturbed H lines due to enhanced excitation of the outer unshocked ejecta. In SN 2009bw the unshocked layers producing the absorption are at about 7300 km s^{-1} while the photospheric absorption move from 6700 to 4400 km s^{-1} between

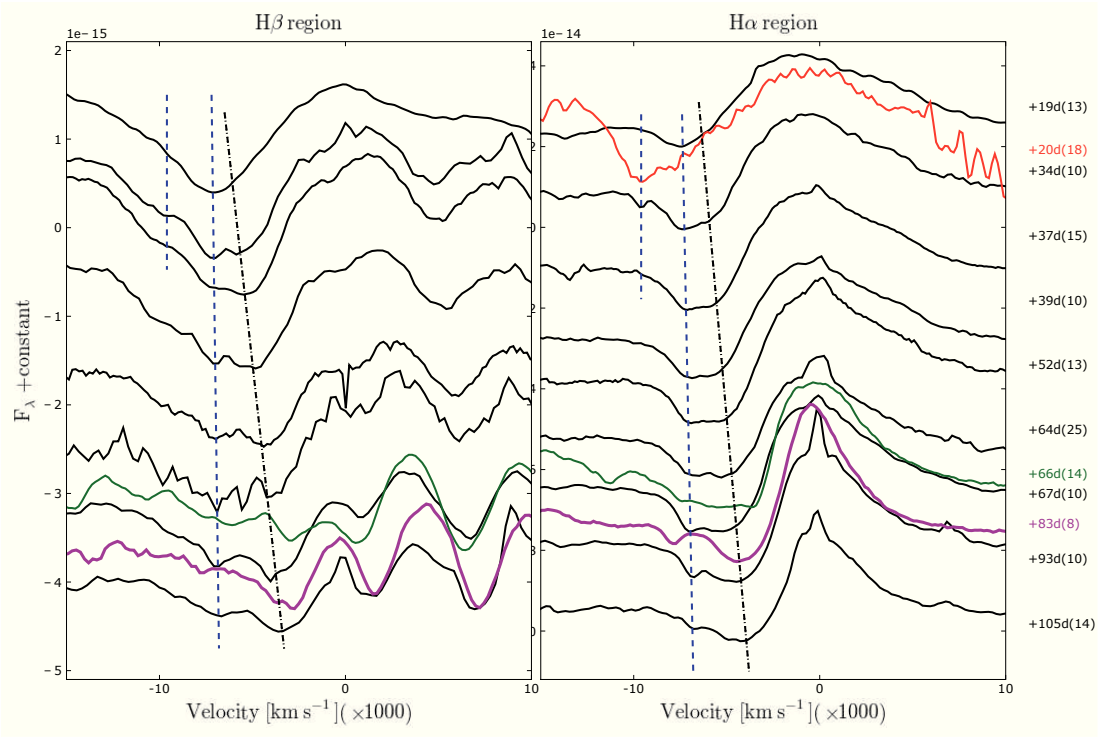

Figure 3.53: Zoom of the Hβ (left-hand panel) and Hα (right-hand panel) spectral region during the plateau phase of SN 2009bw. The x-axes are in expansion velocity coordinates with respect to the rest-frame positions of the lines, respectively. To guide the eye, two dash-dotted lines are drawn in the spectra corresponding expansion velocities, instead two blue dashed lines for each region, at comparable velocities, follow the HV feature of the Balmer lines. The red spectrum is the NIR centered at He I λ10830. We have also reported the spectra of SN 2004dj (purple) and SN1999em (blue) for comparison.

the early and the very late photospheric phase (day 37 to 105). Chugai, Chevalier, and Utrobin (49) also predicted that during the late photospheric stage the physical conditions in the cool dense shell (CDS) behind the reverse shock allow the formation of a notch, a smaller and narrower absorption, at the fastest edge of the line, and recovered it in the spectra of SN 2004dj. We clearly see this notch with similar intensity and position starting from 2 months past explosion of SN 2009bw. The line position is compatible with the expected position of FeII lines at the earliest epoch, but the fact that it does not evolves plays against such identification.

Only one NIR spectrum is available, at an epoch (21d) when the two components of the Balmer lines are blended. The NIR spectrum shows a strong feature at about 10500Å. If we identify it as He I λ10830, the expansion velocity turns out to be larger ($v_{He} \sim 10000$ km s^{-1}) than that of He I λ5876 (which has no sign of a photospheric component), and larger than that of the HV Balmer components. A NIR spectrum of SN 1999em at a similar epoch is available (68), showing an absorption identified by Chugai, Chevalier, and Utrobin (49) as HV He I at a velocity which was marginally higher than those of H and without a photospheric component. The alternative identification with Mg II λ10926 or Fe II λ10862 would imply even larger velocities. In conclusion, the close similarity with the features observed in SN 1999em and SN 2004dj and well modeled by Chugai, Chevalier, and Utrobin (49), leads us to favour the HV Balmer component scenario. Line profile models suggest a typical red supergiant wind with a density of $w = \dot{M}_{-6}/u_{10} \sim 1$, i.e. $\dot{M} \sim 10^{-6}$ M$_\odot$ yr^{-1}, similar to those of SNe 1999em and 2004dj (49), or even higher. Assuming a typical duration of 10^6 yr, the mass lost by the progenitor star is about 1M$_\odot$.

Late photospheric spectra of SN 2009bw show absorption features of CNO elements (see Sect. 3.5) indicating mixing with deep layers, which may be indicators of high metallicity envelope, prone to enhanced mass loss. Similar features in the red part of the optical spectra have been seen also in SN 1999em (175) and SN 1995V (72), both presenting signatures of weak CSM interaction (49, 190). The presence of the C in the photospheric spectra rises the possibility of CO molecules formation, that with their rotation-vibration states are a powerful coolant and are a necessary condition for dust condensation in the ejecta. Indeed SN 1999em

showed both C in the photospheric spectra and dust formation in the inner ejecta after t∼500d (68). In SN 2009bw there is no direct evidence of dust formation (neither photometric nor spectroscopic) though the last two points of the light curves, affected by large uncertainties, may indicate a steepening of the decline with respect to the slope of ^{56}Co.

Moriya *et al.* (156) studied the interaction between SN ejecta and the CSM around RSGs. They showed that, if the temperature and the CSM density are high enough, the CSM around SNe IIP becomes optically thick and the effective photosphere forms at large radii inside the CSM. The interaction-powered phase is characterized by light curves with roundish peaks, flat plateau brighter for large $\dot{M}$ and longer for an extended CSM. The observed expansion velocity at early times is expected to be that of the CSM, then turning to typical SN values when the photosphere recedes into the ejecta. In particular, the early light curves of very bright SNe IIP can be interpreted in terms of interaction with a dense CSM produced by a mass loss at a rate larger than $\sim 10^{-4}$ M$_\odot$ yr^{-1}. The interaction ejecta–CSM applied to the luminous SN 2009kf (29) satisfactorily explained the early multicolor light curves, but failed in explaining the late behaviour and the kinematics, possibly because it was an energetic explosion with large ^{56}Ni production. We have seen above that the line profiles of SN 2009bw would point toward a normal RSG wind with a low value of $\dot{M}$, which is of the order of $\sim 10^{-6}$ M$_\odot$ yr^{-1} (or marginally higher). This is much smaller than the values expected to significantly increase the luminosity. In addition, we have not detected any unusual behaviour in the velocity evolution. Nevertheless, we cannot exclude that a fraction of the observed luminosity during the plateau of SN 2009bw might be due to the transformation of ejecta kinetic energy into radiation via interaction with the CSM. As already highlighted in Sect. 3.7.2.1, this may explain why, differently from our previous experience (116, 194) where the main observables are simultaneously reproduced by our modelling, here we fail to reproduce the kinetic evolution, whilst both the bolometric light curve (cfr. Fig. 3.17) and the spectra in the nebular phase (cfr. Fig. 3.35) are standard, and very similar to those of SN 1999em.

As reported in Sect. 3.7.2.1, the ejecta mass is $\sim 8-12$ M$_\odot$. Accounting for a compact remnant (NS) of ~ 1.6 M$_\odot$ and about 1 M$_\odot$ of mass loss, the initial mass

of the progenitor is of the order of $11-15$ $M_{\odot}$, comparable with that of a massive SAGB stars or a low mass Fe CC-SN progenitor. Despite that, we want to notice that the weak intensity of [O I] $\lambda\lambda 6300-6363$ may be inconsistent with the progenitor mass (too high for the intensity observed), but the similarity between the late spectra of SN 2009bw and SN 1999em and the previous modelling case of the weak interacting SN 2007od (116), are in favour of the goodness of the mass range.

3.7.3 SN 2009dd, SN 2007pk and SN 2010aj

SN 2009dd shows X-ray emission for a few days, but no radio. The first spectrum collected ∼10 days after the shock breack-out shows a possible HV Hα component produced by the shock wave caused by the interaction between the fast moving ejecta and the slow moving CSM, expelled by the progenitor some years before the collapse.

The signs of interaction are different in the case of SN 2007pk. We have verified that the object has been correctly classified as a type IIn, that means with strong interaction between ejecta and CSM (maybe dense). For about a month post explosion there are no absorption components. Only the fourth spectrum (+27d) shows complex structures in the Blamer series with a broad component possibly due to the interaction ejecta-CSM and a narrow due to the unshocked CSM. This spectrum is a rare snapshot of the transition from a type IIn to a type II (P or L) spectrum. To our knowledge the only other object starting as type IIn and evolving after two months in a type II is the SN 2005cl (84, 85).

The only object of this sample that avoids early interaction is SN 2010aj. Possible peculiarities of SN 2010aj are a luminosity larger than average, a steep decline of the last available points that however we believe are not jet nebular and a hint of unusual reddening in the V–I late. For this object speculatively we suggest on early dust formation as in the case of SN 2007od. Such an early dust formation should be possible only in a CDS (cfr. Sec. 3.6) that implies an interaction with a CSM due to a mass loss event occurred ∼280 yr before the explosion (with the same wind and CSM velocity used for SN 2007od).

These three objects, together with the previously discussed and those proposed in Sec. 4 constitute a first sample of bright core collapse SNe with evidence of ejecta CSM interaction (cfr. Tab 3.29) and provide observational evidence of a relation between interaction and enhanced peak luminosity.

4

SNe IIP early interacting: previous additional archival objects

To enlarge the sample of bright SNe, showing also some clues of early interaction, we searched on the ATEL database (`http://www.astronomerstelegram.org/`) and the Padova SNe Group database (restricted only to group users) through GELATO web tool (100), checking possible spectral correlations with the sample shown on Sec. 3. Unfortunately some objects do not have a good coverage or were followed only for few nights.

In the following sections we will show three objects SN 1993ad, SN 1995ad and SN 1996W found in the Padova archive. Their observational coverage is not exceptional but the available data allow the extraction of interesting information. All the data are yet unpublished on referred journals. Nevertheless data of SN 1995ad and SN 1996W were already reported in the Pastorello's PhD thesis (175). All the data reported here for these objects have been checked once again. We do not report the analysis of the individual SNe as done in Sec. 3 but we give our interpretation of some evidences and we compare bolometric curves and spectra with those of the SNe studied so far.

Table 4.1: BVR magnitudes of SN 1993ad and assigned errors.

Date	JD	B	V	R	Inst.
yy/mm/dd	(+2400000)				
93/11/07	49298.50	18.00 (-)			1
93/11/10	49301.50	16.30 (-)	16.60 (-)	16.60 (-)	1
93/11/14	49306.24	16.24 (-)	15.26(.01)		2
93/11/15	49307.26	16.26 (-)	15.15 (.01)	14.77 (.01)	2
93/11/17	49309.25	16.45 (-)	15.12 (.01)	14.75 (.01)	2
93/11/18	49310.33	16.37 (-)	15.20 (.10)	14.79 (.10)	2
94/09/28	49624.50	23.53 (-)	22.83 (-)	21.94 (-)	3
95/05/29	49866.50			>21.77	4

1 = IAUC, 2 = Commission 27 and 42 of the IAU information bulletin on variable stars n.4146 (232), 3 = ESO 3.60m, 4 = ESO 2.2m, 5 = NTT

4.1 Indiviual SNe

4.1.1 SN1993ad

SN 1993ad has been discovered in IC 1501 by Pollas, Cappellaro, and della Valle (188) on November 7 UT 1993. The spectrum acquired by Cappellaro E. and Della Valle M. on 10 UT November identified the SN as a young type II with narrow emission lines of the Blamer series superimposed on a very blue continuum. They noticed also a similarity with the spectrum of SN 1983K ten days before maximum. The position of the SN are at $\alpha = 23^h34^m40^s.97$ and δ =-03^{o}09'33".1 (J2000), 13" East and 22".7 North of the nucleus of the host galaxy IC 1501. The explosion epoch, thanks to the spectra, has been recognized on about JD=2449297±5 (November 05 UT).

The Galactic reddening has been estimated as E_g(B-V)=0.041 (A_g(B)=0.176 205). The Na ID lines related to the parent galaxy are not visible in our spectra. We will adopt the Galaxy absorption as total absorption along the direction of the SN.

NED provides a heliocentric radial velocity corrected for Virgo Infall V_{Virgo} = 5239±34 km s^{-1}, that considering an H_0= 73 km s^{-1}Mpc^{-1} corresponds to a distance modulus μ=34.28±15.

The photometric data available are came from to the bulletin on variable stars (232). In Fig. 4.1 it is visible only the beginning of the plateau in B band and

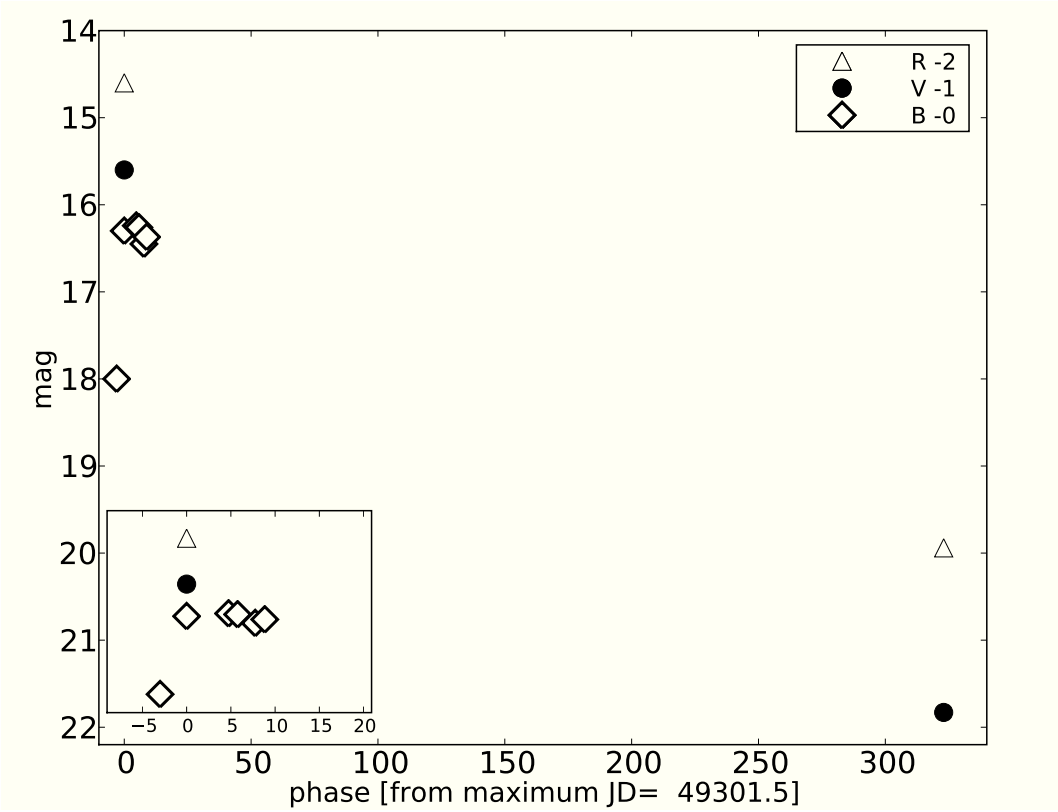

Figure 4.1: Synoptic view of the light curves of SN 1993ad in all available bands. The magnitude shifts from the original value reported on Tab. 4.1 are in the legend. A zoom of the first days is also reported.

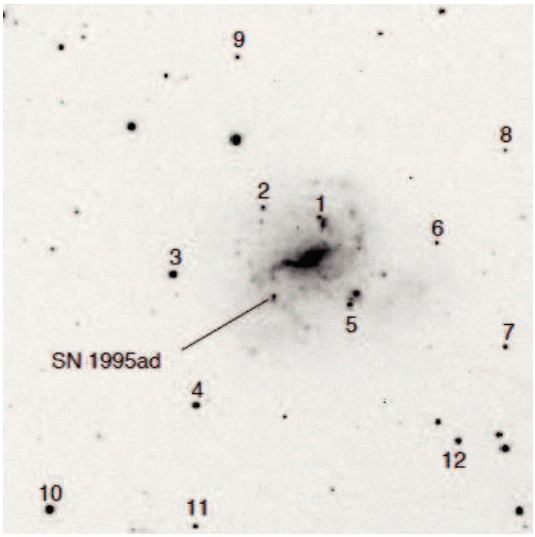

Figure 4.2: R band image of SN 1995ad in NGC 2139 obtained with ESO 3.6m+EFOSC1 on December 29th, 1995. The sequence of stars in the field used to calibrate the optical magnitude of the 1995ad is indicated.

the maximum in the same band. The maximum is M_B ∼-18.21 mag. The data are reported in Tab. 4.1.

4.1.2 SN1995ad

SN 1995ad (Fig. 4.2) was discovered by Evans, Benetti, and Grupe (70), on 28.8 UT of September in the galaxy NGC 2139. Thanks to a spectrum collected the day after the discovery (September 29.30 UT, 70) it has been classified as a type II close to maximum light. The spectrum showed broad P-Cygni profiles of Balmer lines and He I on a blue continuum (T_{bb} ∼13000 K). The coordinates of the SN have been provided by McNaught and Pollas (149) as $\alpha = 06^h01^m06^s.13$ and δ =-23^{o}40'29".0 (J2000), 25" West and 5" South of the nucleus of NGC 2139. The pre-discovery detection (magnitude ∼17.5) obtained on September 22 (35) and the constraints given by spectroscopy lead to estimate the explosion date to be about JD = 2449981±3 (September 20).

The Galactic reddening has been estimated as $A_g(B)$=0.145 (205) corresponding to E(B-V)=0.035. In the spectra are not visible Na ID lines of the parent

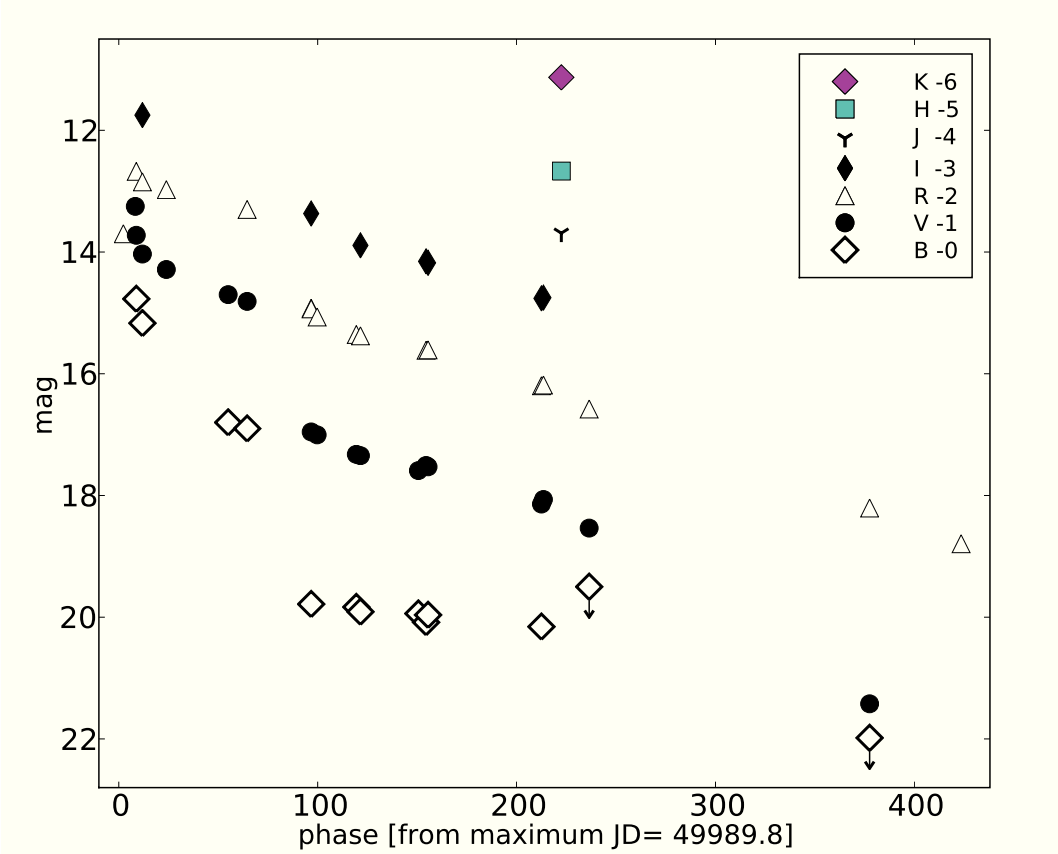

Figure 4.3: Synoptic view of the light curves of SN 1995ad in all available bands. The magnitude shifts from the original value reported on Tab. 4.2 are in the legend.

galaxy. Hereafter we consider the total reddening as given by only Galaxy contribution.

NED provides a heliocentric radial velocity corrected for the Virgo Infall of V_{Virgo}=1647±14 km s^{-1} , which corresponds to a distance modulus μ=31.80±0.15 mag.

The photometric data available in the archive begin close to the discovery and range over a period of more than 400 days. In Fig. 4.2 the sequence stars used for the calibration of the photometry are shown, while the star magnitudes are listed in Tab. A.6. The measurements of SN are reported in Tab. 4.2 & 4.3 . The first interesting issue shown by SN 1995ad is the short duration of the plateau (M_V ∼-16.83) visible in BVR bands (cfr. Fig. 4.3) and resembling that of SN 2007od,

Table 4.2: BVRI magnitudes of SN 1995ad and assigned errors.

Date	JD	B	V	R	I	Inst.
yy/mm/dd	(+2400000)					
95/09/22	49983.29			15.70 (-)		7
95/09/22	49989.60		14.30 (.25)			7
95/09/29	49989.80	14.77 (.20)	14.73 (.15)	14.67 (.15)		1
95/10/02	49992.88	15.17 (.01)	15.03 (.01)	14.85 (.01)	14.75 (.01)	2
95/10/14	50004.90		15.29 (.02)	14.98 (.02)		2
95/11/14	50036.00	16.80 (.25)	15.70 (.20)			7
95/11/24	50045.53	16.90 (.03)	15.81 (.02)	15.30 (.02)		3
95/12/26	50077.71			16.92 (.03)		4
95/12/26	50077.73	19.79 (.01)	17.96 (.06)	16.93 (.03)	16.37 (.02)	4
96/12/29	50080.74		18.00 (.09)	17.07 (.07)		2
96/01/17	50100.42	19.83 (.30)	18.32 (.19)	17.35 (.12)		3
96/01/19	50102.45	19.91 (.25)	18.35 (.12)	17.38 (.10)	16.89 (.10)	5
96/02/18	50131.63	19.94 (.10)	18.59 (.05)			4
96/02/22	50135.65	20.08 (.30)	18.51 (.15)	17.61 (.10)	17.15 (.10)	5
96/02/23	50136.65	19.96 (.30)	18.53 (.15)	17.61 (.10)	17.18 (.10)	5
96/04/20	50193.52	20.16 (.35)	19.14 (.20)	18.20 (.15)	17.76 (.15)	5
96/04/21	50194.55		19.07 (.20)	18.19 (.15)	17.75 (.15)	5
96/05/14	50217.50	>20.5	19.54 (.25)	18.58 (.20)		5
96/10/02	50358.87	>23.0	22.42 (.55)	20.21 (.15)		6
96/11/19	50406.85			20.79 (.40)		5
97/02/19	50489.53			>21.5		2

1 = ESO 1.52m, 2 = ESO 3.6m, 3 = Copernico 4 = ESO 2.2m, 5 = Dutch 0.9m, 6 = Danish 1.54m, 7 = CTIO 1.5m∗

∗ data retrieved from `http://www.noao.edu/ctio/spectrographs/60spec/60spec_ccdinfo.html`

SN 1992H and SN 2010aj. The very late time photometry (t>220d) shows an increment of the slope, from γ_V ∼0.93 at 95-220d, value in agreement with the decay of ^{56}Co in ^{56}Fe, to γ_V ∼2.02 at 210-425d, maybe due to late dust formation in the inner ejecta, as suggested also by the presence of CO molecules (218).

4.1.3 SN1996W

SN 1996W has been discovered by (131) on April 10 UT (and confirmed the following night) at the Beijing Astronomical Observatory (BAO). Nothing was visible at the SN position in an image obtained on March 1. Wang & Wheeler (131) classified it as a type II SN soon after explosion, showing a blue continuum with strong and broad Hα (v∼14300 km s^{-1}) and Hβ. The position of the SN has been given by Suntzeff, Ruiz, and Depoy (224) at $\alpha = 11^h59^m28^s.98$ and

Table 4.3: JHK magnitudes of SN 1995ad and assigned errors, we take into account both measurement errors and uncertainties in the photometric calibration. The measures have been taken at ESO 3.6m.

Date	JD	J	H	K
yy/mm/dd	(+2400000)			
96/04/29	50203.50	17.69 (.20)	17.67 (.30)	17.13 (.50)

δ =-19º15'21".9 (J2000), 17" West and 34" North of the nucleus of the parent galaxy NGC 4027. Thanks to the spectroscopic information, the explosion is estimated to be happened few days before the discovery and through the thesis we will adopt JD = 2450180±5 as epoch of explosion.

The Galactic reddening has been estimated as E(B-V)=0.044 (Ag (B)=0.145 205). In the spectra of SN 1996W the absorption features due to interstellar Na ID lines of host galaxy have been identified. Following Turatto, Benetti, and Cappellaro (235) the reddening due to the parent galaxy is E(B-V)=0.187 ($A_i(B)$=0.77), which provides a total extinction of E_{tot}(B-V)=0.231($A_{tot}(B)$=0.95).

NED provides a velocity corrected for the Virgo Infall V_{Virgo}=1779±29 km s^{-1}, which corresponds to a distance modulus μ=31.93±0.15 mag.

Magnitudes of SN 1996W are reported in Tab 4.4 and shown in Fig. 4.5. The magnitudes of the local sequence of stars, shown together with the SN in Fig. 4.4, are reported in Tab. A.7. The data collected show the first ∼40 days since explosion with a plateau clearly identifiable in bands VRI and the nebular period after 250d. In this phase the slope of the V band is γ_V ∼0.87 suggesting absence of dust. The V band plateau has a bright absolute magnitude of M_V ∼-17.52 justifying the presence of this object in our sample.

4.2 Colour curves and bolometric light curves

After established the distances and the extinctions for these three objects, we can estimate their intrinsic luminosity and compare them with our sample previous presented.

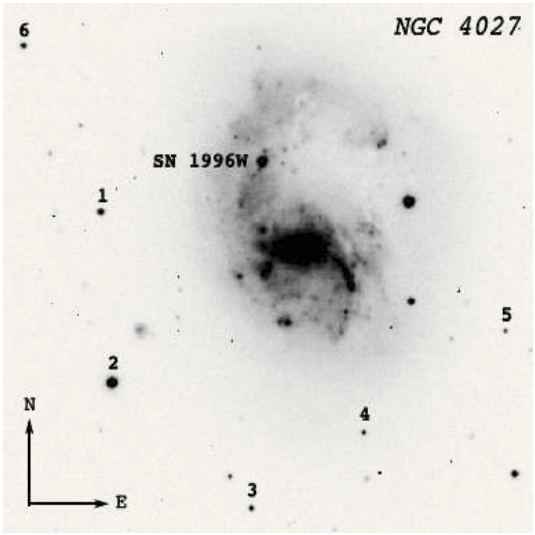

Figure 4.4: R band image of SN 1996W in NGC 4027 obtained with Dutch 0.9m on May 13th, 1996. The sequence of stars in the field used to calibrate the optical magnitude of the 1996W is indicated.

Table 4.4: UBVRI magnitudes of SN 1996W and assigned errors.

Date	JD	U	B	V	R	I	Inst.
yy/mm/dd	(+2400000)						
96/04/10	50183.50			16.00 (-)			6
96/04/11	50184.50			16.00 (-)			6
96/04/13	50186.60			15.10 (-)			6
96/04/16	50190.40		15.53 (.02)	15.18 (.02)	14.77 (.04)		1
96/04/18	50192.40		15.51 (.02)	15.26 (.01)	14.79 (.01)		1
96/04/18	50192.41			15.26 (.01)			1
96/04/19	50192.50		15.45 (.03)	15.15 (.01)	14.77 (.01)	14.60 (.02)	2
96/04/20	50193.50		15.51 (.03)	15.12 (.01)	14.75 (.01)	14.59 (.02)	2
96/04/25	50198.54	15.21 (.30)	15.53 (.15)	15.20 (.10)	14.79 (.10)	14.62 (.15)	3
96/05/09	50212.50		15.89 (.20)	15.22 (.15)	14.74 (.10)	14.49 (.15)	3
96/05/11	50215.63		15.95 (.20)	15.24 (.15)	14.76 (.10)	14.49 (.15)	3
96/05/13	50217.50	16.75 (.05)	16.12 (.03)	15.25 (.03)	14.79 (.03)	14.49 (.03)	2
96/05/14	50218.50	16.82 (.07)	16.15 (.03)	15.26 (.03)	14.79 (.03)	14.50 (.04)	2
96/05/19	50222.54	16.90 (.03)	16.32 (.01)	15.31 (.01)	14.79 (.01)	14.49 (.02)	4
96/12/15	50432.81		19.24 (.13)	18.34 (.12)	17.38 (.06)	17.02 (.05)	4
97/01/30	50478.80		19.33 (.11)	18.55 (.08)	17.76 (.09)	17.41 (.05)	5
97/02/12	50491.50	18.64 (.20)	19.40 (.20)	18.74 (.20)	17.96 (.10)	17.65 (.05)	4
97/03/31	50538.50		19.77 (.20)	19.25 (.20)	18.34 (.20)	17.91 (.10)	2

1 = Copernico, 2 = Dutch 0.9m, 3 = ESO 1.52m, 4 = ESO 2.2m, 5 = Danish 1.54m, 6 = IAUC

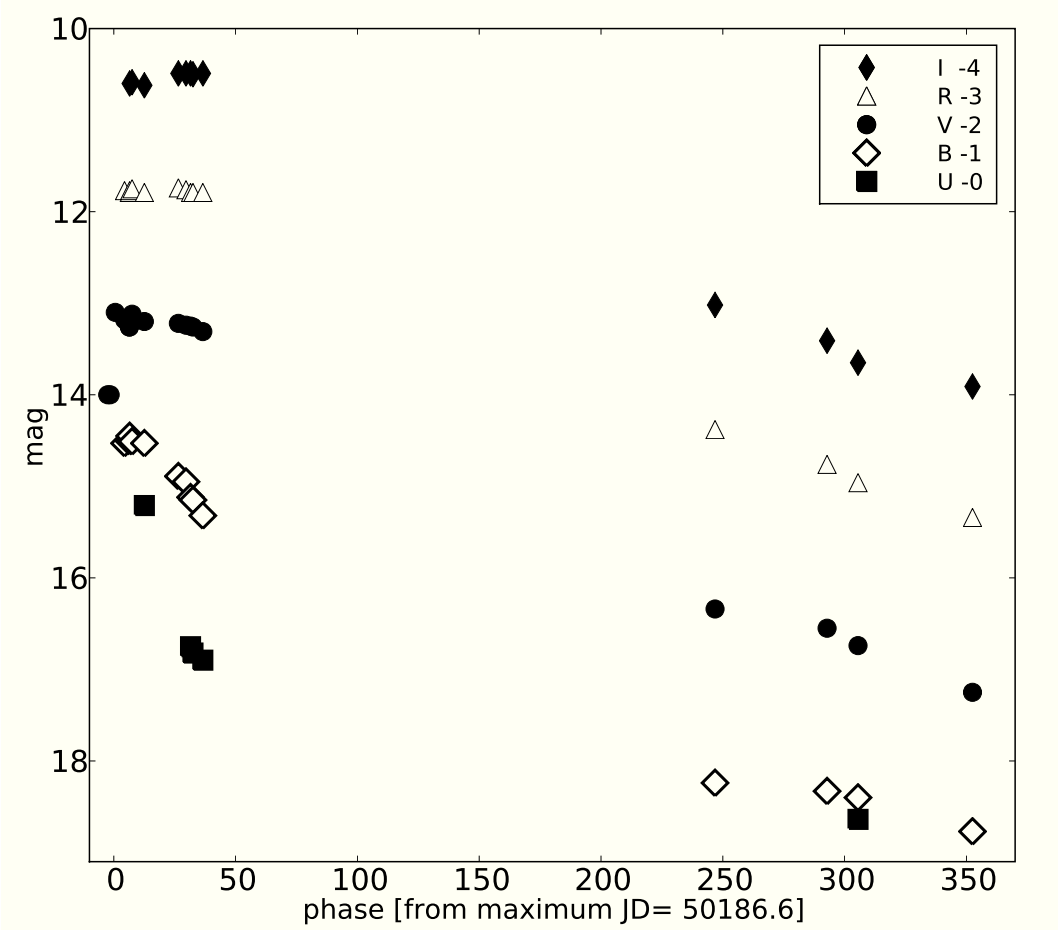

Figure 4.5: Synoptic view of the light curves of SN 1996W in all available bands. The magnitude shifts from the original value reported on Tab. 4.4 are in the legend.

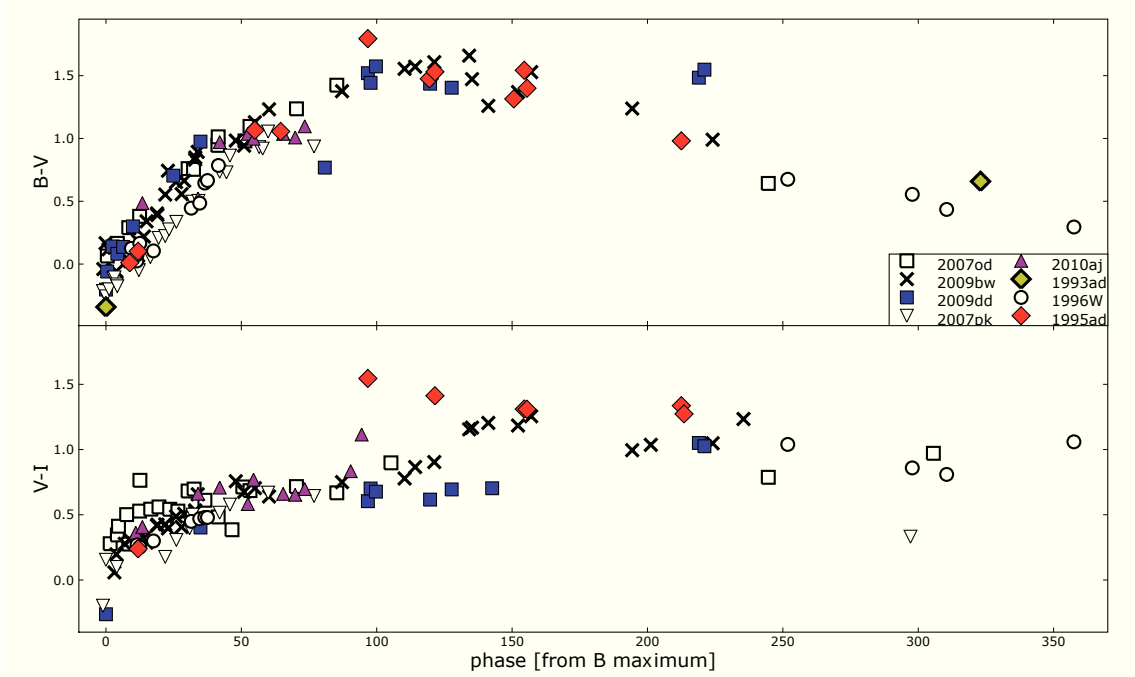

Figure 4.6: Comparison of the dereddened colours of SN 1993ad, SN 1995ad and SN 1996W with those SNe of the sample presented in Sec. 3.

As reported in Sec. 4.1, the evidences lead us to conclude that these SNe have been discovered close to explosion in a range of at maximum ∼10 days.

Considering the distance moduli and the absorption corrections of all the SNe of the sample (8 objects: 5 new and 3 old) we can compare the colour curve of these object between them and respect to the objects presented in Sec. 3.3 and reported in Tab. 3.21.

In Fig. 4.6 we show the time evolution of B–V and V–I colour curves with the other SNe of our sample. All these SNe show in the first 50 days an evolution similar to the other presented, with a rapid increase of the BV colour as the supernova envelope expands. The interesting issue is that after 150 days all the SNe with available data show a decrease to the blue after the constant phase of ∼1.5 mag at about 100d – 150d. The only exception seems SN 2009dd. The decrease is clearly visible in SN 1995ad and in SN 1996W. Also the evolution shown by the V–I diagram is the same for all the SNe of the sample. The exception among the archive SNe is related to SN 1995ad that becomes red before the other.

To better understand the meaning of these colour curves we have also compared these three SNe together with the same reported in Tab. 3.21. The top panel of Fig. 4.7 strengthens the standard increase until 100 days and the costant beahaviour after, as the blue decline of these kind of object, more rapid than those of SN 2004et, SN 1999em and SN 1987A. Instead the V–I is the same of the other objects of the comparison, except, as reported above, of SN 1995ad. The comparison with SNe 1999em and 2004et highlights as SN 1995ad begins to be red ∼30 days before the others.

The (optical) "bolometric" light curves of the SNe chosen in the archive have been compared with those of the new sample and those reported in Tab. 3.21. The emitted flux was computed at the phase in which B, V and R observations were available, respectively for SNe 1993ad, 1996W and 1995ad. As done before, when the observations in a bandpass were unavailable in a given night, the magnitudes were obtained through interpolation. The pre-maximum phase of SNe 1993ad and 1995ad should be uncertain because of observations based only on one band (the band of reference).

The peak luminosity of the SN 1993ad, SN 1995ad and SN 1996W bolometric light curves reached luminosity $L_{bol} = 2.37 \times 10^{42}$ erg s^{-1}, $L_{bol} = 1.55 \times 10^{42}$ erg s^{-1} and $L_{bol} = 2.31 \times 10^{42}$ erg s^{-1} respectively. The tails of the SN 1995ad and SN 1996W bolometric curves have slopes $\gamma \sim 0.88$ mag $(100\mathrm{d})^{-1}$ and $\gamma \sim 0.86$ mag $(100\mathrm{d})^{-1}$ close to the canonical value of $\gamma \sim 0.98$ mag $(100\mathrm{d})^{-1}$ of ^{56}Co decay. The γ value related to SN 1995ad is given by the data until ∼210 days, then before the suspected dust formation.

As said before we compare all the SNe presented in this thesis with those reported in Tab. 3.21, showing the result in Fig. 4.8. The comparison shows as all the archive objects have peak luminosity similar to that of SN 2009bw and SN 2009dd. We can not say a lot about SN 1993ad except that showing a slow decline after the maximum. SN 1995ad is rather comparable to SN 2010aj and presents a behaviour also similar to SN 2007od. The SN 1995ad bolometric luminosity of the tail is slightly greater than SN 1999em and SN 2009bw and slightly lesser of SN 2009dd. Instead, SN 1996W has a decline similar to those of SNe 1992H, 2004et and 2007od, comparable also in luminosity, but shows a luminosity tail greater than SN 2004et and SN 1992H.

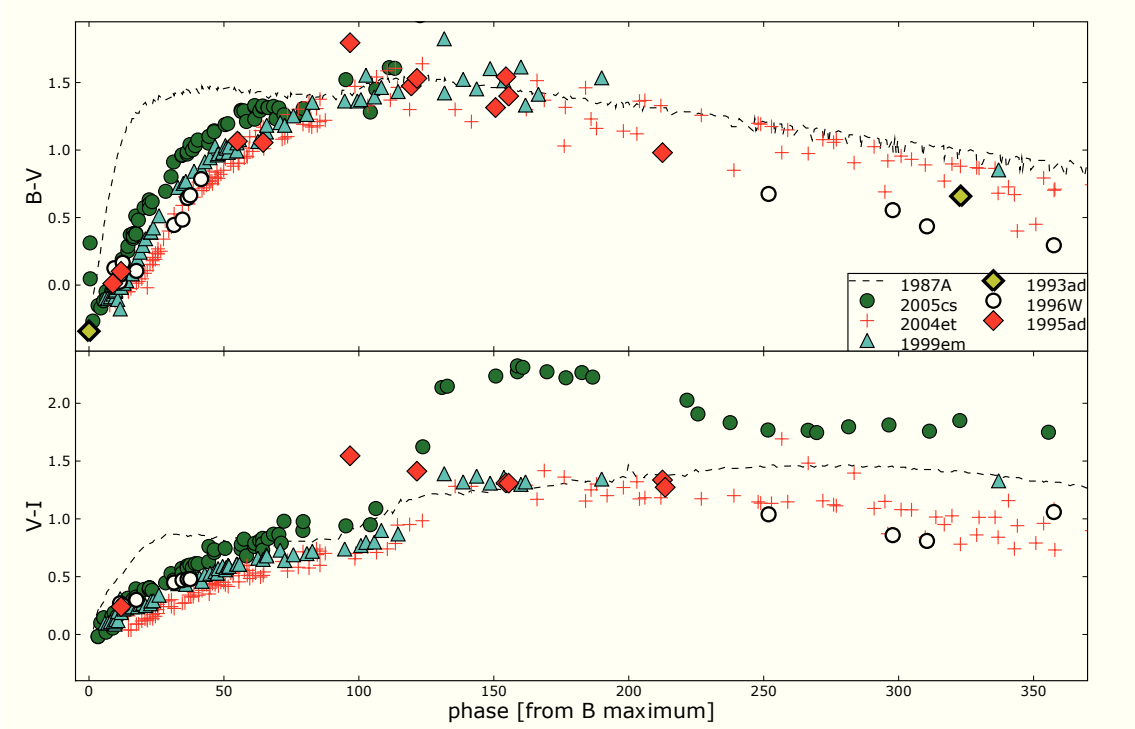

Figure 4.7: Comparison of the dereddened colours of SN 1993ad, SN 1995ad and SN 1996W with those SNe chosen in Sec. 3.3. The phase of SN 1987A is respect to the explosion date

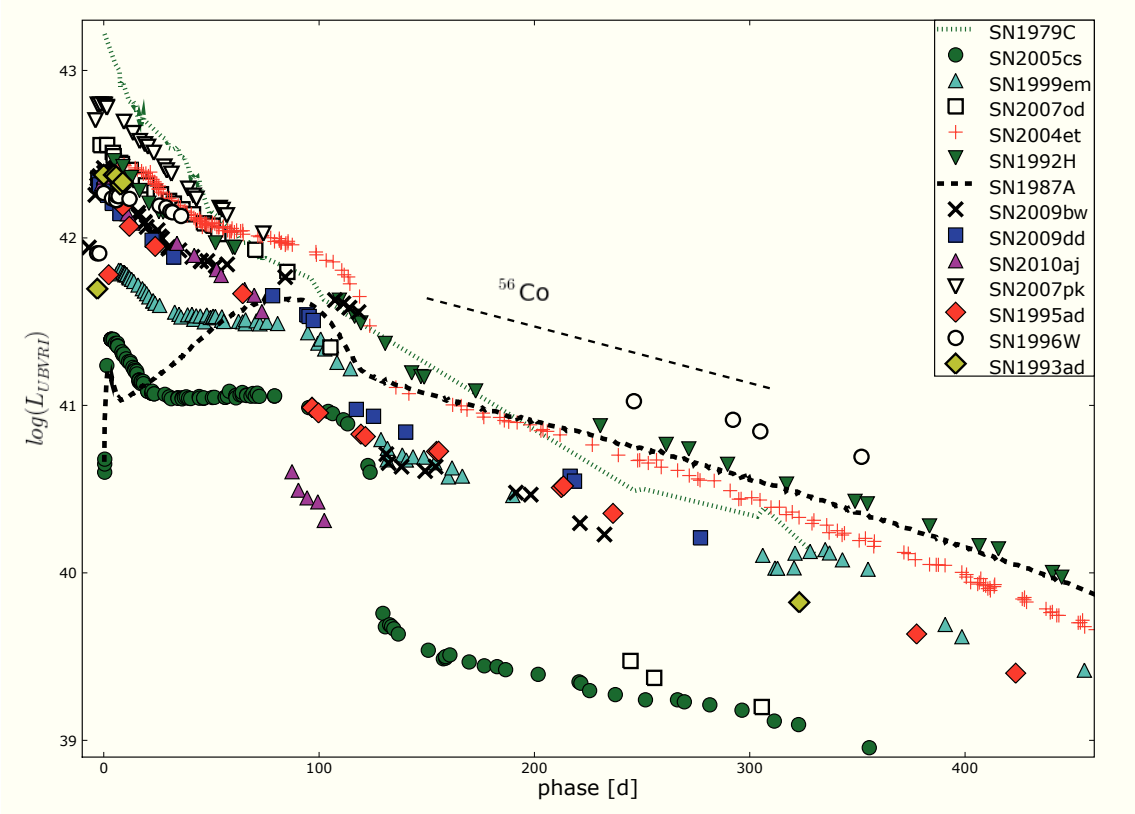

Figure 4.8: Comparison of quasi-bolometric light curves of our sample (SN 2007od, SN 2009bw, SN 2009dd, SN 2007pk, SN 2010aj, SN 1993ad, SN 1995ad and SN 1996W) with those of other type II SNe. Minor misalignments in the epoch of maxima are due to the different epochs adopted for the maxima of the reference band light curve and the quasi-bolometric curve.

The ^{56}Ni mass ejected in the nebular phase can be derived using the Eq. 3.1. The comparison gives M(^{56}Ni)$_{95ad}$ ∼0.033 and M(^{56}Ni)$_{96W}$ ∼0.16. We estimated also the ^{56}Ni mass ejected by SN 1993ad but because of the single point we consider the value of M(^{56}Ni)$_{93ad}$ ∼0.016 as a guess.

From these data the most interesting things are the bright tail of the SN 1996W and the low luminosity point at ∼320d of SN 1993ad coupled with the bright peak.

4.3 Spectroscopy

In this Section we show the spectroscopic evolution of the three objects found in the Padova archive. As reported above, the SN 1993ad has a coverage lesser than the other two SNe that, instead, show a good coverage from the early to the nebular phase with 12 spectra both for SN 1995ad and SN 1996W. The journals of spectroscopic observations are reported in Tab. B.6; B.7 & B.8.

4.3.1 The Dataset

SN 1993ad

Fig. 4.9 shows the evolution of SN 1993ad from 4d to two weeks after maximum, plus two spectra in the nebular phase. The early spectra show a blue continuum. The second (11d) and the third (13d) show a weak and barely visible Hα similar to Hβ. Absorption component of He I and metal lines, probably due to Fe I ions, are also visible.

The most interesting spectrum is the first (4d) of our series. It shows only emission component for the Balmer series and a strong, maybe multicomponent, emission for the He II lines λ4686, and Fe I–II at 5800Å. No He I in emission is visible, as also other iron lines. The Balmer emission profiles are of the order of ∼1000–2000 km s^{-1}, while He II and Fe I–II have width of ∼12000 km s^{-1} and ∼4000 km s^{-1} respectively. Furthermore, the He II profile has a flat top component quite prominent.

The spectrum at 220d shows an [O I] with an $EW_{OI} \sim 1/3 \times EW_{CaII}$ and a flux 0.5 times that of [Ca II], while the last shows an increase of the [O I] with a

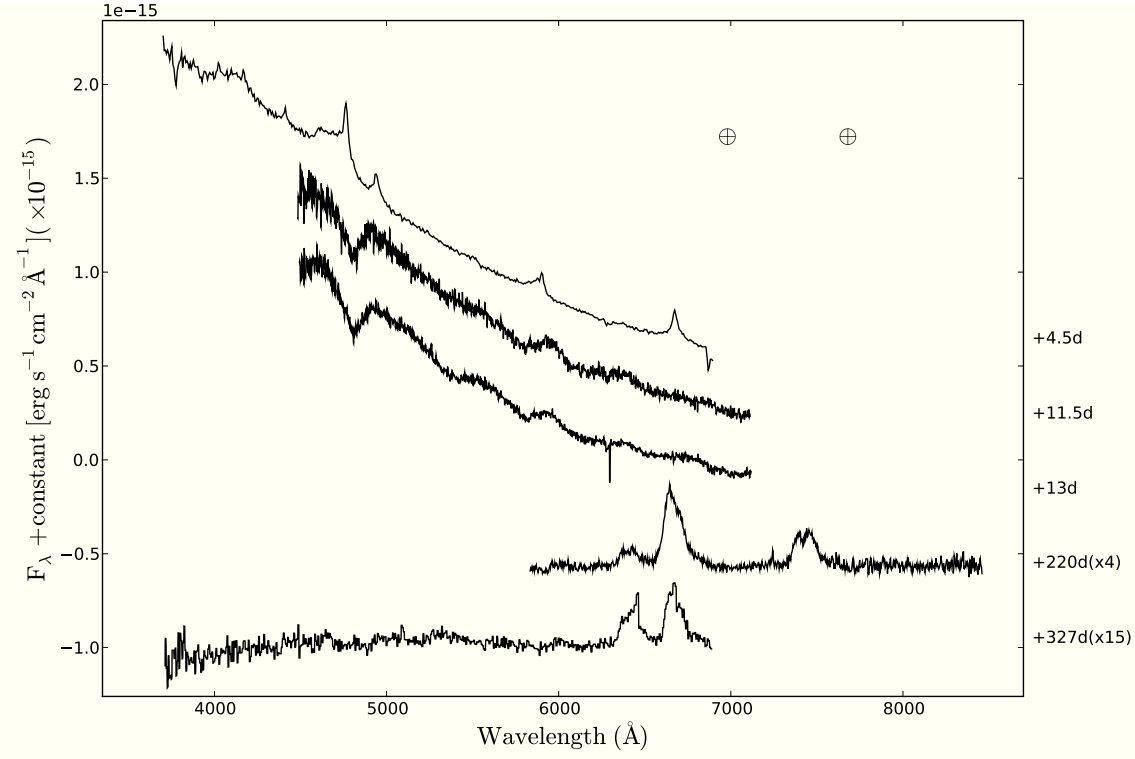

Figure 4.9: The overall spectra evolution of SN 1993ad. Wavelengths are in the observer rest frame. The phase reported for each spectrum is relative to the explosion date (JD 2449297). The ⊕ symbol marks the positions of the most important telluric absorptions. The second and third are shifted upwards by 0.4×10^{-15}; the other spectra are shifted downwards with respect to the previous by 0.2×10^{-15}.

flux comparable to that of Hα. This suggests a massive progenitor for these SNe. Generally massive progenitor are not relate to type II SNe.

The possibility of a massive progenitor, combined with the evidences of the early spectra could lead to the following scenario: a massive star loses the H layer and somewhat of the He layer and after the SNe explosion, the ejecta impacted on the close He CSM (maybe with part of H). In this view the right classification should be as a type Ib and no a type II; the absolute magnitude (cfr. Sec. 4.1.1) and the few points around the maximum should be in agreement with such classification. However, we have not enough informations to clarify this uncommon spectral evolution.

Table 4.5: Observed black-body temperatures and expansion velocities of SN 1993ad.

JD +2400000	Phase* (days)	T (K)	v($H\alpha$) (km s^{-1})	v($H\beta$) (km s^{-1})	v(He I) (km s^{-1})
49301.6	4.6	11830 ± 1000			
49308.6	11.6	9591 ± 1000	8639 ± 402	8455 ± 140	7454 ± 150
49309.7	12.7	10429 ± 1000	8626 ± 400	8270 ± 140	7301± 100

* with respect to the explosion epoch (JD 2449297.0)

In Fig. 4.13 are potted the only two epochs with lines measurements (cfr. Tab. 4.5). The Hα velocities are slightly higher than those of Hβ, while The He I velocities, at similar age, are slower than those of the other SNe of the sample, as visible comparing the three panel of Fig. 4.13.

As shown in Fig. 4.14 the Hα velocity is highly comparable with that of SN 2007od and maybe also with SN 2007pk. Also the temperature evolution is comparable with that of SN 2007od suggesting a similar scenario in the surrounding of SNe explosion.

SN 1995ad

The spectra of SN 1995ad available in the archives start from one weak after explosion until more than 500 days after in nebular phase (see Fig. 4.10). The features visible during the entire evolution are those visible in all type II as the Balmer series, He I, Fe II, Sc II and some other metal lines.

In our analysis the most interesting feature is that of the Hα in the early phase (9d-24d) where the profile remembers that of SN 2007od at similar stage. The Hα profile is flat and has a barely absorption component. The flatness is visible also in the other two spectra, instead from the third spectrum the absorption component becomes clearly visible and measurable (cfr. 4.6). We can not exclude *a priori* that the flat profile is due to the combination of the emission component of the P-Cygni profile blended with the Hα emission of the H II region superimposed (confirmed in all the spectra). However, as suggested by the extensive analysis done on the SN 2007od spectra, one of the cause of a flat top emission could

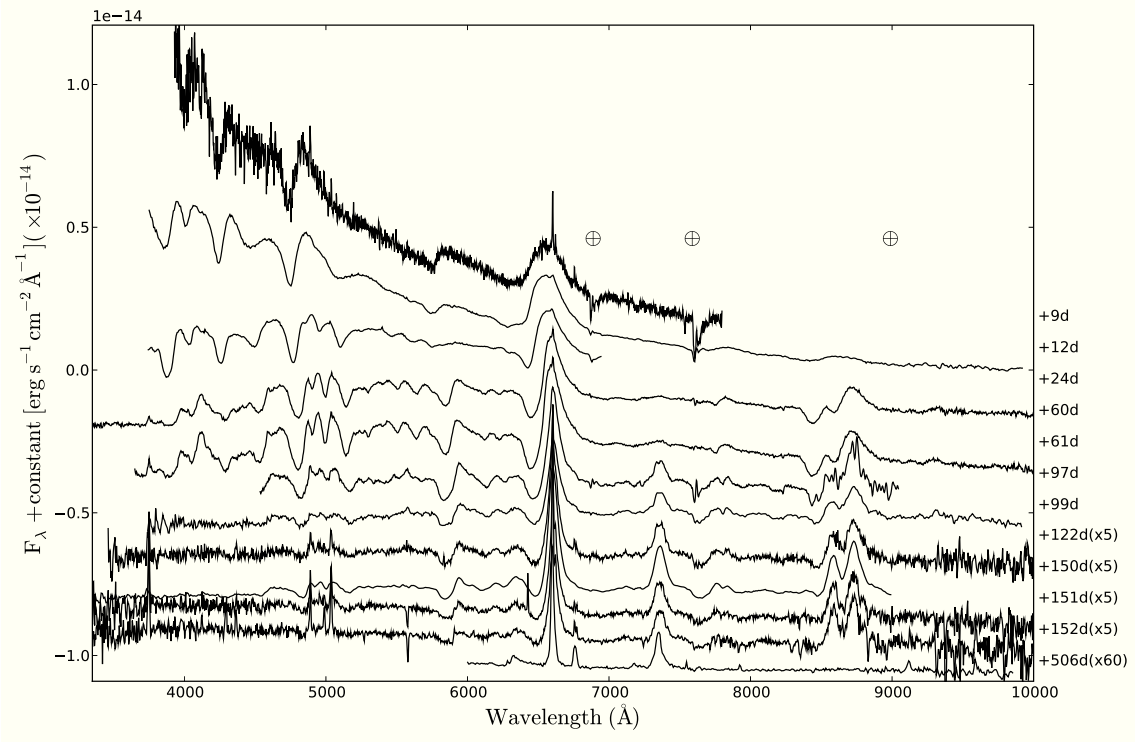

Figure 4.10: The overall spectra evolution of SN 1995ad. Wavelengths are in the observer rest frame. The phase reported for each spectrum is relative to the explosion date (JD 2449981). The $\oplus$ symbol marks the positions of the most important telluric absorptions. The second and third are shifted upwards by 1×10^{-15}; the other spectra are shifted downwards with respect to the previous by 0.7×10^{-15}.

be the interaction between the ejecta and the CSM expelled by the progenitor close, in space and time, to the explosion of SN. To support the issue of the early interaction, following Chugai, Chevalier, and Utrobin (49), we note that possible HV Hα and HV Hβ have been founded in the spectra of the plateau phase (60d and 61d) at a constant velocity of $\sim$10500 km s^{-1}, $\sim$3000 km s^{-1} greater than the respective velocities of Hα and Hβ. Even if the identification of these lines is lesser clear than those in SN 2009bw.

We want to notice that in the nebular spectra is clearly visible the [O I], a good tracing (combined with the [Ca II]) of the progenitor mass.

The expansion velocity of Hα, He I 5876Å, Fe II 5169Å ad Sc II 6264Å are

Table 4.6: Observed black-body temperatures and expansion velocities of SN 1995ad.

JD +2400000	Phase* (days)	T (K)	v($H\alpha$) (km s^{-1})	v(He I) (km s^{-1})	v(Fe II) (km s^{-1})	v(Sc II) (km s^{-1})
49989.8	8.8	16000 ± 1500	11500 ± 1100	8610 ± 570		
49992.9	11.9	9900 ± 400	10930 ± 580	8060 ± 520		
50004.9	23.9	8200 ± 600	7960 ± 270		5760± 200	5100± 350
50040.8	59.9	6900 ± 500	6820 ± 200		3170 ± 110	2770 ± 100
50041.8	60.8	6900 ± 600	6810 ± 210		3120 ± 90	2780 ± 120
50077.8	96.8	5400 ± 600	6160 ± 190		2240 ± 200	
50080.8	99.8	5300± 900	5970 ± 360		2270 ± 280	
50103.7	122.7	5700 ± 400	5720 ± 380		2010 ± 290	1580 ± 210
50131.7	150.7	5500 ± 900	5570 ± 220		1940 ± 130	1280 ± 190
50132.7	151.7	6700 ± 1500	5470 ± 290		1950± 300	1210 ± 200
50133.7	152.7	7200 ± 1300	5320 ± 205		1940 ± 500	

* with respect to the explosion epoch (JD 2449981.0)

reported on Tab. 4.6 and plotted in Fig. 4.13 (Middle panel). The velocity of Hα decreases rapidly in the first 20 days, after the decrease is slower than before. Fe II reaches ∼2000 km s^{-1} at about four moth from explosion, while Sc II reaches ∼1200 after five moth. Both are good indicator of photospheric velocity.

In Fig. 4.14 (Top panel) we compares the Hα evolution of SN 1995ad with those of our sample and other type II SNe. The velocity is comparable with that of SN 2009dd in the first days, even if the behaviour is the same shown by SN 2009bw and SN 1999em but at different days. After it decreases accordingly to those of the other SNe as SN 2007od, SN 2004et and SN 2007pk. In the bottom panel of the same figure the temperature of SN 1995ad has been compared with those of the other SNe. It shows the classical flat behaviour during the plateau phase at ∼5300 K, but increase reaching ∼7000 K at about 150d after the explosion. This behaviour supports the blue colour shown by the B–V colour curve at the same epoch.

SN 1996W

SN 1996W spectroscopic journal is reported in Tab. B.8. The observations (cfr. Fig. 4.11) cover a period of about two months after the explosion and other

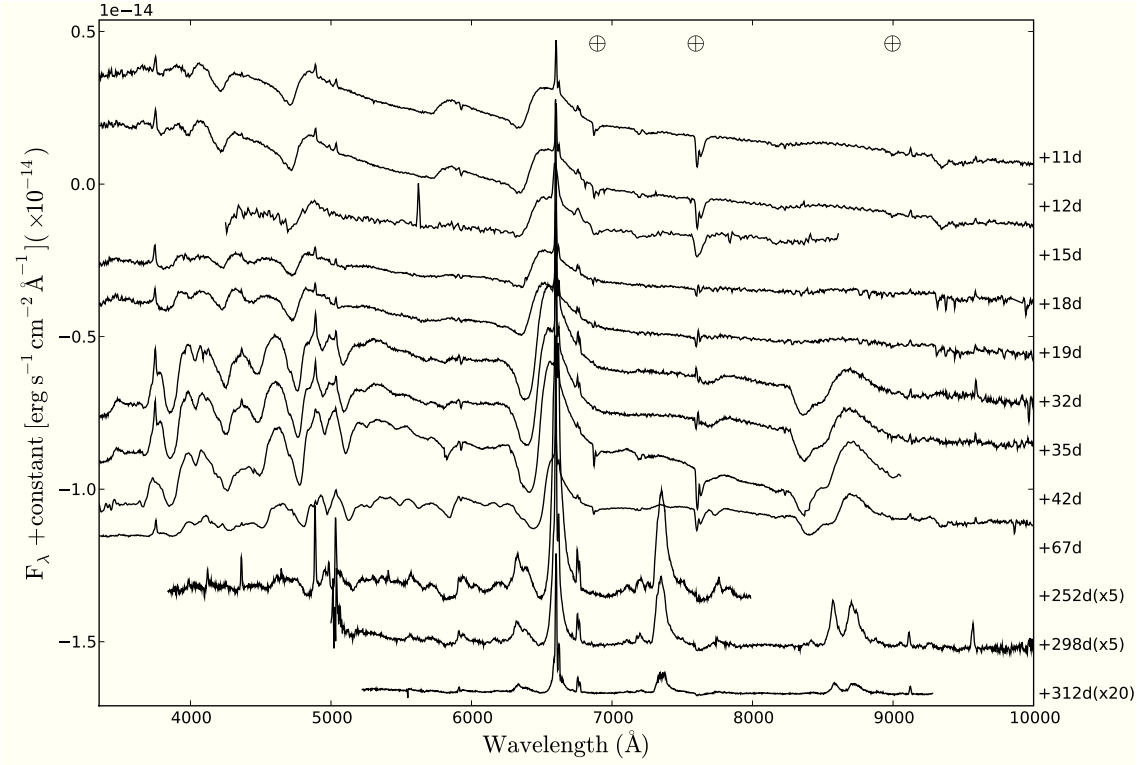

Figure 4.11: The overall spectra evolution of SN 1996W. Wavelengths are in the observer rest frame. The phase reported for each spectrum is relative to the explosion date (JD 2450180). The ⊕ symbol marks the positions of the most important telluric absorptions. The second is shifted upwards by 2×10^{-15}; the other spectra are shifted downwards with respect to the previous by 2.7×10^{-15} (third spectrum) and 1.4×10^{-15} erg s^{-1} cm^{-2} Å^{-1}(others).

two months from ∼250 days post explosion. That means a gap of ∼6 months in the spectral follow-up.

As for SN 1995ad, also this SN shows in their spectra the common element lines in all the phases. Hα, Hβ and He I are visible in the early spectra, while metal lines begin to be visible after 20d, even if the Sc II seems weaker respect to the other SNe until shown and becomes barely visible only in the last spectrum (67d) of the photospheric series. In the nebular spectra are visible the forbidden lines of [Ca II] $\lambda\lambda$7291, 7324 doublet, [O I] $\lambda\lambda$6300-6364 doublet and [Fe II] in the region of 7000–8200 Å.

Also in SN 1996W the most interesting features are related to the Balmer

Table 4.7: Observed black-body temperatures and expansion velocities of SN 1996W.

JD +2400000	Phase* (days)	T (K)	v($H\alpha$) (km s^{-1})	v($H\beta$) (km s^{-1})	v(He I) (km s^{-1})	v(Fe II) (km s^{-1})
50191.6	11.6	10400 ± 300	11570 ± 500	10650 ± 500	9510 ± 500	
50192.6	12.6	10200 ± 300	11330 ± 500	10030 ± 500	9040 ± 500	
50195.4	15.4	10000 ± 200	10890 ± 500	9930 ± 400		
50198.4	18.1	9600 ± 300	10470 ± 500	9420 ± 400		
50198.6	18.5	9500 ± 300	10340 ± 500	9180 ± 400		8710 ± 400
50212.5	32.5	6800 ± 300	8880 ± 300	7250 ± 300		6150 ± 300
50215.6	35.6	6700 ± 300	8770 ± 300	7100 ± 300		5720 ± 300
50222.6	42.6	6600 ± 300	7750 ± 300	6310 ± 300		5010 ± 300
50247.5	67.5	6400 ± 500	5600 ± 300	4450 ± 300		3930 ± 250
50432.8	252.8		3700 ± 200	2830± 200		
50478.5	298.5		3600 ± 200			

* with respect to the explosion epoch (JD 22450180.0)

series. The spectra from 11d to 19d post explosion show an Hα flat top profile resembling those of SN 2007od and SN 1995ad. After this epoch the emission profile has a double component structure (ejecta + H II region emission) that has nothing to do with the interaction. In this case the flat top profile at early stage is more evident than that of SN 1995ad. Again to support this issue we found HV features during entire photospheric evolution. They are another clue to a possible ejecta–CSM interaction happens during the photospheric age. We identified two features on the blue side of Hα and Hβ as HV Hα and HV Hβ respectively. Differently from the case of SN 1995ad, for SN 1996W we identified these lines from the first available spectrum (11d) at velocity of $\sim$11500 km s^{-1} until the last photospheric spectrum (67d). We found also a possible second HV line at $\sim$12500 km s^{-1}, but it is visible only in the Hα region. To better follow the evolution of these important lines we show the photospheric evolutions compare to those of the corresponding Balmer lines in Fig. 4.11. In the figure is shown as the velocity evolution of these two HV is the same.

As for the previous objects we report the velocities of the principal lines (see Tab. 4.7). In Fig. 4.13(right panel) is shown as the velocities of Hα are higher than those of Hβ. The difference enhance at about 20 days. For this object

the only photospheric tracer available is the Fe II, that starts at velocity ∼8700 $\mathrm{km\,s^{-1}}$ (19d) and reaches ∼4000 $\mathrm{km\,s^{-1}}$ at about two months post explosion.

The Hα velocity of SN 1996W as those of SN 1993ad and SN 1995ad are compared with the other SNe previously presented in Fig. 4.13 (Top panel). The velocities of SN 1996W until ∼40 days are higher than the other SNe chosen for the comparison, presenting a monotonic decline different from the other objects. Otherwise, the temperature evolution is pretty similar to that of SN 2007od, with the same slow initial decline. We have to remember that these two objects show both flat profile and HV feature within two weeks, differently for the other that show only HV or flat Hα or nothing.

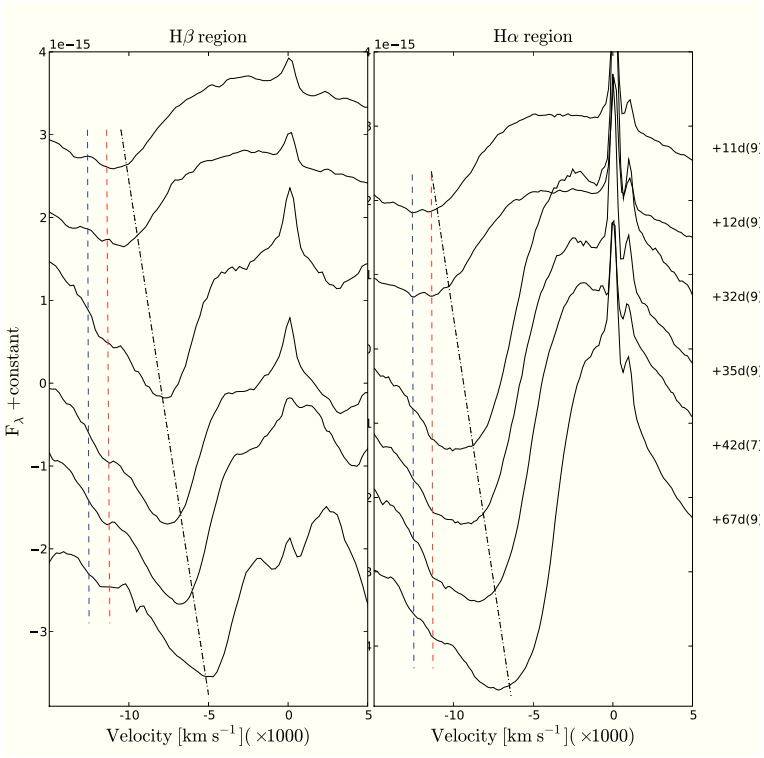

Figure 4.12: Zoom of the 4600Å(left-hand panel) and 6200Å (right-hand panel) spectral region during the plateau phase of SN 1996W. The x-axes are in expansion velocity coordinates with respect to the rest-frame position of Hβ and Hα, respectively. To guide the eye, two dash-dotted lines are drawn in the spectra corresponding expansion velocities, instead two red dashed lines, at comparable velocities, follow the HV feature of the Balmer lines ($\sim$11500 km s^{-1}). The blue dashed lines is tied to the second HV feature at $\sim$12500 km s^{-1} and visible only in the Hα region.

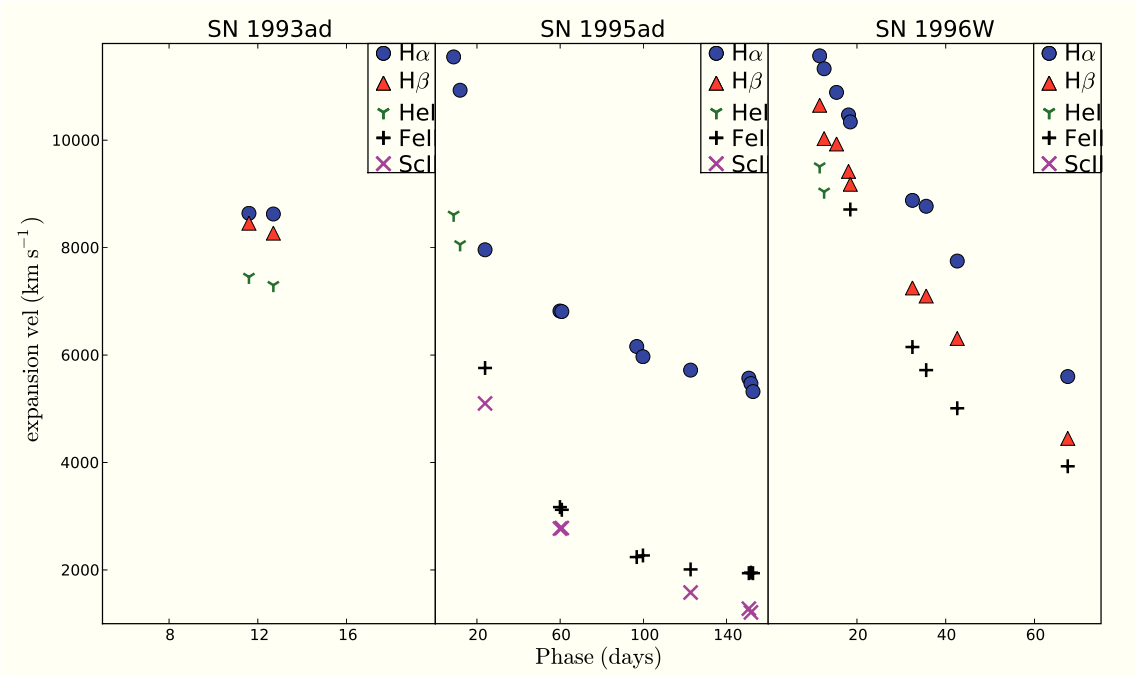

Figure 4.13: Expansion velocity of Hα, Hβ, HeI λ5876, FeII λ5169 and Sc II λ6246 measured from the minima of P-Cygni profiles for SN 1993ad, SN 1995ad and SN 1996W.

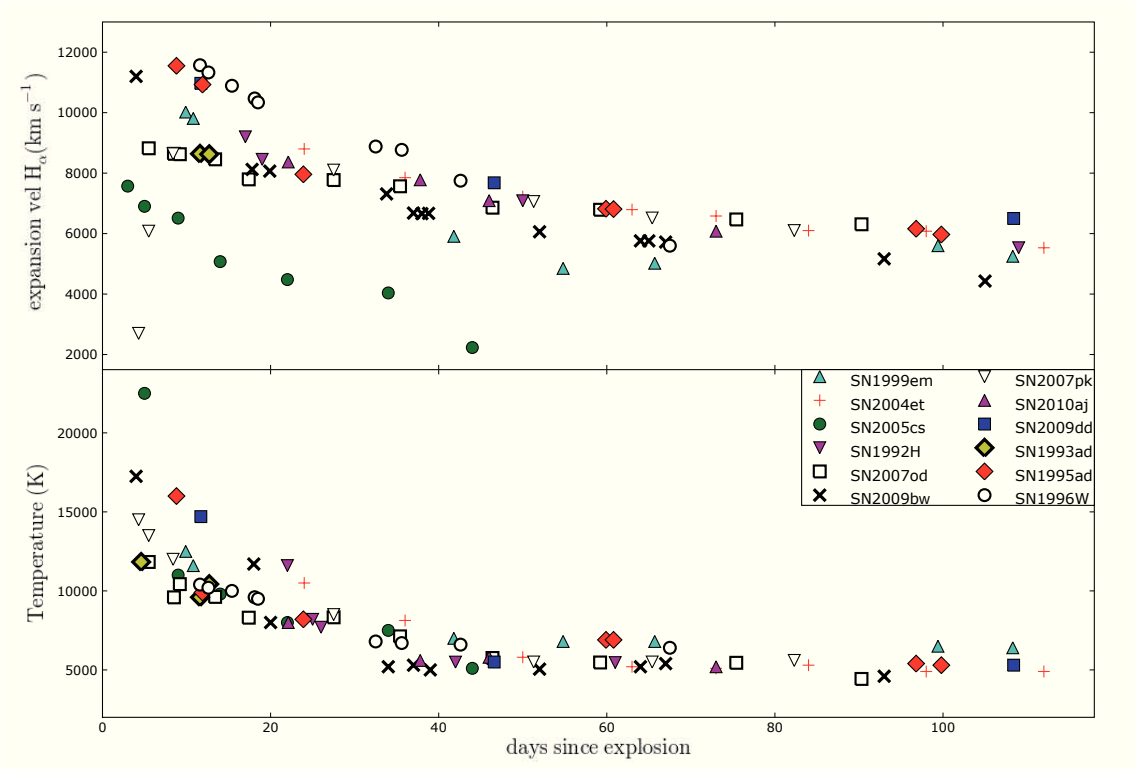

Figure 4.14: Top: comparison of the Hα velocity of our SNe sample (all 8 SNe) with those of other SN II. Bottom: Evolution of the continuum temperature of our SNe sample plus SNe 1999em, 2004et, 2005cs, 1992H.

5

SNe early interacting: analysis of close CSM geometry and mass loss

In the previous Section 1 we have introduced the classification of SNe (taxonomy). Considering all the core collapse SNe (meaning II, IIb, Ib, Ic, Ib/c) seems that the differences in time before the explosion, mass and density of the lost envelope from similar progenitors, lead to different observational quantities and consequentially different, some times complex, classifications. Numerous intermediate objects among SN classes exist (e.g. SNe 1992H, 2005gl and 2011bl) as well as a large variety within each individual class (e.g. 1997D, 1999em, 2007od and 2004et). Several attempts have been made to sort out more physical classification schemes although none of them has proved to be fully satisfactory (180).

Instead in Sec. 1.6, 3 & 4 we have shown what are the SNe objects of this thesis and how can introduce them in the classical scheme. The main characteristics of these SNe are the bright peak and sometimes clues of (weak) interaction in the early or photospheric spectra. To offer a new, unique point of view about type II SNe, we introduce these objects in a more physical scheme, explaining the different subtypes (IIP and IIn) as a function of simple parameters derived from the geometry of the pre–SN star and the amount of mass loss. Starting from the assumption that the majority of the stars have episodes of mass loss after the ZAMS period, we want investigate how the early interaction with CSM can lead

to different optical light curves and spectra in SNe IIP during the photospheric phase. This analysis is also useful as "time machine" to understand the nature of the progenitor and its behaviour on the final stages before the collapse. Assuming that progenitors of SNe IIP are red supergiants (RSGs), massive super–AGB (SAGB) stars or asymptotic giant branch (AGB) stars, we introduce the scenario of the interacting SNe and subsequently we discuss mechanisms and expected anisotropy of the pre-supernova mass loss. At last we describe the early interaction of the ejecta with the CSM in terms of geometry and mass (density) of the CSM.

As written in Sec. 1, the type II SNe showing interaction at early time are the IIn. The interaction between the fast ejecta and the CSM due to the slow wind in pre–SN phase causes the conversion of the ejecta kinetic energy to radiation and creates a fast forward shock wave in the CSM and a reverse shock in the ejecta. As reported by Chevalier and Fransson (44) the shocked material emits energetic radiation whose characteristics strongly depend on the density of both the CSM and the ejecta, and on the properties of the shock. Sometimes the pressure and the temperatures behind the shock are high enough to produce X-ray emission and synchrotron radiation generated by electrons accelerate at relativistic energies by the shock front. In particular, X-ray emission is generally produced behind the reverse shock, where a cool dense shell ($\sim 10^7$ K) formed, otherwise behind the forward shock a hotter shell ($\sim 10^9$ K) has been generated. The interaction produces also ionizing photons that ionize the cool SN gas. The dimension of the ionized region is due to the production rate of ionizing photons, which can be related to Hα luminosity; most of these photons are produced at the reverse shock front in the SN ejecta environment(44). If the SN density profile is flat, the reverse shock wave has a high velocity and the emission is at X-ray wavelength. Instead if the profile is steep, as for RSG model, the velocity of the reverse shock is low and the shock emission is at far-UV wavelengths. Similar structure has been found in quasar ionization structure. Moreover, the shocked SN gas (ejecta) is expected to undergo an early radiative phase, the time of this phase increases if the SN density profile is steeper. The dense shell of gas, created by the cooling, is important for absorbing X-rays produced by the cooling at the reverse shock (44).

However, also progenitor mass loss in type II is self-evident, e.g., SNe IIP as 2004et (121, 139); SNe IIL as 1988Z (50); SNe II as 1979C, 1980K (73, and reference therein) and 1986E (37); SNe IIn as 1998S (129, 193) or the well studied SN 1987A (45). All of these have shown a CSM interaction: early, late of both. Unfortunately many times the SNe are too far away for a radio or x-ray detection and becomes complex to find clear evidence of early interaction. In the light of that, the best observables to check a possible interaction seem to be the optical spectra. Important clues are presence of high velocity features (HV) of the prominent lines (Balmer series and Helium) during the early spectra (16, 116), or during the plateau phase in the form of a less secondary absorption detectable only in the Hα (49). Furthermore, the presence of a boxy (flat) profile of the Hα, similar to the profile of a detached atmosphere or of the interaction with a round CSM (no toroidal) in nebular epochs, is another evidence of possible interaction with a thin, maybe less dense, CSM.

In the last years there are been a few events classified as SNe IIP or IIP-pec that showed these clues of interaction in early phase. These SNe, as for example SN 2007od (116), SN 2009bw (114) or the other objects of our sample, seem to have observable features "intermediate" between standard SNe IIP and IIn. Furthermore, some relatively nearby common SNe IIP, e.g., SN 1999em (16, 190) and SN 2004dj (49), showed minor evidences of interaction with a close CSM.

Another peculiarity of this interacting SNe seems to be the high luminosity, respect the common value (180, 200), shown at peak ($M_V \sim$-18) and during the plateau ($M_V \sim$-17.8) coupled instead with a normal or sometimes faint tale luminosity, as for SN 2007od (4, 116). This difference between the plateau and tail phases could be also relate to a progenitor with a radius bigger than common red supergiants, anyway is difficult explain the line velocities, the bright photospheric phase and the common/low tail luminosity without an early CSM interaction. The interaction should be another source of luminosity added to the principal that justify the brightness reached during the plateau, moreover these interacting SNe show also a short plateau resemble that of SN 1992H (52). It means an H envelope less massive than common, maybe due to the mass loss that generated the close, H rich, CSM.

As shown above by the case of the standard SNe IIP 1999em and 2004dj, the circumstellar interaction seems to be more common than has been thought. This leads our research to better understand the causes related to the mass loss and the role played by CSM in the SNe observables (light curves and spectra).

5.1 Progenitor mass loss: mechanisms and asymmetry

First of all we have to analyze about the origin of CSM. Several potential mechanisms for progenitor mass loss are known. These include: 1) steady wind; 2) radial pulsation driven by partial ionization of the outermost hydrogen layer; 3) eruptive mass loss; and 4) mass transfer in a close binary system. Depending primary on the mechanism, the amount of mass loss could rely on the metallicity as well as the initial mass of the progenitor. These are not mutually exclusive and can also depend by the mass and the evolutive phase of the pre–SN star.

The first mechanism applies to red supergiants, which evolve from initial masses in the range ∼10 to ∼20 $M_{\odot}$, as well as for all massive stars (126). Kudritzki and Puls (125) discussed the fast, line-driven winds of hot stars. These winds become detectable in spectral energy distributions and spectral lines as soon as the stars reach sufficient luminosity. For stars of spectral types O, B, and A, the borderline is 10^4 $L_{\odot}$. On the other hand, cool stars have slow winds u_w ∼10 $km\,s^{-1}$ (198). According to the different prescription used in the evolutionary calculation (105, 147), the steady wind seems necessary to predict the fates of massive stars as function of initial mass and metallicity. Furthermore, mass loss seems to depend on the rotation of the star. As shown in Maeder and Meynet (138), rotation increases the global mass loss rate and also modifies the shape of the star. In rapidly rotating massive stars, the mass loss becomes increasingly anisotropic as the critical rotation parameter increases. However, as shown in Georgy, Meynet, and Maeder (86), rotation near the critical limit (Keplerian velocity at the equator when g_{eff}=0) can favour equatorial-enhanced rather than polar-enhanced mass loss. Thus the formation of asymmetric circumstellar nebulae around fast rotating stars is likely (86). In fact a large fraction

of planetary nebulae are bipolar or elliptical (∼80%), even if it is suggested a noteworthy influence by magnetic field in the asphericity shape of these objects (11, 26). We will assume that by the time of collapse, SNe IIP progenitors are surrounded by equatorial–enhanced CSM.

The second mechanism, radial pulsation driven by partial ionization of hydrogen in the outermost layers, seems to apply to both RSG and AGB stars and is commonly invoked for driving winds from cool stars (159). Heger *et al.* (106) found that strong pulsations in RSGs are similar to those found in AGB stars and suggested the possibility of "superwinds" occurring before the RSGs explode, but only if the luminosity to mass ratio is sufficiently high. The luminosity to mass ratio (L/M) must increase to reach the value required for the superwind phase when rotation is taken in account in the evolutionary model (106). RSGs are generally more susceptible to pulsation instability for larger initial masses (M_{in} >17 to 20 $M_{\odot}$) (250). Therefore, if a superwind could be induced by strong pulsations, it would occur in an earlier evolutionary epoch for a higher mass loss. Normally a superwind phase occurs ∼10^3 to 10^4 yrs before core collapse and is related to massive stars with high enough mass loss rates to finish their evolution as stripped envelope SNe. The only exception should be the SAGB finishing their lives as stripped envelope SNe or electron capture SNe embedded in an optically thick circumstellar shell, created through mass loss during the thermal pulses phase (196). For the reasons presented above this type of mass loss does not apply to the close CSM that is of concern in this thesis. In addition, we have to remember that generally superwinds are less probable than steady wind (106). Episodes of superwind do not exclude mass loss through steady wind at different evolution phases.

Eruptive mass loss is the most unclear mechanism, it may be connected with He-shell flashes, but the exact formation mechanism is still a matter of debate (169). Eruptive outbursts are observed to occur, however, and evidences suggests that they are more effective at shedding mass from a star than are steady winds (213). They can occur regardless of: a) the initial progenitor mass; b) the phase before the explosion as SN; c) a preferential direction of mass loss related to the event. Eruptive mass loss seems to be less sensitive to metallicity than are line driven winds of hot stars (211). This phenomenon is principally relate with

luminous blue variable (LBV) and SNe impostor or pair instability SNe (255). As written above also the He-shell flash are relate with eruptive mass loss, even if this kind of mass loss is generally relate to the thermal pulses in AGB/SAGB stars (143) and not with stronger eruptive phenomena. This kind of mass loss can happen together with the other types, strengthens as some stars can have different modes to lose part of (or entirely) the external layers.

The fourth mechanism is mass transfer due to Roche lobe overflow in close binary systems. Because binarity is common, this mechanism could occur with comparable probability to the steady wind, especially if we consider the tidal forces able to induce the mass loss also without transfer between the two lobes. Furthermore, like the eruptive mechanism this one should be less sensitive to metallicity. For this mechanism, as for the steady wind, it seems reasonable to expect a preferential direction of the mass loss.

As reported above, the mass loss from pre–SN stars can occur in different manners and can depend from the initial mass and the phase, since different kind of mechanism can concern the same object. Being the goal of this thesis chapter a new treatment of SNe II-IIP based on parameters tied to the early interaction, some of the mechanism explained in this sketch about mass loss have not to consider. Eruptive mass loss and superwinds are normally related to more massive stars than the type II progenitors, except the case of SAGB exploding as EC–SNe. The remaining mechanisms are connected with rotation of the star, leading us to believe that progenitor mass loss, occurs immediately preceding a SN II event, is likely to have a preferential direction of ejection, perhaps perpendicular to the rotation axis. The only exception in the scheme is the superwind of the SAGB (stars that can explode as SNe II), that however is a case more rare than the others and does not change the reliability of the assumption. Moreover, including in our understanding also the magnetic field, this additional component should be prone to rotation and not prevent it. This assumption may allow us to better understand the differences between the SNe IIP that show a weak interaction, and the SNe IIn that show a stronger interaction.

5.2 Early interaction

5.2.1 Geometry

Assuming a preferential direction of the mass loss, the next step is to imagine the close CSM as aspherical. The guess could seem strong, but there are a few evidences that can testify this assumption. There are none type IIP, showing a medium-weak interaction, studied through spectro-polarimetry technique. Instead a few type IIn have been well studied. Among them the SNe 2010jl (177), 1998S (129) and 1997eg (108) show an aspherical CSM. Also SN 1987A showed an interaction with an aspherical CSM (187). Hereafter we also assume a homogenous mass loss, without clumpy emission. In some cases evidence of a clumpy wind has been found (50, 116), but normally the clumpy component has a coupled rarefied component that could be aspherical. Then the close CSM, that is the base both for the type IIn and IIP/IIP-pec here analyzed, will be treated as non spherical (see Fig. 5.1).

The spherical ejecta collide with the CSM that, if we assume an orthogonal preferential direction with respect to the star's rotation axis, has an oblate geometry. This introduces a dependence of the observer's viewing angle. In Fig. 5.1 observers in positions A (hereafter OA) and B (hereafter OB) do not see the same thing. In early spectra ($\lesssim$12d), OA sees a boxy profile in the Hα emission, and the lines absorptions are less deep than in normal SNe II; examples are the SNe of our sample. The interaction between the ejecta and the CSM causes toplighting (32), which mutes the absorption and the emission components. Instead the geometry of the CSM, interacting with the ejecta, modify the contribution from the emitting regions and it is responsible for the boxy profile that resembles that seen in some late interactions (50, 116, 193). However, an alternative explanation of this kind of profile could be that some abundance/ionization effect perhaps due to circumstellar interaction reduces the Balmer occupations, implying anyway the circumstellar interaction.

On the other hand, OB during the entire photospheric phase sees the classical SN IIn spectra that result from interaction with a massive CSM.

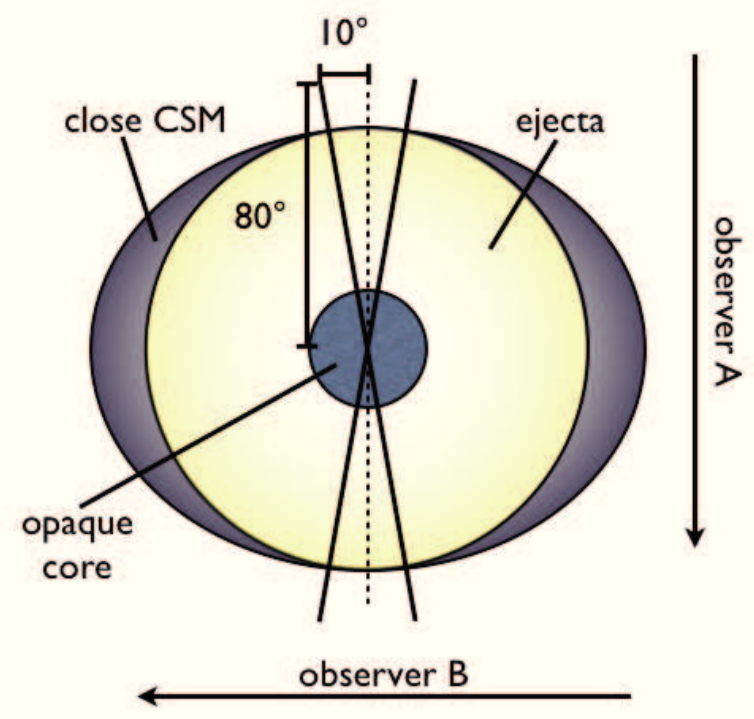

Figure 5.1: CSM-ejecta geometry. View angles and observer directions are also shown.

Stretching the geometry we obtain a torus shape. From the scheme above presented (see Fig. 5.1) to the maximum degeneration along the perpendicular direction of the rotational axis we have a spindle and horn torus[1], both that can be assimilated to the shape described and similar to it, and at last the ring torus shape that can show different width. The last case should be the more uncommon in our kind of object that does not suffer of extreme rotation or strong equatorial eruptive mass loss. Also in the torus case our analysis is still valid.

In early spectra the FWHM of Hα seen by OA ($\sim$9000 km s^{-1}) is about three times greater than that seen generally by OB ($\sim$2700 km s^{-1}). Energy must be conserved. The most probable mechanism to accelerate the CSM is the UV flash at shock breakout. The difference in FWHM (and velocity) is imputed to different explosion energies or CSM densities. The explosion energy of a typical SN IIP such as SN 1999em and a SN II seen by OA is similar (order of a foe). Moreover, the shock breakout energy from a red supergiant is of the order of 10^{48} erg (230), greater respect to $\sim10^{45}$ erg and $\sim10^{46}$–10^{47} erg, that are the necessary energies to accelerate the CSM of SN 1999em and SN 2007od, respectively.

So the only parameter that allows different velocity is the density of the CSM. The close CSM of events like SN 2007od or SN 2009bw is less dense than that of SNe IIn. The difference in density could be explained taking in analysis similar progenitor with different radius. A great radius could explain also the starting high luminosity (powered also by the CSM interaction) shown by the OA objects.

The viewing angle can also affects the bolometric light curve, even if this issue is also relate to the density of the CSM. OA sees a light curve with a plateau and a peak luminosity that exceeds that of a supernova with the same energetics without significant CSM interaction. The plateau is shorter than normal because part of the hydrogen envelope has been removed by the mass loss. Progenitors with different amounts of mass loss seen by OA lead to differences in the duration of the plateau and in the enhancement of the luminosity (e.g. more mass in the CSM implies plateau shorter and luminosity higher than normal). On the other

[1]The torus is a surface of revolution generated by rotating a circle around an axis. When the axis is a chord of the circle the torus is called spindle, if it is tangent to the circle we obtain the horn type, instead when the axis is far away from the circle the ring torus is formed.

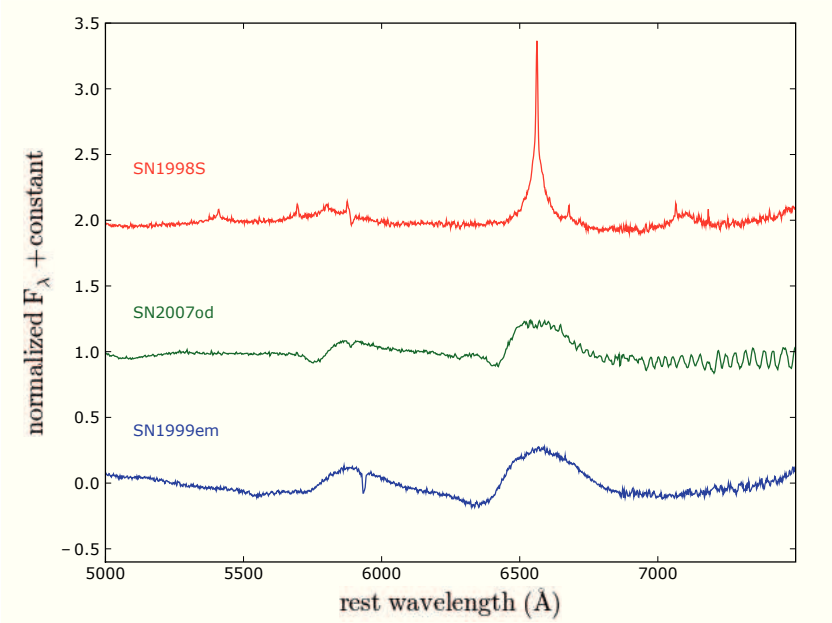

Figure 5.2: Early spectra of a typical SN IIP (SN 1999em), a SN IIP-pec (SN 2007od), and a SN IIn (SN 1998S).

hand, OB sees the typical bolometric light curve of a SN IIn, with a slower rise to and decline from maximum light than for SNe IIP-pec.

After the early phase, from the prospective of OB nothing changes, but for OA the spectra show a quasi-normal P-Cygni profile for all the ions and, when it is visible, a high-velocity Hα absorption during the plateau phase that testifies that the interaction is still ongoing. The presence of such a line has been reported by Chugai, Chevalier, and Utrobin (49) in SNe 1999em and 2004dj, two typical SNe IIP that show early interaction with a less massive CSM, and in SNe 2009bw (114), 1996W (this work) and maybe in SNe 2009dd and 1995ad (both this work). Sometimes also an HV Hβ is visible (e.g. SNe 2009bw and 1996W). However, the presence of HV feature is seen also by OB, since it is an effect due principally to the density (mass) of the CSM. The quasi-normal P-Cygni profile reported above is produced by ejecta that, at this phase, is expanding into the CSM on the sides (perpendicular to OA direction) and swept the thin part of CSM along the OA direction (see Fig. 5.3). This allows OA to see the normal profile instead

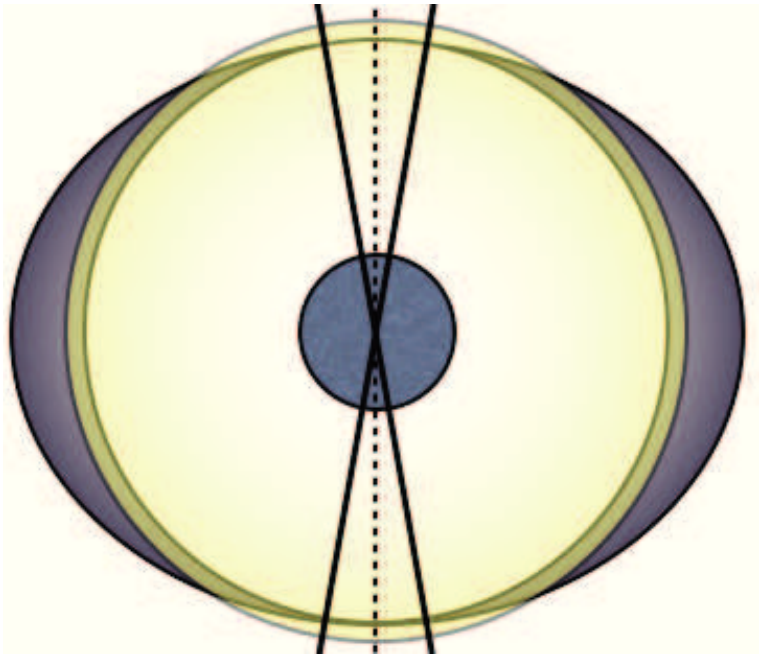

Figure 5.3: Interaction between ejecta and an aspherical CSM after the early phase ($\gtrsim 12 - 15d$).

of a boxy one, but at the same time, because the interaction is still ongoing, as shown principally by the high-velocity Hα and the brightness of the plateau, the toplighting effect is still present and the P-Cygni absorption components are shallower than in a similar SN without the CSM.

Among the main sequence stars are well known some fast rotators as the A0V Altair, the B3V Achenar, the A0V Vega and B7V Regulus α spread from 2 to 17 $R_\odot$ (1.8 to 6.0 $M_\odot$) having rotational velocity of the order of $\sim 300\ km\,s^{-1}$. Vega and Regulus α show also a deformation of the spherical shape with the equatorial radius (a) greater than polar radius (b) of 23% and 30% respectively. Even if these stars have mass smaller than a SN progenitor, they testify as the rotation is common among the stars. Considering that the rotational velocity of a RG can be spread from $\sim$10 $km\,s^{-1}$ to $\sim$100 $km\,s^{-1}$ (39), the fact that rotation enhances mass loss, in star from $9M_\odot$ to $25M_\odot$, varying by a factor from 1.54 to 32.6 (138) and assuming roughly the conservation of the angular momentum we can suppose an asymmetry of our CSM given by $1.1 \lesssim a/b \lesssim 1.3$. Considering the limit of the torus shape, the horn and the spindle must have a>b and $a/b \lesssim 2.0$, instead for the case of ring torus we must have $a/b \gtrsim 3.5$ (182).

Having defined the degree of asymmetry (asphericity) respect to the rotational axis we can handle the angle issue. The limit angle dividing the two scenarios above presented is $\theta \sim 10° \pm 4°$ with respect to the orthogonal axis to the mass loss ejection (then the progenitor's rotation axis). The angle has been evaluated from the rates of SNe IIP–pec and SNe IIn in the last 4 yrs, while the error is given by the propagation of uncertainties on indirect measures applied to the sample of possible interacting SNe (i. e. those not observed early enough and showing spectra like those of typical SNe IIP).

Assuming the same data sample of SNe II, increasing the asphericity to greater value than that reported, θ changes too. If we use an inverse linear proportion law between the asphericity (that means the rate between the two semi axes) and the limit angle we find that for $a/b = 2$, $\theta \sim 7°$, instead for a shape like a ring torus $a/b = 4$ and $\theta \sim 3°$ a value lesser than the error, suggesting how in this case OB probably will see typical spectra of type II or type IIn ever, without dependence from the limit angle.

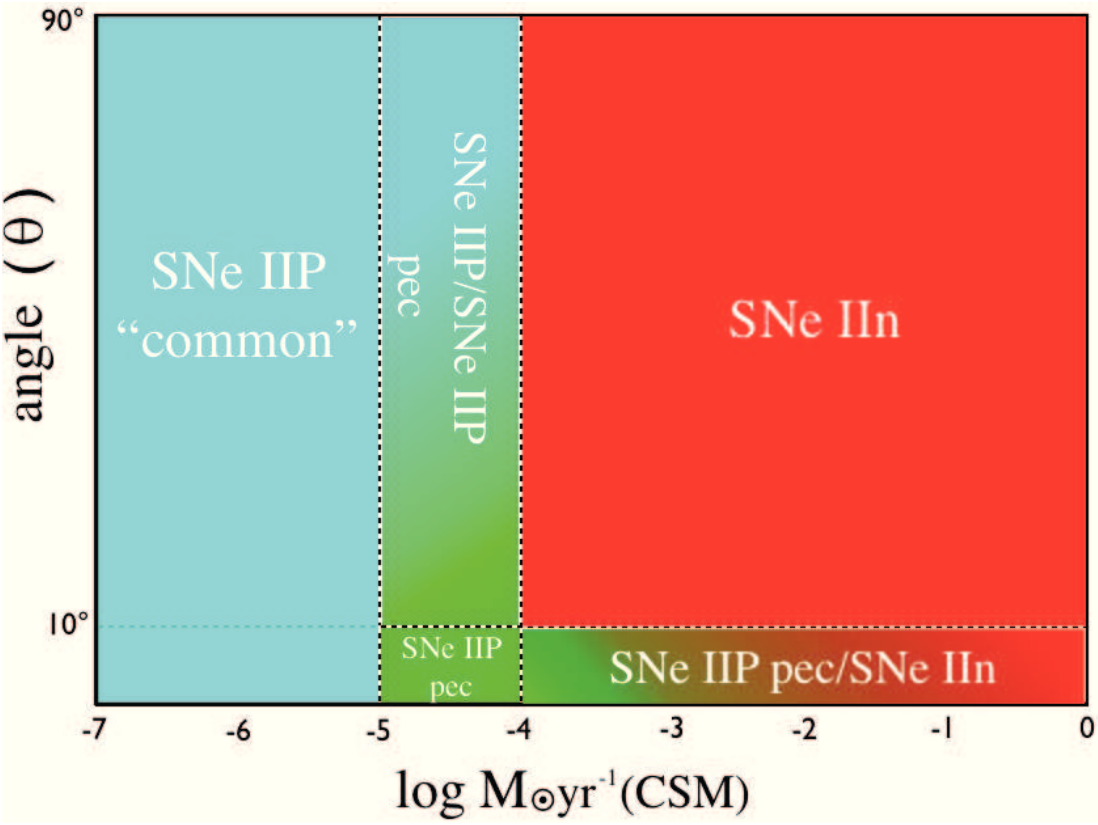

Figure 5.4: Distribution of core collapse SNe, with early interaction due to a close CSM, as function of viewing angle and CSM mass loss rate. Green refers to SNe IIP-pec, red to SNe IIn, and cyan to typical SNe IIP.

Instead increasing the sample of two and three times, counting SNe from 2003 and 1999 respectively we obtain $\theta \sim 13° \pm 6°$ and $\theta \sim 14° \pm 8°$. The increasing of the errors, that reach more than 50% for the last measure were expected because of the lack of swift information (it covers from 2005) and the uncertainties in SNe identification ate early times. From these issues is easily to infer that, without a good temporal coverage, proofs of interaction may be hard to find.

5.2.2 Mass and mass loss rates

The sole CSM geometry is not enough to account for the sequence of typical SNe IIP to IIn by way of the intermediate IIP-pec. We also have to take account the differences in the mass of the CSM.

Assuming an angle averaged mass loss rates $\dot{M}$ and a density profile for CSM following a power law $\rho_{CSM} = \dot{M} 4\pi u_w^{-1} r^{-2}$, where u_w is the wind velocity ranging generally from 5 to 25 $\mathrm{km\,s^{-1}}$ and r is the radius of the CSM (following the discussion above r = a - b), we can obtain a CSM mass value $\propto \dot{M}$ $\mathrm{u_w^{-1}}$ $b(a^2 - b^2)(a-b)^{-2}$.

From the CSM mass dependence appear clearly as there are too many variables. In fact, changing the density profile of the CSM, maybe relate to some peculiar object, the scheme changes and so the physics of interaction, the production of X-ray and radio and maybe also the $\dot{M}$ and the other parameters as u_w. A rough first approximation regarding the mass estimate could be done setting a fix value for the wind, calculating the distances (a and b) through observation (within ∼60 days from shock breakout) and assuming true a priori the power law profile for the CSM density. This allow a linear dependence from the mass loss rates, even if the evaluation of the coefficient is not trivial.

Some peculiarities of the spectra and light curves discussed in Sec. 5.2.1, depending on viewing angle, do not apply if the mass of the CSM is too high or too small. In Fig. 5.4 we suggest a possible distribution of the supernovae according to the mass loss rates ($\mathrm{M_\odot\ yr^{-1}}$) and the viewing angle (θ).

From the OA point of view, a SN IIP-pec is seen only if the mass of the CSM is $\sim 10^{-4}$–10^{-5} $\mathrm{M_\odot\ yr^{-1}}$ (e.g. SNe 2007od Inserra *et al.* (116) 1996W and 1995ad, this work and Pastorello (175)). For smaller values, as for SNe 2004dj and 1999em (190), a typical SN IIP is seen, with the dependence on viewing angle. SN 2009bw could have a mass intermediate between SN 2007od and SN 1999em because it shows the same line profiles and ^{56}Ni mass of SN 1999em but also a bright photospheric luminosity. In this case, if the SN is relatively nearby, the best diagnostics of interaction remain X-ray and radio emission, unless high velocity lines, especially Hα, could be an indication of interaction with a close, less massive CSM. On the other hand, as the CSM mass becomes higher, OA begins to see a SN IIn, again without dependence on viewing angle. In this range two key examples are SNe 2005gl (84, 85) and 2007pk (this work) classified as type IIn revealing P-Cygni profiles like normal type II during the H recombination phase.

OB sees a typical SN IIP if the mass rates of the CSM is $\lesssim 10^{-4}$ $M_\odot$ yr^{-1} and only if the viewing angle is near the limit is there a possibility to observe a SN IIP-pec (e.g. SN 2009bw, 114). At higher values, OB starts to see more SNe IIn than II pec. The large area occupied by SNe IIn in Fig. 5.4 is consistent with the large number of SNe IIn respect to SNe IIP-pec.

As reported above, for low and high CSM mass or mass loss rates (the majority of the events) the shape of the CSM is irrelevant.

6

Final remarks

Aim of this thesis in the observational study of the properties of type II SNe sample belonging to the bright end of the luminosity distribution. In particular, we studied objects that have been considered overall "normal" but with an unusual luminosity at early epochs. We did not concentrate to the single exceptional, peculiar or overluminous objects. Rather, we tried to understand the phenomena causing an increased luminosity in an overall scenario of "normality". The sample of five new objects, plus three found in the Padova-Asiago archive, has been presented and analyzed. The available data set consists on a huge number of spectra and photometric measurements were presented before for a total of more than 90 spectra and 240 photometric epochs, obtained with a many different telescopes and instrumental configurations.This was a large effort in data collection and reduction, on the other the sample results free from systematic effects due to specific instrumentation.

During the thesis we have carefully analyzed the collected data, a summary of the quantitative analyses is given in Tab. 6.1. The extensive photometric and spectroscopic studies of our 2 objects, SN 2007od and SN 2009bw, showed that most probably the source of the brightness is a weak form of early interaction with the CSM. In the other cases the evidences were less compelling but still point in the same directions.

The most important conclusions are the following:

Table 6.1: Main data of the SNe sample.

SNe data	2007od	2009bw	2009dd
adopted distance modulus	$\mu = 32.05 \pm 0.15$	$\mu = 31.53 \pm 0.15$	$\mu = 30.74 \pm 0.15$
SN heliocentric velocity	1734 ± 3 km s^{-1}	1155 ± 6 km s^{-1}	1025 ± 15 km s^{-1}
adopted reddening	E_{tot}(B-V)= 0.04	E_{tot}(B-V)= 0.31	E_{tot}(B-V)= 0.45
explosion day (JD)	$\sim 2454404.5 \pm 5$	$\sim 2454916.5 \pm 2$	$\sim 2454925.5 \pm 5$
L_{bol} peak	6.0×10^{42} erg s^{-1}	2.6×10^{42} erg s^{-1}	2.16×10^{42} erg s^{-1}
(JD)	(2454410 ± 2)	(2454925 ± 2)	(2454937 ± 4)
late time decline mag(100d)$^{-1}$	1.06	1.06	1.07
interval days	208–434	139–239	117–277
M(Ni)	0.02 $M_\odot$	0.022 $M_\odot$	0.034 $M_\odot$
M(ejecta)	5–7.5 $M_\odot$	8.3–12 $M_\odot$	–
explosion energy	0.5×10^{51} ergs	0.3×10^{51} ergs	–
interaction evidences	flat Hα, HVHβ	HVHα, HVHβ	X, possible HVHα

SNe data		2007pk	2010aj
adopted distance modulus		$\mu = 34.23 \pm 0.15$	$\mu = 34.71 \pm 0.15$
SN heliocentric velocity		5116 ± 16 km s^{-1}	6386 ± 20 km s^{-1}
adopted reddening		E_{tot}(B-V)= 0.11	E_{tot}(B-V)= 0.04
explosion day (JD)		$\sim 2454412 \pm 5$	$\sim 2454265.5 \pm 8$
L_{bol} peak		6.26×10^{42} erg s^{-1}	2.68×10^{42} erg s^{-1}
(JD)		(2454420 ± 2)	(2454269 ± 4)
late time decline mag(100d)$^{-1}$		–	4.06
interval days		–	87–103
M(Ni)		–	<0.004 $M_\odot$
M(ejecta)		–	–
explosion energy		–	–
interaction evidences		X, spectra	none

SNe data	1993ad	1995ad	1996W
adopted distance modulus	$\mu = 34.28 \pm 0.15$	$\mu = 31.80 \pm 0.15$	$\mu = 31.93 \pm 0.15$
SN heliocentric velocity	5239 ± 34 km s^{-1}	1647 ± 14 km s^{-1}	1779 ± 29 km s^{-1}
adopted reddening	E_{tot}(B-V)= 0.04	E_{tot}(B-V)=0.04	E_{tot}(B-V)=0.23
explosion day (JD)	$\sim 2449297 \pm 5$	$\sim 2449981 \pm 3$	2450180±5
L_{bol} peak	2.37×10^{42} erg s^{-1}	1.55×10^{42} erg s^{-1}	1.85×10^{42} erg s^{-1}
(JD)	(2454410 ± 2)	(2449989 ± 4)	(2450186 ± 4)
late time decline mag(100d)$^{-1}$	–	0.88	0.86
M(Ni)	$\sim$0.016 $M_\odot$	0.033 $M_\odot$	0.16 $M_\odot$
interaction evidences	early spectra (H, He)	flat Hα	flat Hα
	–	possible HVHα and HVHβ	HVHα, HVHβ

- The bright SNe constitute an heterogenous family of SNe II characterized by bright peaks (average luminosity peak $L_p \sim 4\times10^{42}$ erg s^{-1}), plateau lasting from 30d to 100d, expansion velocities ranging from ∼10000 km s^{-1} at early phase to ∼1000 at the end of the photospheric phase, and temperatures on the plateau T_{pl} ∼5000 K. The observations indicate amounts of ejected ^{56}Ni (a few $\times10^{-2}$ $M_\odot$) in the average for SNe II. Generally these properties are consistent with RSG progenitors of ∼8-15 $M_\odot$ meaning sAGB or iron-CC.

- We have shown that as two SNe of our sample (SN 2007od and SN 2009bw) show clear signs of interaction, with the rise of HV Balmer features during the early phase (SN 2007od) or during the entire photospheric phase (SN 2009bw), and the presence of flat top emission profile for Balmer features (SN 2007od). These signs have been found, even if less prominent, in the other SNe of our sample, leading us to believe that the interaction with a close CSM is more common than previously expected. This interaction transform part of the kinetic energy of the ejecta into luminosity and contribute to the bright display during the early epochs.

- We devoted a particular attention to the study of the photospheric spectra of SN 2007od, modelling them with the LTE code `SYNOW` and the non-LTE code `PHOENIX`. Thanks to this extensive analysis we interpret the line at 4440Å as a combination of Fe II with additional contribution from a possible HV feature of Hβ. At the same time `PHOENIX` calculations show that during the plateau Sc II lines can arise even with standard solar abundances. Also Si II lines are reliably identified in the early spectra. Another important issue is related to the difference between the density profile ($\rho \propto r^{-13}$) needed to reproduce Hα from 8.5d to 17.4d and the density profile required to reproduce the other elements ($\rho \propto r^{-9}$). The evidence for a broken power law density profile shown by SN 2007od might be a specific property of type II SNe or maybe a consequence of a perturbed ejecta, especially in the outermost layers.

- By applying the `SYNOW` code to the photospheric spectra of SN 2009bw we pointed out the presence of the Si II λ6355 feature in the early spectra,

and of CNO element lines in the plateau spectra. Highly ionized C and N features have been tentatively identified in our first spectrum as responsible of the prominent blend at 4600Å. The presence of CNO elements suggests that a dredge up occurred before the explosion, supporting the hypothesis that the progenitor exploded as sAGB or an iron CC-SN.

- In some of the objects of our sample, i.e. SN 2007od, SN 1995ad, SN 2010aj and probably SN 2009bw we noticed signs of early dust formation. The presence of CNO elements and the multiple episodes of mass loss of the progenitor (as seen in SN 2007od) make the environment prone to dust formation, both inside the ejecta and in the CDS, that usually forms close the reverse shock generated from the interaction ejecta-CSM. In our best studied case (SN 2007od) we noticed a boxy line profile of Hα and a blue shift of the emission arising in the SN ejecta. This has been interpreted as the result of the interaction of spherically symmetric SN ejecta expanding in a medium of low average density, with dense clumps. Such configuration, invoked for SN 1988Z (50), allows the early formation of dust in a CDS inside clumps that eventually become incorporated within the SN ejecta. Radiative transfer models (4) have provided estimates of the total dust mass up to 4.2×10^{-3} $M_{\odot}$, which may represent only a lower limit due to the clumpy structure. Only at epochs later than 500d, when the light curve flattens, the interaction dominate over other sources of energy.

- Despite the observational differences, we created a scheme capable to unify all kinds of type II SNe that show weak interaction (our cases), and strong interaction (type IIn). We first considered the mechanisms of mass loss from progenitors of SNe II, excluding *a priori* exotic objects such as LBV or WR stars that produce different types of supernovae. Since mass loss occurs preferentially on the equatorial plane, we expect that the ejecta CSM is asymmetric.

  We suggested that the aspherical geometry explains at the same time all the types of SNe where the ejecta interacts with a close CSM. With the aspherical geometry supported by spectro-polarimetric studies about IIn,

the differences between a SN IIn and a SN IIP, with a weak early interaction, are due principally to two characteristics: the observer viewing angle and the CSM mass loss rate. If the observer line of sight is, within an angle of 10° from the rotation axe, orthogonal to the preferential mass loss direction, and the mass loss rate is $\sim 10^{-4}$–10^{-5} $M_{\odot}$ yr^{-1}, the spectra and the bolometric light curves are those of typical of the bright SN II studied in this thesis. For greater viewing angles and/or larger mass loss the SNe appear as SNe IIn (for various combinations of viewing angles and mass see Fig. 5.4).

Furthermore, most stars that explode as core–collapse supernovae have episodes of mass loss that are not necessarily close in time to the explosion. This leads to two important considerations: 1) a new estimate of the zero age main sequence (ZAMS) mass limits (suggested also in Georgy *et al.* (87) and Smith *et al.* (211)) to smaller values, as for the final mass before the explosion; 2) the possible non-existence of the "red supergiant problem" (209).

The present work highlights the weakness of the current classification scheme for CCSNe. The proliferation of types based only on the morphology of the light curves (IIP, IIL) or in the line profiles (IIn) does not correspond to a real differentiation between the physical processes at stake.

The observational display is heavily affected by too many physical and environmental conditions among which the most important are the size and dimension of the envelope of the star at the explosion, the energy of the explosion, the amount of radiative material synthesized, the amount of fall back on the dense remnant, the presence, geometry and density profile of the CSM.

The understanding of all of theme gives a physical description that starting from the pre-SN evolution includes the accurate treatment of the explosion mechanism, the hydrodynamics of the explosion and the interaction with the environment. Though the single parts are relatively well clear the comprehensive treatment has still to come. To this aim, an extensive preparatory observational background must be prepared.

We are confident to have given a significant contribution to the understanding of CC-SNe but much work remains to be done. The natural continuation of this project is the extension to all kind of CC-SNe.

Appendix A

SNe local sequences

Table A.1: Magnitudes of the local sequence stars in the field of SN 2007od (cfr. Fig. 3.1). The r.m.s. of the measurements are in brackets.

ID	U	B	V	R	I
1	15.25 (.03)	15.21 (.03)	14.44 (.02)	13.99 (.02)	13.70 (.02)
2	17.93 (.01)	17.04 (.01)	15.95 (.02)	15.34 (.02)	14.86 (.02)
3	18.83 (.02)	18.24 (.01)	17.26 (.03)	16.80 (.03)	16.29 (.02)
4	-	17.83 (-)	17.00 (.03)	16.54 (.04)	15.94 (.01)
5	18.58 (.04)	17.54 (.02)	16.43 (.02)	15.76 (.02)	15.23 (.02)
6	18.34 (.04)	18.26 (.03)	17.10 (.02)	16.80 (.02)	16.30 (.03)
7	15.61 (-)	15.77 (.05)	15.11 (.02)	14.82 (.03)	14.37 (.02)
8	18.35 (.01)	17.32 (.02)	16.12 (.02)	15.44 (.02)	14.76 (.02)
9	15.50 (.02)	14.58 (.01)	13.45 (.02)	12.83 (.02)	12.19 (.02)
10	14.58 (.03)	13.85 (.01)	12.86 (.02)	12.30 (.02)	11.74 (.02)
11	18.52 (.01)	18.27 (.03)	17.46 (.03)	17.09 (.03)	16.61 (.02)
12	17.75 (-)	17.96 (.03)	17.31 (.04)	17.06 (.03)	16.64 (.02)
13	-	17.93 (-)	16.78 (.04)	16.08 (.01)	16.01 (.01)

Table A.2: Magnitudes of the local sequence stars in the field of SN 2009bw (cfr. Fig. 3.4). The errors are the r.m.s.

ID	U	B	V	R	I
1	14.48 (.03)	14.41 (.02)	13.73 (.01)	13.36 (.01)	12.97 (.01)
2	16.60 (.03)	15.64 (.02)	14.47 (.02)	13.83 (.01)	13.23 (.01)
3	16.21 (.02)	15.97 (.02)	15.15 (.01)	14.64 (.01)	14.15 (.01)
4	17.01 (.02)	16.42 (.02)	15.41 (.01)	14.85 (.01)	14.27 (.01)
5	17.92 (.02)	17.36 (.02)	16.34 (.01)	15.79 (.02)	15.21 (.02)
6	17.48 (.02)	17.02 (.02)	16.12 (.02)	15.61 (.02)	15.10 (.03)
7	16.60 (.02)	16.46 (.02)	15.68 (.01)	15.24 (.01)	14.78 (.01)
8	16.23 (.02)	16.22 (.02)	15.54 (.01)	15.17 (.02)	14.75 (.01)
9	15.13 (.02)	14.39 (.02)	13.27 (.02)	12.70 (.02)	12.05 (.01)
10	18.04 (.01)	17.73 (.02)	16.86 (.02)	16.45 (.01)	16.01 (.02)
11	18.90 (-)	18.86 (.03)	18.07 (.02)	17.64 (.02)	17.24 (.02)
12	-	19.85 (.02)	18.40 (.02)	17.39 (.01)	16.57 (.01)
13	19.27 (-)	19.22 (.02)	18.50 (.03)	17.99 (.02)	17.59 (.02)
14	-	19.98 (.02)	19.07 (.03)	18.62 (.02)	18.13 (.03)
15	18.55 (-)	18.76 (.02)	17.94 (.02)	17.55 (.01)	17.09 (.02)
16	18.80 (-)	18.65 (.01)	17.59 (.02)	17.00 (.01)	16.45 (.01)
17	20.46 (-)	19.51 (.03)	18.47 (.02)	17.82 (.02)	17.26 (.02)
18	-	20.94 (.02)	19.36 (.03)	18.34 (.02)	17.52 (.02)

Table A.3: Magnitudes of the local sequence stars in the field of SN 2009dd (cfr. Fig. 3.6). The errors are the r.m.s.

ID	U	B	V	R	I
1	16.24 (.07)	17.01 (.02)	16.34 (.01)	16.11 (.01)	15.76 (.02)
2	15.64 (.05)	15.23 (.01)	14.26 (.02)	13.63 (.01)	13.19 (.01)
3	-	19.07 (.02)	17.72 (.02)	16.89 (.01)	16.28 (.02)
4	16.97 (.01)	16.41 (.02)	15.48 (.02)	15.04 (.01)	14.59 (.01)
5	-	19.75 (.02)	19.09 (.02)	18.68 (.02)	18.48 (.03)
6	-	19.91 (.03)	19.06 (.02)	18.32 (.02)	17.77 (.02)
7	-	21.07 (.03)	19.60 (.02)	18.39 (.01)	16.84 (.02)
8	-	20.47 (.02)	19.57 (.02)	18.99 (.02)	18.40 (.02)
9	18.58(-)	17.66 (.02)	16.25 (.03)	15.61 (.01)	14.96 (.02)
10	19.80 (-)	19.00 (.02)	17.95 (.03)	17.52 (.01)	17.12 (.02)

Table A.4: Magnitudes of the local sequence stars in the field of SN 2007pk (cfr. Fig. 3.8). The errors are the r.m.s.

ID	U	B	V	R	I
1	17.00 (.02)	17.11 (.02)	16.53 (.02)	16.21 (.02)	15.82 (.02)
2	19.12 (.02)	18.61 (.03)	17.71 (.01)	17.08 (.03)	16.70 (.02)
3	17.26 (.03)	17.08 (.02)	16.34 (.02)	15.80 (.03)	15.52 (.02)
4	14.70 (.02)	14.79 (.02)	14.35 (.03)	13.85 (.01)	13.54 (.02)
5	16.16 (.02)	16.20 (.02)	15.56 (.02)	15.22 (.03)	14.77 (.03)
6	18.22 (.02)	17.89 (.03)	16.95 (.02)	16.56 (.03)	16.13 (.02)
7	15.81 (.03)	15.86 (.03)	15.26 (.01)	14.93 (.02)	14.69 (.01)
8	15.05 (.02)	14.40 (.03)	13.42 (.03)	12.84 (.02)	12.38 (.01)
9	17.14 (.02)	16.92 (.02)	16.41 (.02)	16.13 (.02)	15.86 (.01)
10	17.54 (.02)	17.48 (.04)	16.79 (.01)	16.45 (.02)	16.14 (.02)
11	17.40 (.02)	17.40 (.03)	16.68 (.01)	16.37 (.02)	16.18 (.05)
12	20.50 (.03)	19.42 (.03)	18.20 (.02)	17.47 (.03)	16.82 (.02)
13	19.20 (.03)	18.76 (.02)	17.90 (.01)	17.42 (.02)	16.90 (.03)

Table A.5: Magnitudes of the local sequence stars in the field of SN 2010aj (cfr. Fig. 3.10). The errors are the r.m.s.

ID	U	B	V	R	I
1	19.14 (.06)	18.52 (.03)	17.62 (.01)	16.99 (.01)	16.48 (.01)
2	17.72 (.06)	17.68 (.02)	17.09 (.04)	16.80 (.01)	16.42 (.02)
3	19.00 (-)	17.91 (.05)	16.39 (.02)	16.31 (.01)	16.07 (.02)
4	18.72 (-)	17.74 (.04)	16.58 (.04)	15.94 (.01)	15.37 (.01)
5	16.90 (.01)	16.77 (.01)	16.05 (.02)	15.62 (.02)	15.24 (.01)
6	14.97 (-)	15.03 (.02)	14.48 (.01)	14.17 (.01)	13.81 (.01)
7	18.89 (-)	18.72 (.01)	17.69 (.07)	17.26 (.01)	16.66 (.07)
8	18.95 (-)	19.27 (.02)	18.66 (.02)	18.37 (.01)	17.83 (.08)
9	18.87 (-)	18.06 (.02)	17.35 (.05)	16.76 (.01)	16.64 (.01)
10	17.91 (-)	18.44 (.04)	17.92 (.01)	17.63 (.01)	17.01 (.08)

Table A.6: Magnitudes of the local sequence stars in the field of SN 1995ad (cfr. Fig. 4.2). The errors are the r.m.s.

ID	U	B	V	R	I
1	-	17.92 (.02)	17.31 (.01)	16.96 (.01)	16.65 (.01)
2	-	17.98 (.01)	17.61 (.01)	17.28 (.01)	16.89 (.01)
3	-	16.25 (.01)	15.29 (.01)	14.78 (.01)	14.29 (.01)
4	-	15.88 (.01)	15.39 (.01)	15.11 (.01)	14.78 (.01)
5	-	17.93 (.02)	17.33 (.01)	16.97 (.01)	16.62 (.04)
6	-	18.63 (.02)	18.08 (.01)	17.74 (.01)	17.43 (.01)
7	-	19.21 (.06)	17.72 (.08)	16.56 (.07)	15.17 (.06)
8	-	18.80 (.02)	18.30 (.07)	18.01 (.05)	17.73 (.02)
9	-	19.59 (.04)	18.14 (.08)	17.23 (.05)	16.32 (.04)
11	-	17.78 (.03)	17.16 (.05)	16.80 (.03)	16.40 (.07)
12	-	16.74 (.01)	16.18 (.05)	15.86 (.06)	15.47 (.10)

Table A.7: Magnitudes of the local sequence stars in the field of SN 1996W (cfr. Fig. 4.4). The errors are the r.m.s.

ID	U	B	V	R	I
2	19.18 (.02)	18.28 (.01)	17.29 (.01)	16.71 (.01)	16.22 (.01)
3	16.90 (.04)	15.94 (.01)	14.90 (.01)	14.28 (.01)	13.76 (.01)
4	19.08 (.02)	18.94 (.02)	18.14 (.01)	17.76 (.01)	17.39 (.02)
5	19.22 (.02)	19.36 (.03)	18.77 (.02)	18.40 (.01)	18.04 (.02)
6	20.03 (.03)	19.88 (.04)	19.29 (.03)	18.83 (.01)	18.47 (.02)

Appendix B

SNe spectroscopic journals

Table B.1: Journal of spectroscopic observations of SN 2007od.

Date	JD +2400000	Phase* (days)	Instrumental setup	Range (Å)	Resolution† (Å)
			SN 2007od		
07/11/04	54409.5	5.5	TNG+DOLORES+LRB‡	3330-7700	14
07/11/07	54412.5	8.5	Pennar+B&C+300tr/mm	3520-8230	10
07/11/08	54413.2	9.2	Copernico+AFOSC+gm4	3500-7820	24
07/11/12	54417.4	13.4	Copernico +AFOSC+gm4,gm2	3640-9150	39
07/11/16	54421.4	17.4	TNG+DOLORES+LRB,LRR‡	3280-9190	14
07/11/27	54431.5	27.5	NTT+EMMI+gm2,gr5	3200-9710	11
07/12/05	54439.4	35.4	Copernico +AFOSC+gm4,gm2	3660-9160	25
07/12/15	54450.4	46.4	TNG+DOLORES+LRB,LRR‡	3400-9100	14
07/12/28	54463.2	59.2	Copernico +AFOSC+gm4,gm2	3780-9150	23
08/01/13	54479.4	75.4	NOT+ALFOSC+gm4	3600-9120	13
08/01/28	54494.3	90.3	Copernico +AFOSC+gm4	3640-7760	23
08/09/05	54714.5	311	TNG+DOLORES+LRR	5050-10250	16
08/10/02	54741.7	338	PALOMAR+DBSP+red	5800-9270	17

* with respect to the explosion epochs (JD 2454404)

† as measured from the full-width at half maximum (FWHM) of the night sky lines

‡ engineering CCD

Table B.2: Journal of spectroscopic observations of SN 2009bw.

Date	JD +2400000	Phase* (days)	Instrumental setup	Range (Å)	Resolution† (Å)
			SN 2009bw		
09/03/29	54920.5	4.0	NOT+ALFOSC+gm4	3600-9000	13
09/04/12	54934.3	17.8	CAHA+CAFOS+b200,r200	3380-10000	10.2
09/04/14	54936.3	19.8	NOT+ALFOSC+gm4	3480-10000	13
09/04/15	54937.3	20.8	TNG+NICS+ij,hk	8750-24600	18,36
09/04/28	54950.3	33.8	CAHA+CAFOS+b200	3480-8730	10.4
09/05/01	54953.5	37	TNG+DOLORES+LRB	3500-7900	15
09/05/02	54954.5	38	TNG+DOLORES+LRR	5000-10000	15
09/05/03	54955.3	39	CAHA+CAFOS+b200	3500-8760	9.8
09/05/16	54968.5	52	BTA+SCORPIO+G400	3870-9830	13
09/05/28	54980.5	64	Copernico +AFOSC+gm4	4500-7760	25
09/05/29	54981.5	65	Copernico +AFOSC+gm2	5330-9020	37
09/05/31	54983.5	67	CAHA+CAFOS+g200	3780-10000	9.5
09/06/26	54509.5	93	CAHA+CAFOS+g200	4000-10000	10.5
09/07/18	55021.5	105	CAHA+CAFOS+g200	4800-10000	13.6
09/08/12	55046.5	130	CAHA+CAFOS+g200	4000-9650	12.4
09/08/13	55047.5	131	NOT+ALFOSC+gm4	4200-9100	18
09/09/04	55069.5	153	CAHA+CAFOS+g200	4000-10000	9
09/10/11	55106.5	190	TNG+DOLORES+LRR	5260-10000	16

* with respect to the explosion epochs (JD 2454916.5)

† as measured from the full-width at half maximum (FWHM) of the night sky lines

Table B.3: Journal of spectroscopic observations of SN 2009dd.

Date	JD +2400000	Phase* (days)	Instrumental setup	Range (Å)	Resolution† (Å)
			SN 2009dd		
09/04/14	54936.7	11.7	NOT+ALFOSC+gm4	3380-8000	13
09/05/20	54971.6	46.6	TNG+DOLORES+LRB,LRR	3400-9220	15
09/07/20	55033.4	108.4	TNG+DOLORES+LRB,LRR	3800-10260	15
09/11/19	55155.7	230.7	CAHA+CAFOS+g200	3800-9900	9.5
09/11/21	55157.7	232.7	TNG+DOLORES+LRR	5100-9600	10.3
10/05/18	55334.5	409.5	TNG+DOLORES+LRR	5030-9270	9.8

* with respect to the explosion epochs (JD 2454925)

† as measured from the full-width at half maximum (FWHM) of the night sky lines

Table B.4: Journal of spectroscopic observations of SN 2007pk.

Date	JD +2400000	Phase* (days)	Instrumental setup	Range (Å)	Resolution† (Å)
			SN 2007pk		
07/11/11	54416.3	4.3	Copernico + AFOSC+gm4	3650-7800	24
07/11/12	54417.5	5.5	Copernico + AFOSC+gm2	5320-9080	36
07/11/16	54421.4	8.4	TNG+DOLORES+LRB,LRR‡	3400-9000	14
07/12/05	54439.5	27.5	Copernico +AFOSC+gm4,gm2	3700-9050	25
07/12/28	54463.3	51.3	Copernico +AFOSC+gm4,gm2	3780-9180	23
08/01/11	54477.4	65.4	NOT+ALFOSC+gm4	3580-9120	14
08/01/12	54478.4	66.4	TNG+NICS+ij	8660-13480	18
08/01/28	54494.3	82.3	Copernico +AFOSC+gm4	3670-7770	23
08/09/05	54714.5	302.5	TNG+DOLORES+LRR	5150-10230	16
08/10/02	54741.7	329.7	PALOMAR+DBSP+red	5800-9990	17

* with respect to the explosion epochs (JD 2454412)

† as measured from the full-width at half maximum (FWHM) of the night sky lines

‡ engineering CCD

Table B.5: Journal of spectroscopic observations of SN 2010aj.

Date	JD +2400000	Phase* (days)	Instrumental setup	Range (Å)	Resolution† (Å)
			SN 2010aj		
10/03/30	55287.6	22.1	WHT+ISIS+R300B,R158R	3130-11130	5.4-6.3
10/04/14	55303.3	37.8	NTT+EFOSC2+gm16	3800-7500	13
10/04/24	55311.5	46	TNG+DOLORES+LRB,LRR	3380-9900	10
10/05/21	55338.5	73	TNG+DOLORES+LRB,LRR	3500-9700	10
11/02/11	55604.3	356.8	NTT+EFOSC2+gm13	3650-9300	17

* with respect to the explosion epochs (JD 2455265.5)

† as measured from the full-width at half maximum (FWHM) of the night sky lines

Table B.6: Journal of spectroscopic observations of SN 1993ad.

Date	JD +2400000	Phase* (days)	Instrumental setup	Range (Å)	Resolution† (Å)
			SN 1993ad		
93/11/10	49301.6	4.6	ESO 3.6m+EFOSC1+b300	3700-6900	14
93/11/17	49308.6	11.6	ESO 2.2m+EFOSC2+gr6	4480-7115	11
93/11/18	49309.7	12.7	ESO 2.2m+EFOSC2+gr6	3750-6940	11
94/06/14	49517.5	220.5	ESO 2.2m+EFOSC2+gr5	5830-8500	11
94/09/29	49624.6	327.6	ESO 3.6m+EFOSC1+b300	3715-6890	14

* with respect to the explosion epochs (JD 2449297.0)

† as measured from the full-width at half maximum (FWHM) of the night sky lines

Table B.7: Journal of spectroscopic observations of SN 1995ad.

Date	JD +2400000	Phase* (days)	Instrumental setup	Range (Å)	Resolution† (Å)
			SN 1995ad		
95/09/29	49989.8	8.8	ESO 1.5m+B&C	3930-7790	5
95/10/02	49992.9	11.9	ESO 3.6m+EFOSC1	3750-9920	14+17
95/10/14	50004.9	23.9	ESO 3.6m+EFOSC1	3750-6940	19
95/11/19	50040.8	59.9	ESO 1.5m+B&C	3100-10710	10
95/11/20	50041.8	60.8	ESO 1.5m+B&C	3100-10710	25
95/12/26	50077.8	96.8	ESO 2.2m+EFOSC2	3720-9040	11+11+60
95/12/29	50080.8	99.8	ESO 3.6m+EFOSC1	3740-9910	14+17
96/01/21	50103.7	122.7	ESO 1.5m+B&C	3460-11100	9
96/02/18	50131.7	150.7	ESO 2.2m+EFOSC2	3350-8980	11
96/02/19	50132.7	151.7	ESO 1.5m+B&C	3040-10000	9
96/02/20	50133.7	152.7	ESO 1.5m+B&C	3040-10000	9
97/02/11	50490.6	509.6	ESO 3.6m+EFOSC1	6000-9850	23

* with respect to the explosion epochs (JD 2449981.0)

† as measured from the full-width at half maximum (FWHM) of the night sky lines

Table B.8: Journal of spectroscopic observations of SN 1996W.

Date	JD +2400000	Phase* (days)	Instrumental setup	Range (Å)	Resolution† (Å)
			SN 1996W		
96/04/18	50191.6	11.6	ESO 1.5m+B&C+gr2	3160-10650	9
96/04/19	50192.6	12.6	ESO 1.5m+B&C+gr2	3160-10650	9
96/06/21	50195.4	15.4	Copernico+B&C+150tr.	4250-8600	29
96/04/24	50198.4	18.1	ESO 1.5m+B&C+gr2	3130-10430	9
96/04/25	50198.6	18.5	ESO 1.5m+B&C+gr2	3130-10430	9
96/05/09	50212.5	32.5	ESO 1.5m+B&C+gr2	3120-10590	9
96/05/12	50215.6	35.6	ESO 1.5m+B&C+gr2	3120-10590	9
96/05/19	50222.6	42.6	ESO 2.2m+EFOSC2+gr5,gr6	2850-9050	7+7
96/06/12	50247.5	67.5	ESO 1.5m+B&C+gr2	2900-10460	9
96/12/15	50432.8	252.8	ESO 2.2m+EFOSC2+gr6	3840-7980	10
97/01/30	50478.5	298.5	Danish 1.54m+DFOSC+gr5	5000-10180	8
97/02/13	50492.7	312.7	ESO 2.2m+EFOSC2+gr5	5220-9280	9

* with respect to the explosion epochs (JD 2450180.0)

† as measured from the full-width at half maximum (FWHM) of the night sky lines

References

[1] Agnoletto, I., Benetti, S., Cappellaro, E., Zampieri, L., Turatto, M., Mazzali, P., Pastorello, A., Della Valle, M., Bufano, F., Harutyunyan, A., Navasardyan, H., Elias-Rosa, N., Taubenberger, S., Spiro, S., and Valenti, S.: 2009, *Astrophys. J.* **691**, 1348. 148

[2] Alard, C.: 2000, *Astronomy and Astrophysics Supplement Series* **144**, 363. 37

[3] Aldering, G., Antilogus, P., Bailey, S., Baltay, C., Bauer, A., Blanc, N., Bongard, S., Copin, Y., Gangler, E., Gilles, S., Kessler, R., Kocevski, D., Lee, B.C., Loken, S., Nugent, P., Pain, R., Pécontal, E., Pereira, R., Perlmutter, S., Rabinowitz, D., Rigaudier, G., Scalzo, R., Smadja, G., Thomas, R.C., Wang, L., and Weaver, B.A.: 2006, *Astrophys. J.* **650**, 510. 8

[4] Andrews, J.E., Gallagher, J.S., Clayton, G.C., Sugerman, B.E.K., Chatelain, J.P., Clem, J., Welch, D.L., Barlow, M.J., Ercolano, B., Fabbri, J., Wesson, R., and Meixner, M.: 2010, *Astrophys. J.* **715**, 541. vi, vii, 48, 51, 52, 78, 83, 133, 134, 136, 137, 138, 141, 142, 143, 147, 183, 199

[5] Arnett W. D., 1996, Supernovae and Nucleosynthesis, Princeton University Press, Princeton 22, 82, 131

[6] Arnett, W.D., Bahcall, J.N., Kirshner, R.P., and Woosley, S.E.: 1989, *Annual Review of Astronomy and Astrophysics* **27**, 629. 74

[7] Arnett, W.D., Branch, D., and Wheeler, J.C.: 1985, *Nature* **314**, 337. 7

[8] Arnett, W.D.: 1982, *Astrophys. J.* **253**, 785. 7

[9] Asplund, M., Grevesse, N., Sauval, A.J., and Scott, P.: 2009, *Annual Review of Astronomy and Astrophysics* **47**, 481. 150

[10] Balberg, S., Zampieri, L., and Shapiro, S.L.: 2000, *Astrophys. J.* **541**, 860.

[11] Balick, B. and Frank, A.: 2002, *Annual Review of Astronomy and Astrophysics* **40**, 439 185

[12] Balinskaia, I.S., Bychkov, K.V., and Neizvestnyi, S.I.: 1980, *Astron. Astroph.* **85**, L19. 74

[13] Barbon, R., Buondí, V., Cappellaro, E., and Turatto, M.: 1999, *Astronomy and Astrophysics Supplement Series* **139**, 531. 5, 8, 10

[14] Barbon, R., Benetti, S., Cappellaro, E., Patat, F., Turatto, M., and Iijima, T.: 1995, *Astronomy and Astrophysics Supplement Series* **110**, 513. 10

[15] Barbon, R., Ciatti, F., and Rosino, L.: 1979, *Astron. Astroph.* **72**, 287. 4, 11

[16] Baron, E., Nugent, P.E., Branch, D., and Hauschildt, P.H.: 2004, *Astrophys. J.* **616**, L91. 183

[17] Baron, E., Branch, D., Hauschildt, P.H., Filippenko, A.V., Kirshner, R.P., Challis, P.M., Jha, S., Chevalier, R., Fransson, C., Lundqvist, P., Garnavich, P., Leibundgut, B., McCray, R., Michael, E., Panagia, N., Phillips, M.M., Pun, C.S.J., Schmidt, B., Sonneborn, G., Suntzeff, N.B., Wang, L., and Wheeler, J.C.: 2000, *Astrophys. J.* **545**, 444. 74, 85, 91

[18] Baron, E., Hauschildt, P.H., Branch, D., Kirshner, R.P., and Filippenko, A.V.: 1996, *Monthly Notices of the Royal Astronomical Society* **279**, 799. 18, 127

[19] Baron, E., Hauschildt, P.H., Branch, D., Austin, S., Garnavich, P., Ann, H.B., Wagner, R.M., Filippenko, A.V., Matheson, T., and Liebert, J.: 1995, *Astrophys. J.* **441**, 170. 127

[20] Baron, E., Hauschildt, P.H., and Branch, D.: 1994, *Astrophys. J.* **426**, 334. 127

[21] Baron, E., Hauschildt, P.H., Branch, D., Wagner, R.M., Austin, S.J., Filippenko, A.V., and Matheson, T.: 1993, *Astrophys. J.* **416**, L21. 127

[22] Benetti, S., Cappellaro, E., Mazzali, P.A., Turatto, M., Altavilla, G., Bufano, F., Elias-Rosa, N., Kotak, R., Pignata, G., Salvo, M., and Stanishev, V.: 2005, *Astrophys. J.* **623**, 1011. 7

[23] Benetti, S.: 2000, *Memorie della Societa Astronomica Italiana* **71**, 323. 13

[24] Benetti, S., Patat, F., Turatto, M., Contarini, G., Gratton, R., and Cappellaro, E.: 1994, *Astron. Astroph.* **285**, L13. 10

[25] Bertoldi, F., Carilli, C.L., Cox, P., Fan, X., Strauss, M.A., Beelen, A., Omont, A., and Zylka, R.: 2003, *Astron. Astroph.* **406**, L55. 20

[26] Blackman, E.G., Frank, A., Markiel, J.A., Thomas, J.H., and Van Horn, H.M.: 2001, *Nature* **409**, 485. 185

[27] Blair, W.P., Ghavamian, P., Long, K.S., Williams, B.J., Borkowski, K.J., Reynolds, S.P., and Sankrit, R.: 2007, *Astrophys. J.* **662**, 998. 22

[28] Blondin, S. and Calkins, M.: 2007, *Central Bureau Electronic Telegrams* **1119**, 1. 44

[29] Botticella, M.T., Trundle, C., Pastorello, A., Rodney, S., Rest, A., Gezari, S., Smartt, S.J., Narayan, G., Huber, M.E., Tonry, J.L., Young, D., Smith, K., Bresolin, F., Valenti, S., Kotak, R., Mattila, S., Kankare, E., Wood-Vasey, W.M., Riess, A., Neill, J.D., Forster, K., Martin, D.C., Stubbs, C.W., Burgett, W.S., Chambers, K.C., Dombeck, T., Flewelling, H., Grav, T., Heasley, J.N., Hodapp, K.W., Kaiser, N., Kudritzki, R., Luppino, G., Lupton, R.H., Magnier, E.A., Monet, D.G., Morgan, J.S., Onaka, P.M., Price, P.A., Rhoads, P.H., Siegmund, W.A., Sweeney, W.E., Wainscoat, R.J., Waters, C., Waterson, M.F., and Wynn-Williams, C.G.: 2010, *Astrophys. J.* **717**, L52. 154

[30] Botticella, M.T., Pastorello, A., Smartt, S.J., Meikle, W.P.S., Benetti, S., Kotak, R., Cappellaro, E., Crockett, R.M., Mattila, S., Sereno, M., Patat, F., Tsvetkov, D., van Loon, J.T., Abraham, D., Agnoletto, I., Arbour, R., Benn, C., di Rico, G., Elias-Rosa, N., Gorshanov, D.L., Harutyunyan, A., Hunter, D., Lorenzi, V., Keenan, F.P., Maguire, K., Mendez, J., Mobberley, M., Navasardyan, H., Ries, C., Stanishev, V., Taubenberger, S., Trundle, C., Turatto, M., and Volkov, I.M.: 2009, *Monthly Notices of the Royal Astronomical Society* **398**, 1041. 5, 22

[31] Branch, D., Benetti, S., Kasen, D., Baron, E., Jeffery, D.J., Hatano, K., Stathakis, R.A., Filippenko, A.V., Matheson, T., Pastorello, A., Altavilla, G., Cappellaro, E., Rizzi, L., Turatto, M., Li, W., Leonard, D.C., and Shields, J.C.: 2002, *Astrophys. J.* **566**, 1005. 9, 118

[32] Branch, D., Jeffery, D.J., Blaylock, M., and Hatano, K.: 2000, *Publications of the Astronomical Society of the Pacific* **112**, 217. 91, 109, 151, 187

[33] Branch, D., Nomoto, K., and Filippenko, A.V.: 1990, *Comments on Astrophysics* **15**, 221. 12

[34] Branch, D., Falk, S.W., Uomoto, A.K., Wills, B.J., McCall, M.L., and Rybski, P.: 1981, *Astrophys. J.* **244**, 780. 87

[35] Broughton, J.: 1998, *International Astronomical Union Circular* **6852**, 2. 160

[36] Cappellaro, E., Mazzali, P.A., Benetti, S., Danziger, I.J., Turatto, M., della Valle, M., and Patat, F.: 1997, *Astron. Astroph.* **328**, 203. 7, 83

[37] Cappellaro, E., Danziger, I.J., and Turatto, M.: 1995, *Monthly Notices of the Royal Astronomical Society* **277**, 106. 134, 183

[38] Cardelli, J.A., Clayton, G.C., and Mathis, J.S.: 1989, *Astrophys. J.* **345**, 245. 46

[39] Carney, B.W., Gray, D.F., Yong, D., Latham, D.W., Manset, N., Zelman, R., and Laird, J.B.: 2008, *The Astronomical Journal* **135**, 892. 192

[40] Cenko, S.B., Cobb, B.E., Kleiser, I.K., and Filippenko, A.V.: 2010, *Central Bureau Electronic Telegrams* **2209**, 1. 69, 70

[41] Cernuschi, F., Marsicano, F., and Codina, S.: 1967, *Annales d'Astrophysique* **30**, 1039. 20

[42] Chandra, P. and Soderberg, A.: 2007, *The Astronomer's Telegram* **1271**, 1. 64

[43] Chevalier, R.A.: 2008, *IAU Symposium* **255**, 175. 142

[44] Chevalier, R.A. and Fransson, C.: 1994, *Astrophys. J.* **420**, 268. 13, 24, 134, 182

[45] Chevalier, R.A.: 1988, *Nature* **332**, 514. 183

[46] Chevalier, R.A.: 1982, *Astrophys. J.* **259**, L85. 8

[47] Chevalier, R.A.: 1982, *Astrophys. J.* **259**, 302 8

[48] Chevalier, R.A.: 1982, *Astrophys. J.* **258**, 790. 134, 137

[49] Chugai, N.N., Chevalier, R.A., and Utrobin, V.P.: 2007, *Astrophys. J.* **662**, 1136. 23, 24, 114, 141, 151, 153, 173, 183, 190

[50] Chugai, N.N. and Danziger, I.J.: 1994, *Monthly Notices of the Royal Astronomical Society* **268**, 173. 137, 183, 187, 199

[51] Clocchiatti, A. and Wheeler, J.C.: 1997, *Astrophys. J.* **491**, 375. 9

[52] Clocchiatti, A., Benetti, S., Wheeler, J.C., Wren, W., Boisseau, J., Cappellaro, E., Turatto, M., Patat, F., Swartz, D.A., Harkness, R.P., Brotherton, M.S., Wills, B., Hemenway, P., Cornell, M., Frueh, M., and Kaiser, M.B.: 1996, *The Astronomical Journal* **111**, 1286. 11, 50, 57, 64, 74, 87, 110, 183

[53] Cortini, G. and Dimai, A.: 2009, *Central Bureau Electronic Telegrams* **1764**, 1. 58

[54] de, S., Baron, E., and Hauschildt, P.H.: 2010, *Monthly Notices of the Royal Astronomical Society* **407**, 658. 127

[55] de, S., Baron, E., and Hauschildt, P.H.: 2010, *Monthly Notices of the Royal Astronomical Society* **401**, 2081. 127

[56] de Blok, W.J.G. and van der Hulst, J.M.: 1998, *Astron. Astroph.* **335**, 421. 142

[57] Dessart L., & Hillier, D. J., 2007, *Monthly Notices of the Royal Astronomical Society* , **383**, 57. 127

[58] Dessart, L. and Hillier, D.J.: 2005, *Astron. Astroph.* **437**, 667. 87

[59] Dickey, J.M. and Lockman, F.J.: 1990, *Annual Review of Astronomy and Astrophysics* **28**, 215. 151

[60] Dwek, E., Galliano, F., and Jones, A.P.: 2007, *Astrophys. J.* **662**, 927. 22, 23

[61] Dwek, E.: 2004, *Astrophys. J.* **607**, 848. 23

[62] Dunne, L., Eales, S., Ivison, R., Morgan, H., and Edmunds, M.: 2003, *Nature* **424**, 285. 22

[63] Elias-Rosa, N., Van Dyk, S.D., Li, W., Silverman, J.M., Foley, R.J., Ganeshalingam, M., Mauerhan, J.C., Kankare, E., Jha, S., Filippenko, A.V., Beckman, J.E., Berger, E., Cuillandre, J.-C., and Smith, N.: 2011, *ArXiv e-prints*, arXiv:1108.2645. 21

[64] Elias-Rosa, N., Van Dyk, S.D., Li, W., Miller, A.A., Silverman, J.M., Ganeshalingam, M., Boden, A.F., Kasliwal, M.M., Vinkó, J., Cuillandre, J.-C., Filippenko, A.V., Steele, T.N., Bloom, J.S., Griffith, C.V., Kleiser, I.K.W., and Foley, R.J.: 2010, *Astrophys. J.* **714**, L254. 21

[65] Elias-Rosa, N., Van Dyk, S.D., Li, W., Morrell, N., Gonzalez, S., Hamuy, M., Filippenko, A.V., Cuillandre, J.-C., Foley, R.J., and Smith, N.: 2009, *Astrophys. J.* **706**, 1174. 21

[66] Elias-Rosa, N., van Dyk, S.D., Agnoletto, I., and Benetti, S.: 2009, *Central Bureau Electronic Telegrams* **1765**, 1. 58, 60

[67] Elmhamdi, A., Chugai, N.N., and Danziger, I.J.: 2003, *Astron. Astroph.* **404**, 1077. 52, 83, 143

[68] Elmhamdi, A., Danziger, I.J., Chugai, N., Pastorello, A., Turatto, M., Cappellaro, E., Altavilla, G., Benetti, S., Patat, F., and Salvo, M.: 2003, *Monthly Notices of the Royal Astronomical Society* **338**, 939. 22, 74, 85, 108, 110, 133, 136, 143, 148, 153, 154

[69] Ercolano, B., Barlow, M.J., and Sugerman, B.E.K.: 2007, *Monthly Notices of the Royal Astronomical Society* **375**, 753. 143

[70] Evans, R., Benetti, S., and Grupe, D.: 1995, *International Astronomical Union Circular* **6239**, 1. 160

[71] Fassia, A., Meikle, W.P.S., Chugai, N., Geballe, T.R., Lundqvist, P., Walton, N.A., Pollacco, D., Veilleux, S., Wright, G.S., Pettini, M., Kerr, T., Puchnarewicz, E., Puxley, P., Irwin, M., Packham, C., Smartt, S.J., and Harmer, D.: 2001, *Monthly Notices of the Royal Astronomical Society* **325**, 907. 74, 93, 100

[72] Fassia, A., Meikle, W.P.S., Geballe, T.R., Walton, N.A., Pollacco, D.L., Rutten, R.G.M., and Tinney, C.: 1998, *Monthly Notices of the Royal Astronomical Society* **299**, 150. 87, 131, 153

[73] Fesen, R.A., Gerardy, C.L., Filippenko, A.V., Matheson, T., Chevalier, R.A., Kirshner, R.P., Schmidt, B.P., Challis, P., Fransson, C., Leibundgut, B., and van Dyk, S.D.: 1999, *The Astronomical Journal* **117**, 725. 134, 183

[74] Filippenko, A.V., Silverman, J.M., and Foley, R.J.: 2007, *Central Bureau Electronic Telegrams* **1129**, 2. 64, 100

[75] Filippenko, A.V.: 1997, *Annual Review of Astronomy and Astrophysics* **35**, 309. 11, 14

[76] Filippenko, A.V., Barth, A.J., Matheson, T., Armus, L., Brown, M., Espey, B.R., Fan, X.-M., Goodrich, R.W., Ho, L.C., Junkkarinen, V.T., Koo, D.C., Lehnert, M.D., Martel, A.R., Mazzarella, J.M., Miller, J.S., Smith, G.H., Tytler, D., and Wirth, G.D.: 1995, *Astrophys. J.* **450**, L11. 8

[77] Filippenko, A.V.: 1988, *The Astronomical Journal* **96**, 1941. 10

[78] Fisher A., 2000, PhD thesis, Univ. Oklahoma 91, 118

[79] Fox, O., Skrutskie, M.F., Chevalier, R.A., Kanneganti, S., Park, C., Wilson, J., Nelson, M., Amirhadji, J., Crump, D., Hoeft, A., Provence, S., Sargeant, B., Sop, J., Tea, M., Thomas, S., and Woolard, K.: 2009, *Astrophys. J.* **691**, 650. 22

[80] Fransson, C. and Chevalier, R.A.: 1989, *Astrophys. J.* **343**, 323. 142

[81] Fransson, C. and Chevalier, R.A.: 1987, *Astrophys. J.* **322**, L15. 142

[82] Fryer, C.L.: 1999, *Astrophys. J.* **522**, 413. 147

[83] Gal-Yam, A., Mazzali, P., Ofek, E.O., Nugent, P.E., Kulkarni, S.R., Kasliwal, M.M., Quimby, R.M., Filippenko, A.V., Cenko, S.B., Chornock, R., Waldman, R., Kasen, D., Sullivan, M., Beshore, E.C., Drake, A.J., Thomas, R.C., Bloom, J.S., Poznanski, D., Miller, A.A., Foley, R.J., Silverman, J.M., Arcavi, I., Ellis, R.S., and Deng, J.: 2009, *Nature* **462**, 624. 19

[84] Gal-Yam, A. and Leonard, D.C.: 2009, *Nature* **458**, 865. 155, 194

[85] Gal-Yam, A., Leonard, D.C., Fox, D.B., Cenko, S.B., Soderberg, A.M., Moon, D.-S., Sand, D.J., Li, W., Filippenko, A.V., Aldering, G., and Copin, Y.: 2007, *Astrophys. J.* **656**, 372. 155, 194

[86] Georgy, C., Meynet, G., and Maeder, A.: 2011, *Astron. Astroph.* **527**, A52. 184

[87] Georgy, C., Meynet, G., Walder, R., Folini, D., and Maeder, A.: 2009, *Astron. Astroph.* **502**, 611. 200

[88] Gerardy, C.L., Höflich, P., Fesen, R.A., Marion, G.H., Nomoto, K., Quimby, R., Schaefer, B.E., Wang, L., and Wheeler, J.C.: 2004, *Astrophys. J.* **607**, 391. 23

[89] Gerardy, C.L., Fesen, R.A., Nomoto, K., Garnavich, P.M., Jha, S., Challis, P.M., Kirshner, R.P., Höflich, P., and Wheeler, J.C.: 2002, *Astrophys. J.* **575**, 1007. 22

[90] Gerardy, C.L., Fesen, R.A., Höflich, P., and Wheeler, J.C.: 2000, *The Astronomical Journal* **119**, 2968. 22

[91] Gibson, B.K., Stetson, P.B., Freedman, W.L., Mould, J.R., Kennicutt, R.C., Jr., Huchra, J.P., Sakai, S., Graham, J.A., Fassett, C.I., Kelson, D.D., Ferrarese, L., Hughes, S.M.G., Illingworth, G.D., Macri, L.M., Madore, B.F., Sebo, K.M., and Silbermann, N.A.: 2000, *Astrophys. J.* **529**, 723. 7

[92] Grevesse, N. and Sauval, A.J.: 1998, *Space Science Reviews* **85**, 161. 120

[93] Hamuy, M., Phillips, M.M., Suntzeff, N.B., Maza, J., González, L.E., Roth, M., Krisciunas, K., Morrell, N., Green, E.M., Persson, S.E., and McCarthy, P.J.: 2003, *Nature* **424**, 651. 5, 8, 23

[94] Hamuy, M.: 2003, *Astrophys. J.* **582**, 905. 25, 82

[95] Hamuy, M.: 2003, Review for Core Collapse of Massive Stars, Ed. C.L. Fryer, Kluwer, Dordrecht v, 12

[96] Hamuy, M., Pinto, P.A., Maza, J., Suntzeff, N.B., Phillips, M.M., Eastman, R.G., Smith, R.C., Corbally, C.J., Burstein, D., Li, Y., Ivanov, V., Moro-Martin, A., Strolger, L.G., de Souza, R.E., dos Anjos, S., Green, E.M., Pickering, T.E., González, L., Antezana, R., Wischnjewsky, M., Galaz, G., Roth, M., Persson, S.E., and Schommer, R.A.: 2001, *Astrophys. J.* **558**, 615.

[97] Hamuy, M.A.: 2001, *Ph.D. Thesis.*

[98] Hamuy, M., Suntzeff, N.B., Heathcote, S.R., Walker, A.R., Gigoux, P., and Phillips, M.M.: 1994, *Publications of the Astronomical Society of the Pacific* **106**, 566. 40

[99] Hamuy, M., Walker, A.R., Suntzeff, N.B., Gigoux, P., Heathcote, S.R., and Phillips, M.M.: 1992, *Publications of the Astronomical Society of the Pacific* **104**, 533. 40

[100] Harutyunyan, A.H., Pfahler, P., Pastorello, A., Taubenberger, S., Turatto, M., Cappellaro, E., Benetti, S., Elias-Rosa, N., Navasardyan, H., Valenti, S., Stanishev, V., Patat, F., Riello, M., Pignata, G., and Hillebrandt, W.: 2008, *Astron. Astroph.* **488**, 383. 50, 57, 61, 67, 73, 108, 157

[101] Hauschildt P. H., Baron, E. 2004, Mitt. Math. Ges., 24, 1 118

[102] Hauschildt, P.H. and Baron, E.: 1999, *Journal of Computational and Applied Mathematics* **109**, 41. 118

[103] Hauschildt, P.H.: 1992, *Journal of Quantitative Spectroscopy and Radiative Transfer* **47**, 433 118

[104] Heger, A., Woosley, S.E., and Spruit, H.C.: 2005, *Astrophys. J.* **626**, 350.

[105] Heger, A., Fryer, C.L., Woosley, S.E., Langer, N., and Hartmann, D.H.: 2003, *Astrophys. J.* **591**, 288. 19, 142, 184

[106] Heger, A., Jeannin, L., Langer, N., and Baraffe, I.: 1997, *Astron. Astroph.* **327**, 224. 185

[107] Hillebrandt, W., Sim, S.A., and Röpke, F.K.: 2007, *Astron. Astroph.* **465**, L17. 7

[108] Hoffman, J.L., Leonard, D.C., Chornock, R., Filippenko, A.V., Barth, A.J., and Matheson, T.: 2008, *Astrophys. J.* **688**, 1186 187

[109] Hoyle, F. and Wickramasinghe, N.C.: 1970, *Nature* **226**, 62. 20

[110] Howell, D.A., Sullivan, M., Nugent, P.E., Ellis, R.S., Conley, A.J., Le Borgne, D., Carlberg, R.G., Guy, J., Balam, D., Basa, S., Fouchez, D., Hook, I.M., Hsiao, E.Y., Neill, J.D., Pain, R., Perrett, K.M., and Pritchet, C.J.: 2006, *Nature* **443**, 308. 7

[111] Immler, S., Russell, B.R., and Brown, P.J.: 2009, *The Astronomer's Telegram* **2106**, 1. 58, 116

[112] Immler, S., Pooley, D., Brown, P.J., Li, W., and Filippenko, A.V.: 2007, *The Astronomer's Telegram* **1284**, 1. 64

[113] Immler, S. and Brown, P.J.: 2007, *The Astronomer's Telegram* **1259**, 1. 44, 141

[114] Inserra, C.et al. *ArXiv e-prints*, arXiv:1102.5468 2009bw. 27, 29, 64, 84, 118, 139, 183, 190, 195

[115] Inserra, C., Baron, E., and Turatto, M.: *ArXiv e-prints*, arXiv:1102.5468 2009bw. 118, 139

[116] Inserra, C., Turatto, M., Pastorello, A., Benetti, S., Cappellaro, E., Pumo, M.L., Zampieri, L., Agnoletto, I., Bufano, F., Botticella, M.T., Della Valle, M., Elias Rosa, N., Iijima, T., Spiro, S., and Valenti, S.: 2011, *ArXiv e-prints*, arXiv:1102.5468. 27, 29, 57, 58, 64, 84, 118, 119, 122, 126, 128, 139, 147, 154, 155, 183, 187, 194

[117] Iwamoto, K., Nakamura, T., Nomoto, K., Mazzali, P.A., Danziger, I.J., Garnavich, P., Kirshner, R., Jha, S., Balam, D., and Thorstensen, J.: 2000, *Astrophys. J.* **534**, 660. 9

[118] Iwamoto, K., Mazzali, P.A., Nomoto, K., Umeda, H., Nakamura, T., Patat, F., Danziger, I.J., Young, T.R., Suzuki, T., Shigeyama, T., Augusteijn, T., Doublier, V., Gonzalez, J.-F., Boehnhardt, H., Brewer, J., Hainaut, O.R., Lidman, C., Leibundgut, B., Cappellaro, E., Turatto, M., Galama, T.J., Vreeswijk, P.M., Kouveliotou, C., van Paradijs, J., Pian, E., Palazzi, E., and Frontera, F.: 1998, *Nature* **395**, 672. 9

[119] Jeffery, D.J., Branch, D., and Baron, E.: 2006, *ArXiv Astrophysics e-prints*, arXiv:astro-ph/0609804. 7

[120] Jeffery, D.J. and Branch, D.: 1990, *Supernovae, Jerusalem Winter School for Theoretical Physics*, 149. 85

[121] Kotak, R., Meikle, W.P.S., Farrah, D., Gerardy, C.L., Foley, R.J., Van Dyk, S.D., Fransson, C., Lundqvist, P., Sollerman, J., Fesen, R., Filippenko, A.V., Mattila, S., Silverman, J.M., Andersen, A.C., Höflich, P.A., Pozzo, M., and Wheeler, J.C.: 2009, *Astrophys. J.* **704**, 306. 20, 22, 50, 133, 134, 143, 147, 183

[122] Kotak, R., Meikle, P., van Dyk, S.D., Höflich, P.A., and Mattila, S.: 2005, *Astrophys. J.* **628**, L123. 133

[123] Kozasa, T., Hasegawa, H., and Nomoto, K.: 1991, *Astron. Astroph.* **249**, 474. 137

[124] Krause, O., Birkmann, S.M., Rieke, G.H., Lemke, D., Klaas, U., Hines, D.C., and Gordon, K.D.: 2004, *Nature* **432**, 596. 22

[125] Kudritzki, R.-P. and Puls, J.: 2000, *Annual Review of Astronomy and Astrophysics* **38**. 184

[126] Lamers, H.J.G.L.M. and Cassinelli, J.P.: 1999, *Introduction to Stellar Winds*, by Henny J. G. L. M. Lamers and Joseph P. Cassinelli, pp. 452. ISBN 0521593980. Cambridge, UK: Cambridge University Press, June 1. 184

[127] Landolt, A.U.: 1992, *The Astronomical Journal* **104**, 340. 38

[128] Leibundgut, B. and Suntzeff, N.B.: 2003, *Supernovae and Gamma-Ray Bursters* **598**, 77. v, 16

[129] Leonard, D.C., Filippenko, A.V., Barth, A.J., and Matheson, T.: 2000, *Astrophys. J.* **536**, 183, 187

[130] Li, W., Jha, S., Filippenko, A.V., Bloom, J.S., Pooley, D., Foley, R.J., and Perley, D.A.: 2006, *Publications of the Astronomical Society of the Pacific* **118**, 37. 39, 46

[131] Li, W.D., Qiu, Y.L., Qiao, Q.Y., Ma, J., Hu, J.Y., Wang, L., and Wheeler, J.C.: 1996, *International Astronomical Union Circular* **6379**, 1. 162

[132] Lidman, C., Cuby, J.G., Vanzi, L., Billeres, M., Hainaut, O. R., and Pompei, E.: 2002, SOFI - User's Maual issue 1.4, 2002 November 5. 39

[133] Lucy, L.B.: 1991, *Astrophys. J.* **383**, 308. 8

[134] Lucy E. et al.,1991, in Supernovae, ed. S.E. Woosley, Springer-Verlag, New York, p.82 22, 131

[135] Lucy, L.B., Danziger, I.J., Gouiffes, C., and Bouchet, P.: 1989, *IAU Colloq. 120: Structure and Dynamics of the Interstellar Medium* **350**, 164. 136

[136] Maeda, K., Benetti, S., Stritzinger, M., Röpke, F.K., Folatelli, G., Sollerman, J., Taubenberger, S., Nomoto, K., Leloudas, G., Hamuy, M., Tanaka, M., Mazzali, P.A., and Elias-Rosa, N.: 2010, *Nature* **466**, 82. 8

[137] Maeder, A.: 2002, *Astron. Astroph.* **392**, 575.

[138] Maeder, A. and Meynet, G.: 2000, *Astron. Astroph.* **361**, 159. 184, 192

[139] Maguire, K., di Carlo, E., Smartt, S.J., Pastorello, A., Tsvetkov, D.Y., Benetti, S., Spiro, S., Arkharov, A.A., Beccari, G., Botticella, M.T., Cappellaro, E., Cristallo, S., Dolci, M., Elias-Rosa, N., Fiaschi, M., Gorshanov, D., Harutyunyan, A., Larionov, V.M., Navasardyan, H., Pietrinferni, A., Raimondo, G., di Rico, G., Valenti, S., Valentini, G., and Zampieri, L.: 2010, *Monthly Notices of the Royal Astronomical Society* **404**, 981. 22, 50, 57, 64, 74, 78, 85, 110, 133, 183

[140] Malesani, D., Tagliaferri, G., Chincarini, G., Covino, S., Della Valle, M., Fugazza, D., Mazzali, P.A., Zerbi, F.M., D'Avanzo, P., Kalogerakos, S., Simoncelli, A., Antonelli, L.A., Burderi, L., Campana, S., Cucchiara, A., Fiore, F., Ghirlanda, G., Goldoni, P., Götz, D., Mereghetti, S., Mirabel, I.F., Romano, P., Stella, L., Minezaki, T., Yoshii, Y., and Nomoto, K.: 2004, *Astrophys. J.* **609**, L5. 9

[141] Matheson, T., Filippenko, A.V., Chornock, R., Leonard, D.C., and Li, W.: 2000, *The Astronomical Journal* **119**, 2303. 9

[142] Mattila, S., Meikle, W.P.S., Lundqvist, P., Pastorello, A., Kotak, R., Eldridge, J., Smartt, S., Adamson, A., Gerardy, C.L., Rizzi, L., Stephens, A.W., and van Dyk, S.D.: 2008, *Monthly Notices of the Royal Astronomical Society* **389**, 141. 5, 22, 137

[143] Mattsson, L., Höfner, S., and Herwig, F.: 2007, *Astron. Astroph.* **470**, 339. 186

[144] Maund, J.R., Fraser, M., Ergon, M., Pastorello, A., Smartt, S.J., Sollerman, J., Benetti, S., Botticella, M.-., Bufano, F., Danziger, I.J., Kotak, R., Magill, L., Stephens, A.W., and Valenti, S.: 2011, *ArXiv e-prints*, arXiv:1106.2565. 21

[145] Mazzali, P.A., Benetti, S., Altavilla, G., Blanc, G., Cappellaro, E., Elias-Rosa, N., Garavini, G., Goobar, A., Harutyunyan, A., Kotak, R., Leibundgut, B., Lundqvist, P., Mattila, S., Mendez, J., Nobili, S., Pain, R., Pastorello, A., Patat, F., Pignata, G., Podsiadlowski, P., Ruiz-Lapuente, P., Salvo, M., Schmidt, B.P., Sollerman, J., Stanishev, V., Stehle, M., Tout, C., Turatto, M., and Hillebrandt, W.: 2005, *Astrophys. J.* **623**, L37 23

[146] Mazzali, P.A., Deng, J., Maeda, K., Nomoto, K., Umeda, H., Hatano, K., Iwamoto, K., Yoshii, Y., Kobayashi, Y., Minezaki, T., Doi, M., Enya, K., Tomita, H., Smartt, S.J., Kinugasa, K., Kawakita, H., Ayani, K., Kawabata, T., Yamaoka, H., Qiu, Y.L., Motohara, K., Gerardy, C.L., Fesen, R., Kawabata, K.S., Iye, M., Kashikawa, N., Kosugi, G., Ohyama, Y., Takada-Hidai, M., Zhao, G., Chornock, R., Filippenko, A.V., Benetti, S., and Turatto, M.: 2002, *Astrophys. J.* **572**, L61. 9

[147] Meynet, G., Maeder, A., Schaller, G., Schaerer, D., and Charbonnel, C.: 1994, *Astronomy and Astrophysics Supplement Series* **103**, 97 184

[148] McGaugh, S.S.: 1994, *Astrophys. J.* **426**, 135. 142

[149] McNaught, R.H. and Pollas, C.: 1995, *International Astronomical Union Circular* **6242**, 2. 160

[150] Meikle, W.P.S., Mattila, S., Pastorello, A., Gerardy, C.L., Kotak, R., Sollerman, J., Van Dyk, S.D., Farrah, D., Filippenko, A.V., Höflich, P., Lundqvist, P., Pozzo, M., and Wheeler, J.C.: 2007, *Astrophys. J.* **665**, 608. 22, 23

[151] Mihalas, D.: 1970, *Series of Books in Astronomy and Astrophysics, San Francisco: Freeman, —c1970* 118

[152] Mikuz, H. and Maticic, S.: 2007, *Central Bureau Electronic Telegrams* **1116**, 1. 44, 45, 46, 50

[153] Minkowski, R.: 1941, *Publications of the Astronomical Society of the Pacific* **53**, 224. 2

[157] Montes, M.J., Weiler, K.W., Van Dyk, S.D., Panagia, N., Lacey, C.K., Sramek, R.A., and Park, R.: 2000, *Astrophys. J.* **532**, 1124. 13, 46, 54, 60, 66, 70, 128

[155] Morgan, H.L. and Edmunds, M.G.: 2003, *Monthly Notices of the Royal Astronomical Society* **343**, 427. 23

[156] Moriya, T., Tominaga, N., Blinnikov, S.I., Baklanov, P.V., and Sorokina, E.I.: 2011, *Monthly Notices of the Royal Astronomical Society*, 697. 139, 154

[157] Mould, J.R., Huchra, J.P., Freedman, W.L., Kennicutt, R.C., Jr., Ferrarese, L., Ford, H.C., Gibson, B.K., Graham, J.A., Hughes, S.M.G., Illingworth, G.D., Kelson, D.D., Macri, L.M., Madore, B.F., Sakai, S., Sebo, K.M., Silbermann, N.A., and Stetson, P.B.: 2000, *Astrophys. J.* **529**, 786. 13, 46, 54, 60, 66, 70, 128

[158] Moskvitin, A.S., Sonbas, E., Sokolov, V.V., Fatkhullin, T.A., and Castro-Tirado, A.J.: 2010, *ArXiv e-prints*, arXiv:1004.2633. 118

[159] Neilson, H.R. and Lester, J.B.: 2008, *Astrophys. J.* **684**, 569. 185

[160] Newton, J., Puckett, T., and Orff, T.: 2010, *Central Bureau Electronic Telegrams* **2201**, 1. 69

[161] Nomoto, K., Wanajo, S., Kamiya, Y., Tominaga, N., and Umeda, H.: 2009, *IAU Symposium* **254**, 355. 17

[162] Nomoto, K., Maeda, K., Tominaga, N., Ohkubo, T., Deng, J., and Mazzali, P.A.: 2005, *Astrophysics and Space Science* **298**, 81. 5

[163] Nomoto, K., Uenishi, T., Kobayashi, C., Umeda, H., Ohkubo, T., Hachisu, I., and Kato, M.: 2003, *From Twilight to Highlight: The Physics of Supernovae*, 115. 7

[164] Nomoto, K.I., Iwamoto, K., and Suzuki, T.: 1995, *Physics Reports* **256**, 173. 12

[165] Nozawa, T., Kozasa, T., Habe, A., Dwek, E., Umeda, H., Tominaga, N., Maeda, K., and Nomoto, K.: 2007, *Astrophys. J.* **666**, 955. 23

[166] Nozawa, T., Kozasa, T., Umeda, H., Maeda, K., and Nomoto, K.: 2003, *Astrophys. J.* **598**, 785. 22

[167] Nissinen M., Heikkinen E.P, Hentunen V.-P., 2009, CBET, 1743, 1 52

[168] Oke, J.B.: 1990, *The Astronomical Journal* **99**, 1621. 40

[169] Olofsson, H., Carlstrom, U., Eriksson, K., Gustafsson, B., and Willson, L.A.: 1990, *Astron. Astroph.* **230**, L13. 185

[170] Parisky, X. and Li, W.: 2007, *Central Bureau Electronic Telegrams* **1129**, 1. 64

[171] Pastorello, A., Valenti, S., Zampieri, L., Navasardyan, H., Taubenberger, S., Smartt, S.J., Arkharov, A.A., Bärnbantner, O., Barwig, H., Benetti, S., Birtwhistle, P., Botticella, M.T., Cappellaro, E., Del Principe, M., di Mille, F., di Rico, G., Dolci, M., Elias-Rosa, N., Efimova, N.V., Fiedler, M., Harutyunyan, A., Höflich, P.A., Kloehr, W., Larionov, V.M., Lorenzi, V., Maund, J.R., Napoleone, N., Ragni, M., Richmond, M., Ries, C., Spiro, S., Temporin, S., Turatto, M., and Wheeler, J.C.: 2009, *Monthly Notices of the Royal Astronomical Society* **394**, 2266. 58, 74, 110, 143

[178] Pastorello, A., Smartt, S.J., Mattila, S., Eldridge, J.J., Young, D., Itagaki, K., Yamaoka, H., Navasardyan, H., Valenti, S., Patat, F., Agnoletto, I., Augusteijn, T., Benetti, S., Cappellaro, E., Boles, T., Bonnet-Bidaud, J.-M., Botticella, M.T., Bufano, F., Cao, C., Deng, J., Dennefeld, M., Elias-Rosa, N., Harutyunyan, A., Keenan, F.P., Iijima, T., Lorenzi, V., Mazzali, P.A., Meng, X., Nakano, S., Nielsen, T.B., Smoker, J.V., Stanishev, V., Turatto, M., Xu, D., and Zampieri, L.: 2007, *Nature* **447**, 829. 8, 19

[173] Pastorello, A., Sauer, D., Taubenberger, S., Mazzali, P.A., Nomoto, K., Kawabata, K.S., Benetti, S., Elias-Rosa, N., Harutyunyan, A., Navasardyan, H., Zampieri, L., Iijima, T., Botticella, M.T., di Rico, G., Del Principe, M., Dolci, M., Gagliardi, S., Ragni, M., and Valentini, G.: 2006, *Monthly Notices of the Royal Astronomical Society* **370**, 1752. 85, 87, 108, 109

[174] Pastorello, A., Zampieri, L., Turatto, M., Cappellaro, E., Meikle, W.P.S., Benetti, S., Branch, D., Baron, E., Patat, F., Armstrong, M., Altavilla, G., Salvo, M., and Riello, M.: 2004, *Monthly Notices of the Royal Astronomical Society* **347**, 74. 75

[175] Pastorello A., 2003, PhD. thesis, Univ.Padova 25, 27, 83, 85, 87, 131, 153, 157, 194

[176] Pastorello, A., Turatto, M., Benetti, S., Cappellaro, E., Danziger, I.J., Mazzali, P.A., Patat, F., Filippenko, A.V., Schlegel, D.J., and Matheson, T.: 2002, *Monthly Notices of the Royal Astronomical Society* **333**, 27. 13

[177] Patat, F., Taubenberger, S., Benetti, S., Pastorello, A., and Harutyunyan, A.: 2011, *Astron. Astroph.* **527**, L6. 187

[178] Patat, F., Chandra, P., Chevalier, R., Justham, S., Podsiadlowski, P., Wolf, C., Gal-Yam, A., Pasquini, L., Crawford, I.A., Mazzali, P.A., Pauldrach, A.W.A., Nomoto, K., Benetti, S., Cappellaro, E., Elias-Rosa, N., Hillebrandt, W., Leonard, D.C., Pastorello, A., Renzini, A., Sabbadin, F., Simon, J.D., and Turatto, M.: 2007, *Science* **317**, 924. 8, 19

[179] Patat, F., Chugai, N., and Mazzali, P.A.: 1995, *Astron. Astroph.* **299**, 715. 10

[180] Patat, F., Barbon, R., Cappellaro, E., and Turatto, M.: 1994, *Astron. Astroph.* **282**, 731. 11, 50, 52, 57, 58, 69, 78, 82, 181, 183

[181] Phillips, M.M.: 1993, *Astrophys. J.* **413**, L105. 7

[182] Pinkall U., Mathematical Models from the Collections of Universities and Museums., Ed. G. Fischer., Braunschweig, Germany: Vieweg 192

[183] Pei, Y.C., Fall, S.M., and Bechtold, J.: 1991, *Astrophys. J.* **378**, 6. 20

[184] Pettini, M. and Pagel, B.E.J.: 2004, *Monthly Notices of the Royal Astronomical Society* **348**, L59. 150

[185] Pettini, M., King, D.L., Smith, L.J., and Hunstead, R.W.: 1997, *Astrophys. J.* **478**, 536. 22

[186] Pilyugin, L.S., Vílchez, J.M., and Contini, T.: 2004, *Astron. Astroph.* **425**, 849. 150

[187] Podsiadlowski, P., Fabian, A.C., and Stevens, I.R.: 1991, *Nature* **354**, 43. 187

[188] Pollas, C., Cappellaro, E., and della Valle, M.: 1993, *International Astronomical Union Circular* **5887**, 1. 158

[189] Poole, T.S., Breeveld, A.A., Page, M.J., Landsman, W., Holland, S.T., Roming, P., Kuin, N.P.M., Brown, P.J., Gronwall, C., Hunsberger, S., Koch, S., Mason, K.O., Schady, P., vanden Berk, D., Blustin, A.J., Boyd, P., Broos, P., Carter, M., Chester, M.M., Cucchiara, A., Hancock, B., Huckle, H., Immler, S., Ivanushkina, M., Kennedy, T., Marshall, F., Morgan, A., Pandey, S.B., de Pasquale, M., Smith, P.J., and Still, M.: 2008, *Monthly Notices of the Royal Astronomical Society* **383**, 627. 39

[190] Pooley, D., Lewin, W.H.G., Fox, D.W., Miller, J.M., Lacey, C.K., Van Dyk, S.D., Weiler, K.W., Sramek, R.A., Filippenko, A.V., Leonard, D.C., Immler, S., Chevalier, R.A., Fabian, A.C., Fransson, C., and Nomoto, K.: 2002, *Astrophys. J.* **572**, 932. 23, 85, 141, 151, 153, 183, 194

[191] Poznanski, D., Ganeshalingam, M., Silverman, J.M., and Filippenko, A.V.: 2011, *Monthly Notices of the Royal Astronomical Society* **415**, L81. 54

[192] Pozzo, M., Meikle, W.P.S., Rayner, J.T., Joseph, R.D., Filippenko, A.V., Foley, R.J., Li, W., Mattila, S., and Sollerman, J.: 2006, *Monthly Notices of the Royal Astronomical Society* **368**, 1169. 133

[193] Pozzo, M., Meikle, W.P.S., Fassia, A., Geballe, T., Lundqvist, P., Chugai, N.N., and Sollerman, J.: 2004, *Monthly Notices of the Royal Astronomical Society* **352**, 457. 22, 133, 137, 143, 183, 187

[194] Pumo, M.L. and Zampieri, L.: 2011, *ArXiv e-prints*, arXiv:1108.0688 148, 154

[195] Pumo, M.L., Zampieri, L., and Turatto, M.: 2010, *Memorie della Societa Astronomica Italiana Supplementi* **14**, 123. 84, 144, 147

[196] Pumo, M.L., Turatto, M., Botticella, M.T., Pastorello, A., Valenti, S., Zampieri, L., Benetti, S., Cappellaro, E., and Patat, F.: 2009, *Astrophys. J.* **705**, L138. 143, 145, 185

[197] Quimby R. M., Wheeler J. C., Höflich P., Akerlof C. W., Brown P. J., Rykoff E. S., 2007, ApJ, 666, 1093 74, 93

[198] Reimers, D.: 1977, *Astron. Astroph.* **61**, 217 184

[199] Rho, J., Jarrett, T.H., Reach, W.T., Gomez, H., and Andersen, M.: 2009, *Astrophys. J.* **693**, L39. 22

[200] Richardson, D., Branch, D., Casebeer, D., Millard, J., Thomas, R.C., and Baron, E.: 2002, *The Astronomical Journal* **123**, 745 9, 11, 50, 57, 183

[201] Roy, R., Kumar, B., Moskvitin, A.S., Benetti, S., Fatkhullin, T.A., Kumar, B., Misra, K., Bufano, F., Martin, R., Sokolov, V.V., Pandey, S.B., Chandola, H.C., and Sagar, R.: 2011, *Monthly Notices of the Royal Astronomical Society*, 637. 118

[202] Rutten, R.J.: 2003, *Radiative Transfer in Stellar Atmospheres, by Robert J. Rutten. Lecture Notes Utrecht University, 255 pages, 2003.* 91

[203] Salamanca, I., Terlevich, R.J., and Tenorio-Tagle, G.: 2002, *Monthly Notices of the Royal Astronomical Society* **330**, 844. 14

[204] Sandstrom, K.M., Bolatto, A.D., Stanimirović, S., van Loon, J.T., and Smith, J.D.T.: 2009, *Astrophys. J.* **696**, 2138. 22

[205] Schlegel, D.J., Finkbeiner, D.P., and Davis, M.: 1998, *Astrophys. J.* **500**, 525. 45, 52, 58, 64, 70, 158, 160, 163

[206] Schlegel, E.M.: 1990, *Monthly Notices of the Royal Astronomical Society* **244**, 269. 13

[207] Schmidt, B.P., Kirshner, R.P., Eastman, R.G., Phillips, M.M., Suntzeff, N.B., Hamuy, M., Maza, J., and Aviles, R.: 1994, *Astrophys. J.* **432**, 42. 18

[208] Schmidt, B.P., Kirshner, R.P., Schild, R., Leibundgut, B., Jeffery, D., Willner, S.P., Peletier, R., Zabludoff, A.I., Phillips, M.M., Suntzeff, N.B., Hamuy, M., Wells, L.A., Smith, R.C., Baldwin, J.A., Weller, W.G., Navarette, M., Gonzalez, L., Filippenko, A.V., Shields, J.C., Steidel, C.C., Perlmutter, S., Pennypacker, C., Smith, C.K., Porter, A.C., Boroson, T.A., Stathakis, R., Cannon, R., Peters, J., Horine, E., Freeman, K.C., Womble, D.S., Stone, R.P.S., Marschall, L.A., Phillips, A.C., Saha, A., and Bond, H.E.: 1993, *The Astronomical Journal* **105**, 2236. 87

[209] Smartt, S.J.: 2009, *Annual Review of Astronomy and Astrophysics* **47**, 63. 11, 20, 200

[210] Smartt, S.J., Eldridge, J.J., Crockett, R.M., and Maund, J.R.: 2009, *Monthly Notices of the Royal Astronomical Society* **395**, 1409. 20, 21

[211] Smith, N., Li, W., Filippenko, A.V., and Chornock, R.: 2011, *Monthly Notices of the Royal Astronomical Society*, 314. 20, 185, 200

[212] Smith, N., Li, W., Foley, R.J., Wheeler, J.C., Pooley, D., Chornock, R., Filippenko, A.V., Silverman, J.M., Quimby, R., Bloom, J.S., and Hansen, C.: 2007, *Astrophys. J.* **666**, 1116. 14

[213] Smith, N. and Owocki, S.P.: 2006, *Astrophys. J.* **645**, L45. 185

[214] Smoker, J.V., Davies, R.D., Axon, D.J., and Hummel, E.: 2000, *Astron. Astroph.* **361**, 19. 142

[215] Smoker, J.V., Axon, D.J., and Davies, R.D.: 1999, *Astron. Astroph.* **341**, 725. 142

[216] Sollerman, J., Cumming, R.J., and Lundqvist, P.: 1998, *Astrophys. J.* **493**, 933. 58

[217] Spyromilio, J., Leibundgut, B., and Gilmozzi, R.: 2001, *Astron. Astroph.* **376**, 188. 133

[218] Spyromilio, J. and Leibundgut, B.: 1996, *Monthly Notices of the Royal Astronomical Society* **283**, L89. 133, 162

[219] Stanek, K.Z., Matheson, T., Garnavich, P.M., Martini, P., Berlind, P., Caldwell, N., Challis, P., Brown, W.R., Schild, R., Krisciunas, K., Calkins, M.L., Lee, J.C., Hathi, N., Jansen, R.A., Windhorst, R., Echevarria, L., Eisenstein, D.J., Pindor, B., Olszewski, E.W., Harding, P., Holland, S.T., and Bersier, D.: 2003, *Astrophys. J.* **591**, L17. 9

[220] Stanimirović, S., Bolatto, A.D., Sandstrom, K., Leroy, A.K., Simon, J.D., Gaensler, B.M., Shah, R.Y., and Jackson, J.M.: 2005, *Astrophys. J.* **632**, L103. 22

[221] Stanishev, V., Adamo, A., and Micheva, G.: 2009, *Central Bureau Electronic Telegrams* **1746**, 1. 52, 91

[222] Stockdale, C.J., Weiler, K.W., Immler, S., Panagia, N., van Dyk, S.D., Ryder, S., Marcaide, J.M., Pooley, D., Sramek, R.A., Williams, C.L.M., and Kelley, M.T.: 2009, *The Astronomer's Telegram* **2016**, 1. 58

[223] Suntzeff, N.B., Phillips, M.M., Covarrubias, R., Navarrete, M., Pérez, J.J., Guerra, A., Acevedo, M.T., Doyle, L.R., Harrison, T., Kane, S., Long, K.S., Maza, J., Miller, S., Piatti, A.E., Clariá, J.J., Ahumada, A.V., Pritzl, B., and Winkler, P.F.: 1999, *The Astronomical Journal* **117**, 1175. 7

[224] Suntzeff, N.B., Ruiz, M.-T., and Depoy, D.: 1996, *International Astronomical Union Circular* **6380**, 2. 162

[225] Suntzeff, N.B. and Bouchet, P.: 1990, *The Astronomical Journal* **99**, 650. 110, 114

[226] Szalai, T., Vinkó, J., Balog, Z., Gáspár, A., Block, M., and Kiss, L.L.: 2011, *Astron. Astroph.* **527**, A61. 22

[227] Temim, T., Gehrz, R.D., Woodward, C.E., Roellig, T.L., Smith, N., Rudnick, L., Polomski, E.F., Davidson, K., Yuen, L., and Onaka, T.: 2006, *The Astronomical Journal* **132**, 1610. 22

[228] Thompson, L.A.: 1982, *Astrophys. J.* **257**, L63. 21

[229] Todini, P. and Ferrara, A.: 2001, *Monthly Notices of the Royal Astronomical Society* **325**, 726. 22

[230] Tominaga, N., Morokuma, T., Blinnikov, S.I., Baklanov, P., Sorokina, E.I., and Nomoto, K.: 2011, *The Astrophysical Journal Supplement Series* **193** 189

[231] Tsamis, Y.G., Barlow, M.J., Liu, X.-W., Danziger, I.J., and Storey, P.J.: 2003, *Monthly Notices of the Royal Astronomical Society* **338**, 687. 91

[232] Tsvetkov, D.Y. and Pavlyuk, N.N.: 1995, *Information Bulletin on Variable Stars* **4146**, 1. 158

[233] Tully R. B., 1988, Nearby Galaxies Catalogue, Cambridge University Press, Cambridge and New York, p.221 46

[234] Turatto, M., Benetti, S., and Pastorello, A.: 2007, *Supernova 1987A: 20 Years After: Supernovae and Gamma-Ray Bursters* **937**, 187. v, 5, 6

[235] Turatto, M., Benetti, S., and Cappellaro, E.: 2003, *From Twilight to Highlight: The Physics of Supernovae*, 200. 46, 52, 58, 163

[236] Turatto, M.: 2003, *Supernovae and Gamma-Ray Bursters* **598**, 21. v, 3, 5

[237] Turatto, M., Suzuki, T., Mazzali, P.A., Benetti, S., Cappellaro, E., Danziger, I.J., Nomoto, K., Nakamura, T., Young, T.R., and Patat, F.: 2000, *Astrophys. J.* **534**, L57. 24

[238] Turatto, M., Cappellaro, E., Danziger, I.J., Benetti, S., Gouiffes, C., and della Valle, M.: 1993, *Monthly Notices of the Royal Astronomical Society* **262**, 128. 14

[239] Turatto, M., Cappellaro, E., Barbon, R., della Valle, M., Ortolani, S., and Rosino, L.: 1990, *The Astronomical Journal* **100**, 771. 52, 58

[240] Utrobin, V.P. and Chugai, N.N.: 2011, *Astron. Astroph.* **532**, A100. 124

[241] Utrobin, V.P. and Chugai, N.N.: 2005, *Astron. Astroph.* **441**, 271. 127

[242] Utrobin, V.P.: 2004, *Astronomy Letters* **30**, 293. 145

[243] Valenti, S., Pastorello, A., Cappellaro, E., Benetti, S., Mazzali, P.A., Manteca, J., Taubenberger, S., Elias-Rosa, N., Ferrando, R., Harutyunyan, A., Hentunen, V.P., Nissinen, M., Pian, E., Turatto, M., Zampieri, L., and Smartt, S.J.: 2009, *Nature* **459**, 674. 5

[244] Valenti, S., Benetti, S., Cappellaro, E., Patat, F., Mazzali, P., Turatto, M., Hurley, K., Maeda, K., Gal-Yam, A., Foley, R.J., Filippenko, A.V., Pastorello, A., Challis, P., Frontera, F., Harutyunyan, A., Iye, M., Kawabata, K., Kirshner, R.P., Li, W., Lipkin, Y.M., Matheson, T., Nomoto, K., Ofek, E.O., Ohyama, Y., Pian, E., Poznanski, D., Salvo, M., Sauer, D.N., Schmidt, B.P., Soderberg, A., and Zampieri, L.: 2008, *Monthly Notices of the Royal Astronomical Society* **383**, 1485. 9

[245] Van Dyk, S.D., Li, W., and Filippenko, A.V.: 2003, *Publications of the Astronomical Society of the Pacific* **115**, 1. 20

[246] Van Dyk, S.D., Garnavich, P.M., Filippenko, A.V., Höflich, P., Kirshner, R.P., Kurucz, R.L., and Challis, P.: 2002, *Publications of the Astronomical Society of the Pacific* **114**, 1322. 21

[247] Van Dyk, S.D., Peng, C.Y., King, J.Y., Filippenko, A.V., Treffers, R.R., Li, W., and Richmond, M.W.: 2000, *Publications of the Astronomical Society of the Pacific* **112**, 1532. 21

[248] Van Dyk, S.D., Peng, C.Y., Barth, A.J., and Filippenko, A.V.: 1999, *The Astronomical Journal* **118**, 2331. 5, 8, 10

[249] van Zee, L., Salzer, J.J., Haynes, M.P., O'Donoghue, A.A., and Balonek, T.J.: 1998, *The Astronomical Journal* **116**, 2805.

[250] Yoon, S.-C. and Cantiello, M.: 2010, *Astrophys. J.* **717**, L62. 185

[251] Wheeler, J.C. and Benetti, S.: 2000, *Allen's Astrophysical Quantities*, 451. v, 4, 9

[252] Wheeler, J.C., Harkness, R.P., Clocchiatti, A., Benetti, S., Brotherton, M.S., Depoy, D.L., and Elias, J.: 1994, *Astrophys. J.* **436**, L135. 9

[253] Wheeler, J.C., Harkness, R.P., Barker, E.S., Cochran, A.L., and Wills, D.: 1987, *Astrophys. J.* **313**, L69. 8

[254] Woosley, S.E., Heger, A., and Weaver, T.A.: 2002, *Reviews of Modern Physics* **74**, 1015. 143

[255] Woosley, S.E., Blinnikov, S., and Heger, A.: 2007, *Nature* **450**, 39 186

[256] Woosley, S.E., Heger, A., and Weaver, T.A.: 2002, *Reviews of Modern Physics* **74**, 1015.

[257] Woosley, S.E., Hartmann, D., and Pinto, P.A.: 1989, *Astrophys. J.* **346**, 395. 83

[258] Woosley, S.E., Pinto, P.A., Martin, P.G., and Weaver, T.A.: 1987, *Astrophys. J.* **318**, 664. 21

[259] Woosley, S.E. and Weaver, T.A.: 1986, *Annual Review of Astronomy and Astrophysics* **24**, 205. 10

[260] Zampieri, L.: 2007, *The Multicolored Landscape of Compact Objects and Their Explosive Origins* **924**, 358. 144

[261] Zampieri, L., Pastorello, A., Turatto, M., Cappellaro, E., Benetti, S., Altavilla, G., Mazzali, P., and Hamuy, M.: 2003, *Monthly Notices of the Royal Astronomical Society* **338**, 711. 84, 144, 147

[262] Zampieri, L.: 2002, *Recent Developments in General Relativity*, 301. 147